Advances in Droplet Microfluidics for High-Throughput Experimentation

by

Emory M. Payne

A dissertation submitted in partial fulfillment
of the requirements for the degree of
Doctor of Philosophy
(Chemistry)
in the University of Michigan
2023

Doctoral Committee:

Professor Robert T. Kennedy, Chair
Professor Ryan C. Bailey
Professor Kristina Håkansson
Professor Alison R. H. Narayan

Emory M. Payne

emoryp@umich.edu

ORCID iD: 0000-0002-5956-8392

Dedication

To my parents, Mary Lou and Steve, for their constant love and support.

Acknowledgements

I am extremely grateful for the support that I have received over the past few years, and I truly could not have done any of it without the proverbial village that has helped me. First and foremost, I would like to thank Professor Robert Kennedy for allowing me to work under his supervision. The mentorship, direction, and thoughtfulness that he provided is the glue that holds this dissertation together. I will always value how I was treated as an equal throughout my time in his group, and I am forever grateful for the opportunities that he provided me with.

Next, thank you to my committee: Professors Ryan Bailey, Kristina Håkansson and Alison Narayan. They have each showed me endless support and pushed me to think beyond my experiments to better my thesis. I am so honored to have been able to work with and learn from each of them. I would also like to thank honorary committee member Dr. Jeffrey Moore of Merck who was a constant force for providing scientific and moral support. I thank collaborators Professor Paul Haddad (University of Tasmania), Dr. Maryam Taraji (AWRI), and Dr. Eric Abbate (Inscripta Inc) for the value that they contributed to this work. I want to thank Professor Molly Costanza-Robinson and MaryAnn DeMaria for exemplifying what a scientist is; without either of them I would certainly not be writing this thesis.

I have been so lucky to work with and learn from incredibly talented scientists. Thank you to Dr. Daniel Holland-Moritz, Dr. Daniel Steyer, and Dr. Shane Wells for mentoring such an aggressively eager first year student and teaching the fine motor skills necessary to succeed at the microscale. I will also thank Dr. Steven Doonan for instilling in me the great American tradition

of droplet microfluidics. Thank you to Bridget Murray and Laura Penabad-Peña for being excellent coworkers – I am so excited to see their continued success.

I would be remiss not to mention the other Kennedy Kids that I have had the pleasure to work with. Dr. Alec Valenta and Dr. Cara D'Amico were at times the only reason I came to lab – they showed me true friendship and exemplified how to throw a very classy wine and cheese night. Thank you to Drs. Sorensen and Zegalia whose comradery and advice was always welcome. Thank you to Brady Anderson, who has been an extraordinary friend, roommate, soundboard, and squash rival throughout candidacy, covid, seminar, data meeting, job search, break-ups, and broken doors. Thank you to Peter-Phillip Booth and Ashley Lenhart for their endless support, desk snacks, and just the right amount of judgement through so many bagel Wednesdays and trips to Walgreens. Thank you to Hayley Herderschee for her excellent song suggestions over the last few years. To all of the members of the Kennedy lab: I am so thankful for your friendship, patience, and help.

Thank you to Marina, Josh, Kayla, Ruby, Anna, and Claire for our shared game nights, bar crawls, hockey games, and dinner parties. I also want to thank Rosie and Iliana, whose late presence in my time at Michigan made the last few months so enjoyable despite our shared trauma of contracting covid at ASMS. I am so grateful for the relationships I have built with each of you.

Finally, thank you to my family for, really, everything. Thank you to my parents for doing everything in their power to ensure I had every resource available to get to this point. Thank you to Aidan for always being my role-model despite picking the polar opposite career path than I did. Thank you to Juanita Pardo Sanchez for being my biggest supporter for the past few years. I cannot imagine having finished this work without your constant love, support, and positivity. I recognize that none of you wanted to hear about the difficulty of coupling droplets to electrospray, but I appreciate your feigned enthusiasm regardless.

Table of Contents

List of Tables

List of Figures

Abstract

High throughput experimentation (HTE) is increasingly important in both academic and industrial research environments. While the utility in screening large libraries for many applications is promising, the analytical testing remains a major bottleneck to discovering desired samples. New analytical tools are required that can process and screen large datasets with minimal time and waste. This work focuses on the development and advancement of droplet microfluidics to achieve HTE.

A limiting factor to droplet microfluidics as a screening technology is the transfer of small molecules between droplet samples. This work first investigates droplet carryover or "crosstalk" using electrospray ionization mass spectrometry (ESI-MS). Using this label-free analysis method, 36 small molecules are screened for extent of crosstalk, and the behavior is modelled using physicochemical properties. Important drivers of crosstalk are elucidated, such as analyte hydrophobicity, surfactant identity, oil composition, surfactant concentration, and flow duration. A new surfactant is tested which is shown to selectively retain small molecules that resemble the surfactant head chemical structure.

We next apply fundamental droplet investigations to the development of novel unit operations for the processing of droplet samples. In one tool, dielectrophoresis (DEP) is used to split and trap 400 – 1000 pL microfluidic droplets in flow at rates of 25 droplets/s. The splitting effect is characterized to show the utility of the tool in microfluidic workflows with varying droplet sizes and applications. A second tool, high-dilution reagent addition, is developed to enable temporal control for synthetic and biological screening. Two microfluidic device designs are

developed to dilute droplet samples from 2 – 150-fold with less than 1% carryover between droplet samples. One device was shown to be compatible with droplets generated from a multiwell plate, which was applied to testing a photocatalysis reaction with 1% reagent consumption compared to μL-scale experiments. The second device is shown to provide 10-fold dilution at > 40 droplets/s without carryover and a 97% success rate, which is a significant improvement on previous designs.

The development of a microfluidic liquid-liquid extraction is shown as an advanced tool for sample processing. A microfluidic chip is designed to achieve slug flow nanoextraction (SFNE). An automated system is built using the device, employing an autosampler to inject samples into the chip, and an in-line UV detector to analyze small molecules partitioning between aqueous and organic phases. Flow modulation and analytical performance is characterized using the automated SFNE system. A mini-screen of octanol-water partition coefficients is performed using the system, leading to a platform that meets industry standards with 10-fold less time and 40-fold less volume than a previous miniaturized method.

Lastly, the development a droplet-based analytical method to test and sort cell variants for lysine production is presented. An ESI-MS method is shown to perform reliable detection of lysine from 10-30 nL microfluidic droplets even with a complex cell media background. Individual *E. coli* cells are encapsulated and grown in microfluidic droplets, and lysine production from a known *E. coli* variant is measured. Using mass-activated droplet sorting, the above strategies were used to analyze and sort cells with high lysine production, with 5.8-fold improvement of lysine production from a mixed variant population after 2.5 h of sorting. The resulting pool is immediately translatable to validation methods such as sequencing.

Chapter 1 Introduction

Adapted in part from Payne, E.M. *et al, Lab Chip* **2020** *20,* 2247-2262
with permission from the Royal Society of Chemistry.

1.1 High Throughput Screening

High-throughput screening is a valuable technology in chemical and biochemical research for the discovery of new reactions, catalysts, or pharmaceuticals. The ability to generate and test large libraries of small molecules, enzymes, or cells variants for a chemical activity of interest improves the likelihood of finding "hits" or samples with desired activity. In addition to screening chemical activity (e.g. reaction yields), screening pharmacological properties (e.g. partitioning coefficients/pKas,[1] or inhibition concentrations[2]) is a useful process for characterizing large candidate libraries during drug development. As technology advances to process and screen large sample libraries, many new chemical applications become feasible.

One application that has been enabled by screening technology development is protein or metabolic engineering, which follows iterative rounds of design and testing of cell or enzyme variants. This process relies on mutation to develop biocatalysts which have desired activity. Examples of recent biocatalysis efforts include enzymes designed by Merck for the biosynthesis of the diabetes medication sitagliptin[3] and the anti-HIV pharmaceutical islatravir[4] and by academic groups to perform biaryl cross coupling[5] and plastic biodegradation.[6] However, the discovery of active enzymes requires the generation and screening of 10^3-10^5 variants.[7] While these demonstrations are powerful, the method is limited by the ability to generate, prepare, and analyze individual variants for the target activity. Directed evolution is just one example where large

library testing is useful, but it represents an application which has been enabled by the ability to generate and test samples. Developing tools for high throughput experimentation (HTE) can enable workflows such as directed evolution, expand efforts to discover novel reactions, and characterize larger sample libraries.

Technology has advanced significantly for the generation, manipulation, and analysis of samples for HTS. While HTS relied on 96-well plates in the early 1990s, screening technology rapidly improved through higher sample density and handling potential of multi-well plates (MWPs) into the 2000s.[8] In 1536-well arrays, the minimum volume is 3 μL, which is a reduction from >100 μL required for 96-well plates. Additionally, robotic solid and liquid handlers can perform thousands of assays per day in a MWP format which automates library generation and processing.

However, as MWP formats have become more miniaturized, reliable sample handing,[9] evaporation,[10] and effective mixing[11] have become challenging during HTE, leading to variability and inaccuracy. Additionally, for sample libraries with $>10^7$ members, the material cost and waste of thousands of MWPs, consumables, and reagents is significant. While robots can improve time efficiency for processing these samples, high-end liquid handlers that allow for full automation can cost > $250,000.[9]

Another hurdle in HTS technology is the development of analytical methods. HTS using methods such as fluorescence activated cell sorting (FACS) or traditional optical plate-reader assays are strong options if the chemical activity can be surface displayed on cells or produce optical signal. However, as many relevant systems (reactions, biocatalysts) do not produce fluorescent or colorimetric products, information rich techniques are needed for analysis.

High pressure liquid chromatography (HPLC) coupled to UV-visible, refractive index, electrochemical, or mass spectrometry (MS) detection is a reliable analytical method for HTS. HPLC provides chemical separation allowing for the analysis of target analytes from a reaction mixture. Coupling HPLC with MS provides an additional dimension of selectivity, where ionizable analytes can be structurally characterized or quantified. While HPLC-based screening is well-established, typical quantification methods will expend > 5 min and > 2.5 mL of solvent per sample. Many HPLC methods can be shortened, with robust techniques routinely achieving 1-3 minutes per sample. Even at this throughput, screening library sizes of 10^4 samples would require ~1 month of instrument run time. Higher throughput methods for HPLC have been developed such as multiple injections in a single chromatographic run (MISER), which can improve throughput almost 10-fold.[12,13] Others are developing ultrafast isocratic separations in microcolumns which reduces any inter-run equilibration,[14] but screening has not been achieved using this method yet.

Other analytical approaches have circumvented the need for chromatographic separation techniques. As MS resolution and scanning speed has improved, some applications can perform analysis with minimal sample preparation without a front-end separation technique. Recently, high-throughput sample injection methods have been reviewed,[15] which is summarized in Figure 1-1. While this figure is not comprehensive in evaluating each methods' repeatability or sensitivity, it provides a benchmark for the minimization and throughput of screening.

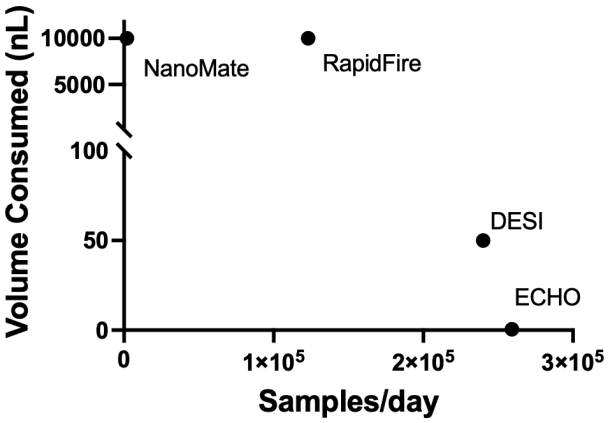

Figure 1-1: High-throughput sample injection methods for mass spectrometry. Values retrieved from Kempa et. al, 2019.

NanoMate (TriVersa), RapidFire (Agilent Technologies), and EchoMS (SCIEX) are three commercial front-end sampling methods for rapid introduction into mass spectrometers. The NanoMate provides chip-based separation and electrospray into a mass spectrometer, but requires high volume and throughput is relatively low.[16] The RapidFire is a robotic sample handler which can sip from MWPs, perform in-line solid-phase microextraction, then inject for direct MS. The throughput of the RapidFire ranges from 5 – 60 seconds/sample, dependent on inclusion of an extraction step or other sampling conditions.[17–19] The EchoMS is a sample introduction method which leverages acoustic ejection of samples from a MWP. By vibrating the bottom of custom MWPs, small (~50 pL) sample droplets can be ejected into the mass spectrometer.[20] New sample introduction methods are being developed, such as high-density sample spotting followed by desorption electrospray ionization (DESI) MS.[21,22] This approach is achieved by arraying samples in a MWP, dipping pin arrays into the liquid samples, then depositing sample onto a substrate which can be imaged using DESI-MS imaging. In principle, samples can be retrieved from the MWPs after analysis in each of these formats, but the volume required for the analysis is limited to the MWPs used. Therefore, volume required for analysis is unequal to volume consumed as in

Figure 1-1. These methods, in tandem with robotic liquid handlers to prepare samples, are increasingly employed in research environments for HTE.

Each of the methods described above are only compatible with MWPs, which limits HTS with respect to volume (< 3 μL), cost, reliability, and accessibility. Methods that can address the flexibility, cost, and reagent consumption while providing a cohesive method for sample preparation and analysis would fill a significant gap in the analytical technology for HTS.

1.2 Droplet Microfluidics

Droplet microfluidics enables the translation of chemical and biological assays to scales and rates unachievable in conventional laboratory workflows. The term droplet microfluidics is used to generalize microfluidic manipulation using immiscible phases by segmenting a sample ("dispersed") phase, typically water, with an immiscible solvent ("continuous phase"), typically a hydrophobic (e.g. mineral oil) or fluorinated oil. Droplet sizes range from fL-μL volumes and can be manipulated when confined to microfabricated devices or capillaries.

The impetus for using water-in-oil emulsions grew initially from a desire to develop low-cost alternatives to robotic liquid handlers for HTE. Microfluidic segmentation presents $10^3 – 10^6$ fold volume reductions of bioassays compared to MWP-based methods.[23] Compared with other microfluidic methods, use of droplets provides solutions to some drawbacks of single liquid phase systems such as ineffective sample diffusion, low analytical throughput, surface fouling, and inefficient mixing.[24,25]

Droplets are relatively simple to generate in a wide range of volumes, compositions, and throughputs. They may be stored, transported, and analyzed, facilitating modular operations.[26] Droplet-based sample manipulations routinely exceed 1000 Hz, which is orders of magnitude faster than robotic high-throughput liquid handling.[27,28]

In the well plate-screening paradigm, samples are retained in wells on a 96, 384, or 1536-well plate, allowing for reactions to be performed in volumes as low as 3 µL. The spatial separation of samples in discrete wells provides the ability for thousands of parallel reactions to take place in a compact, traceable, and addressable format. With chemistry and biology confined to wells, researchers can culture and sequence cells, add reagents, aliquot sample, perform sample cleanup, and analyze with a wide range of instrumentation. The ability to manipulate and analyze each sample based on its position is critical to the utility of this format. For a novel screening platform to compare, it is essential that it reliably perform all of these functions; however, to be widely adopted, such a screening technology must also provide advantages over these existing workflows.

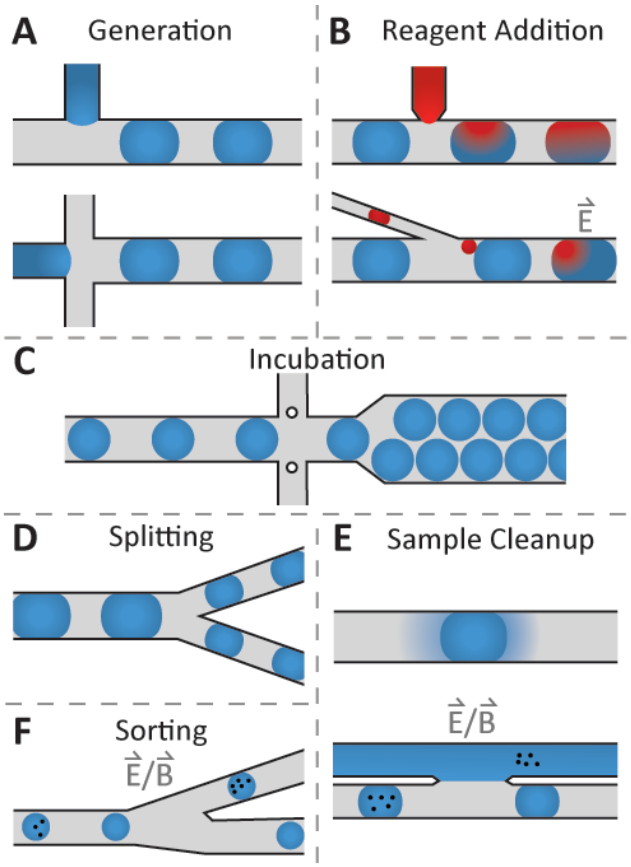

Figure 1-2: Common droplet unit operations with flow proceeding left to right. A) Droplet generation by T-junction or flow focusing. B) Reagent addition by direct injection and pairwise merging. C) On-chip incubation by oil drain and channel expansion. D) Splitting by channel bifurcation. E) Sample cleanup by continuous phase partitioning or solid phase extraction. F) Sorting by dielectro- or magneto-phoresis.

Research in droplet microfluidics has largely addressed each of the core functionalities of well plate screening.[26] Spatial separation is achieved by breaking fluids into individual droplets using either a T-junction or flow focusing geometry (Figure 1-2A). The resultant droplets range in volume from single femtoliters to tens of nanoliters with extremely low variability (< 1% relative standard deviation, RSD on droplet volume),[29–32] a significant reduction from the microliters needed in MWPs. A variety of microfluidic geometries allow multiple substances to be co-encapsulated in these droplets as they are made, at controlled ratios and with minimal sample to sample variation.[33–35] Droplet generation in the kilohertz range dwarf the fluid handling capabilities of robotics and proposed methods for parallelization hold the potential to push these speeds even higher.[36]

Once droplets have been formed, it is critical to maintain their spatial and chemical separation in bulk format. Structure is maintained through the use of surfactants,[37,38] which mimic the function of phospholipid membranes in biological systems, i.e. they limit droplet merging and chemical transfer when in contact.[37] Use of surfactants also allows for droplet stability at temperatures up to 98°C,[37,39] enabling complex reactions such as droplet-based polymerase chain reaction (PCR),[40] or elevated temperature incubations for extended periods.[41]

In MWPs, the spatial separation of samples has facilitated the use of robotics for the addition of reagent to individual reactions. The reproducibility and reliability of such systems is critical to modern screening technologies. In droplet microfluidics, overcoming the challenge to create a comparable form of reagent addition has been critical to the use of the technology for complex chemical reactions. Reagent addition has been achieved by direct injection into droplets, pairwise droplet merging, and double emulsion strategies.[42] Direct injectors (e.g. Pico-injectors) bring single-phase reagent into contact with a cross flow of droplets, allowing for brief merger

between the aqueous components, then re-segmentation after the addition of the reagent (Figure 1-2B).[43–45] When surfactant stabilized, reagent addition by pico-injection may be actuated by use of an external electric field.[44] Direct injection into droplets has been demonstrated with up to 2-fold increase in droplet volume, at rates of 1000 droplets/s, which exceeds that of robotic handling by several orders of magnitude.[46,47] Aside from limited volume addition, direct injection designs have been characterized by high (5-10%) droplet to droplet carryover, so methods such as wash droplets,[48] reagent flushing,[45] and multiple small injectors[43] can reduce carryover to < 1%.

While direct injection has allowed complex reaction workflows to be performed in droplets, it does not allow for combinatorial reaction screening to be performed in the same way that it may be in MWPs. One method to address this is to combine two libraries of droplets to produce a combinatorial set of samples. In continuous flow, two streams of droplets may be combined in pairs and merged to produce an output stream of combined droplets (Figure 1B).[42,49–51] This method has been shown with up to 25-fold addition,[52] and at 250 droplets/s.[51] However, achieving one-to-one merging of the two droplet streams is difficult, and instances of missed or double droplet merger events have been characterized as up to 14% of all droplets processed in this way.[53] Due to this inconsistency, this droplet merger format has not been widely applied for achieving reagent addition.

In any chemical reaction, sample incubation is critical to allow the desired reaction to occur prior to screening. In the droplet format, this may be achieved by removing droplets from a device and storing them in bulk. Incubation can also be achieved on-chip, which is commonly achieved by reducing fluidic velocity on-chip by draining oil and allowing droplets to close-pack (Figure 1-2C).[54,55] Devices with integrated delay lines are useful for simplifying workflows to single devices when incubation is necessary. On-chip incubation lines are often aided by channel expansion or

multi-layer fabrication, where an increase in channel volume contributes to both decreased fluidic velocity and increased droplet containment.[33,55,56] This strategy can reduce the footprint of a microfluidic device while increasing the incubation time.

Sampling from well plates in traditional screening workflows is common; small volumes of sample may be pulled for analysis, further reactions, or long-term storage. In droplet format, sampling can be performed by splitting droplets in flow using microchannel bifurcations (Figure 1-2D),[29,45] electrostatic forces,[57] or acoustics waves.[58] Splitting has been achieved across a range of droplet sizes ranging from 6.5 fL to > 1 μL,[59] and the split ratios can be as asymmetric as sampling 95 – 5% of total droplet volume.[60]

Solid and liquid phase extractions are regularly performed in plate format to prepare samples for analytical assessment, and similar sample cleanup has been demonstrated in droplets (Figure 1-2E).[46,61–65] Droplet splitting may be used to perform solid phase extractions (SPE), allowing selective retention of targeted analytes in droplets via bead based capture and wash workflows.[66,67] The throughput of droplet SPE is modest compared to that of droplet generation or splitting (regularly exceeding 1000 droplets/s),[68] likely due to the mixing occurring in droplets keeping SPE beads in suspension. However, SPE has been achieved in a droplet format at 5 droplets/s with < 60% enrichment of DNA.[69]

Once analysis is performed, it is often necessary to further manipulate the sample. On MWPs, this function is trivial assuming that the analytical method does not consume all of the sample. For flowing droplets, however, collecting desired samples for further use requires a collection or sorting method. The most common strategy for doing so is dielectrophoresis (DEP) where a droplet may be deflected by an electric field to exit a device via a selected channel (Figure 1-2F).[70,71] DEP of 65 pL droplets has been shown at 30 kHz, resulting in 10^8 droplets sorted per

hour.[72] Other sorting strategies have been achieved using external magnetic fields,[73,74] acoustic waves,[75] or through other physical properties of droplets.[56,76] Coupling these sorting techniques with rapid analytical assessment can provide high throughput approaches to hit identification and selection, and enables downstream discovery and analysis.[77–79]

MWP screening methodologies are a well-established, robust approach to HTS but microfluidic droplets are quickly becoming a viable alternative. A demonstration of directed evolution using microfluidic droplets summarized the economy for their particular HTS, showing drastic cost and time efficiency using droplets (Table 1-1).[80]

Table 1-1: Comparison of time and costs for complete screen using two methods[80]

	Robot	Microfluidic drops
Total reactions	5×10^7	5×10^7
Reaction volume	100 µL	6 pL
Total volume	5,000 L	150 µL
Reactions/day	73,000	1×10^8
Total time	**~2 years**	**~7 h**
Number of plates/devices	260,000	2
Cost of plates/devices	$520,000	$1.00
Cost of tips	$10 million	$0.30
Amortized cost of instruments	$280,000	$1.70
Substrate	$4.75 million	$0.25
Total cost	**$15.81 million**	**$2.50**

Droplets represent an attractive opportunity to scale down expensive chemical use in HTS, reduce unsustainable consumable use in the screening process, and rapidly analyze millions of

samples, all while using automated workflows that run at rates that are orders of magnitude higher than industry standard techniques.

1.3 Analysis of Droplet Samples

Rapid analysis is a critical bottleneck in HTS. The challenge for analysis in droplet microfluidics in obtaining high information content in minimal reaction volumes at high rates. The analysis of droplet content has relied heavily on a few techniques that have been applied widely. Most notably, droplet HTS has been performed extensively using fluorescent detection. Laser induced fluorescence (LIF) is a common technique for droplet analysis as it is easily applied to droplet analysis; LIF approaches have rapid acquisition rates, which allow for multiple sample points across a single droplet even at high throughputs with low limits of detection and high sensitivity. When coupled to DEP sorting, LIF based droplet selection has been demonstrated as fast as 30 kHz with > 99% accuracy,[72] throughput similar to fluorescence activated cell sorting >100 kHz.[81]

However, LIF based workflows require fluorescent reporters, which are often challenging to incorporate into chemical and biological assays. In many chemical or biochemical screens, the native target is not fluorescently active and adding a fluorescent tag may change the activity of interest. To address this limit, secondary reporters have been utilized to give a signal output from non-fluorescently active assays.[79,82,83] Applications of these reporter systems are limited and must be designed on an *ad hoc* basis. Therefore, while fluorescence activated droplet sorting (FADS) is rapid and reliable, it is not generalizable enough to use in most screening applications, such as reactions, evolution experiments, and small molecule characterization studies.

Many alternative approaches have been investigated for the analysis of droplet samples. Absorbance based detection schemes have been explored as a complimentary strategy for droplet

analysis.[79] However, the low specificity and high limits of detection limit this approach to reactions that produce a change significant enough to be detected above the background reaction matrix.[84] Absorbance detection is more challenging in droplets due to the limited path length through which to detect across a droplet. To counter this, more sensitive methods such as differential detection photothermal interferometry have been reported for absorbance readouts from droplets.[85] High-speed charged coupled device (CCD) cameras have been employed for the screening of colorimetric outputs in droplets.[82,86] Though CCD cameras have been used primarily to interrogate droplet size, a system in which droplets change turbidity or refractive index may be accessible for this type of detection as well.[87]

Spectroscopic techniques such as droplet Raman and infrared detection, as well as droplet nuclear magnetic resonance (NMR) spectroscopy, have been developed but are under-utilized in droplet HTS. Raman has been applied to single cell detection in droplets but has not been widely employed for many HTS workflows due to high noise levels and low sensitivity.[88] Strategies for improvement of sensitivity and selectivity are a major topic of research,[89,90] which may lead to improved detection methods for DEP triggering.[88] Infrared detection has been applied to imaging droplets in flow, but HTS has not been demonstrated, likely due to the high interference from the aqueous background.[91,92] NMR analysis of microliter segmented plugs has been shown as a multiplexed detection from LC effluent,[93] but has similarly not been applied to HTS. Droplet NMR spectroscopy may be an exciting future development with the improvement of miniaturized high-field magnets.[94,95]

1.4 Mass Spectrometry of Droplet Samples

Mass spectrometry (MS) analysis of droplets has been explored as an alternative approach, expanding the tool set for droplet analysis through label free detection. Analytes must be ionized

for mass spectrometry detection or analysis. Electrospray ionization (ESI) and matrix assisted laser desorption ionization (MALDI) are two commonly used approaches for ionizing and generating gas phase analytes for MS. ESI and MALDI are similar in that ionization occurs via proton transfer or adduction and both are considered "soft" ionization techniques where the chemical structure is primarily maintained throughout ionization.

MALDI is largely performed on a sample in solid form. Samples are mixed with a MALDI matrix and placed onto a substrate and dried.[96] The subsequent dried droplet is ablated using a laser, which generates a plume perpendicular to the surface (Figure 1-3A). In the plume, the high energy initiates cascades of proton transfer which ultimately produce some charged molecules that are detectable by MS. The purpose of the matrix is to absorb energy from the laser, and to promote proton transfer with the molecules in the sample.[97] The effectiveness of MALDI as a charging method lies in the ability to create imperfect matrix/analyte co-crystals for best ablation and proton transfer. MALDI is affected by the choice of matrix, drying solvent/method, and laser power, which can each be selected based on targeted analyte or application.

In ESI, liquid flow is pumped through a needle with a high voltage applied either to a conductive needle or directly to the liquid stream, which promotes the aerosolization of the liquid flow.[98] Neutral analytes can be charged via proton transfer or though adduction of charged ions such as Na^+,NH_4^+, or Cl^- among many types of adducts. In the aerosol droplets, charges accumulate on the surface of microdroplets, including salts and analytes (Figure 1-3B). Microdroplets shrink and split in the presence of high heat and vacuum, and charged species can be ejected from the droplet due to the accumulation of surface charge.[99] Charged molecules ejected from the droplet result in gas phase ions that can be detected by MS.[100] The process of ionizing an analyte of interest is strongly dependent on the sample matrix, salt concentration, and surface activity of molecules.

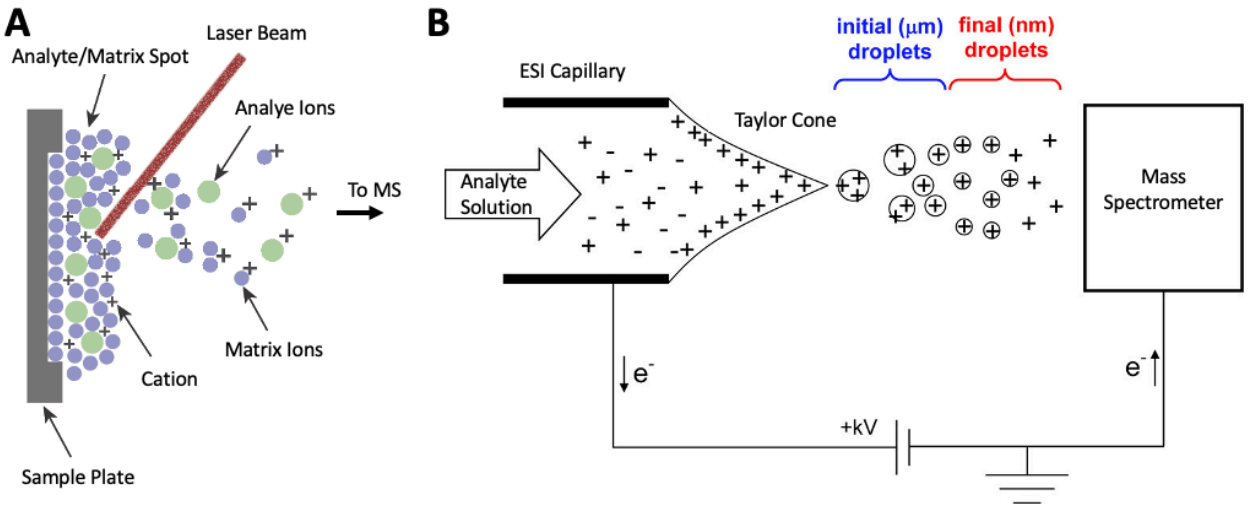

Figure 1-3: General mechanisms of standard soft-ionization sources. (A) Schematic of MALDI adapted from Spectra Physics. (B) Schematic of ESI adapted from Konerman et al., 2013.

Both ESI and MALDI show significant promise for enabling label-free droplet analysis using MS. The methods provide similar data, while providing advantages for given applications. MALDI requires droplet deposition, matrix addition, and sample drying prior to analysis which limits throughput, while ESI is fully destructive and flow rates must be compatible with the scanning speed of the mass spectrometer. Significant effort has been dedicated to addressing these limitations.

Several groups have achieved droplet deposition for MS-imaging analysis.[6,101–103] Droplet MALDI has the advantage of flexibility in droplet size as the laser ablation area is often smaller than droplet diameters commonly used. Similarly, MALDI is not fully destructive like ESI, allowing researchers to return to samples of interest after analysis. Haidas and coworkers reported the ability to spot and analyze up to 2400 droplets on a standard glass slide,[104] and others have fabricated microwell plates for droplet deposition at higher densities.[103] While droplet MALDI cannot be performed as an online technique for analysis, which restricts throughput, spotting droplets at densities of 100,000 samples/plate at 2,000 Hz makes the method feasible.[105] Additionally, droplet spotting can be performed using DEP, where only droplets that contain

sample are spotted for analysis.[103,105] This method ensures that the slow analysis time is maximized on samples of interest, rather than samples which are empty. Others are developing droplet MALDI with advanced sample tracking and ablation, which reduces the analysis time where no sample has been deposited.[106]

ESI of droplets is advantageous as it may be integrated into the outlet of a microfluidic system. As mass spectrometers become faster and more sensitive, techniques such as tandem mass spectrometry have enabled selective analysis of droplet samples. Droplet ESI-MS generates bursts of analysis as aqueous droplets are sprayed, followed by non-conductive oil (Figure 1-4).[107] Throughputs for droplet ESI are modest in comparison to optical detection; recently 300 pL droplet samples have been analyzed at up to 10 Hz using nano-ESI[108] and 800 pL have been shown to be detectable at up to 33 Hz with software modifications to commercially available mass spectrometers.[109] At these throughputs, droplet ESI provides an order of magnitude increase in samples screened per day compared to ECHO-MS (Figure 1-1), while benefiting from upstream processing such as reagent addition and clean up. Droplet ESI is also currently limited by droplet size; most studies have thus far operated with 10 – 50 nL droplets.[52,107,110–112] However, recent work using nano-ESI has shown droplet detection in volumes as small as 65 pL.[108] A constraint in coupling microfluidics with ESI is compatibility between scan speeds of mass spectrometers and droplet size and flow rates; droplets are often too small to maintain sustained electrospray for thorough droplet analysis. Additionally, as ESI is destructive, a method for preserving a duplicate sample is necessary. Our group has recently developed mass activated droplet sorting to this end, which splits a sample droplet where one is analyzed by ESI-MS, and the other is sorted based on the intensity of target analytes.[52]

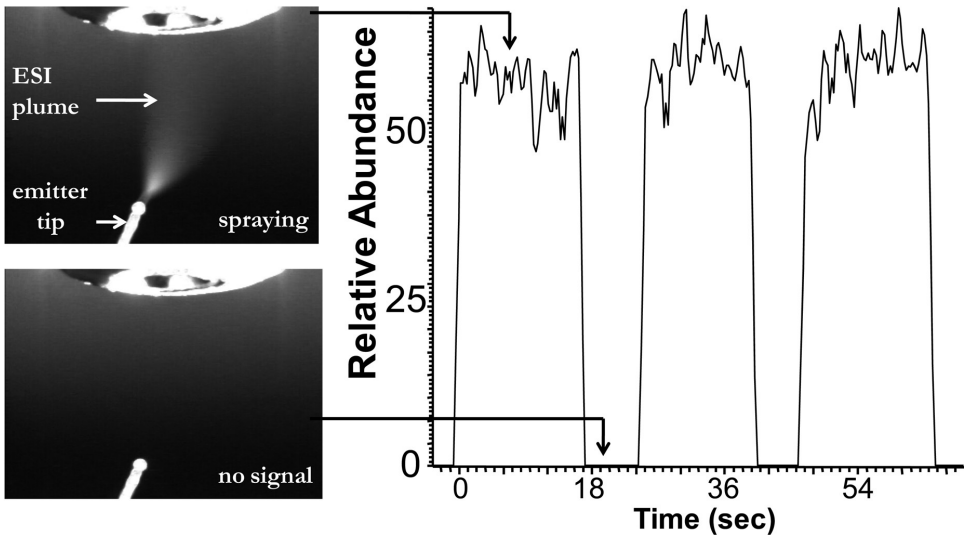

Figure 1-4: Example of droplet ESI-MS. When the aqueous droplet splays, signal intensity is observed, while when the carrier phase is sprayed no signal is observed. Figure adapted from Pei et. al, 2009.

1.5 Challenges in Droplet Microfluidics

The advances in droplet manipulation over the past decade have positioned droplet microfluidics to deeply alter the methods by which HTS is performed. Droplet microfluidics has the ability to emulate many of the key unit operations in traditional well plate screens, with advantages in sample size and throughput. Despite these advantages, droplets have not yet gained traction as a common method for HTS. Efforts to commercialize these systems have been limited to only a few niche applications.[113]

To effectively process and analyze samples discretely, it is critical that droplets reliably maintain their contents through the course of any incubation or manipulation without analyte partitioning. Early research with mineral oil as the continuous phase for droplet segmentation revealed that some analytes, particularly small molecules, demonstrated partitioning into hydrophobic oil.[114] Fluorinated oil and surfactants offered an alternative carrier phase to contain analytes,[115] but chemical leakage from droplet samples has also been observed in these systems. Several groups have investigated molecular retention and leakage in droplet emulsions using

fluorescent detection with fluorophores as model analytes.[38,116–118] Buffer pH, fluorophore solubility and hydrophobicity, and micellar transport have all been proposed as contributors to analyte loss both into the surrounding oil phase and into neighboring droplet samples. No definitive mechanism of molecular transport has been agreed upon.[119] Investigation into both the fundamental mechanism and prevention of crosstalk may expand droplet functionality to workflows inaccessible due to chemical leakage.[118]

Additionally, available tools for droplet analysis is a limiting factor to adoption of the technology. As has been previously discussed, droplets are by and large analyzed with fluorescent measurement. However, most applications where HTS would be useful do not have fluorescent products or reporters. Using information rich techniques such as MS will open the possibility for screening a diverse range of analytes that have been previously unavailable. The development of compatible tools for these analysis methods is also required to enable new screening methods. For example, droplets used for ESI-MS are typically larger, so existing droplet methods (generation, reagent addition, splitting, sorting) must be changed to fit the necessary droplet size. Using the developed tools for droplet processing and analysis, new high-throughput screens can be achieved.

1.6 Dissertation Overview

This dissertation aims to advance the development of droplet microfluidic tools which are useful in HTE. The scope of the work ranges from understanding fundamental droplet dynamics to screening a variety of systems. Droplet microfluidics is demonstrated as a powerful technique for testing small molecule physicochemical properties, reaction conditions in synthetic chemistry, and biocatalysts for use in synthetic biology.

We first investigate undesirable transport between droplet samples. In **Chapter 2**, a method was developed to quantify small molecule crosstalk in droplet microfluidic systems using MS. A

variety of small molecules were tested for crosstalk and modelled using physicochemical properties, which provided insight into the extent of transfer between droplets. A range of variables were tested, including fluorinated oil, surfactant, and flow parameters, representing a significant step towards understanding the effect.

In **Chapter 3**, droplet behavior in alternating electric fields investigated. With a combination of electrophoretic and hydrodynamic design, droplets were discovered to split and trap in high field regions. This novel behavior was used to develop microfluidic devices which can controllably split droplets in flow without the need for complex microfabrication. By using an electric field as the driving splitting force, on-demand droplet splitting is enabled. The effect is characterized with droplets ranging from 400 – 1000 pL in volume, with < 6% variability on droplet size.

Chapter 4 describes the development of high-volume addition for droplet microfluidics, which is necessary for applications such as ESI-MS. The first device is capable of diluting droplets 2 – 150-fold with < 1% carryover using a step-injection geometry, building upon previous direct-injection designs limited to 2-fold addition. An additional device, based on the droplet merger design, demonstrates carryover-free droplet dilution with 97% success rate, outperforming previously developed methods. The reagent addition tool is demonstrated in a proof of principle high throughput screen of photocatalyst substrates in collaboration with the Stephenson Lab at the University of Michigan.

The aim of **Chapter 5** was to build on previous work for performing liquid-liquid extractions in a droplet context. A microfluidic device was developed to generate 4 nL liquid-liquid exactions leveraging slug-flow nanoextraction. Library introduction into the droplet format was performed using an HPLC autosampler, which sampled from a MWP into the microfluidic

device. Flow was modulated to generate two- and three-liquid phase pairs. The resulting droplets flowed directly through a UV spectrophotometer. This fully automated system was applied to the screening of octanol-water partitioning coefficients, and a mini-screen of seven active pharmaceutical ingredients was achieved. The method agreed with established methods within acceptable guidelines and represented 10- and 40-fold reductions in time and volume respectively.

In **Chapter 6**, a workflow is presented for the growth, analysis, and sorting of cell samples using droplet ESI-MS for synthetic biology. A droplet MS method was developed to analyze lysine, the target product from the cells, over cell media background. *E. coli* were shown to effectively grow and produce lysine following single cell encapsulation in droplets. Finally, mass-activated droplet sorting was performed on droplets containing cells, enabling the selection of a cell variant with high lysine production. The droplet workflow was shown to be directly compatible with cell growth in liquid cultures, enabling downstream verification methods.

1.7 References

(1) Bahr, M. N.; Nandkeolyar, A.; Kenna, J. K.; Nevins, N.; Da Vià, L.; Işık, M.; Chodera, J. D.; Mobley, D. L. Automated High Throughput PKa and Distribution Coefficient Measurements of Pharmaceutical Compounds for the SAMPL8 Blind Prediction Challenge. *J Comput Aided Mol Des* **2021**, *35* (11), 1141–1155. https://doi.org/10.1007/s10822-021-00427-0.

(2) Dalvit, C.; Ardini, E.; Fogliatto, G. P.; Mongelli, N.; Veronesi, M. Reliable High-Throughput Functional Screening with 3-FABS. *Drug Discovery Today* **2004**, *9* (14), 595–602. https://doi.org/10.1016/S1359-6446(04)03161-7.

(3) Savile, C. K.; Janey, J. M.; Mundorff, E. C.; Moore, J. C.; Tam, S.; Jarvis, W. R.; Colbeck, J. C.; Krebber, A.; Fleitz, F. J.; Brands, J.; Devine, P. N.; Huisman, G. W.; Hughes, G. J. Biocatalytic Asymmetric Synthesis of Chiral Amines from Ketones Applied to Sitagliptin Manufacture. *Science* **2010**. https://doi.org/10.1126/science.1188934.

(4) Huffman, M. A.; Fryszkowska, A.; Alvizo, O.; Borra-Garske, M.; Campos, K. R.; Canada, K. A.; Devine, P. N.; Duan, D.; Forstater, J. H.; Grosser, S. T.; Halsey, H. M.; Hughes, G. J.; Jo, J.; Joyce, L. A.; Kolev, J. N.; Liang, J.; Maloney, K. M.; Mann, B. F.; Marshall, N. M.; McLaughlin, M.; Moore, J. C.; Murphy, G. S.; Nawrat, C. C.; Nazor, J.; Novick, S.; Patel, N. R.; Rodriguez-Granillo, A.; Robaire, S. A.; Sherer, E. C.; Truppo, M. D.; Whittaker, A. M.; Verma, D.; Xiao, L.; Xu, Y.; Yang, H. Design of an in Vitro

Biocatalytic Cascade for the Manufacture of Islatravir. *Science* **2019**, *366* (6470), 1255–1259. https://doi.org/10.1126/science.aay8484.
(5) Zetzsche, L. E.; Yazarians, J. A.; Chakrabarty, S.; Hinze, M. E.; Murray, L. A. M.; Lukowski, A. L.; Joyce, L. A.; Narayan, A. R. H. Biocatalytic Oxidative Cross-Coupling Reactions for Biaryl Bond Formation. *Nature* **2022**, *603* (7899), 79–85. https://doi.org/10.1038/s41586-021-04365-7.
(6) Bell, E. L.; Smithson, R.; Kilbride, S.; Foster, J.; Hardy, F. J.; Ramachandran, S.; Tedstone, A. A.; Haigh, S. J.; Garforth, A. A.; Day, P. J. R.; Levy, C.; Shaver, M. P.; Green, A. P. Directed Evolution of an Efficient and Thermostable PET Depolymerase. *Nat Catal* **2022**, *5* (8), 673–681. https://doi.org/10.1038/s41929-022-00821-3.
(7) Tracewell, C. A.; Arnold, F. H. Directed Enzyme Evolution: Climbing Fitness Peaks One Amino Acid at a Time. *Current Opinion in Chemical Biology* **2009**, *13* (1), 3–9. https://doi.org/10.1016/j.cbpa.2009.01.017.
(8) Mayr, L. M.; Bojanic, D. Novel Trends in High-Throughput Screening. *Current Opinion in Pharmacology* **2009**, *9* (5), 580–588. https://doi.org/10.1016/j.coph.2009.08.004.
(9) Tegally, H.; San, J. E.; Giandhari, J.; de Oliveira, T. Unlocking the Efficiency of Genomics Laboratories with Robotic Liquid-Handling. *BMC Genomics* **2020**, *21* (1), 729. https://doi.org/10.1186/s12864-020-07137-1.
(10) Spruill, S. E.; Lu, J.; Hardy, S.; Weir, B. Assessing Sources of Variability in Microarray Gene Expression Data. *BioTechniques* **2002**, *33* (4), 916–923. https://doi.org/10.2144/02334mt05.
(11) Dopp, J. L.; Jo, Y. R.; Reuel, N. F. Methods to Reduce Variability in E. Coli-Based Cell-Free Protein Expression Experiments. *Synthetic and Systems Biotechnology* **2019**, *4* (4), 204–211. https://doi.org/10.1016/j.synbio.2019.10.003.
(12) Welch, C. J.; Gong, X.; Schafer, W.; Pratt, E. C.; Brkovic, T.; Pirzada, Z.; Cuff, J. F.; Kosjek, B. MISER Chromatography (Multiple Injections in a Single Experimental Run): The Chromatogram Is the Graph. *Tetrahedron: Asymmetry* **2010**, *21* (13), 1674–1681. https://doi.org/10.1016/j.tetasy.2010.05.029.
(13) Zawatzky, K.; Biba, M.; Regalado, E. L.; Welch, C. J. MISER Chiral Supercritical Fluid Chromatography for High Throughput Analysis of Enantiopurity. *Journal of Chromatography A* **2016**, *1429*, 374–379. https://doi.org/10.1016/j.chroma.2015.12.057.
(14) Kaplitz, A. S.; Kresge, G. A.; Selover, B.; Horvat, L.; Franklin, E. G.; Godinho, J. M.; Grinias, K. M.; Foster, S. W.; Davis, J. J.; Grinias, J. P. High-Throughput and Ultrafast Liquid Chromatography. *Anal. Chem.* **2020**, *92* (1), 67–84. https://doi.org/10.1021/acs.analchem.9b04713.
(15) E. Kempa, E.; A. Hollywood, K.; A. Smith, C.; E. Barran, P. High Throughput Screening of Complex Biological Samples with Mass Spectrometry – from Bulk Measurements to Single Cell Analysis. *Analyst* **2019**, *144* (3), 872–891. https://doi.org/10.1039/C8AN01448E.
(16) Kertesz, V.; Van Berkel, G. J. Fully Automated Liquid Extraction-Based Surface Sampling and Ionization Using a Chip-Based Robotic Nanoelectrospray Platform. *Journal of Mass Spectrometry* **2010**, *45* (3), 252–260. https://doi.org/10.1002/jms.1709.
(17) Supercharge Your Lab's Productivity: Agilent RapidFire 365 High-Throughput Mass Spectrometry System, 2018. https://www.agilent.com/cs/library/brochures/5991-2422EN_SinglePages.pdf (accessed 2020-02-11).

(18) Leveridge, M.; Collier, L.; Edge, C.; Hardwicke, P.; Leavens, B.; Ratcliffe, S.; Rees, M.; Stasi, L. P.; Nadin, A.; Reith, A. D. A High-Throughput Screen to Identify LRRK2 Kinase Inhibitors for the Treatment of Parkinson's Disease Using RapidFire Mass Spectrometry. *J Biomol Screen* **2016**, *21* (2), 145–155. https://doi.org/10.1177/1087057115606707.
(19) Hutchinson, S. E.; Leveridge, M. V.; Heathcote, M. L.; Francis, P.; Williams, L.; Gee, M.; Munoz-Muriedas, J.; Leavens, B.; Shillings, A.; Jones, E.; Homes, P.; Baddeley, S.; Chung, C.; Bridges, A.; Argyrou, A. Enabling Lead Discovery for Histone Lysine Demethylases by High-Throughput RapidFire Mass Spectrometry. *J Biomol Screen* **2012**, *17* (1), 39–48. https://doi.org/10.1177/1087057111416660.
(20) Sinclair, I.; Stearns, R.; Pringle, S.; Wingfield, J.; Datwani, S.; Hall, E.; Ghislain, L.; Majlof, L.; Bachman, M. Novel Acoustic Loading of a Mass Spectrometer: Toward Next-Generation High-Throughput MS Screening. *J Lab Autom.* **2016**, *21* (1), 19–26. https://doi.org/10.1177/2211068215619124.
(21) Chen, H.; Talaty, N. N.; Takáts, Z.; Cooks, R. G. Desorption Electrospray Ionization Mass Spectrometry for High-Throughput Analysis of Pharmaceutical Samples in the Ambient Environment. *Anal. Chem.* **2005**, *77* (21), 6915–6927. https://doi.org/10.1021/ac050989d.
(22) P. Sobreira, T. J.; Avramova, L.; Szilagyi, B.; L. Logsdon, D.; P. Loren, B.; Jaman, Z.; T. Hilger, R.; S. Hosler, R.; R. Ferreira, C.; Koswara, A.; H. Thompson, D.; Graham Cooks, R.; K. Nagy, Z. High-Throughput Screening of Organic Reactions in Microdroplets Using Desorption Electrospray Ionization Mass Spectrometry (DESI-MS): Hardware and Software Implementation. *Analytical Methods* **2020**, *12* (28), 3654–3669. https://doi.org/10.1039/D0AY00072H.
(23) Chiu, D. T.; Lorenz, R. M.; Jeffries, G. D. M. Droplets for Ultrasmall-Volume Analysis. *Anal. Chem.* **2009**, *81* (13), 5111–5118. https://doi.org/10.1021/ac900306q.
(24) Baroud, C. N.; Gallaire, F.; Dangla, R. Dynamics of Microfluidic Droplets. *Lab Chip* **2010**, *10* (16), 2032–2045. https://doi.org/10.1039/C001191F.
(25) Thorsen, T.; Roberts, R. W.; Arnold, F. H.; Quake, S. R. Dynamic Pattern Formation in a Vesicle-Generating Microfluidic Device. *Phys. Rev. Lett.* **2001**, *86* (18), 4163–4166. https://doi.org/10.1103/PhysRevLett.86.4163.
(26) Shang, L.; Cheng, Y.; Zhao, Y. Emerging Droplet Microfluidics. *Chem. Rev.* **2017**, *117* (12), 7964–8040. https://doi.org/10.1021/acs.chemrev.6b00848.
(27) Major, J. Challenges and Opportunities in High Throughput Screening: Implications for New Technologies. *J Biomol Screen* **1998**, *3* (1), 13–17. https://doi.org/10.1177/108705719800300102.
(28) Zhong, J.; Riordon, J.; C. Wu, T.; Edwards, H.; R. Wheeler, A.; Pardee, K.; Aspuru-Guzik, A.; Sinton, D. When Robotics Met Fluidics. *Lab on a Chip* **2020**, *20* (4), 709–716. https://doi.org/10.1039/C9LC01042D.
(29) Link, D. R.; Anna, S. L.; Weitz, D. A.; Stone, H. A. Geometrically Mediated Breakup of Drops in Microfluidic Devices. *Phys. Rev. Lett.* **2004**, *92* (5), 054503. https://doi.org/10.1103/PhysRevLett.92.054503.
(30) Kim, H.; Luo, D.; Link, D.; Weitz, D. A.; Marquez, M.; Cheng, Z. Controlled Production of Emulsion Drops Using an Electric Field in a Flow-Focusing Microfluidic Device. *Appl. Phys. Lett.* **2007**, *91* (13), 133106. https://doi.org/10.1063/1.2790785.
(31) Zhu, P.; Wang, L. Passive and Active Droplet Generation with Microfluidics: A Review. *Lab on a Chip* **2017**, *17* (1), 34–75. https://doi.org/10.1039/C6LC01018K.

(32) Lorenz, R. M.; Edgar, J. S.; Jeffries, G. D. M.; Chiu, D. T. Microfluidic and Optical Systems for the On-Demand Generation and Manipulation of Single Femtoliter-Volume Aqueous Droplets. *Analytical Chemistry* **2006**, *78* (18), 6433–6439. https://doi.org/10.1021/ac060748l.
(33) Xu, Y.; Lee, J.-H.; Li, Z.; Wang, L.; Ordog, T.; C. Bailey, R. A Droplet Microfluidic Platform for Efficient Enzymatic Chromatin Digestion Enables Robust Determination of Nucleosome Positioning. *Lab on a Chip* **2018**, *18* (17), 2583–2592. https://doi.org/10.1039/C8LC00599K.
(34) Zhu, P.; Tang, X.; Wang, L. Droplet Generation in Co-Flow Microfluidic Channels with Vibration. *Microfluid Nanofluid* **2016**, *20* (3), 47. https://doi.org/10.1007/s10404-016-1717-2.
(35) Zhang, K.; Kang, D.-K.; Monsur Ali, M.; Liu, L.; Labanieh, L.; Lu, M.; Riazifar, H.; N. Nguyen, T.; A. Zell, J.; A. Digman, M.; Gratton, E.; Li, J.; Zhao, W. Digital Quantification of MiRNA Directly in Plasma Using Integrated Comprehensive Droplet Digital Detection. *Lab on a Chip* **2015**, *15* (21), 4217–4226. https://doi.org/10.1039/C5LC00650C.
(36) Ou, C.-Y.; Vu, T.; T. Grunwald, J.; Toledano, M.; Zimak, J.; Toosky, M.; Shen, B.; A. Zell, J.; Gratton, E.; J. Abram, T.; Zhao, W. An Ultrasensitive Test for Profiling Circulating Tumor DNA Using Integrated Comprehensive Droplet Digital Detection. *Lab on a Chip* **2019**, *19* (6), 993–1005. https://doi.org/10.1039/C8LC01399C.
(37) Baret, J.-C. Surfactants in Droplet-Based Microfluidics. *Lab on a Chip* **2012**, *12* (3), 422–433. https://doi.org/10.1039/C1LC20582J.
(38) Wagner, O.; Thiele, J.; Weinhart, M.; Mazutis, L.; Weitz, D. A.; Huck, W. T. S.; Haag, R. Biocompatible Fluorinated Polyglycerols for Droplet Microfluidics as an Alternative to PEG-Based Copolymer Surfactants. *Lab Chip* **2016**, *16* (1), 65–69. https://doi.org/10.1039/C5LC00823A.
(39) Chowdhury, M. S.; Zheng, W.; Kumari, S.; Heyman, J.; Zhang, X.; Dey, P.; Weitz, D. A.; Haag, R. Dendronized Fluorosurfactant for Highly Stable Water-in-Fluorinated Oil Emulsions with Minimal Inter-Droplet Transfer of Small Molecules. *Nature Communications* **2019**, *10* (1), 1–10. https://doi.org/10.1038/s41467-019-12462-5.
(40) Dressman, D.; Yan, H.; Traverso, G.; Kinzler, K. W.; Vogelstein, B. Transforming Single DNA Molecules into Fluorescent Magnetic Particles for Detection and Enumeration of Genetic Variations. *PNAS* **2003**, *100* (15), 8817–8822. https://doi.org/10.1073/pnas.1133470100.
(41) Kiss, M. M.; Ortoleva-Donnelly, L.; Beer, N. R.; Warner, J.; Bailey, C. G.; Colston, B. W.; Rothberg, J. M.; Link, D. R.; Leamon, J. H. High-Throughput Quantitative Polymerase Chain Reaction in Picoliter Droplets. *Anal. Chem.* **2008**, *80* (23), 8975–8981. https://doi.org/10.1021/ac801276c.
(42) Sciambi, A.; Abate, A. R. Adding Reagent to Droplets with Controlled Rupture of Encapsulated Double Emulsions. *Biomicrofluidics* **2013**, *7* (4), 044112. https://doi.org/10.1063/1.4817793.
(43) Li, L.; Boedicker, J. Q.; Ismagilov, R. F. Using a Multijunction Microfluidic Device To Inject Substrate into an Array of Preformed Plugs without Cross-Contamination: Comparing Theory and Experiments. *Anal. Chem.* **2007**, *79* (7), 2756–2761. https://doi.org/10.1021/ac062179n.

(44) Abate, A. R.; Hung, T.; Mary, P.; Agresti, J. J.; Weitz, D. A. High-Throughput Injection with Microfluidics Using Picoinjectors. *PNAS* **2010**. https://doi.org/10.1073/pnas.1006888107.
(45) Doonan, S. R.; Bailey, R. C. K-Channel: A Multifunctional Architecture for Dynamically Reconfigurable Sample Processing in Droplet Microfluidics. *Anal. Chem.* **2017**, *89* (7), 4091–4099. https://doi.org/10.1021/acs.analchem.6b05041.
(46) Mary, P.; Studer, V.; Tabeling, P. Microfluidic Droplet-Based Liquid−Liquid Extraction. *Anal. Chem.* **2008**, *80* (8), 2680–2687. https://doi.org/10.1021/ac800088s.
(47) Fallah-Araghi, A.; Baret, J.-C.; Ryckelynck, M.; Griffiths, A. D. A Completely in Vitro Ultrahigh-Throughput Droplet-Based Microfluidic Screening System for Protein Engineering and Directed Evolution. *Lab Chip* **2012**, *12* (5), 882. https://doi.org/10.1039/c2lc21035e.
(48) Shestopalov, I.; D. Tice, J.; F. Ismagilov, R. Multi-Step Synthesis of Nanoparticles Performed on Millisecond Time Scale in a Microfluidic Droplet-Based System. *Lab on a Chip* **2004**, *4* (4), 316–321. https://doi.org/10.1039/B403378G.
(49) Zec, H.; D. Rane, T.; Wang, T.-H. Microfluidic Platform for On-Demand Generation of Spatially Indexed Combinatorial Droplets. *Lab on a Chip* **2012**, *12* (17), 3055–3062. https://doi.org/10.1039/C2LC40399D.
(50) Lee, M.; W. Collins, J.; M. Aubrecht, D.; A. Sperling, R.; Solomon, L.; Ha, J.-W.; Yi, G.-R.; A. Weitz, D.; N. Manoharan, V. Synchronized Reinjection and Coalescence of Droplets in Microfluidics. *Lab on a Chip* **2014**, *14* (3), 509–513. https://doi.org/10.1039/C3LC51214B.
(51) Mazutis, L.; Baret, J.-C.; Treacy, P.; Skhiri, Y.; Fallah Araghi, A.; Ryckelynck, M.; Taly, V.; D. Griffiths, A. Multi-Step Microfluidic Droplet Processing: Kinetic Analysis of an in Vitro Translated Enzyme. *Lab on a Chip* **2009**, *9* (20), 2902–2908. https://doi.org/10.1039/B907753G.
(52) Holland-Moritz, D. A.; Wismer, M. K.; Mann, B. F.; Farasat, I.; Devine, P.; Guetschow, E. D.; Mangion, I.; Welch, C. J.; Moore, J. C.; Sun, S.; Kennedy, R. T. Mass Activated Droplet Sorting (MADS) Enables High-Throughput Screening of Enzymatic Reactions at Nanoliter Scale. *Angewandte Chemie International Edition* **2020**, *59* (11), 4470–4477. https://doi.org/10.1002/anie.201913203.
(53) Mazutis, L.; Baret, J.-C.; Treacy, P.; Skhiri, Y.; Fallah Araghi, A.; Ryckelynck, M.; Taly, V.; D. Griffiths, A. Multi-Step Microfluidic Droplet Processing: Kinetic Analysis of an in Vitro Translated Enzyme. *Lab on a Chip* **2009**, *9* (20), 2902–2908. https://doi.org/10.1039/B907753G.
(54) Cochrane, W. G.; Hackler, A. L.; Cavett, V. J.; Price, A. K.; Paegel, B. M. Integrated, Continuous Emulsion Creamer. *Anal. Chem.* **2017**, *89* (24), 13227–13234. https://doi.org/10.1021/acs.analchem.7b03070.
(55) Frenz, L.; Blank, K.; Brouzes, E.; D. Griffiths, A. Reliable Microfluidic On-Chip Incubation of Droplets in Delay-Lines. *Lab on a Chip* **2009**, *9* (10), 1344–1348. https://doi.org/10.1039/B816049J.
(56) Horvath, D. G.; Braza, S.; Moore, T.; Pan, C. W.; Zhu, L.; Pak, O. S.; Abbyad, P. Sorting by Interfacial Tension (SIFT): Label-Free Enzyme Sorting Using Droplet Microfluidics. *Analytica Chimica Acta* **2019**, *1089*, 108–114. https://doi.org/10.1016/j.aca.2019.08.025.

(57) Ruiter, R. de; Pit, A. M.; Oliveira, V. M. de; Duits, M. H. G.; Ende, D. van den; Mugele, F. Electrostatic Potential Wells for On-Demand Drop Manipulation in Microchannels. *Lab Chip* **2014**, *14* (5), 883–891. https://doi.org/10.1039/C3LC51121A.
(58) Ho Jung, J.; Destgeer, G.; Ha, B.; Park, J.; Jin Sung, H. On-Demand Droplet Splitting Using Surface Acoustic Waves. *Lab on a Chip* **2016**, *16* (17), 3235–3243. https://doi.org/10.1039/C6LC00648E.
(59) Yang, Y.-J.; Feng, X.; Xu, N.; Pang, D.-W.; Zhang, Z.-L. Generation of Sub-Femtoliter Droplet by T-Junction Splitting on Microfluidic Chips. *Appl. Phys. Lett.* **2013**, *102* (12), 123502. https://doi.org/10.1063/1.4798510.
(60) Verbruggen, B.; Tóth, T.; Atalay, Y. T.; Ceyssens, F.; Verboven, P.; Puers, R.; Nicolai, B.; Lammertyn, J. Design of a Flow-Controlled Asymmetric Droplet Splitter Using Computational Fluid Dynamics. *Microfluid Nanofluid* **2013**, *15* (2), 243–252. https://doi.org/10.1007/s10404-013-1139-3.
(61) Doonan, S.; Bailey, R.; C. Bailey, R. Droplet CAR-Wash: Continuous Picoliter-Scale Immunocapture and Washing. *Lab on a Chip* **2019**, *19* (9), 1589–1598. https://doi.org/10.1039/C9LC00125E.
(62) He, Y.; Pei, J.; Srinivasakannan, C.; Li, S.; Peng, J.; Guo, S.; Zhang, L.; Yin, S. Extraction of Samarium Using a Serpentine Y-Junction Microreactor with 2-Ethylhexyl Phosphonic Acid Mono-2-Ethylhexyl. *Hydrometallurgy* **2018**, *179*, 175–180. https://doi.org/10.1016/j.hydromet.2018.06.006.
(63) Xu, C.; Xie, T. Review of Microfluidic Liquid–Liquid Extractors. *Ind. Eng. Chem. Res.* **2017**, *56* (27), 7593–7622. https://doi.org/10.1021/acs.iecr.7b01712.
(64) Wang, X.; Sun, M.; Ferguson, S. A.; Hoff, J. D.; Qin, Y.; Bailey, R. C.; Meyerhoff, M. E. Ionophore-Based Biphasic Chemical Sensing in Droplet Microfluidics. *Angewandte Chemie International Edition* **2019**, *58* (24), 8092–8096. https://doi.org/10.1002/anie.201902960.
(65) Wells, S. S.; Kennedy, R. T. High-Throughput Liquid–Liquid Extractions with Nanoliter Volumes. *Anal. Chem.* **2020**, acs.analchem.9b04915. https://doi.org/10.1021/acs.analchem.9b04915.
(66) Serra, M.; Ferraro, D.; Pereiro, I.; Viovy, J.-L.; Descroix, S. The Power of Solid Supports in Multiphase and Droplet-Based Microfluidics: Towards Clinical Applications. *Lab on a Chip* **2017**, *17* (23), 3979–3999. https://doi.org/10.1039/C7LC00582B.
(67) Lee, H.; Xu, L.; Oh, K. W. Droplet-Based Microfluidic Washing Module for Magnetic Particle-Based Assays. *Biomicrofluidics* **2014**, *8* (4), 044113. https://doi.org/10.1063/1.4892495.
(68) Zhu, Y.; Fang, Q. Analytical Detection Techniques for Droplet Microfluidics—A Review. *Analytica Chimica Acta* **2013**, *787*, 24–35. https://doi.org/10.1016/j.aca.2013.04.064.
(69) Gu, S.-Q.; Zhang, Y.-X.; Zhu, Y.; Du, W.-B.; Yao, B.; Fang, Q. Multifunctional Picoliter Droplet Manipulation Platform and Its Application in Single Cell Analysis. *Anal. Chem.* **2011**, *83* (19), 7570–7576. https://doi.org/10.1021/ac201678g.
(70) Ahn, K.; Kerbage, C.; Hunt, T. P.; Westervelt, R. M.; Link, D. R.; Weitz, D. A. Dielectrophoretic Manipulation of Drops for High-Speed Microfluidic Sorting Devices. *Appl. Phys. Lett.* **2006**, *88* (2), 024104. https://doi.org/10.1063/1.2164911.
(71) Caen, O.; Schütz, S.; Jammalamadaka, M. S. S.; Vrignon, J.; Nizard, P.; Schneider, T. M.; Baret, J.-C.; Taly, V. High-Throughput Multiplexed Fluorescence-Activated Droplet

Sorting. *Microsyst Nanoeng* **2018**, *4* (1), 1–10. https://doi.org/10.1038/s41378-018-0033-2.
(72) Sciambi, A.; Abate, A. R. Accurate Microfluidic Sorting of Droplets at 30 KHz. *Lab on a Chip* **2015**, *15* (1), 47–51. https://doi.org/10.1039/C4LC01194E.
(73) Gijs, M. A. M. Magnetic Bead Handling On-Chip: New Opportunities for Analytical Applications. *Microfluid Nanofluid* **2004**, *1* (1), 22–40. https://doi.org/10.1007/s10404-004-0010-y.
(74) Zhang, K.; Liang, Q.; Ma, S.; Mu, X.; Hu, P.; Wang, Y.; Luo, G. On-Chip Manipulation of Continuous Picoliter-Volume Superparamagnetic Droplets Using a Magnetic Force. *Lab on a Chip* **2009**, *9* (20), 2992–2999. https://doi.org/10.1039/B906229G.
(75) Franke, T.; R. Abate, A.; A. Weitz, D.; Wixforth, A. Surface Acoustic Wave (SAW) Directed Droplet Flow in Microfluidics for PDMS Devices. *Lab on a Chip* **2009**, *9* (18), 2625–2627. https://doi.org/10.1039/B906819H.
(76) Zielke, C.; Pan, C. W.; Gutierrez Ramirez, A. J.; Feit, C.; Dobson, C.; Davidson, C.; Sandel, B.; Abbyad, P. Microfluidic Platform for the Isolation of Cancer-Cell Subpopulations Based on Single-Cell Glycolysis. *Anal. Chem.* **2020**. https://doi.org/10.1021/acs.analchem.9b05738.
(77) Schmid, L.; A. Weitz, D.; Franke, T. Sorting Drops and Cells with Acoustics: Acoustic Microfluidic Fluorescence-Activated Cell Sorter. *Lab on a Chip* **2014**, *14* (19), 3710–3718. https://doi.org/10.1039/C4LC00588K.
(78) Baret, J.-C.; Miller, O. J.; Taly, V.; Ryckelynck, M.; El-Harrak, A.; Frenz, L.; Rick, C.; Samuels, M. L.; Hutchison, J. B.; Agresti, J. J.; Link, D. R.; Weitz, D. A.; Griffiths, A. D. Fluorescence-Activated Droplet Sorting (FADS): Efficient Microfluidic Cell Sorting Based on Enzymatic Activity. *Lab Chip* **2009**, *9* (13), 1850. https://doi.org/10.1039/b902504a.
(79) Gielen, F.; Hours, R.; Emond, S.; Fischlechner, M.; Schell, U.; Hollfelder, F. Ultrahigh-Throughput–Directed Enzyme Evolution by Absorbance-Activated Droplet Sorting (AADS). *Proc Natl Acad Sci USA* **2016**, *113* (47), E7383–E7389. https://doi.org/10.1073/pnas.1606927113.
(80) Agresti, J. J.; Antipov, E.; Abate, A. R.; Ahn, K.; Rowat, A. C.; Baret, J.-C.; Marquez, M.; Klibanov, A. M.; Griffiths, A. D.; Weitz, D. A. Ultrahigh-Throughput Screening in Drop-Based Microfluidics for Directed Evolution. *PNAS* **2010**, *107* (9), 4004–4009. https://doi.org/10.1073/pnas.0910781107.
(81) Faraghat, S. A.; Hoettges, K. F.; Steinbach, M. K.; Veen, D. R. van der; Brackenbury, W. J.; Henslee, E. A.; Labeed, F. H.; Hughes, M. P. High-Throughput, Low-Loss, Low-Cost, and Label-Free Cell Separation Using Electrophysiology-Activated Cell Enrichment. *PNAS* **2017**, *114* (18), 4591–4596. https://doi.org/10.1073/pnas.1700773114.
(82) M. Nightingale, A.; Hassan, S.; H. Evans, G. W.; M. Coleman, S.; Niu, X. Nitrate Measurement in Droplet Flow: Gas-Mediated Crosstalk and Correction. *Lab on a Chip* **2018**, *18* (13), 1903–1913. https://doi.org/10.1039/C8LC00092A.
(83) Debon, A.; Pott, M.; Obexer, R.; Green, A. P.; Friedrich, L.; Griffiths, A. D.; Hilvert, D. Ultrahigh-Throughput Screening Enables Efficient Single-Round Oxidase Remodelling. *Nat Catal* **2019**, *2* (9), 740–747. https://doi.org/10.1038/s41929-019-0340-5.
(84) Duncombe, T. A.; Dittrich, P. S. Droplet Barcoding: Tracking Mobile Micro-Reactors for High-Throughput Biology. *Current Opinion in Biotechnology* **2019**, *60*, 205–212. https://doi.org/10.1016/j.copbio.2019.05.004.

(85) M. Maceiczyk, R.; Hess, D.; Y. Chiu, F. W.; Stavrakis, S.; J. deMello, A. Differential Detection Photothermal Spectroscopy: Towards Ultra-Fast and Sensitive Label-Free Detection in Picoliter & Femtoliter Droplets. *Lab on a Chip* **2017**, *17* (21), 3654–3663. https://doi.org/10.1039/C7LC00946A.
(86) Gao, Z.; Peng, H.; Zhu, M.; Wu, L.; Jia, C.; Zhou, H.; Zhao, J. A Facile Strategy for Visualizing and Modulating Droplet-Based Microfluidics. *Micromachines* **2019**, *10* (5), 291. https://doi.org/10.3390/mi10050291.
(87) Nguyen, N.-T.; Lassemono, S.; Chollet, F. A. Optical Detection for Droplet Size Control in Microfluidic Droplet-Based Analysis Systems. *Sensors and Actuators B: Chemical* **2006**, *117* (2), 431–436. https://doi.org/10.1016/j.snb.2005.12.010.
(88) Wang, X.; Ren, L.; Su, Y.; Ji, Y.; Liu, Y.; Li, C.; Li, X.; Zhang, Y.; Wang, W.; Hu, Q.; Han, D.; Xu, J.; Ma, B. Raman-Activated Droplet Sorting (RADS) for Label-Free High-Throughput Screening of Microalgal Single-Cells. *Anal. Chem.* **2017**, *89* (22), 12569–12577. https://doi.org/10.1021/acs.analchem.7b03884.
(89) Jeon, J.; Choi, N.; Chen, H.; Moon, J.-I.; Chen, L.; Choo, J. SERS-Based Droplet Microfluidics for High-Throughput Gradient Analysis. *Lab Chip* **2019**, *19* (4), 674–681. https://doi.org/10.1039/C8LC01180J.
(90) Cecchini, M. P.; Hong, J.; Lim, C.; Choo, J.; Albrecht, T.; deMello, A. J.; Edel, J. B. Ultrafast Surface Enhanced Resonance Raman Scattering Detection in Droplet-Based Microfluidic Systems. *Anal. Chem.* **2011**, *83* (8), 3076–3081. https://doi.org/10.1021/ac103329b.
(91) Chan, K. L. A.; Niu, X.; deMello, A. J.; Kazarian, S. G. Generation of Chemical Movies: FT-IR Spectroscopic Imaging of Segmented Flows. *Anal. Chem.* **2011**, *83* (9), 3606–3609. https://doi.org/10.1021/ac200497a.
(92) Chan, K. L. A.; Kazarian, S. G. FT-IR Spectroscopic Imaging of Reactions in Multiphase Flow in Microfluidic Channels. *Anal. Chem.* **2012**, *84* (9), 4052–4056. https://doi.org/10.1021/ac300019m.
(93) Lin, Y.; Schiavo, S.; Orjala, J.; Vouros, P.; Kautz, R. Microscale LC-MS-NMR Platform Applied to the Identification of Active Cyanobacterial Metabolites. *Anal. Chem.* **2008**, *80* (21), 8045–8054. https://doi.org/10.1021/ac801049k.
(94) Kautz, R. A.; Goetzinger, W. K.; Karger, B. L. High-Throughput Microcoil NMR of Compound Libraries Using Zero-Dispersion Segmented Flow Analysis. *J. Comb. Chem.* **2005**, *7* (1), 14–20. https://doi.org/10.1021/cc0498940.
(95) Schroeder, F. C.; Gronquist, M. Extending the Scope of NMR Spectroscopy with Microcoil Probes. *Angewandte Chemie International Edition* **2006**, *45* (43), 7122–7131. https://doi.org/10.1002/anie.200601789.
(96) Šedo, O.; Sedláček, I.; Zdráhal, Z. Sample Preparation Methods for MALDI-MS Profiling of Bacteria. *Mass Spectrometry Reviews* **2011**, *30* (3), 417–434. https://doi.org/10.1002/mas.20287.
(97) Niehaus, M.; Soltwisch, J. New Insights into Mechanisms of Material Ejection in MALDI Mass Spectrometry for a Wide Range of Spot Sizes. *Sci Rep* **2018**, *8* (1), 7755. https://doi.org/10.1038/s41598-018-25946-z.
(98) Konermann, L.; Ahadi, E.; Rodriguez, A. D.; Vahidi, S. Unraveling the Mechanism of Electrospray Ionization. *Anal. Chem.* **2013**, *85* (1), 2–9. https://doi.org/10.1021/ac302789c.

(99) Daub, C. D.; Cann, N. M. How Are Completely Desolvated Ions Produced in Electrospray Ionization: Insights from Molecular Dynamics Simulations. *Anal. Chem.* **2011**, *83* (22), 8372–8376. https://doi.org/10.1021/ac202103p.
(100) Kebarle, P.; Verkerk, U. H. Electrospray: From Ions in Solution to Ions in the Gas Phase, What We Know Now. *Mass Spectrometry Reviews* **2009**, *28* (6), 898–917. https://doi.org/10.1002/mas.20247.
(101) Küster, S. K.; Fagerer, S. R.; Verboket, P. E.; Eyer, K.; Jefimovs, K.; Zenobi, R.; Dittrich, P. S. Interfacing Droplet Microfluidics with Matrix-Assisted Laser Desorption/Ionization Mass Spectrometry: Label-Free Content Analysis of Single Droplets. *Anal. Chem.* **2013**, *85* (3), 1285–1289. https://doi.org/10.1021/ac3033189.
(102) Küster, S. K.; Pabst, M.; Jefimovs, K.; Zenobi, R.; Dittrich, P. S. High-Resolution Droplet-Based Fractionation of Nano-LC Separations onto Microarrays for MALDI-MS Analysis. *Anal. Chem.* **2014**, *86* (10), 4848–4855. https://doi.org/10.1021/ac4041982.
(103) Cole, R. H.; Tang, S.-Y.; Siltanen, C. A.; Shahi, P.; Zhang, J. Q.; Poust, S.; Gartner, Z. J.; Abate, A. R. Printed Droplet Microfluidics for on Demand Dispensing of Picoliter Droplets and Cells. *PNAS* **2017**, *114* (33), 8728–8733. https://doi.org/10.1073/pnas.1704020114.
(104) Haidas, D.; Bachler, S.; Köhler, M.; Blank, L. M.; Zenobi, R.; Dittrich, P. S. Microfluidic Platform for Multimodal Analysis of Enzyme Secretion in Nanoliter Droplet Arrays. *Anal. Chem.* **2019**, *91* (3), 2066–2073. https://doi.org/10.1021/acs.analchem.8b04506.
(105) Xu, L.; Chang, K.-C.; Payne, E. M.; Modavi, C.; Liu, L.; Palmer, C. M.; Tao, N.; Alper, H. S.; Kennedy, R. T.; Cornett, D. S.; Abate, A. R. Mapping Enzyme Catalysis with Metabolic Biosensing. *Nat Commun* **2021**, *12* (1), 6803. https://doi.org/10.1038/s41467-021-27185-9.
(106) Bell, S. E.; Park, I.; Rubakhin, S. S.; Bashir, R.; Vlasov, Y.; Sweedler, J. V. Droplet Microfluidics with MALDI-MS Detection: The Effects of Oil Phases in GABA Analysis. *ACS Meas. Au* **2021**, *1* (3), 147–156. https://doi.org/10.1021/acsmeasuresciau.1c00017.
(107) Pei, J.; Li, Q.; Lee, M. S.; Valaskovic, G. A.; Kennedy, R. T. Analysis of Samples Stored as Individual Plugs in a Capillary by Electrospray Ionization Mass Spectrometry. *Anal. Chem.* **2009**, *81* (15), 6558–6561. https://doi.org/10.1021/ac901172a.
(108) Steyer, D. J.; Kennedy, R. T. High-Throughput Nanoelectrospray Ionization-Mass Spectrometry Analysis of Microfluidic Droplet Samples. *Anal. Chem.* **2019**, *91* (10), 6645–6651. https://doi.org/10.1021/acs.analchem.9b00571.
(109) Kempa, E.; Smith, C.; Li, X.; Bellina, B.; Richardson, K.; Pringle, S.; Barran, P. Coupling Droplet Microfluidics with Mass Spectrometry for Ultrahigh-Throughput Analysis up to and Above 30Hz. **2020**. https://doi.org/10.26434/chemrxiv.11836731.v1.
(110) Sun, S.; Slaney, T. R.; Kennedy, R. T. Label Free Screening of Enzyme Inhibitors at Femtomole Scale Using Segmented Flow Electrospray Ionization Mass Spectrometry. *Anal. Chem.* **2012**, *84* (13), 5794–5800. https://doi.org/10.1021/ac3011389.
(111) Li, Q.; Pei, J.; Song, P.; Kennedy, R. T. Fraction Collection from Capillary Liquid Chromatography and Off-Line Electrospray Ionization Mass Spectrometry Using Oil Segmented Flow. *Anal. Chem.* **2010**, *82* (12), 5260–5267. https://doi.org/10.1021/ac100669z.
(112) Diefenbach, X. W.; Farasat, I.; Guetschow, E. D.; Welch, C. J.; Kennedy, R. T.; Sun, S.; Moore, J. C. Enabling Biocatalysis by High-Throughput Protein Engineering Using

Droplet Microfluidics Coupled to Mass Spectrometry. *ACS Omega* **2018**, *3* (2), 1498–1508. https://doi.org/10.1021/acsomega.7b01973.
(113) Holtze, C.; Weisse, S. A.; Vranceanu, M. Commercial Value and Challenges of Drop-Based Microfluidic Screening Platforms–An Opinion. *Micromachines* **2017**, *8* (6), 193. https://doi.org/10.3390/mi8060193.
(114) Courtois, F.; Olguin, L. F.; Whyte, G.; Theberge, A. B.; Huck, W. T. S.; Hollfelder, F.; Abell, C. Controlling the Retention of Small Molecules in Emulsion Microdroplets for Use in Cell-Based Assays. *Anal. Chem.* **2009**, *81* (8), 3008–3016. https://doi.org/10.1021/ac802658n.
(115) Roach, L. S.; Song, H.; Ismagilov, R. F. Controlling Nonspecific Protein Adsorption in a Plug-Based Microfluidic System by Controlling Interfacial Chemistry Using Fluorous-Phase Surfactants. *Anal. Chem.* **2005**, *77* (3), 785–796. https://doi.org/10.1021/ac049061w.
(116) Janiesch, J.-W.; Weiss, M.; Kannenberg, G.; Hannabuss, J.; Surrey, T.; Platzman, I.; Spatz, J. P. Key Factors for Stable Retention of Fluorophores and Labeled Biomolecules in Droplet-Based Microfluidics. *Analytical Chemistry* **2015**, *87* (4), 2063–2067. https://doi.org/10.1021/ac504736e.
(117) Gruner, P.; Riechers, B.; Semin, B.; Lim, J.; Johnston, A.; Short, K.; Baret, J.-C. Controlling Molecular Transport in Minimal Emulsions. *Nature Communications* **2016**, *7*, 10392. https://doi.org/10.1038/ncomms10392.
(118) Etienne, G.; Vian, A.; Biočanin, M.; Deplancke, B.; Amstad, E. Cross-Talk between Emulsion Drops: How Are Hydrophilic Reagents Transported across Oil Phases? *Lab on a Chip* **2018**, *18* (24), 3903–3912. https://doi.org/10.1039/C8LC01000E.
(119) Chen, Y.; Wijaya Gani, A.; Tang, S. K. Y. Characterization of Sensitivity and Specificity in Leaky Droplet-Based Assays. *Lab on a Chip* **2012**, *12* (23), 5093. https://doi.org/10.1039/c2lc40624a.

Chapter 2 Evaluation of Analyte Transfer Between Droplets by Mass Spectrometry

This was performed in collaboration with Maryam Taraji (MT) at the Australian Wine Research Institute and Bridget E. Murray (BEM) at University of Michigan. MT performed physiochemical calculations and principle component analysis resulting in Figure 2-2. BEM performed the multi-well plate droplet generation and analysis resulting in Figure 2-8.

2.1 Introduction

Droplet microfluidics has emerged as a promising tool for high-throughput experimentation (HTE) and screening. Droplets and segmented flow have been used successfully for screening enzyme variants,[1–3] rare genetic material,[4–6] and reaction conditions[7,8] with higher reagent and time efficiency compared to traditional screening methods. Similarly, droplets have been applied to achieve high temporal analysis, e.g. understanding reaction kinetics[9–12] and in vivo sensing (e.g., neurotransmitters from microdialysis sampling).[13–16] Regardless of application, it is critical that droplets remain chemically distinct to achieve reliable results; however, chemical transport or crosstalk between droplets has been observed under some conditions.[17,18] Small molecule crosstalk has been identified as limiting the technology from broader use in HTE.[19] In this report, we investigate crosstalk to better understand conditions that result in molecular transport between droplets and identify variables that control the effect.

Microfluidic droplets are made by segmenting an aqueous flow with an immiscible carrier phase to create individual sample chambers for processing and analysis.[20,21] Often, a surfactant is dissolved in the carrier phase to facilitate stabilization of droplets in flow.[22] Many early reports of

droplets for HTE used hydrocarbons as carrier fluid (e.g., mineral oil, silicone oil, decane);[21,23–25] however, chemical diffusion between droplets was observed.[17,26–28] Analytes were observed to partition directly through the oil due to moderate solubility[17,29,30] as well as be transported by reverse micelles.[27,31,32] The addition of bovine serum albumin (BSA)[27] and complex sugars (e.g. dextran)[28] successfully mitigated chemical transport of fluorophores in these water-in-hydrocarbon emulsions.

Fluorocarbon oils have become preferred for segmentation due to both low solubility of analytes in fluorous phases and superior stability of droplets.[33,34] Despite these advances, small molecule transfer has still been observed between neighboring droplets. Direct partitioning has been largely discounted as a mechanism due to the low solubility of small molecules in fluorocarbons,[35] but some have hypothesized a small amount of crosstalk can still occur through semi-fluorinated oils.[36] Recent investigations of fluorosurfactant stabilized systems have supported the view that reverse micelles are a mechanism for droplet to droplet transport.[18,37] These findings have led to the development of new surfactants that are reported to reduce crosstalk.[36,38,39] Previous solutions to droplet crosstalk in mineral oil-based systems, such as BSA, have not been successful in mitigating crosstalk with fluorocarbon carrier fluids.[18]

Investigations into droplet crosstalk have relied on spectroscopic analysis based on fluorescent,[18,26–28,37,40] colorimetric,[41] or secondary reporters[38,41] to determine the extent of transfer. Additionally, these reports focus on one analyte or compound class (e.g., substituted Alexa Fluor or ATTO dyes)[40] which provides a narrow scope for understanding crosstalk. Consequently, a general understanding of the extent and mechanism of fluorocarbon-based droplet crosstalk remains lacking.[42] An approach for measuring crosstalk for a broad range of conditions

and analytes is needed to expand the understanding of mechanisms and direct future development of droplet microfluidics.

In this report, we investigate droplet crosstalk using electrospray mass spectrometry (ESI-MS). ESI-MS is a flexible tool for label-free analysis, as many chemicals are ionizable. Droplet microfluidics has been successfully coupled with ESI-MS previously.[43–45] In this method, each droplet flows through the ESI emitter allowing for discrete droplet analysis by MS.[46] For this study, empty and analyte-containing droplets are alternately generated by a microfluidic device and analyzed using ESI-MS. Crosstalk is measurable by the amount of analyte loss from the analyte droplets and gain to the "blank" or empty droplets. This approach allows for evaluation of the effect of variables such as analyte structure, carrier phase, and surfactant. We quantify and model the carryover for a variety of small molecules which span many compound classes that are relevant for droplet microfluidics and HTE. We then investigate a number of parameters to study crosstalk between droplets in flow, such as the type of fluorinated oil, surfactant structure, surfactant concentration, and flow duration. Relevant results obtained from these online droplet generation experiments are also tested for droplets generated and incubated for prolonged periods, which mimics many screening workflows.[19,47]

2.2 Materials and Methods

Reagents and Materials. All small molecule standards and fluorinated oils were purchased from Sigma Aldrich (St. Louis, MO) unless otherwise stated. Hydrofluoroether 7500 (HFE 7500, Novec 7500) was purchased from Oakwood Chemicals (Estill, SC). The surfactants used were commercially available as 2% w/v in HFE 7500: FluoSurf from Dolomite Microfluidics (Norwell, MA), PicoSurf from Sphere Fluidics (Cambridge, UK), and dSurf from Fluigent (Suffolk, MA). 008-Fluorosurfactant from RAN Biotechnologies (Beverly, MA) was purchased

neat and dissolved in the respective oil. The carboxylate-Krytox surfactant was synthesized (See SI). Polydimethylsiloxane (PDMS) was purchased from Curbell Plastics (Livonia, MI).

Device Design and Fabrication. Microfluidic geometry was designed using AutoCAD from Autodesk Inc (San Rafael, CA). Corresponding transparencies were printed by Fineline Imaging (Colorado Springs, CO). Master molds were generated with 200 μm feature height using standard photolithography procedures; SU8 2050 negative epoxy photoresist was spun onto silicon wafers from University Wafer (South Boston, MA), patterned with ultraviolet irradiation through the transparent mask, and developed to leave polymerized features. PDMS was prepared 1:10 activator to monomer ratio, degassed, and poured over the SU8 master. Fluidic ports were produced in the PDMS stamps. PDMS stamps fabricated with fluidic channels were bound to standard glass slides using oxygen plasma activation generated by a Harrick Plasma Inc. PDC-32G (Ithaca, NY). Microfluidic devices were flushed with 2% tridecafluoro-1,1,2,2-tetrahydrooctyl tricholorosilane in perfluorodecalin for surface treatment.

Device Operation. A microfluidic chip was used to generate droplets of alternating content to study crosstalk between the adjacent droplets (Figure 2-1A). Liquid flow was generated using Hamilton (Reno, NV) gastight syringes with Chemyx Inc. Fusion 400 syringe pumps. Syringes were connected to microbore polytetrafluoroethylene (PTFE) tubing from Cole Parmer (Vernon Hills, IL) which was inserted into the microfluidic device ports. The microfluidic device was coupled to the electrospray ionization source with 150 μm x 300 μm perfluoroalkoxy alkane (PFA) tubing from IDEX (Lake Forest, IL).

The microfluidic device generated alternating droplets with 0.3 μL/min on the aqueous flows and 1 μL/min on the oil flow (Figure 2-1). For generating a stream of droplets from just one source, one aqueous stream was pumped at 0.6 μL/min with the other stream stopped. Analyte-

containing droplets contained 200 μM of the respective test analyte, and 20 μM choline in 10 mM ammonium formate buffered at pH 8.5. Blank droplets contained 20 μM acetylcholine in 10 mM ammonium formate. Unless otherwise stated, droplets flowed through 50.8 cm (20") of PFA capillary to the mass spectrometer, which corresponds to ~5.5 min of flow time. Device operation was observed with a Nikon (Tokyo, Japan) TS2 inverted microscope equipped with a Cognex (Natick, MA) In-Sight 7600 tracking camera.

Prolonged storage experiments. Droplet populations were generated using standard flow focusing microfluidic devices and stored in glass vials. Droplets were mixed by adding oil above the droplets while draining oil below to distribute droplet populations evenly. After incubation, droplets were reinjected into an oil respacing microfluidic device and transferred to PFA tubing. Flow rates were consistent as chopper experiments.

Multiwell Plate Droplet Generation. Oil-segmented droplets (15-20 nL) were created from a 384-well plate (Corning, Kennebunk, ME). 25 μL of 10 mM pH 8.5 ammonium formate buffer was pipetted into one well and 25 μL of either 200 μM caffeine or 200 μM acetylpyridine in 10 mM pH 8.5 ammonium formate buffer was pipetted into a second well. The samples were covered with 100 μL of perflourodecalin or HFE 7500. Epoxy was placed around the two wells to hold the oil. A 25 μL gas tight Hamilton syringe (Reno, NV) was attached to 150 μm i.d. x 360 μm o.d. perfluoroalkoxy alkane tubing from IDEX (Lake Forest, IL) with a low dead volume union from Valco Instruments Co., Inc. (Houston, TX). The syringe and tubing were filled with oil prior to droplet generation. The syringe was withdrawn at 1.2 μL/min using a Fusion 400 syringe pump (Chemyx Inc., Stafford, TX). The tubing was moved within and between wells using a computer numerical control machine (CNC, Cameron Micro Drill Press, Sonora, CA). G-code was used to program the CNC machine so that the tubing was held in the aqueous layer for 1.5 s and the oil

layer for 1 s while the syringe was withdrawing. Five replicate droplets were created from each well, and a total of 300 droplets were made per generation cycle.

Carboxylate Surfactant Synthesis. To prepare the ionic Krytox surfactant, 157FS(H) Krytox from DuPont (Wilmington, DE) was dissolved in methanol in a round bottom flask. Sodium hydroxide was added dropwise to precipitate carboxylate salt. After overnight stirring, precipitate was filtered, rinsed with methanol, and centrifuged to separate from methanol. Surfactant was placed under vacuum overnight, then dissolved at 2 wt.% in HFE 7500.

Mass Spectrometry. The mass spectrometer was an Agilent 6135b single quadrupole fitted with a capillary electrophoresis sheath flow electrospray source (G1607B). Electrospray was achieved with 2.5 kV, with 350 °C drying gas set at 30 L/min, a source pressure of 10 PSI, and 135 eV of fragmentor energy. The sheath liquid was water pumped at 30 μL/min. The mass spectrometer was operated in selected ion mode, monitoring for the nominal protonated mass for each of the test analytes and the nominal molecular weight of the marker compounds which each carry a permanent positive charge. Dwell time on the instrument was set at 1 ms per mass.

Computation and Principal Component Analysis. Physicochemical properties were calculated based on analyte structures and aqueous pH (8.5) using MarvinSketch version 18.24 and JChem for Excel version 20.20.0.732 from ChemAxon (Budapest, Hungary). Tanimoto similarity values were calculated using the same software. Multivariate principal component analysis (PCA) was performed using normalized descriptor parameters based on variable loadings using Unscrambler version 11.0.

2.3 Results and Discussion

Crosstalk Measurement and Repeatability. To study crosstalk, a train of 10 nL droplets that alternated between containing analyte and just buffer (“blank”) was generated from a

microfluidic "chopper" (Figure 2-1A).[48] The droplet array was pumped into an ESI-MS source to measure the analyte signal in the analyte containing and blank droplets. The ESI source generated spray directly from the PFA tubing, so droplets did not interact with any stainless steel or fused-silica surfaces which could contribute to carryover via adhesion or interaction during spray.[49] Therefore, analyte signal in the blanks is attributed to crosstalk during transport to the detector. By doubling one aqueous flow rate and stopping the other within the chopper, a homogeneous train of analyte or blank droplets could be generated. As such, populations of analyte and blank droplets can be analyzed without interaction as controls. Analyte and blank droplet solutions were spiked with choline and acetylcholine, respectively, which preliminary studies showed did not exhibit crosstalk, to enable tracking of each droplet type.

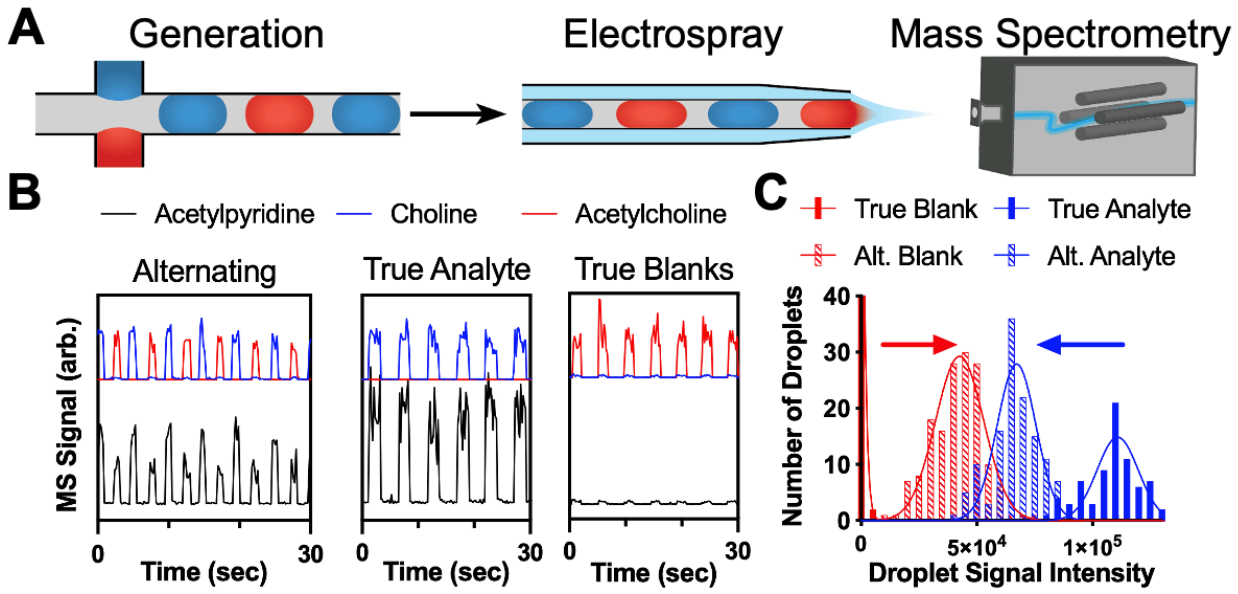

Figure 2-1: Overview of microfluidic mass spectrometry method for evaluating crosstalk. (A) Droplets are generated using a microfluidic chopper, which alternately generates blank (red) and analyte containing (blue) droplets. The droplets flow through an electrospray emitter and are individually ionized and analyzed. (B) Example droplet traces from acetylpyridine crosstalk measurement. Droplets are alternated to evaluate the acetylpyridine signal intensity in blank droplets, marked with acetylcholine. Unmixed droplet trains are analyzed to evaluate the minimum and maximum signal without transfer. (C) Histogram of all droplets analyzed in the experiment. The pre-mixed samples (solid bars) shift intensities during mixing (dashed bars) indicating signal loss from analyte containing droplets and signal gain in blank droplets (demonstrated with blue and red arrows, respectively).

To demonstrate the method for quantitative crosstalk determination, acetylpyridine was used as a model test analyte. It was previously observed that acetylpyridine was transported between droplets,[44] so it served as a good model compound with relatively high carryover. This test used 2 wt.% 008-fluorosurfactant (008-FS) in HFE 7500, which is commonly used for droplets for cell or small molecule screening.[47,50,51] Droplets (with and without alternation) were generated to the MS as above (Figure 2-1B). Four populations of droplets were generated corresponding to analyte-containing and blank droplets with and without interaction. A histogram acetylpyridine signal for these droplets shows the signal increase in blanks which interacted with analyte droplets, corresponding to crosstalk (Figure 2-1C). A dimensionless crosstalk coefficient can be calculated from mean droplet ESI signals:

Equation 2-1

$$Crosstalk = \frac{(alternating\ blank) - (true\ blank)}{true\ analyte-containing}$$

This crosstalk coefficient quantifies the increase in signal intensity from background noise normalized to the average signal of true analyte-containing droplets. The crosstalk coefficient controls for ionization efficiency and background observed during ESI-MS, allowing for comparisons between analytes with varying ionization efficiencies and background intensities. The maximum theoretical value for the crosstalk coefficient is 0.5, corresponding to equal average signal intensity in blank and analyte-containing droplets post mixing. When doubled, the crosstalk coefficient can be interpreted as a percent carryover.

The crosstalk coefficient for the acetylpyridine test was 0.364 ± 0.009 (n = 369 total droplets), or ~75% carryover. Notably, this crosstalk occurred with only 5.5 min of incubation time which is substantially less than the hours or days of incubation time used in many high-throughput screens.[6,47]

Analysis of the acetylpyridine crosstalk measurement shows equal increase in signal for average blank droplet as decrease in average analyte-containing droplet, demonstrating conservation of analyte between the analyte and blank droplets. The repeatability of this measurement was evaluated and is summarized in Table 2-1. Triplicate, intra-day technical replicates (i.e. same sample, device, and tubing) result in a relative standard deviation (RSD) of 3% while inter-day, experimental replicates (i.e. separate solutions, microfluidic devices, and tubing) show 8% RSD. These results suggest that this measurement is repeatable and can be used to make comparisons after perturbing the system.

Table 2-1: Repeatability of acetylpyridine crosstalk measurements

Replicate Type	Trial	Acetylpyridine Crosstalk Value	Average Crosstalk	n	SEM	% RSD
Intra-day	Test 1	0.406	0.3985	3	0.01	3%
	Test 2	0.391				
	Test 3	0.430				
Inter-day	Day 1	0.414	0.3755	4	0.02	8%
	Day 2	0.348				
	Day 3	0.352				
	Day 4	0.388				

Crosstalk Analysis of a Diverse Set of Small Molecules. We next sought to measure crosstalk for a variety of compounds to better understand how molecular properties contribute to the effect. Crosstalk values were determined for 36 analytes in 2 wt.% 008-FS in HFE 7500 and are summarized in the Appendix. In the dataset, 20 of the 36 compounds exhibited crosstalk between 0.005 – 0.5 crosstalk units (1 – 100% carryover) and 12 compounds had values < 0.005

which is the lower limit measurable by ESI-MS. Four compounds exhibited significant carryover into the oil which inhibited droplet analysis (e.g. equal analyte signal in aqueous and oil phases). These compounds were classified together as >0.5 crosstalk (>100% carryover).

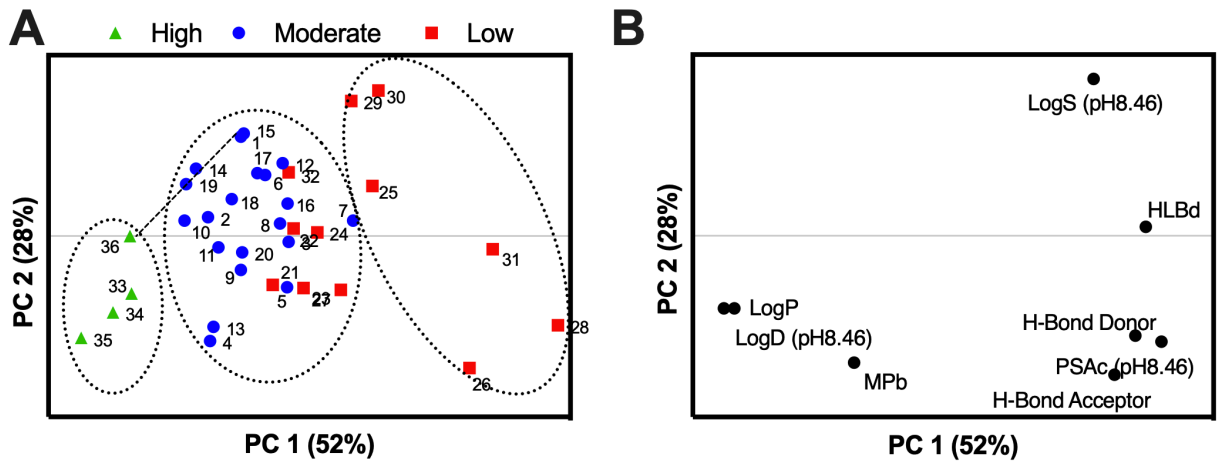

Figure 2-2: Principal component analysis of test set. (A) Score and (B) loading plots of 36-compound crosstalk test set generated using the physical descriptors. Points are labelled according to the entry in Table S2. Colors correspond with extent of crosstalk determined with the chopper experiment; low (<0.005 crosstalk) is red, moderate (0.005 – 0.5) is blue, and high (>0.5) is green.

Physiochemical descriptors were calculated for each of the analytes in the data set to evaluate the properties contributing to crosstalk. Each physicochemical property calculable with ChemAxon software was used (LogS, LogD, LogP, number of hydrogen bond acceptor and donor groups, molecular polarizability, polar surface area, and hydrophobic-lipophilic balance). The analytes studied represent high structural diversity as determined by a Tanimoto similarity matrix (Appendix), which analyzes chemical similarity based on ChemAxon hashed fingerprint descriptors. By studying dissimilar compounds according to this analysis, a large chemical space is explored which can help identify chemical trends that are significant.[52,53]

Principal component analysis was performed using the normalized chemical descriptors resulting in score and loading plots shown in Figure 2-2. Each point in the loading plot in Figure 2-2A is labelled according to the entry in the Appendix. The LogS value for analytes with

quaternary amines acetylcholine, choline, and neostigmine (29, 30, 32 respectively) cannot be calculated with ChemAxon due to the permanent charge; however, due to the extremely low crosstalk observed these analytes were included in the analysis. After PCA of the physical descriptors, we color coded the datapoint for each analyte based on the extent of crosstalk (red is low/undetectable crosstalk, blue is moderate crosstalk, and green is high crosstalk).

Three regions in Figure 2-2A emerge corresponding with high, moderate, and low crosstalk indicated by the dashed ovals. Generally, compounds exhibiting high crosstalk are in the bottom left of the plot, while compounds exhibiting low crosstalk are in the top right. According to the loading plot (Figure 2-2B), high LogP and LogD character corresponds with high crosstalk values, whereas high polarity (high LogS, more H-bond donor/acceptor groups, and high polar surface area) corresponds with the low/undetectable crosstalk compounds. A homologous series of substituted amines (triethyl- tripropyl, and tributyl-amine) is included as entries 1, 19, and 36 respectively, which shows a trend of general hydrophobicity (superimposed dashed line). These results suggest that hydrophobic analytes have a greater tendency for crosstalk in this carrier fluid-surfactant system.

Within these regions though, some analytes classified as low crosstalk by our experimental measurement are positioned within the expected moderate crosstalk group. We predicted that these analytes may transfer if given longer incubation time. To test this, we performed a 2 h incubation (see methods) of these compounds as well as a random selection of four other compounds within the low cluster to determine if incubation time affected their crosstalk. Analytes 21, 22, 23, and 24, which were in the moderate cluster showed moderate carryover at 2 h (Figure 2-3). Each of the analytes tested within the low cluster (28, 29, 30, 31) remained low with less than 1% carryover after 2 h incubation.

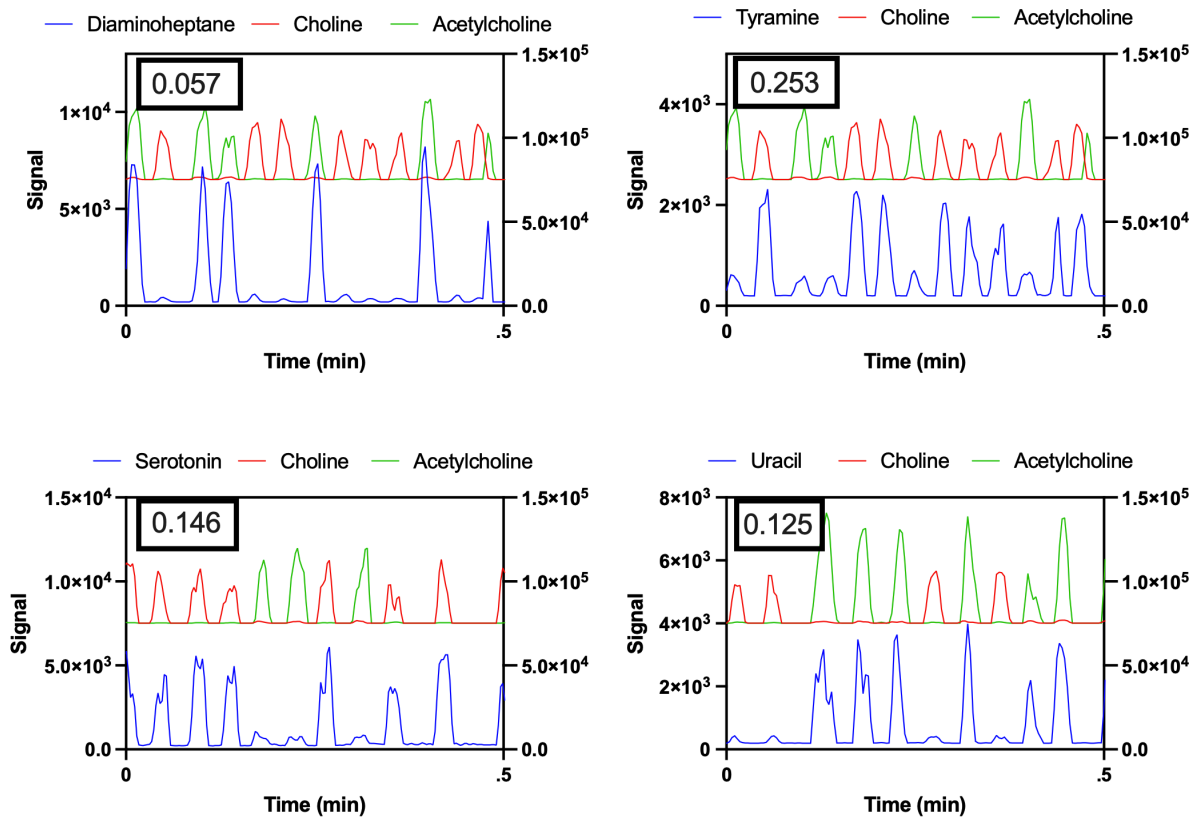

Figure 2-3: Droplet traces from prolonged incubation of low-carryover analytes. Blue traces represent the test compound, while red trace (choline) marks analyte droplets and green trace (acetylcholine) marks blank droplets. Crosstalk values were calculated and are shown in the top left of the traces. Kynurenic acid, choline, and acetylcholine had crosstalk values < 0.005.

Analytes 27 and 32 do not follow the expected behavior predicted by the descriptor classification. The two analytes show less than 1% carryover with the 2 h incubation despite clustering within the moderate group. Analyte 32, neostigmine, clusters with the moderate crosstalk region due to the exclusion of a LogS value in the calculation. With the ability to calculate LogS for permanently charged analytes, it is expected that compound 32 would cluster accurately. Despite these two outliers, the model accurately reflects the transport for 34 of 36 analytes studied, which is significant for the many droplet microfluidic platforms that require an extended incubation period.

The amino acids tested showed long term containment to the original droplet, which is encouraging for droplet microfluidic methods that require amino acids. Similarly, many of the

analytes that demonstrated crosstalk only after prolonged incubation were neurotransmitters. Previous studies using droplets to analyze neurotransmitters have not required long term storage, but rather test droplets quickly after generation, so the conditions under which these analytes exhibit crosstalk may not be of concern.[13–16] These observations indicate how these results can be interpreted depending on the application envisioned for droplet microfluidics.

Role of Surfactant and Oil Phase on Crosstalk. The PCA model predicts carryover based on analyte chemical properties; however, it is based on results using the most common surfactant and oil (008-FS in HFE 7500). Therefore, we also examined how changing the carrier fluid system affected carryover. Figure 2-4A shows how crosstalk of two test analytes, acetylpyridine and caffeine, varied with several commonly used surfactants.[13,54,55] Fluoro-phase from Dolomite Microfludics, a silica nanoparticle-based droplet stabilizer believed to inhibit micelle formation,[36] was also tested but was incompatible with ESI-MS analysis.

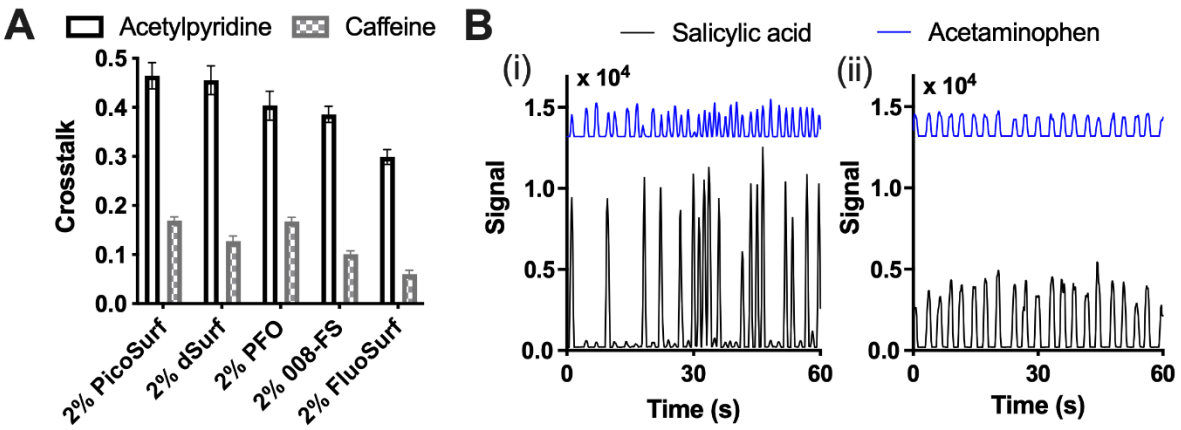

Figure 2-4: Effect of surfactant structure on crosstalk. (A) Crosstalk values for acetylpyridine (black) and caffeine (gray) in HFE 7500 with commercial surfactants dissolved at 2 wt.%. Acetylpyridine has higher crosstalk for each surfactant compared to caffeine. 2 wt.% PicoSurf demonstrates higher crosstalk for both compounds compared with 2 wt.% FluoSurf. (B) Traces of four-hour droplet incubation with (i) 2 wt.% carboxylate surfactant in HFE 7500 and (ii) 2 wt.% 008-FS in HFE 7500. Acetaminophen (blue trace, offset) marks each droplet. Salicylic acid (black) was added to half of the droplets prior to mixing. Salicylic acid does not transfer with the carboxylate surfactant but appears in every droplet with the 008-FS.

Changing the surfactant affected the crosstalk measured for both analytes. Though the commercial surfactants have proprietary structures, they likely all share similar polyethylene glycol (PEG) or polypropylene glycol head groups and Krytox (poly(perfluoropropylene glycol)-carboxylates) derivative tails as described previously.[34] Differences between surfactants appear to have both general effects on small molecule transport, as suggested by relatively high carryover by PicoSurf for both acetylpyridine and caffeine, and analyte-specific effects, demonstrated by the degree of change between the two test analytes.

We hypothesize that a driving interaction is affinity between the small molecule and the surfactant head group which saturates the droplet surface. To test this, we synthesized a surfactant with a carboxylate head group and a Krytox tail group, similar to Krytox-PEG surfactants (e.g., 008-FS).[34] We tested acidic analytes which should have minimal interaction with the carboxylate head group due to charge repulsion. None of the five acidic analytes demonstrated crosstalk in the chopper experiment. To further test this surfactant, we incubated analyte-containing (salicylic acid) and blank droplets for 4 h. Using the carboxylate surfactant, salicylic acid showed extremely low crosstalk (crosstalk coefficient < 0.05), while using 008-FS resulted in full crosstalk (crosstalk coefficient of 0.5, Figure 2-4B). Full carryover was observed when the carboxylate surfactant was tested with quaternary amine marker compounds such as choline and acetylcholine, likely due to strong ionic attraction between headgroup and the analytes. These findings support our hypothesis that small molecule affinity for the surfactant head group is an important driver for crosstalk. These results suggest that tailoring surfactants for given analytes may be beneficial to reduce crosstalk.

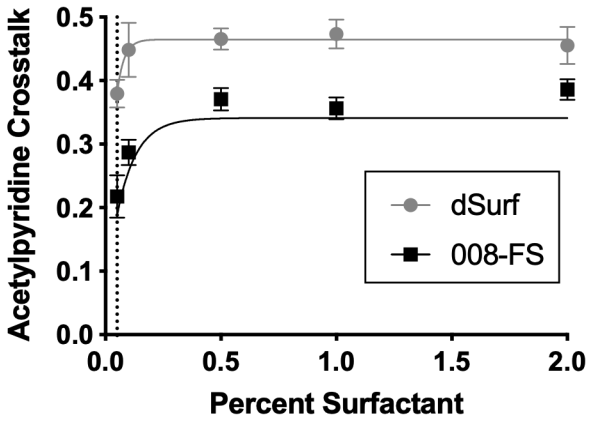

Figure 2-5: Effect of 008-FS and dSurf concentration on crosstalk in HFE 7500. Crosstalk is reduced as the surfactant concentration approaches the CMC (0.05, notated with dashed vertical line).

We then tested the role of surfactant concentration on carryover. Acetylpyridine was tested with several surfactant concentrations using two surfactants with available critical micelle concentration (CMC) data from the manufacturers (Figure 2-5). In both cases, crosstalk decreased at low concentrations, which agrees with a previous study using Jeffamine surfactants.[18] Attempts to test surfactant concentrations below the CMC (0.05 and 0.06 wt.% for dSurf and 008-FS, respectively) resulted in failure to generate alternating droplets due to merging at the chopper junction. In other surfactant systems, micelle concentration and size increase as surfactant concentration increases above the CMC, while free surfactant concentration is consistent.[56,57] A possible explanation for the increase in crosstalk from 0.05 – 0.5% surfactant in Figure 2-5 is the increasing possibility of micelle generation in the oil. With increasing surfactant concentration, micelles are more readily generated containing analyte.

While both surfactants in Figure 2-5 demonstrate an increase in crosstalk with increasing surfactant concentrations, crosstalk plateaus with surfactants above 0.5 wt.%. In this test, neither surfactant resulted in full transfer of acetylpyridine (0.47 and 0.34 for dSurf and 008-FS respectively). This suggests that the surfactant or micelle generation limits carryover at low concentrations (0.05-0.5 wt.% in Figure 2-5), and other factors limit crosstalk at higher

concentrations (>0.5 wt.%). While lower surfactant percentages appear to reduce crosstalk, droplet stability is also reduced.

The carrier phase properties can also be affected by changing the fluorinated oil. Figure 2-6 shows the carryover of acetylpyridine and caffeine for 2 wt.% 008-FS in HFE 7500, PFD, and FC-40 which are common carrier oils for droplet screening.[13,40,58] Substantial decreases were observed by replacing HFE 7500 with the two perfluorinated oils. The low crosstalk observed in the FC-40 oil agrees with the low carryover reported previously regarding fluorescent dye retention in surfactant-doped FC-40.[40]

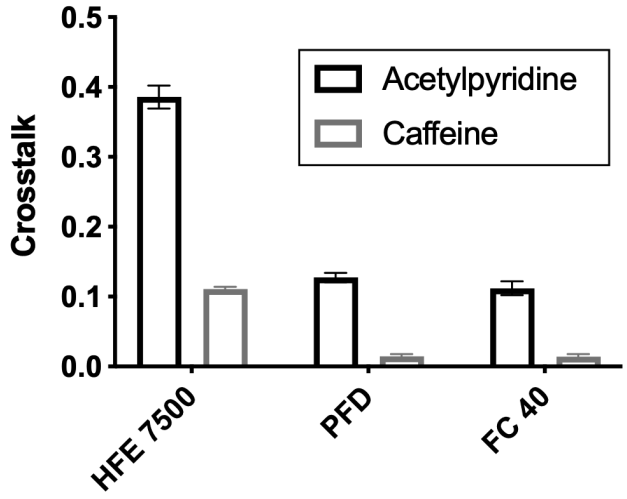

Figure 2-6: Effect of fluorinated oil on crosstalk. Crosstalk was measured with 2 wt.% 008-FS in HFE 7500, perfluorodecalin (PFD), and FC-40. Crosstalk is reduced when switching from the HFE oil to perfluourinated oils.

We tested increasing the concentration of 008-FS to 5 wt.% in FC-40 oil as in Figure 2-5 with the HFE 7500 oil. Acetylpyridine carryover increased with increasing surfactant in FC-40 (Figure 2-7) then reached a plateau, consistent with the trend in Figure 2-5. Manufacturer data on the solubility or CMC in alternative oils is not available, so it is difficult to explain the behavior mechanistically. One possible explanation for this behavior is related to differences in surfactant interaction with different oils.[56] HFE 7500 contains a non-fluorinated ether group compared to

PFD or FC-40 which could lead to higher density of 008-FS reverse micelles at lower concentrations, higher solubility of free surfactant, or differences in the micelle structures.

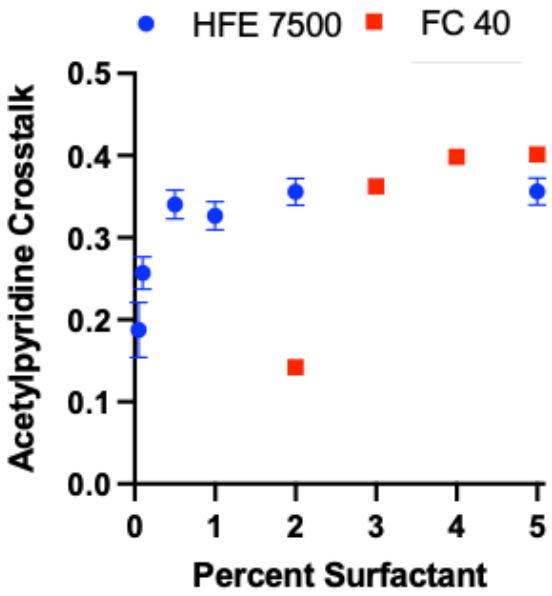

Figure 2-7: Effect of surfactant concentration on crosstalk in HFE 7500 and FC 40. Crosstalk decreases as surfactant concentration decreases in both oils.

A second explanation for the difference in crosstalk with different oils is direct paritioning (no surfactant mediation) through the oil. It is not possible to use the chopper device for this test due to the coalescence of the two streams at the junction, so droplets were generated from a multi-wellplate described previously.[43] Alternating arrays of five analyte-containing and five blank droplets were generated using both HFE 7500 and PFD without surfactant and infused into the mass spectrometer. This approach does not provide a quantitative comparison to on-chip experiments, but it can be used to provide insight into surfactant-free systems. Carryover was still observed (Figure 2-8); acetylpyridine had higher crosstalk than caffeine and HFE 7500 had higher carryover than PFD. Though the carryover was less than with surfactant present, this test shows that some degree of crosstalk is possible by direct partitioning through the fluorinated oils. The possibility of mechanical carryover via PFA tubing adsorption was ruled out, as the signal increase

in blank droplets was equal for blank droplets preceding and following generation of analyte droplets. Similarly, droplets generated first (those that had longer total flow) had equal carryover as droplets generated last (with less total flow), so adherence to tubing walls is unlikely.

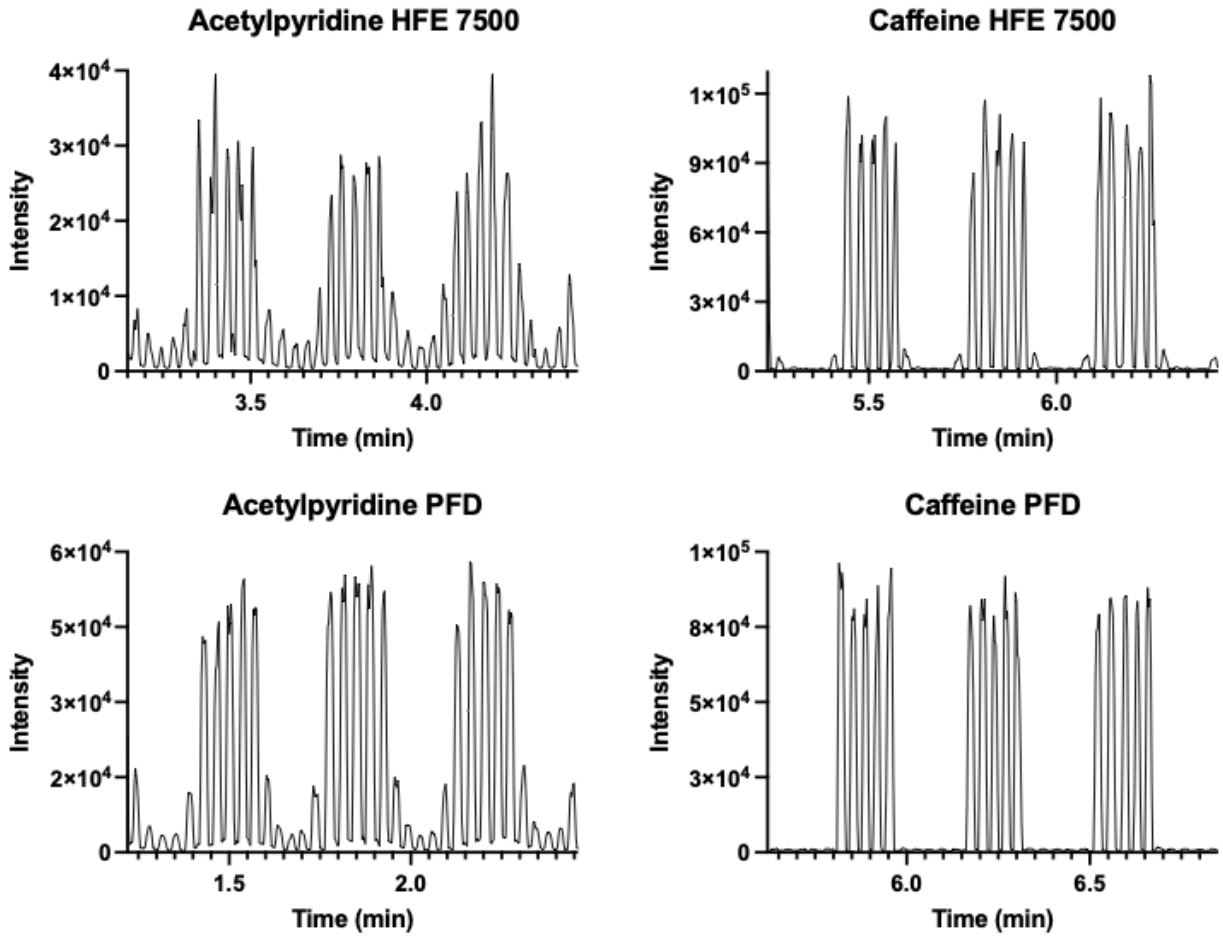

Figure 2-8: Crosstalk test without surfactant. Droplet traces without surfactant for acetylpyridine and caffeine in HFE 7500 and PFD. Droplets were generated in alternating pairs of five analyte droplets and five blank droplets. Each trace shows 35 droplets, 15 analyte and 20 blanks. Carryover improves from acetylpyridine to caffeine, and from HFE 7500 to PFD.

Based on these results, we propose that crosstalk can occur both by surfactant-mediated carryover and in the absense of surfactant, via direct partitioning through oil. While the partitioning without surfactant appears to be lower than the surfactant systems, more investigation is required to determine if a small percentage of surfactant (e.g. 0.01 wt.% 008-FS) can reduce direct

partitioning through oil without leading to the micelle-mediated transport observed above the CMC.

Role of Flow in Crosstalk. Some crosstalk studies have focused on droplets in flow,[37,59] while most focus on droplets in storage.[18,27,28,38,40] Flow is a requirement to all droplet microfluidics, so an understanding of crosstalk in flow is central to all applications using droplet microfluidics.

To test if the incubation time within the tubing has an effect, trains of droplets were generated using the chopper device then flow was stopped. In two experiments (15 and 20 min of static incubation) flow was resumed (total flow time was kept at 5.5 min). These timepoints are ~3 and 4-fold increases in incubation time compared to the total time flowing. There was no significant change between signal intensities in blank droplets when parked for 15 or 20 min (Figure 2-9). If direct partitioning through the oil were a major mechanism for crosstalk, it is expected that this test would have yielded a significant change. This suggests that with a surfactant present, carryover does not increase when droplets are static at the time scales used here. With this experiment, droplets are not in contact with each other, so direct interaction between droplets is not possible. We hypothesized that if the carryover is not occurring passively in this system, a dynamic process such as flow may increase crosstalk.

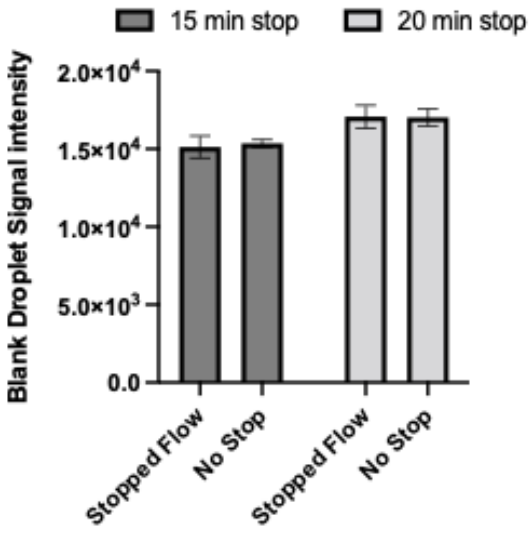

Figure 2-9: Blank droplet signal intensities after stopped flow incubation. Alternating droplets were generated then flow was stopped for 15 or 20 minutes. Stopped blank droplet signal intensity was compared to freshly generated blank droplets which were not stopped. Electrospray tip position was changed slightly between experiments due to the flow stoppage, which accounts for changes in signal intensity between 15 and 20 minute stop experiments.

We tested this by varying the capillary length from the device to the mass spectrometer, which increases the incubation time while maintaining flow. The length of capillary ranged from 16.8 – 152 cm corresponding to 1.8 to 17 min incubation time. An increase in acetylpyridine crosstalk was observed with increasing capillary length (Figure 2-10A). Crosstalk increased linearly until full carryover was measured above 75 cm. Caffeine crosstalk also increased linearly with capillary length (Figure 2-10B). These observations suggest that the carryover in flow is related to the amount of contact the droplet has with the tubing or device walls.

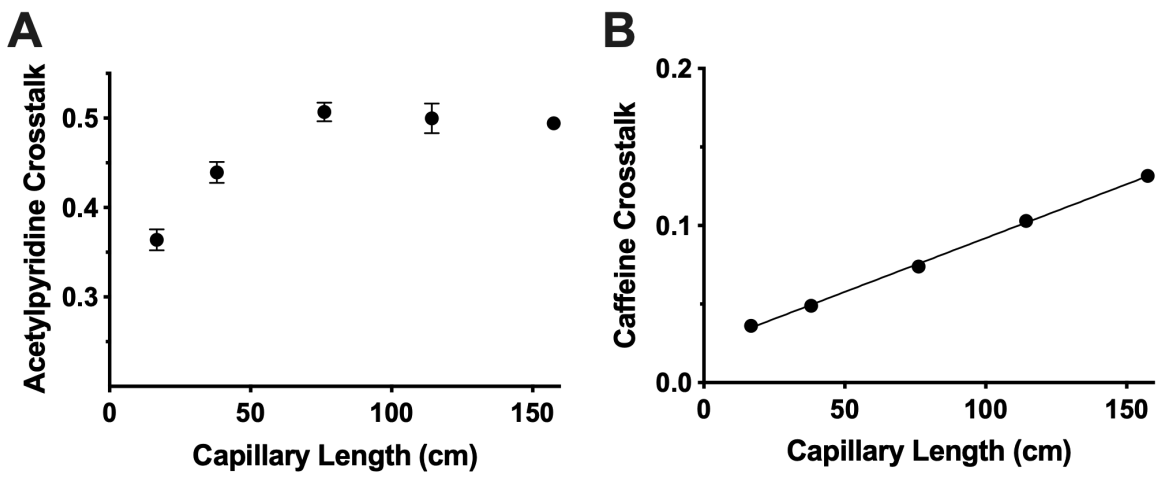

Figure 2-10: Crosstalk as a function of length of capillary to the mass spectrometer. (A) Acetylpyridine crosstalk increases until it reaches full carryover. (B) Caffeine crosstalk increases linearly with capillary length (R2 > 0.99).

A possible explanation is that friction or shear force between the droplet and the tubing walls is the process that drives transfer of small molecules. Others have investigated shear force in surfactant stabilized systems.[60,61] At Reynolds numbers comparable to our system, prediction models have shown that shear stress causes droplet shedding in the form of "non-satellite droplets" or micelles due to differences in interfacial tension on the tubing interface compared to the oil interface.[61] These models did not investigate the contents of the micelle structures generated by shear, but it is reasonable that they contain small molecules from the initial droplet if the small molecules have affinity for the surfactant or oil.

Shear-driven micelle generation fits with our earlier hypothesis that in flow, micelles are loaded with analyte cargo based on affinity with the surfactant, leading to crosstalk. A potential limiting factor of crosstalk in the presence of ample surfactant (Figure 2-5, >0.5%) is the ability to shear micelles that contain analyte. With sufficient surfactant for micelle generation, analyte affinity, and sufficient tubing for shear-based loading of micelles, significant carryover is observed. More investigation must be done to compare these findings with the crosstalk behavior for droplets stored with prolonged contact. For example, if the increased crosstalk observed after

prolonged storage is due to micelles produced by flow during droplet generation, or if an additional mechanism is acting in these formats.

2.4 Conclusions

Small molecule transport between droplet samples in flow was investigated using mass spectrometry. A method was developed to quickly and reliably evaluate the carryover of small molecules that are not fluorescent. A panel of compounds was tested for crosstalk with a range of chemical properties, and PCA suggested a correlation between the severity of crosstalk and the hydrophobic character of the small molecule. A variety of fluorinated surfactants and oils were tested, which suggested that crosstalk occurs partially as a result of micelle-mediated transport. A new surfactant head group was synthesized and tested based on these results which resulted in decreased carryover compared to a commercially available surfactant. Observations of increasing crosstalk with increasing flow path suggest a friction or shear force that may drive the generation of analyte-containing micelles from droplets in flow.

We propose a mode of crosstalk where small molecules partition to the droplet surface driven either by surfactant affinity or oil solubility. In the presence of surfactant, analyte-containing reverse micelles can be sheared off during flow and transported to neighboring droplets. Without surfactant, some analytes can diffuse through the perfluorinated oil. Analytes partition at varying rates and conditions, which can be factored into the design of droplet-based experiments.

2.5 References

(1) Agresti, J. J.; Antipov, E.; Abate, A. R.; Ahn, K.; Rowat, A. C.; Baret, J.-C.; Marquez, M.; Klibanov, A. M.; Griffiths, A. D.; Weitz, D. A. Ultrahigh-Throughput Screening in Drop-Based Microfluidics for Directed Evolution. *PNAS* **2010**, *107* (9), 4004–4009. https://doi.org/10.1073/pnas.0910781107.

(2) Sjostrom, S. L.; Bai, Y.; Huang, M.; Liu, Z.; Nielsen, J.; Joensson, H. N.; Andersson Svahn, H. High-Throughput Screening for Industrial Enzyme Production Hosts by Droplet Microfluidics. *Lab Chip* **2014**, *14* (4), 806–813. https://doi.org/10.1039/C3LC51202A.
(3) Fallah-Araghi, A.; Baret, J.-C.; Ryckelynck, M.; D. Griffiths, A. A Completely in Vitro Ultrahigh-Throughput Droplet-Based Microfluidic Screening System for Protein Engineering and Directed Evolution. *Lab on a Chip* **2012**, *12* (5), 882–891. https://doi.org/10.1039/C2LC21035E.
(4) Terekhov, S. S.; Smirnov, I. V.; Stepanova, A. V.; Bobik, T. V.; Mokrushina, Y. A.; Ponomarenko, N. A.; Belogurov, A. A.; Rubtsova, M. P.; Kartseva, O. V.; Gomzikova, M. O.; Moskovtsev, A. A.; Bukatin, A. S.; Dubina, M. V.; Kostryukova, E. S.; Babenko, V. V.; Vakhitova, M. T.; Manolov, A. I.; Malakhova, M. V.; Kornienko, M. A.; Tyakht, A. V.; Vanyushkina, A. A.; Ilina, E. N.; Masson, P.; Gabibov, A. G.; Altman, S. Microfluidic Droplet Platform for Ultrahigh-Throughput Single-Cell Screening of Biodiversity. *PNAS* **2017**, *114* (10), 2550–2555. https://doi.org/10.1073/pnas.1621226114.
(5) Macosko, E. Z.; Basu, A.; Satija, R.; Nemesh, J.; Shekhar, K.; Goldman, M.; Tirosh, I.; Bialas, A. R.; Kamitaki, N.; Martersteck, E. M.; Trombetta, J. J.; Weitz, D. A.; Sanes, J. R.; Shalek, A. K.; Regev, A.; McCarroll, S. A. Highly Parallel Genome-Wide Expression Profiling of Individual Cells Using Nanoliter Droplets. *Cell* **2015**, *161* (5), 1202–1214. https://doi.org/10.1016/j.cell.2015.05.002.
(6) Xu, L.; Chang, K.-C.; Payne, E. M.; Modavi, C.; Liu, L.; Palmer, C. M.; Tao, N.; Alper, H. S.; Kennedy, R. T.; Cornett, D. S.; Abate, A. R. Mapping Enzyme Catalysis with Metabolic Biosensing. *Nat Commun* **2021**, *12* (1), 6803. https://doi.org/10.1038/s41467-021-27185-9.
(7) Sun, A. C.; Steyer, D. J.; Allen, A. R.; Payne, E. M.; Kennedy, R. T.; Stephenson, C. R. J. A Droplet Microfluidic Platform for High-Throughput Photochemical Reaction Discovery. *Nature Communications* **2020**, *11* (1), 6202. https://doi.org/10.1038/s41467-020-19926-z.
(8) Cochrane, W. G.; Malone, M. L.; Dang, V. Q.; Cavett, V.; Satz, A. L.; Paegel, B. M. Activity-Based DNA-Encoded Library Screening. *ACS Comb Sci* **2019**, *21* (5), 425–435. https://doi.org/10.1021/acscombsci.9b00037.
(9) L. Sjostrom, S.; N. Joensson, H.; Andersson Svahn, H. Multiplex Analysis of Enzyme Kinetics and Inhibition by Droplet Microfluidics Using Picoinjectors. *Lab on a Chip* **2013**, *13* (9), 1754–1761. https://doi.org/10.1039/C3LC41398E.
(10) Frenz, L.; Blank, K.; Brouzes, E.; D. Griffiths, A. Reliable Microfluidic On-Chip Incubation of Droplets in Delay-Lines. *Lab on a Chip* **2009**, *9* (10), 1344–1348. https://doi.org/10.1039/B816049J.
(11) Hassan, S.; M. Nightingale, A.; Niu, X. Continuous Measurement of Enzymatic Kinetics in Droplet Flow for Point-of-Care Monitoring. *Analyst* **2016**, *141* (11), 3266–3273. https://doi.org/10.1039/C6AN00620E.
(12) Hess, D.; Dockalova, V.; Kokkonen, P.; Bednar, D.; Damborsky, J.; deMello, A.; Prokop, Z.; Stavrakis, S. Exploring Mechanism of Enzyme Catalysis by On-Chip Transient Kinetics Coupled with Global Data Analysis and Molecular Modeling. *Chem* **2021**, *7* (4), 1066–1079. https://doi.org/10.1016/j.chempr.2021.02.011.
(13) Bell, S. E.; Park, I.; Rubakhin, S. S.; Bashir, R.; Vlasov, Y.; Sweedler, J. V. Droplet Microfluidics with MALDI-MS Detection: The Effects of Oil Phases in GABA Analysis. *ACS Meas. Au* **2021**, *1* (3), 147–156. https://doi.org/10.1021/acsmeasuresciau.1c00017.

(14) Ngernsutivorakul, T.; Steyer, D. J.; Valenta, A. C.; Kennedy, R. T. In Vivo Chemical Monitoring at High Spatiotemporal Resolution Using Microfabricated Sampling Probes and Droplet-Based Microfluidics Coupled to Mass Spectrometry. *Anal. Chem.* **2018**, *90* (18), 10943–10950. https://doi.org/10.1021/acs.analchem.8b02468.
(15) Alizadeh, N.; Salimi, A. Polymer Dots as a Novel Probe for Fluorescence Sensing of Dopamine and Imaging in Single Living Cell Using Droplet Microfluidic Platform. *Analytica Chimica Acta* **2019**, *1091*, 40–49. https://doi.org/10.1016/j.aca.2019.08.036.
(16) Brink, F. T. G. van den; Phisonkunkasem, T.; Asthana, A.; G. Bomer, J.; Maagdenberg, A. M. J. M. van den; A. Tolner, E.; Odijk, M. A Miniaturized Push–Pull-Perfusion Probe for Few-Second Sampling of Neurotransmitters in the Mouse Brain. *Lab on a Chip* **2019**, *19* (8), 1332–1343. https://doi.org/10.1039/C8LC01137K.
(17) Calderó, G.; García-Celma, M. J.; Solans, C.; Plaza, M.; Pons, R. Influence of Composition Variables on the Molecular Diffusion from Highly Concentrated Water-in-Oil Emulsions (Gel−Emulsions). *Langmuir* **1997**, *13* (3), 385–390. https://doi.org/10.1021/la9603380.
(18) Skhiri, Y.; Gruner, P.; Semin, B.; Brosseau, Q.; Pekin, D.; Mazutis, L.; Goust, V.; Kleinschmidt, F.; Harrak, A. E.; Brian Hutchison, J.; Mayot, E.; Bartolo, J.-F.; D. Griffiths, A.; Taly, V.; Baret, J.-C. Dynamics of Molecular Transport by Surfactants in Emulsions. *Soft Matter* **2012**, *8* (41), 10618–10627. https://doi.org/10.1039/C2SM25934F.
(19) Payne, E. M.; Holland-Moritz, D. A.; Sun, S.; Kennedy, R. T. High-Throughput Screening by Droplet Microfluidics: Perspective into Key Challenges and Future Prospects. *Lab Chip* **2020**, *20* (13), 2247–2262. https://doi.org/10.1039/D0LC00347F.
(20) Zhu, P.; Wang, L. Passive and Active Droplet Generation with Microfluidics: A Review. *Lab on a Chip* **2017**, *17* (1), 34–75. https://doi.org/10.1039/C6LC01018K.
(21) Thorsen, T.; Roberts, R. W.; Arnold, F. H.; Quake, S. R. Dynamic Pattern Formation in a Vesicle-Generating Microfluidic Device. *Phys. Rev. Lett.* **2001**, *86* (18), 4163–4166. https://doi.org/10.1103/PhysRevLett.86.4163.
(22) Baret, J.-C. Surfactants in Droplet-Based Microfluidics. *Lab on a Chip* **2012**, *12* (3), 422–433. https://doi.org/10.1039/C1LC20582J.
(23) Pietrini, A. V.; Luisi, P. L. Cell-Free Protein Synthesis through Solubilisate Exchange in Water/Oil Emulsion Compartments. *ChemBioChem* **2004**, *5* (8), 1055–1062. https://doi.org/10.1002/cbic.200400014.
(24) Chao, W.-C.; Collins, J.; Bachman, M.; Li, G. P.; Lee, A. Droplet Arrays in Microfluidic Channels for Combinatorial Screening Assays. *Angewandte Chemie International Edition* **2003**, *42* (7).
(25) Ward, T.; Faivre, M.; Abkarian, M.; Stone, H. A. Microfluidic Flow Focusing: Drop Size and Scaling in Pressure versus Flow-Rate-Driven Pumping. *ELECTROPHORESIS* **2005**, *26* (19), 3716–3724. https://doi.org/10.1002/elps.200500173.
(26) Chen, H.; Fang, Q.; Yin, X.-F.; Fang, Z.-L. Microfluidic Chip-Based Liquid–Liquid Extraction and Preconcentration Using a Subnanoliter-Droplet Trapping Technique. *Lab Chip* **2005**, *5* (7), 719–725. https://doi.org/10.1039/B416964F.
(27) Courtois, F.; Olguin, L. F.; Whyte, G.; Theberge, A. B.; Huck, W. T. S.; Hollfelder, F.; Abell, C. Controlling the Retention of Small Molecules in Emulsion Microdroplets for Use in Cell-Based Assays. *Anal. Chem.* **2009**, *81* (8), 3008–3016. https://doi.org/10.1021/ac802658n.

(28) Sandoz, P. A.; Chung, A. J.; Weaver, W. M.; Di Carlo, D. Sugar Additives Improve Signal Fidelity for Implementing Two-Phase Resorufin-Based Enzyme Immunoassays. *Langmuir* **2014**, *30* (23), 6637–6643. https://doi.org/10.1021/la5004484.
(29) Trotta, M.; Gasco, M. R.; Morel, S. Release of Drugs from Oil-Water Microemulsions. *Journal of Controlled Release* **1989**, *10* (3), 237–243. https://doi.org/10.1016/0168-3659(89)90073-4.
(30) Calderó, G.; García-Celma, M. J.; Solans, C.; Pons, R. Effect of PH on Mandelic Acid Diffusion in Water in Oil Highly Concentrated Emulsions (Gel-Emulsions). *Langmuir* **2000**, *16* (4), 1668–1674. https://doi.org/10.1021/la990971w.
(31) Poulin, P.; Bibette, J. Adhesion of Water Droplets in Organic Solvent. *Langmuir* **1998**, *14* (22), 6341–6343. https://doi.org/10.1021/la9801413.
(32) Thiam, A. R.; Bremond, N.; Bibette, J. From Stability to Permeability of Adhesive Emulsion Bilayers. *Langmuir* **2012**, *28* (15), 6291–6298. https://doi.org/10.1021/la3003349.
(33) Studer, A.; Hadida, S.; Ferritto, R.; Kim, S.-Y.; Jeger, P.; Wipf, P.; Curran, D. P. Fluorous Synthesis: A Fluorous-Phase Strategy for Improving Separation Efficiency in Organic Synthesis. *Science* **1997**. https://doi.org/10.1126/science.275.5301.823.
(34) Holtze, C.; C. Rowat, A.; J. Agresti, J.; B. Hutchison, J.; E. Angilè, F.; J. Schmitz, C. H.; Köster, S.; Duan, H.; J. Humphry, K.; A. Scanga, R.; S. Johnson, J.; Pisignano, D.; A. Weitz, D. Biocompatible Surfactants for Water-in- Fluorocarbon Emulsions. *Lab on a Chip* **2008**, *8* (10), 1632–1639. https://doi.org/10.1039/B806706F.
(35) Sun, S.; Zawatzky, K.; Regalado, E. L.; Mangion, I. K.; Welch, C. J. Are Fluorine-Rich Pharmaceuticals Lost by Partition into Fluorous Phases? *Journal of Pharmaceutical and Biomedical Analysis* **2016**, *128*, 106–110. https://doi.org/10.1016/j.jpba.2016.05.025.
(36) Pan, M.; Rosenfeld, L.; Kim, M.; Xu, M.; Lin, E.; Derda, R.; Tang, S. K. Y. Fluorinated Pickering Emulsions Impede Interfacial Transport and Form Rigid Interface for the Growth of Anchorage-Dependent Cells. *ACS Appl. Mater. Interfaces* **2014**, *6* (23), 21446–21453. https://doi.org/10.1021/am506443e.
(37) Gruner, P.; Riechers, B.; Semin, B.; Lim, J.; Johnston, A.; Short, K.; Baret, J.-C. Controlling Molecular Transport in Minimal Emulsions. *Nature Communications* **2016**, *7*, 10392. https://doi.org/10.1038/ncomms10392.
(38) Chowdhury, M. S.; Zheng, W.; Kumari, S.; Heyman, J.; Zhang, X.; Dey, P.; Weitz, D. A.; Haag, R. Dendronized Fluorosurfactant for Highly Stable Water-in-Fluorinated Oil Emulsions with Minimal Inter-Droplet Transfer of Small Molecules. *Nature Communications* **2019**, *10* (1), 1–10. https://doi.org/10.1038/s41467-019-12462-5.
(39) Suman Chowdhury, M.; Zheng, W.; Kumar Singh, A.; Hao Ong, I. L.; Hou, Y.; A. Heyman, J.; Faghani, A.; Amstad, E.; A. Weitz, D.; Haag, R. Linear Triglycerol-Based Fluorosurfactants Show High Potential for Droplet-Microfluidics-Based Biochemical Assays. *Soft Matter* **2021**, *17* (31), 7260–7267. https://doi.org/10.1039/D1SM00890K.
(40) Janiesch, J.-W.; Weiss, M.; Kannenberg, G.; Hannabuss, J.; Surrey, T.; Platzman, I.; Spatz, J. P. Key Factors for Stable Retention of Fluorophores and Labeled Biomolecules in Droplet-Based Microfluidics. *Analytical Chemistry* **2015**, *87* (4), 2063–2067. https://doi.org/10.1021/ac504736e.
(41) M. Nightingale, A.; Hassan, S.; H. Evans, G. W.; M. Coleman, S.; Niu, X. Nitrate Measurement in Droplet Flow: Gas-Mediated Crosstalk and Correction. *Lab on a Chip* **2018**, *18* (13), 1903–1913. https://doi.org/10.1039/C8LC00092A.

(42) Gruner, P.; Riechers, B.; Chacòn Orellana, L. A.; Brosseau, Q.; Maes, F.; Beneyton, T.; Pekin, D.; Baret, J.-C. Stabilisers for Water-in-Fluorinated-Oil Dispersions: Key Properties for Microfluidic Applications. *Current Opinion in Colloid & Interface Science* **2015**, *20* (3), 183–191. https://doi.org/10.1016/j.cocis.2015.07.005.
(43) Sun, S.; Slaney, T. R.; Kennedy, R. T. Label Free Screening of Enzyme Inhibitors at Femtomole Scale Using Segmented Flow Electrospray Ionization Mass Spectrometry. *Anal. Chem.* **2012**, *84* (13), 5794–5800. https://doi.org/10.1021/ac3011389.
(44) Steyer, D. J.; Kennedy, R. T. High-Throughput Nanoelectrospray Ionization-Mass Spectrometry Analysis of Microfluidic Droplet Samples. *Anal. Chem.* **2019**, *91* (10), 6645–6651. https://doi.org/10.1021/acs.analchem.9b00571.
(45) Kempa, E.; Smith, C.; Li, X.; Bellina, B.; Richardson, K.; Pringle, S.; Barran, P. Coupling Droplet Microfluidics with Mass Spectrometry for Ultrahigh-Throughput Analysis up to and Above 30Hz. **2020**. https://doi.org/10.26434/chemrxiv.11836731.v1.
(46) Pei, J.; Li, Q.; Lee, M. S.; Valaskovic, G. A.; Kennedy, R. T. Analysis of Samples Stored as Individual Plugs in a Capillary by Electrospray Ionization Mass Spectrometry. *Anal. Chem.* **2009**, *81* (15), 6558–6561. https://doi.org/10.1021/ac901172a.
(47) Holland-Moritz, D. A.; Wismer, M. K.; Mann, B. F.; Farasat, I.; Devine, P.; Guetschow, E. D.; Mangion, I.; Welch, C. J.; Moore, J. C.; Sun, S.; Kennedy, R. T. Mass Activated Droplet Sorting (MADS) Enables High-Throughput Screening of Enzymatic Reactions at Nanoliter Scale. *Angewandte Chemie International Edition* **2020**, *59* (11), 4470–4477. https://doi.org/10.1002/anie.201913203.
(48) Deal, K. S.; Easley, C. J. Self-Regulated, Droplet-Based Sample Chopper for Microfluidic Absorbance Detection. *Anal. Chem.* **2012**, *84* (3), 1510–1516. https://doi.org/10.1021/ac202791d.
(49) Diefenbach, X. W.; Farasat, I.; Guetschow, E. D.; Welch, C. J.; Kennedy, R. T.; Sun, S.; Moore, J. C. Enabling Biocatalysis by High-Throughput Protein Engineering Using Droplet Microfluidics Coupled to Mass Spectrometry. *ACS Omega* **2018**, *3* (2), 1498–1508. https://doi.org/10.1021/acsomega.7b01973.
(50) Cole, R. H.; Tang, S.-Y.; Siltanen, C. A.; Shahi, P.; Zhang, J. Q.; Poust, S.; Gartner, Z. J.; Abate, A. R. Printed Droplet Microfluidics for on Demand Dispensing of Picoliter Droplets and Cells. *PNAS* **2017**, *114* (33), 8728–8733. https://doi.org/10.1073/pnas.1704020114.
(51) Kulesa, A.; Kehe, J.; Hurtado, J. E.; Tawde, P.; Blainey, P. C. Combinatorial Drug Discovery in Nanoliter Droplets. *PNAS* **2018**, *115* (26), 6685–6690. https://doi.org/10.1073/pnas.1802233115.
(52) Lajiness, M. S. Dissimilarity-Based Compound Selection Techniques. *Perspectives in Drug Discovery and Design* **1996**, *7* (1), 65–84. https://doi.org/10.1007/BF03380182.
(53) Bajusz, D.; Rácz, A.; Héberger, K. Why Is Tanimoto Index an Appropriate Choice for Fingerprint-Based Similarity Calculations? *Journal of Cheminformatics* **2015**, *7* (1), 20. https://doi.org/10.1186/s13321-015-0069-3.
(54) Zilionis, R.; Nainys, J.; Veres, A.; Savova, V.; Zemmour, D.; Klein, A. M.; Mazutis, L. Single-Cell Barcoding and Sequencing Using Droplet Microfluidics. *Nat Protoc* **2017**, *12* (1), 44–73. https://doi.org/10.1038/nprot.2016.154.
(55) Srisa-Art, M.; Dyson, E. C.; deMello, A. J.; Edel, J. B. Monitoring of Real-Time Streptavidin−Biotin Binding Kinetics Using Droplet Microfluidics. *Anal. Chem.* **2008**, *80* (18), 7063–7067. https://doi.org/10.1021/ac801199k.

(56) Sheng, J. J. Chapter 7 - Surfactant Flooding. In *Modern Chemical Enhanced Oil Recovery*; Sheng, J. J., Ed.; Gulf Professional Publishing: Boston, 2011; pp 239–335. https://doi.org/10.1016/B978-1-85617-745-0.00007-3.
(57) Lee, K. S.; Lee, J. H. Chapter 4 - Hybrid Chemical EOR Using Low-Salinity and Smart Waterflood. In *Hybrid Enhanced Oil Recovery using Smart Waterflooding*; Lee, K. S., Lee, J. H., Eds.; Gulf Professional Publishing, 2019; pp 65–110. https://doi.org/10.1016/B978-0-12-816776-2.00004-0.
(58) Payne, E. M.; Wells, S. S.; Kennedy, R. T. Continuous and Automated Slug Flow Nanoextraction for Rapid Partition Coefficient Measurement. *Analyst* **2021**, *146* (18), 5722–5731. https://doi.org/10.1039/D1AN01156A.
(59) Nightingale, A. M.; Phillips, T. W.; Bannock, J. H.; de Mello, J. C. Controlled Multistep Synthesis in a Three-Phase Droplet Reactor. *Nature Communications* **2014**, *5* (1), 1–8. https://doi.org/10.1038/ncomms4777.
(60) Mulligan, M. K.; Rothstein, J. P. The Effect of Confinement-Induced Shear on Drop Deformation and Breakup in Microfluidic Extensional Flows. *Physics of Fluids* **2011**, *23* (2), 022004. https://doi.org/10.1063/1.3548856.
(61) Wang, G.; Zhu, C.; Fu, T.; Ma, Y. Formation Mechanism and Criterion of Tail Satellite Droplets for Moving Droplet in Microchannel. *Chemical Engineering Science* **2021**, *238*, 116607. https://doi.org/10.1016/j.ces.2021.116607.

Chapter 3 On-Demand Microfluidic Droplet Splitting Using an External Electric Field

3.1 Introduction.

Miniaturization of chemical and biochemical assays using microfluidics is contingent on enabling sample and reagent manipulations inside microchannels. A variety of microfluidic droplet processing tools have been developed that attain processing rates and volumes unachievable by robotic liquid handling.[1] Previously developed droplet-based sample processing unit operations include reagent addition,[2,3] analyte extraction,[4–6] dielectrophoretic sorting,[7,8] and sample aliquoting (splitting).[9–11] Combining these unit operations allows for automated workflows at the microscale. Such workflows have proven useful for reducing reagent usage, increasing throughput, and enabling testing of limited samples.

Many droplet manipulations rely strictly on pressure and flow control within geometric structures. It can be advantageous, however, to incorporate external forces in tandem with fluidic forces to enable either new functions or functions that do not require complex pressure control. For example, electric fields may be used passively to reduce surface tension to facilitate reagent addition to droplets,[3] and to induce dielectrophoretic force to steer aqueous droplets.[7] By adding a uniform electric field to a bifurcated channel for splitting, droplet polarization occurs prior to splitting, resulting in charged droplets.[12] Continuous flow operations, such as droplet generation, may be performed by using electrophoresis rather than pressure driven flow.[13,14] Similarly, magnetic forces have been used for droplet generation,[15,16] sorting,[17,18] and coalescence[19] with the use of magnetic particles and ferrofluids. The use of lasers can enable sorting,[20] coalescence,[21] and

splitting[22] through various modes such as laser induced heating. Integrating surface acoustic waves (SAWs) has been investigated for droplet generation[23,24] and splitting[25,26] since it does not degrade the droplet contents as lasers might.

Use of external forces also enable on-demand (i.e. activated) functions in microfluidic systems, which is useful for selecting or changing a particular sample in high-throughput screening. On-demand reagent addition has been achieved with electric fields to dose a predetermined array of droplets with reagent.[3] Dielectrophoretic droplet sorting has been demonstrated to enable collection of a droplet when it meets criteria based on fluorescence,[8] absorbance,[27] Raman activity,[28] or a mass signature.[29] SAWs have been used for on-demand droplet splitting to enable parallel design experimentation (i.e. multiplexed droplet analysis).[30,31] It has been demonstrated that a magnetic force can be actuated with microfabricated valving to perform on-demand sample extractions of magnetic beads.[32]

Although magnetic fields and SAWs have been implemented in on-demand techniques, activating these forces require multicomponent fabrication, miniaturized transducers, or electromagnets.[25,26,30,33] Adding additional components can increase fabrication cost and time, and represent an additional point of failure for device operation. However, electric fields are easy to implement by designing liquid electrode channels into the microfluidic device.[34] With liquid electrodes, no multicomponent fabrication is needed which improves fabrication fidelity and ease.

Droplet splitting is used in a variety of workflows to preserve a portion of sample for later analysis[29,35,36] or to control droplet contents (e.g. particle enrichment).[37–39] Splitting is typically performed using fluidic methods by driving all droplets through a bifurcated channel.[40] Performing droplet splitting on-demand is useful for multiplexed droplet analysis, such as when one analysis technique is destructive or will change the sample.[29,30] For example, when performing droplet mass

spectrometry or deposition techniques, aliquoting all droplets consumes analysis time or space while having a duplicate sample is beneficial for downstream analysis or sequencing.[29,36,41] On-demand droplet splitting has also been applied to generating combinatorial libraries of droplet trains,[42] which can increase library diversity while keeping initial sample libraries managable.[43]

On-demand droplet splitting has been demonstrated through use of surface acoustic waves,[30,31] which suffers from multicomponent fabrication described previously. Recently, on-demand splitting has been achieved by pneumatic valves,[42,44] which requires multilayer fabrication, extensive programming of pressure or vacuum sources, and a complex resistive channel network. Using electric fields is appealing due to the lack of complex fabrication techniques and microfabrication, but splitting has not been demonstrated thus far. Droplet deformation in electric fields has been investigated and shown promise for potential electric field-based splitting.[45] Direct current (DC) fields have been shown to evoke cascading fission of droplets into a large number of fragments,[46] but controlled splitting was not investigated.

Here, we explore a novel phenomenon in droplet microfluidics, and demonstrate the utility for on-demand droplet splitting. Droplets are split by applying an electric field in conjunction with a channel expansion (Figure 3-1). This technique serves as an alternative approach to droplet splitting using standard geometrical splitters for high-throughput droplet workflows. Field-induced droplet splitting is consistently achieved at pL – nL droplet sizes. This technique allows for actionable droplet splitting due to the programmable nature of the electric field, as opposed to a static geometric splitter.

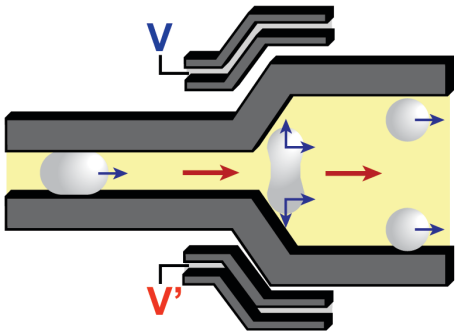

Figure 3-1: Schematic of field-induced droplet splitting. Red arrows demonstrate direction of flow, blue arrows represent simplified forces acting on the droplet. Potentials are applied to independent electrode channels represented by V and V'.

3.2 Materials and Methods

Reagents and materials. All chemicals were purchased from SigmaAldrich unless otherwise specified. HFE-7500 (3M) was used as fluorinated carrier fluid with 2 wt. % 008-fluorosurfactant (RAN Biotechnologies). To increase contrast for imaging purposes, green food dye (McCormick) was added to droplets when collecting images and videos.

Device fabrication. Device design was performed using AutoCAD (Autodesk, Inc.) and a corresponding transparent mask was produced (Fineline Imaging). Standard photolithography procedures were followed.[47] Briefly, SU8 2050 negative epoxy photoresist (MicroChem Corp.) was spun to the desired thickness (100 μm) on silicon wafers (University Wafer). Wafers were patterned with the desired geometry with ultraviolet irradiation through the mask. Undeveloped photoresist was removed to produce a negative mold of the device. Polydimethylsiloxane (PDMS, Curbell Plastics) was mixed in a 1:10 activator to monomer ratio and poured over the patterned wafer. Cured devices were punched with a 30-gauge needle to add flow ports then bonded to glass slides with oxygen plasma activation (PDC-32G, Harrick Plasma, Inc.). Bound devices were flushed with perfluorodecalin (Oakwood Products Inc.) with 2% tridecafluoro-1,1,2,2-tetrahydrooctyl tricholorosilane for surface treatment.

Device operation. Device flow control was performed using an Elveflow OB1 MK3+ pressure controller supplied with nitrogen gas. Pressure was applied to the headspace of reagent vials with 30 ga PTFE tubing (Cole-Parmer) inserted into the device ports. Pressures were modulated using Elveflow Smart Interface software.

Device operation was performed and monitored using two inverted microscope systems. Primarily, a Nikon TS100 inverted microscope equipped with a Phantom Miro C110 high speed camera was used for visualization and data collection. For fluorescent imaging, a DMi8 light microscope (Leica Microsystems) with a VEO 640L high speed camera (Vision Research Inc.) was used. Fluorescent excitation and emission was achieved using a FITC filter cube (Leica Microsystems). Data analysis was performed using ImageJ (NIH). For all experimentation, surfactant stabilized droplets were generated using flow focusing devices and stored in a modified vial as reported elsewhere.[29,48]

Electric field generation. Electric fields were generated using a home built high voltage system. A high voltage inverter (CXA-L0512-NJL; TDK-Lambda) was supplied with 12 V DC and was adjusted using a variable resistor. The potentiometer modulated applied voltages between 0 – 1.5 kV_{pp}. The AC field alternated at 45 Hz as dictated by the invertor used. Output 1 (denoted V) is connected to the high voltage invertor through a potentiometer while the "ground" output (denoted V') is floated. Due to the floated ground, the alternating field necessary for the field-based operations is produced Electrode channels were connected to syringes filled with 3 M NaCl. The voltage generator was attached to these NaCl filled syringes with alligator clips.[34] A true ground moat was generated by connecting a salt-water electrode with a wire connected to house ground. Voltages were monitored with a Siglent SDS 1104X-E oscilloscope.

3.3 Results and Discussion

Operating Principles. To perform droplet splitting with electric fields, devices were designed as shown in Figure 3-2A. Immiscible carrier phase was flowed into inlet 1 and pre-formed droplets were re-injected into inlet 2. Droplets were respaced by the carrier fluid in the re-injection region, then traveled to the splitting region. In the splitting region, the droplet fluidic channel expands. Voltages were applied to the electrodes at inlets 3 and 4 in Figure 3-2A to produce an electric field across the splitting region. To prevent droplet coalescence in the re-injection region, a grounded salt-water moat surrounds the droplet inlet (5 in Figure 3-2A). After the splitting region, the main fluidic channel bifurcates to two outlets to collect split droplets (6 in Figure 3-2A).

In traditional droplet sorting schemes, the electric field is applied on one side of the channel and droplets experience dielectrophoretic force in the direction of the field.[7] To induce opposing dielectrophoretic forces, two electrodes with AC potentials 180° out of phase were employed. A recorded voltage trace of the two applied electrodes is shown in Figure 3-2B. Each electrode alternated at 45 kHz.

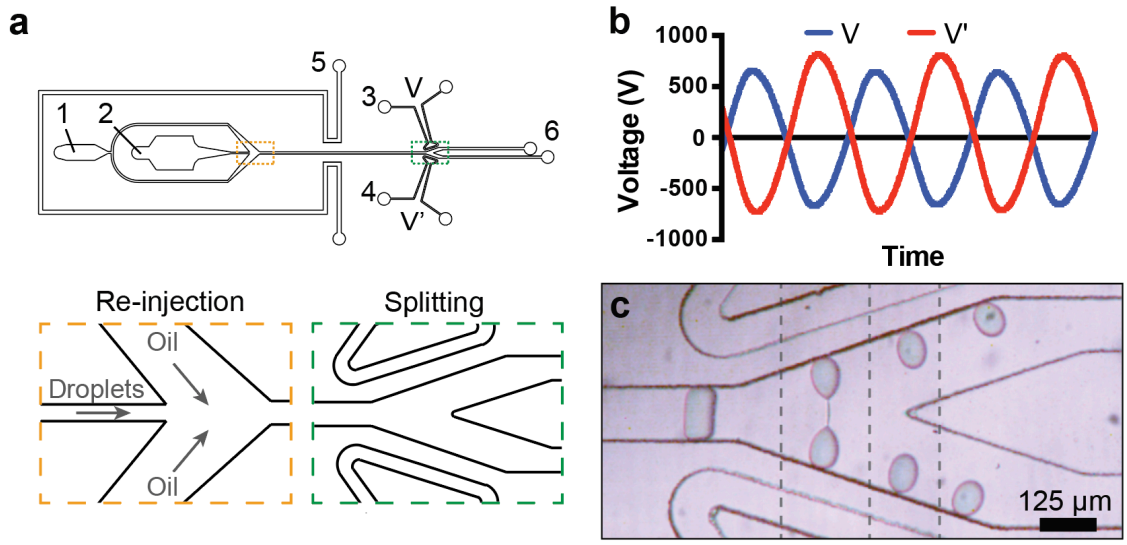

Figure 3-2 Field-induced droplet splitting operating principles. (A) Schematic of simple droplet splitting device. Fluidic connections are labeled: 1-carrier fluid inlet, 2-droplet re-injection inlet, 3 electrode inlet V, 4-electrode inlet V', 5-shielding electrode inlet, 6-outlets. Insets show expanded views of the re-injection and splitting regions. (B) Example waveform of electric potential applied to V and V'. Example trace shown is over 70 µs. (C) Composite micrograph of a single 850 pL droplet splitting over 30 ms. Dashed lines represent edge of stitched still-frames.

Figure 3-2C shows one droplet splitting within the splitting region shown in Figure 3-2A. For this test, a population of 850 pL droplets containing 1% green food dye was pumped into the device at 10 droplets/s. Micrographs were taken over 30 ms and stitched together (denoted with dashed lines) to show a time course of the droplet splitting progression (Figure 3-2C). Droplets expand within the incoming channel upon their introduction to the field due to the rapidly alternating dielectrophoretic force perpendicular to the direction of droplet flow. The competing dielectrophoretic forces act most strongly upon the droplet pole nearest the respective electrode, causing stretching and ultimately splitting. After splitting, the droplets are held to the channel walls due to the dielectrophoretic forces from the two opposing electrodes. In addition to bifurcated channels (one channel split to two outlets as in Figure 3-2), field-induced droplet splitting also occurs in simple channel expansions where the droplet may split in a local high field then flow to a single outlet (Figure 3-3). On-demand droplet splitting to a single outlet has been shown using SAWs for particle enrichment and increased droplet generation throughput.[30]

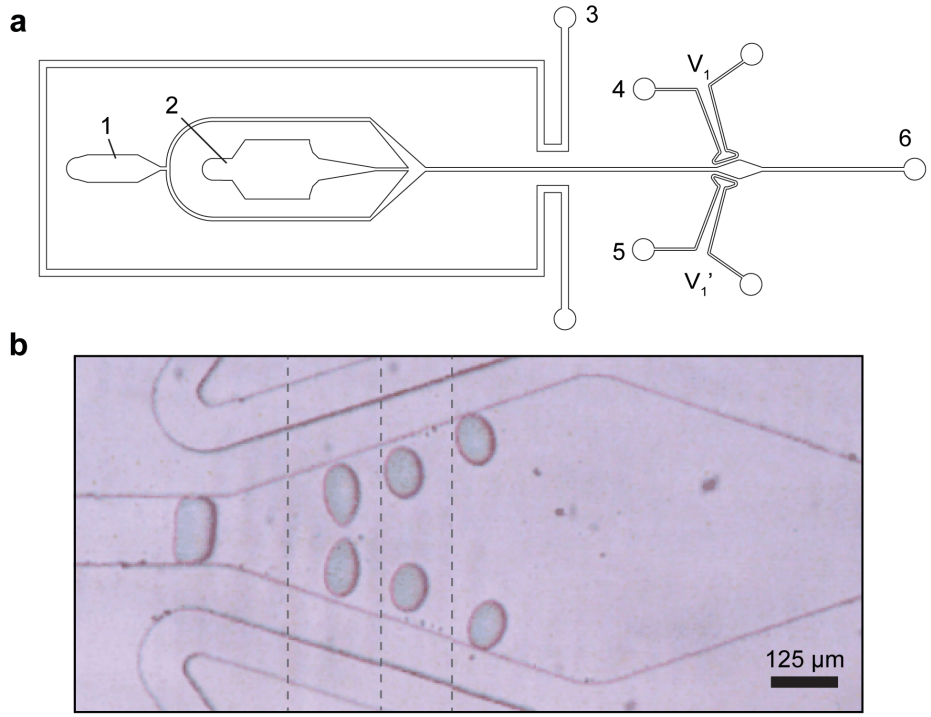

Figure 3-3: Device design for field assisted droplet splitting with a simple channel expansion. (A) Channel expands then continues to a single outlet. Fluidic connections are labeled: 1-oil inlet, 2-droplet re-injection inlet, 3-shielding electrode inlet, 4- electrode inlet V, 5- electrode inlet V', 6-outlet. (B) Time lapse micrograph of a single 600 pL droplet splitting in the channel expansion. Dotted lines represent edges of the stitched frames.

Electric Field Requirements. Dielectrophoretic principles demonstrate that the force upon the droplet is proportional to field strength.[7] Similarly, field-induced droplet splitting depends on the strength of the field, i.e the competing dielectrophoretic forces must be strong enough to overcome the surface tension of the droplets. To demonstrate this threshold, 850 pL droplets were re-injected into a splitting device and the applied voltage was increased incrementally while measuring the applied voltage. As shown in Figure 3-4, from 0 – 420 V_{pp} no effect was observed; the droplets collided with the bifurcating pillar and alternated flow to each of the two outlets. Dielectrophoretic sorting was observed above 420 V_{pp} likely due to slight asymmetry of field intensity generated by our HV setup. At 813 V_{pp} droplet splitting began. When applying a sufficiently high voltage to electrode V but applying a true ground at electrode V', no splitting is observed. Additionally, applying AC potentials that are not 180° out of phase with each

other to electrodes V and V' did not result in droplet splitting. We conclude that two voltages must be applied that are of the same frequency and magnitude, and that are strong enough to induce significant DEP to overcome droplet surface tension.

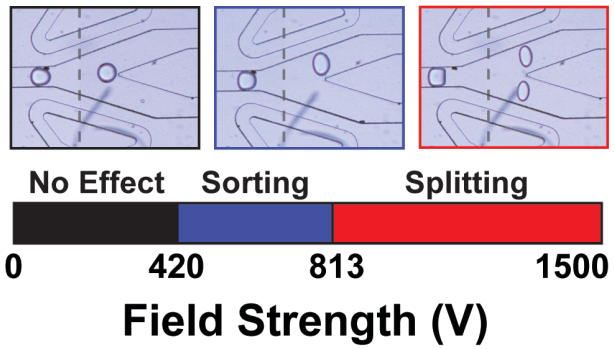

Figure 3-4: Effect of increasing field strength on droplet manipulation. Composite micrographs are shown for 850 pL droplets entering the splitting region at low (black), moderate (blue), and high (red) fields. Dashed lines represent edge of stitched still-frames. Effective DEP sorting was observed above 420 V_{pp} and field-assisted splitting was observed above 813 V_{pp}

Device Design Requirements. Although droplet splitting is actuated using an electric field, the channel geometry is a contributing factor to droplet splitting. It is necessary that the electrodes be symmetrical about the splitting region to induce the equal dielectrophoretic forces. Additionally, droplets must be able to expand significantly (>2x the droplet diameter) within the splitting region, which allows the two droplet halves to separate enough to split (Figure 3-5). Droplet splitting was observed for droplets both larger and smaller than channel height, which was held at 100 μm for all experiments. As such, splitting occurs in the plane of electric field, and whether or not droplets contact the top or bottom of the channel does not appear to be significant.

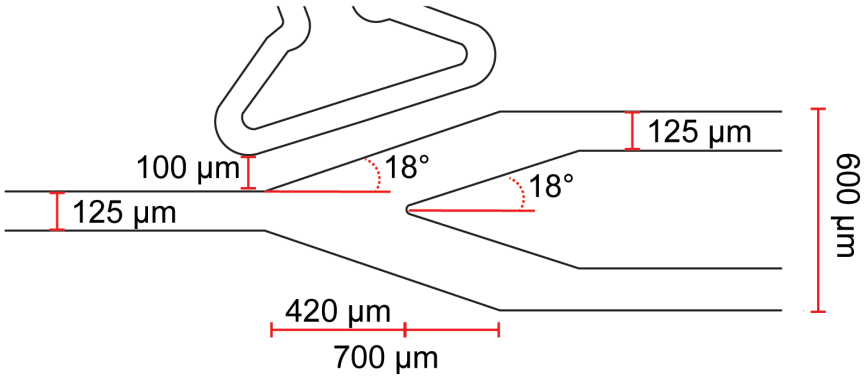

Figure 3-5: Detailed microfluidic geometry for performing droplet splitting. This design was tested for splitting of 400 – 1000 pL droplets. Devices were designed as shown and fabricated with 100 µm channel height. Lower electrode is removed for labeling purposes but is symmetrical relative to the channel. Incoming droplet channel is 125 µm, then expands at an 18° over 700 µm to achieve 600 µm separation. The outlet channels are 125 µm. The electrodes are fabricated 100 µm from the channel, with slight overlap with the incoming channel to allow for deformation before entering splitting region

It was discovered that splitting regions with a less drastic expansion resulted in dielectrophoretic trapping (Figure 3-6A), indicating that the rate of channel expansion is also a contributing factor. With a smaller channel expansion, the droplets are slowed and stopped due to the competing dielectrophoretic forces without reaching the critical channel dimensions for splitting (Figure 3-6B). For this demonstration, a population of 750 pL droplets with 1% green food dye was generated, stored, and re-injected into trapping devices with the field held at 1.5 kV. Droplets were trapped as a prolate within high field regions despite oil constantly flowing to the outlet. The prolate shape is due to the competing dielectrophoretic forces distorting the droplets. Upon entry of a second 750 pL droplet in this geometry, the droplet displaces the first with both droplets flowing to the outlet, leaving the region available for a new droplet to be trapped. The trapping effect can be used to merge sequential droplets with higher oil flow rates. Similar to on-demand droplet splitting, on-demand trapping may be achieved by pulsing the electric field to capture a droplet before releasing it after a predetermined time.

Droplet traps are useful for droplet analysis, where monitoring inter-droplet reactions by UV, fluorescence, or Raman detection can be performed on a single droplet due to increased

residence time within a detection point. Physical trapping mechanisms have been developed, but may not be turned off and rely on complex valving and fabrication protocols.[49–51] Droplet and particle trapping is commonly reported in digital microfluidics,[52], and dielectrophoretic particle/droplet trapping,[53,54] but has not been reported for continuous flow droplet microfluidics.

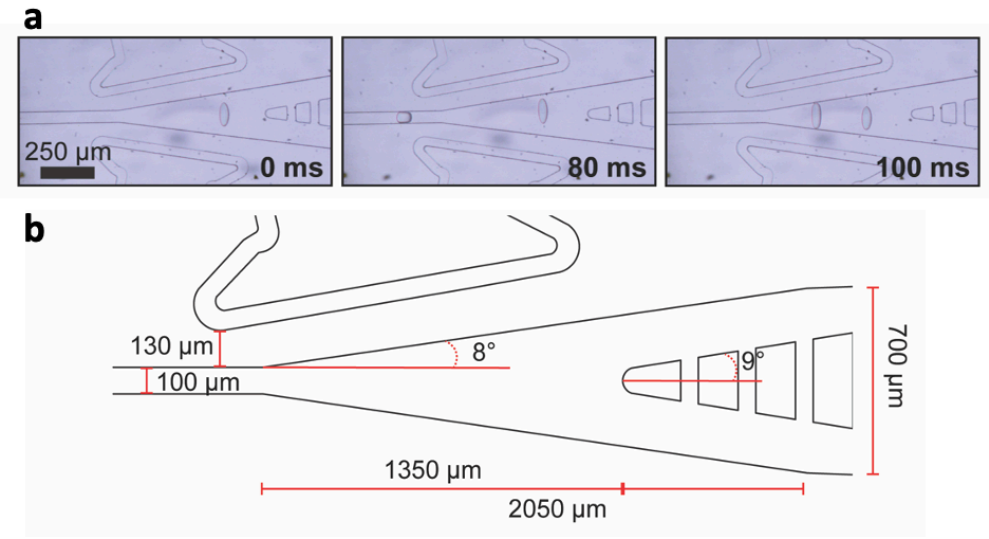

Figure 3-6: Droplet trapping using electric fields. (A). Micrographs of droplet trapping over 100 ms. With a 1 kVpp field applied to the electrodes, a 750 pL droplet is confined within the field as a prolate. The droplet is parked within a 75 µm window as long as the field is sustained. A second droplet is shown to enter the high field region, which displaces the first and both flow to the outlets. (B). Device design for trapping 750 pL droplets. Incoming channel is 100 µm then expands at 8° over 2050 µm to achieve 700 µm separation. The electrodes are fabricated 130 µm from the channel with slight overlap to begin trapping before entering the trapping region. The electrodes are elongated to span the entire region, allowing for effective droplet trapping.

Splitting Characterization. A drawback to many microfluidic operations is the inability to process droplet populations with volume heterogeneity, which may arise from thermocycling or shear stresses during reinjection.[55] Passive droplet size sorters have been integrated into larger droplet workflows to address this concern, such that unit operations may continue as intended with a monodisperse population.[56] For droplet splitting with static geometric splitters, incoming droplet size heterogeneity may lead to ineffective splitting due to the variable back pressures caused by inconsistent split ratios or an inability to split sheared droplets altogether. To assess the flexibility of field-induced droplet splitting by a single device design, populations of 420, 600 and 1000 pL surfactant stabilized droplets were generated using standard flow focusing devices, mixed, and

stored. The populations were re-injected into the splitting device geometry shown in Figure 3-2A. All droplets from the three populations experienced field-induced droplet splitting. For each population, the variability in the resulting split droplet volume was below 10% relative standard deviation (Table 3-1), suggesting field-induced droplet splitting is consistent despite a range of droplet sizes. The % RSD on 1000 pL droplet samples was undetermined as each split droplet resulted in the same size according to image analysis. Higher resolution cameras may have detected a difference, the variability is still very low. All splitting ratios (volume ratio of the daughter droplets) were approximately equal indicating no relationship between droplet split ratio was observed as a function of voltage. We observed no upper limit of throughputs achievable, though we investigated up to 25 droplets/s. Similar splitting demonstrations have reported throughputs between 2-13 droplets/s.[30,31,44,57]

Table 3-1: Splitting volumes and variability

Initial droplet volume (pL)	% RSD on final droplet volume	n (droplets)
420	4.9	13
600	6.1	21
1000	n/a	17

For many splitting needs, such as multiplexed analysis of droplet samples, it is necessary that the splitting event does not change the chemical composition. Previously, it has been shown that embedded electrodes cause in-droplet separation of charged species,[12,57] such as fluorescein (anionic at pH 7.4). To determine if chemical composition was altered by field-induced droplet splitting, 1 nL droplets containing 1 μM fluorescein buffered to pH 7.4 (Tris) were split and monitored through fluorescent imaging (Figure 3-7A). Equal fluorescent intensities were observed in the split droplets, suggesting chemical composition is equivalent post-split (Figure 3-7B). Separation does not occur in this system since no uniform electric field is used. This feature makes

the electric field-induced splitting method useful for aliquoting purposes where changing the sample is not desired.

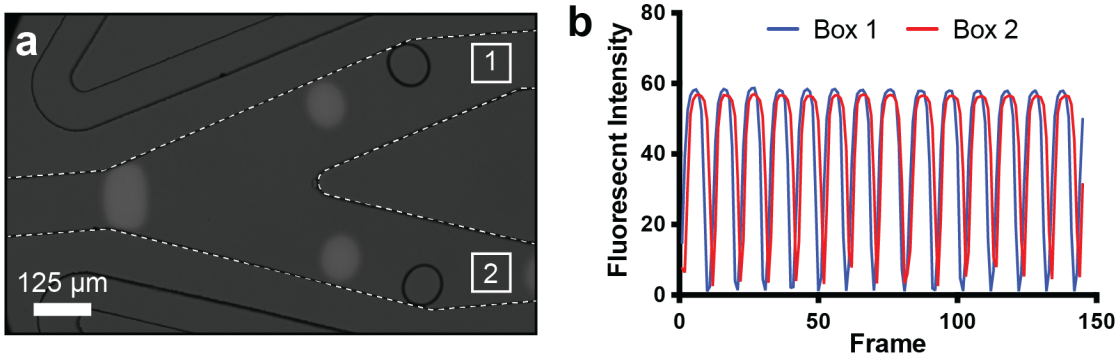

Figure 3-7: Test of chemical composition through splitting. (A) Fluorescent image of fluorescein-containing droplets splitting in an electric field overlaid on a brightfield image of the same region. Dashed lines show the channel boarders. The boxes denote locations of fluorescent measurements. (B) Fluorescent signal of post-split droplets by monitoring along the top (box 1) and the bottom (box 2) channels over 150 frames (14 droplets).

A main advantage of electric field-induced splitting over geometric splitting is the potential to select specific droplets for splitting. We tested the feasibility for on-demand splitting by manually turning the electric field generation device on and off as 800 pL droplets flowed through the device. While the electric field was off the droplet remains intact but when turned on the droplets split. The effect is rapid, e.g. one droplet does not split while a second droplet 200 ms later experiences field-induced droplet splitting. The limitations of droplet splitting throughput are dictated by the electric field actuation, which has been shown to be possible at 30 kHz for FADS.[58]

On demand droplet splitting may be useful in a variety of workflows, for example after detecting presence of a feature (e.g. by LIF) the droplet may be split for downstream functions or storage. A merged droplet detected by LIF can be selectively split and reintegrated into the droplet population as a way of filtering and correcting heterogeneous droplet populations. Additionally, for destructive, lower throughput approaches such as electrospray mass spectrometry[59] droplets can be preliminarily screened using optical detection, and only droplets of interest are aliquoted for MS. This technique would be useful for deconvolution of empty droplets during data analysis

or live tracking during mass-activated droplet sorting.[29] Similarly, on-demand droplet splitting may be useful for droplet deposition techniques,[41] where a pre-analyzed droplet may be split for deposition for sequencing or complementary analytical techniques such as matrix assisted laser desorption ionization (MALDI) mass spectrometry.[60,61] This technique could be used to reduce droplet deposition of empty droplets, while still maintaining a droplet duplicate for sequencing or further analysis after MALDI.

3.4 Conclusions

A new technique for droplet splitting inside microfluidic devices is demonstrated over a range of droplet sizes. By nature of the electric field as the mechanism for droplet fission, a "splitting-on-demand" platform is possible, which may be useful in larger droplet microfluidic workflows. Design (geometry and electric field) considerations are included for implementing droplet splitting into existing workflows. The ability to perform droplet DEP in multiple directions may allow for a broader range of droplet operations in addition to the splitting and trapping shown here. Integrating multiple electric fields is an easy technique for droplet manipulation beyond the scope of simple sorting strategies demonstrated until now.

3.5 References

(1) Chiu, D. T.; Lorenz, R. M.; Jeffries, G. D. M. Droplets for Ultrasmall-Volume Analysis. *Anal. Chem.* **2009**, *81* (13), 5111–5118. https://doi.org/10.1021/ac900306q.

(2) Li, L.; Boedicker, J. Q.; Ismagilov, R. F. Using a Multijunction Microfluidic Device To Inject Substrate into an Array of Preformed Plugs without Cross-Contamination: Comparing Theory and Experiments. *Anal. Chem.* **2007**, *79* (7), 2756–2761. https://doi.org/10.1021/ac062179n.

(3) Abate, A. R.; Hung, T.; Mary, P.; Agresti, J. J.; Weitz, D. A. High-Throughput Injection with Microfluidics Using Picoinjectors. *PNAS* **2010**, *107* (45), 19163–19166. https://doi.org/10.1073/pnas.1006888107.

(4) Lee, H.; Xu, L.; Oh, K. W. Droplet-Based Microfluidic Washing Module for Magnetic Particle-Based Assays. *Biomicrofluidics* **2014**, *8* (4), 044113. https://doi.org/10.1063/1.4892495.

(5) Mary, P.; Studer, V.; Tabeling, P. Microfluidic Droplet-Based Liquid−Liquid Extraction. *Anal. Chem.* **2008**, *80* (8), 2680–2687. https://doi.org/10.1021/ac800088s.
(6) Wells, S. S.; Kennedy, R. T. High-Throughput Liquid–Liquid Extractions with Nanoliter Volumes. *Anal. Chem.* **2020**, acs.analchem.9b04915. https://doi.org/10.1021/acs.analchem.9b04915.
(7) Ahn, K.; Kerbage, C.; Hunt, T. P.; Westervelt, R. M.; Link, D. R.; Weitz, D. A. Dielectrophoretic Manipulation of Drops for High-Speed Microfluidic Sorting Devices. *Appl. Phys. Lett.* **2006**, *88* (2), 024104. https://doi.org/10.1063/1.2164911.
(8) Baret, J.-C.; J. Miller, O.; Taly, V.; Ryckelynck, M.; El-Harrak, A.; Frenz, L.; Rick, C.; L. Samuels, M.; Brian Hutchison, J.; J. Agresti, J.; R. Link, D.; A. Weitz, D.; D. Griffiths, A. Fluorescence-Activated Droplet Sorting (FADS): Efficient Microfluidic Cell Sorting Based on Enzymatic Activity. *Lab on a Chip* **2009**, *9* (13), 1850–1858. https://doi.org/10.1039/B902504A.
(9) Shang, L.; Cheng, Y.; Zhao, Y. Emerging Droplet Microfluidics. *Chemical Reviews* **2017**, *117* (12), 7964–8040. https://doi.org/10.1021/acs.chemrev.6b00848.
(10) Link, D. R.; Anna, S. L.; Weitz, D. A.; Stone, H. A. Geometrically Mediated Breakup of Drops in Microfluidic Devices. *Phys. Rev. Lett.* **2004**, *92* (5), 054503. https://doi.org/10.1103/PhysRevLett.92.054503.
(11) Nie, J.; Kennedy, R. T. Sampling from Nanoliter Plugs via Asymmetrical Splitting of Segmented Flow. *Anal. Chem.* **2010**, *82* (18), 7852–7856. https://doi.org/10.1021/ac101723x.
(12) Link, D. R.; Grasland-Mongrain, E.; Duri, A.; Sarrazin, F.; Cheng, Z.; Cristobal, G.; Marquez, M.; Weitz, D. A. Electric Control of Droplets in Microfluidic Devices. *Angewandte Chemie* **2006**, *118* (16), 2618–2622. https://doi.org/10.1002/ange.200503540.
(13) Huang, Y.; L. Wang, Y.; N. Wong, T. AC Electric Field Controlled Non-Newtonian Filament Thinning and Droplet Formation on the Microscale. *Lab on a Chip* **2017**, *17* (17), 2969–2981. https://doi.org/10.1039/C7LC00420F.
(14) Teo, A. J. T.; Yan, M.; Dong, J.; Xi, H.-D.; Fu, Y.; Tan, S. H.; Nguyen, N.-T. Controllable Droplet Generation at a Microfluidic T-Junction Using AC Electric Field. *Microfluid Nanofluid* **2020**, *24* (3), 21. https://doi.org/10.1007/s10404-020-2327-6.
(15) Wu, Y.; Fu, T.; Ma, Y.; Z. Li, H. Ferrofluid Droplet Formation and Breakup Dynamics in a Microfluidic Flow-Focusing Device. *Soft Matter* **2013**, *9* (41), 9792–9798. https://doi.org/10.1039/C3SM51860D.
(16) Tan, S.-H.; Nguyen, N.-T.; Yobas, L.; Kang, T. G. Formation and Manipulation of Ferrofluid Droplets at a MicrofluidicT-Junction. *J. Micromech. Microeng.* **2010**, *20* (4), 045004. https://doi.org/10.1088/0960-1317/20/4/045004.
(17) Zhang, K.; Liang, Q.; Ma, S.; Mu, X.; Hu, P.; Wang, Y.; Luo, G. On-Chip Manipulation of Continuous Picoliter-Volume Superparamagnetic Droplets Using a Magnetic Force. *Lab on a Chip* **2009**, *9* (20), 2992–2999. https://doi.org/10.1039/B906229G.
(18) Chen, A.; Byvank, T.; Chang, W.-J.; Bharde, A.; Vieira, G.; L. Miller, B.; J. Chalmers, J.; Bashir, R.; Sooryakumar, R. On-Chip Magnetic Separation and Encapsulation of Cells in Droplets. *Lab on a Chip* **2013**, *13* (6), 1172–1181. https://doi.org/10.1039/C2LC41201B.
(19) Varma, V. B.; Ray, A.; Wang, Z. M.; Wang, Z. P.; Ramanujan, R. V. Droplet Merging on a Lab-on-a-Chip Platform by Uniform Magnetic Fields. *Scientific Reports* **2016**, *6* (1), 37671. https://doi.org/10.1038/srep37671.

(20) Jung, J. H.; Lee, K. H.; Lee, K. S.; Ha, B. H.; Oh, Y. S.; Sung, H. J. Optical Separation of Droplets on a Microfluidic Platform. *Microfluidics and Nanofluidics* **2014**, *16* (4), 635–644. https://doi.org/10.1007/s10404-013-1263-0.
(21) Jung, J. H.; Lee, K. H.; Destgeer, G.; Lee, K. S.; Cho, H.; Ha, B. H.; Sung, H. J. In Situ Seriate Droplet Coalescence under an Optical Force. *Microfluidics and Nanofluidics* **2015**, *18* (5–6), 1247–1254. https://doi.org/10.1007/s10404-014-1522-8.
(22) Baroud, C. N.; Vincent, M. R. de S.; Delville, J.-P. An Optical Toolbox for Total Control of Droplet Microfluidics. *Lab Chip* **2007**, *7* (8), 1029–1033. https://doi.org/10.1039/B702472J.
(23) Schmid, L.; Franke, T. Acoustic Modulation of Droplet Size in a T-Junction. *Appl. Phys. Lett.* **2014**, *104* (13), 133501. https://doi.org/10.1063/1.4869536.
(24) Schmid, L.; Franke, T. SAW-Controlled Drop Size for Flow Focusing. *Lab Chip* **2013**, *13* (9), 1691–1694. https://doi.org/10.1039/C3LC41233D.
(25) Sesen, M.; Alan, T.; Neild, A. Microfluidic Plug Steering Using Surface Acoustic Waves. *Lab Chip* **2015**, *15* (14), 3030–3038. https://doi.org/10.1039/C5LC00468C.
(26) Collignon, S.; Friend, J.; Yeo, L. Planar Microfluidic Drop Splitting and Merging. *Lab Chip* **2015**, *15* (8), 1942–1951. https://doi.org/10.1039/C4LC01453G.
(27) Gielen, F.; Hours, R.; Emond, S.; Fischlechner, M.; Schell, U.; Hollfelder, F. Ultrahigh-Throughput–Directed Enzyme Evolution by Absorbance-Activated Droplet Sorting (AADS). *PNAS* **2016**, *113* (47), E7383–E7389. https://doi.org/10.1073/pnas.1606927113.
(28) Wang, X.; Ren, L.; Su, Y.; Ji, Y.; Liu, Y.; Li, C.; Li, X.; Zhang, Y.; Wang, W.; Hu, Q.; Han, D.; Xu, J.; Ma, B. Raman-Activated Droplet Sorting (RADS) for Label-Free High-Throughput Screening of Microalgal Single-Cells. *Anal. Chem.* **2017**, *89* (22), 12569–12577. https://doi.org/10.1021/acs.analchem.7b03884.
(29) Holland-Moritz, D. A.; Wismer, M. K.; Mann, B. F.; Farasat, I.; Devine, P.; Guetschow, E. D.; Mangion, I.; Welch, C. J.; Moore, J. C.; Sun, S.; Kennedy, R. T. Mass Activated Droplet Sorting (MADS) Enables High-Throughput Screening of Enzymatic Reactions at Nanoliter Scale. *Angewandte Chemie International Edition* **2020**, *59* (11), 4470–4477. https://doi.org/10.1002/anie.201913203.
(30) Ho Jung, J.; Destgeer, G.; Ha, B.; Park, J.; Jin Sung, H. On-Demand Droplet Splitting Using Surface Acoustic Waves. *Lab on a Chip* **2016**, *16* (17), 3235–3243. https://doi.org/10.1039/C6LC00648E.
(31) Park, J.; Ho Jung, J.; Park, K.; Destgeer, G.; Ahmed, H.; Ahmad, R.; Jin Sung, H. On-Demand Acoustic Droplet Splitting and Steering in a Disposable Microfluidic Chip. *Lab on a Chip* **2018**, *18* (3), 422–432. https://doi.org/10.1039/C7LC01083D.
(32) Serra, M.; Gontran, E.; Hajji, I.; Malaquin, L.; Viovy, J.-L.; Descroix, S.; Ferraro, D. Development of a Droplet Microfluidics Device Based on Integrated Soft Magnets and Fluidic Capacitor for Passive Extraction and Redispersion of Functionalized Magnetic Particles. *Advanced Materials Technologies* **2020**, *5* (4), 1901088. https://doi.org/10.1002/admt.201901088.
(33) Pamme, N. Magnetism and Microfluidics. *Lab on a Chip* **2006**, *6* (1), 24–38. https://doi.org/10.1039/B513005K.
(34) Sciambi, A.; Abate, A. Generating Electric Fields in PDMS Microfluidic Devices with Salt Water Electrodes. *Lab on a Chip* **2014**, *14* (15), 2605–2609. https://doi.org/10.1039/C4LC00078A.

(35) B. Berry, S.; J. Lee, J.; Berthier, J.; Berthier, E.; B. Theberge, A. Droplet Incubation and Splitting in Open Microfluidic Channels. *Analytical Methods* **2019**, *11* (35), 4528–4536. https://doi.org/10.1039/C9AY00758J.
(36) Chen, Z.; Chen, B.; He, M.; Hu, B. Droplet-Splitting Microchip Online Coupled with Time-Resolved ICPMS for Analysis of Released Fe and Pt in Single Cells Treated with FePt Nanoparticles. *Anal. Chem.* **2020**, *92* (18), 12208–12215. https://doi.org/10.1021/acs.analchem.0c01217.
(37) Fornell, A.; Liu, Z.; Tenje, M. Optimisation of the Droplet Split Design for High Acoustic Particle Enrichment in Droplet Microfluidics. *Microelectronic Engineering* **2020**, *226*, 111303. https://doi.org/10.1016/j.mee.2020.111303.
(38) Pan, X.; Zeng, S.; Zhang, Q.; Lin, B.; Qin, J. Sequential Microfluidic Droplet Processing for Rapid DNA Extraction. *ELECTROPHORESIS* **2011**, *32* (23), 3399–3405. https://doi.org/10.1002/elps.201100078.
(39) Cho, S. K.; Zhao, Y.; Kim, C.-J. "CJ." Concentration and Binary Separation of Micro Particles for Droplet-Based Digital Microfluidics. *Lab Chip* **2007**, *7* (4), 490–498. https://doi.org/10.1039/B615665G.
(40) Chen, Y.; Gao, W.; Zhang, C.; Zhao, Y. Three-Dimensional Splitting Microfluidics. *Lab on a Chip* **2016**, *16* (8), 1332–1339. https://doi.org/10.1039/C6LC00186F.
(41) Cole, R. H.; Tang, S.-Y.; Siltanen, C. A.; Shahi, P.; Zhang, J. Q.; Poust, S.; Gartner, Z. J.; Abate, A. R. Printed Droplet Microfluidics for on Demand Dispensing of Picoliter Droplets and Cells. *PNAS* **2017**, *114* (33), 8728–8733. https://doi.org/10.1073/pnas.1704020114.
(42) Agnihotri, S. N.; Raveshi, M. R.; Bhardwaj, R.; Neild, A. Microfluidic Valves for Selective On-Chip Droplet Splitting at Multiple Sites. *Langmuir* **2020**, *36* (5), 1138–1146. https://doi.org/10.1021/acs.langmuir.9b03515.
(43) Um, E.; E. Rogers, M.; A. Stone, H. Combinatorial Generation of Droplets by Controlled Assembly and Coalescence. *Lab on a Chip* **2013**, *13* (23), 4674–4680. https://doi.org/10.1039/C3LC50957E.
(44) Raveshi, M. R.; Agnihotri, S. N.; Sesen, M.; Bhardwaj, R.; Neild, A. Selective Droplet Splitting Using Single Layer Microfluidic Valves. *Sensors and Actuators B: Chemical* **2019**, *292*, 233–240. https://doi.org/10.1016/j.snb.2019.04.115.
(45) Xi, H.-D.; Guo, W.; Leniart, M.; Chong, Z. Z.; Tan, S. H. AC Electric Field Induced Droplet Deformation in a Microfluidic T-Junction. *Lab Chip* **2016**, *16* (16), 2982–2986. https://doi.org/10.1039/C6LC00448B.
(46) Chaudhuri, J.; Timung, S.; Dandamudi, C. B.; Mandal, T. K.; Bandyopadhyay, D. Discrete Electric Field Mediated Droplet Splitting in Microchannels: Fission, Cascade, and Rayleigh Modes. *Electrophoresis* **2017**, *38* (2), 278–286. https://doi.org/10.1002/elps.201600276.
(47) Xia, Y.; Rogers, J. A.; Paul, K. E.; Whitesides, G. M. Unconventional Methods for Fabricating and Patterning Nanostructures. *Chem. Rev.* **1999**, *99* (7), 1823–1848. https://doi.org/10.1021/cr980002q.
(48) Mahler, L.; Tovar, M.; Weber, T.; Brandes, S.; Rudolph, M. M.; Ehgartner, J.; Mayr, T.; Figge, M. T.; Roth, M.; Zang, E. Enhanced and Homogeneous Oxygen Availability during Incubation of Microfluidic Droplets. *RSC Adv.* **2015**, *5* (123), 101871–101878. https://doi.org/10.1039/C5RA20118G.

(49) Huebner, A.; Bratton, D.; Whyte, G.; Yang, M.; deMello, A. J.; Abell, C.; Hollfelder, F. Static Microdroplet Arrays: A Microfluidic Device for Droplet Trapping, Incubation and Release for Enzymatic and Cell-Based Assays. *Lab Chip* **2009**, *9* (5), 692–698. https://doi.org/10.1039/B813709A.
(50) Wang, W.; Yang, C.; Ming Li, C. On-Demand Microfluidic Droplet Trapping and Fusion for on-Chip Static Droplet Assays. *Lab on a Chip* **2009**, *9* (11), 1504–1506. https://doi.org/10.1039/B903468D.
(51) Leung, K.; Zahn, H.; Leaver, T.; Konwar, K. M.; Hanson, N. W.; Pagé, A. P.; Lo, C.-C.; Chain, P. S.; Hallam, S. J.; Hansen, C. L. A Programmable Droplet-Based Microfluidic Device Applied to Multiparameter Analysis of Single Microbes and Microbial Communities. *PNAS* **2012**, *109* (20), 7665–7670. https://doi.org/10.1073/pnas.1106752109.
(52) Hunt, T. P.; Issadore, D.; Westervelt, R. M. Integrated Circuit/Microfluidic Chip to Programmably Trap and Move Cells and Droplets with Dielectrophoresis. *Lab on a Chip* **2008**, *8* (1), 81–87. https://doi.org/10.1039/B710928H.
(53) Holmes, D.; Green, N. G.; Morgan, H. Microdevices for Dielectrophoretic Flow - through Cell Separation. *IEEE Engineering in Medicine and Biology Magazine* **2003**, *22* (6), 85–90. https://doi.org/10.1109/MEMB.2003.1266051.
(54) Voldman, J.; Gray, M. L.; Toner, M.; Schmidt, M. A. A Microfabrication-Based Dynamic Array Cytometer. *Anal. Chem.* **2002**, *74* (16), 3984–3990. https://doi.org/10.1021/ac0256235.
(55) Payne, E. M.; Holland-Moritz, D. A.; Sun, S.; Kennedy, R. T. High-Throughput Screening by Droplet Microfluidics: Perspective into Key Challenges and Future Prospects. *Lab Chip* **2020**, *20* (13), 2247–2262. https://doi.org/10.1039/D0LC00347F.
(56) Fallah-Araghi, A.; Baret, J.-C.; Ryckelynck, M.; D. Griffiths, A. A Completely in Vitro Ultrahigh-Throughput Droplet-Based Microfluidic Screening System for Protein Engineering and Directed Evolution. *Lab on a Chip* **2012**, *12* (5), 882–891. https://doi.org/10.1039/C2LC21035E.
(57) Saucedo-Espinosa, M. A.; Dittrich, P. S. In-Droplet Electrophoretic Separation and Enrichment of Biomolecules. *Anal. Chem.* **2020**, *92* (12), 8414–8421. https://doi.org/10.1021/acs.analchem.0c01044.
(58) Sciambi, A.; Abate, A. R. Accurate Microfluidic Sorting of Droplets at 30 KHz. *Lab on a Chip* **2015**, *15* (1), 47–51. https://doi.org/10.1039/C4LC01194E.
(59) Steyer, D. J.; Kennedy, R. T. High-Throughput Nanoelectrospray Ionization-Mass Spectrometry Analysis of Microfluidic Droplet Samples. *Anal. Chem.* **2019**, *91* (10), 6645–6651. https://doi.org/10.1021/acs.analchem.9b00571.
(60) Haidas, D.; Bachler, S.; Köhler, M.; Blank, L. M.; Zenobi, R.; Dittrich, P. S. Microfluidic Platform for Multimodal Analysis of Enzyme Secretion in Nanoliter Droplet Arrays. *Anal. Chem.* **2019**, *91* (3), 2066–2073. https://doi.org/10.1021/acs.analchem.8b04506.
(61) Küster, S. K.; Fagerer, S. R.; Verboket, P. E.; Eyer, K.; Jefimovs, K.; Zenobi, R.; Dittrich, P. S. Interfacing Droplet Microfluidics with Matrix-Assisted Laser Desorption/Ionization Mass Spectrometry: Label-Free Content Analysis of Single Droplets. *Anal. Chem.* **2013**, *85* (3), 1285–1289. https://doi.org/10.1021/ac3033189.

Chapter 4 Design of Strategies for High-Dilution Addition to Droplets

Figures 4-7 and 4-8 were reproduced from Sun, A. *et al, Nat. Commun.* **2020** *11 (1), 1-6* with permission from Springer Nature

4.1 Introduction

In high-throughput experiment and screening, addition of liquids by pipetting into sample vessels such as test tubes or microwell plates is a fundamental process that controls the chemistry or biology within the vessel. The ability to change the composition of a reaction with temporal control is extremely useful for performing a reaction. Adding material to a pre-existing sample can be used for reagent addition (e.g. adding the substrate to a reaction), dilution, or for buffer exchanges. Therefore, when translating MWP workflows into a miniaturized droplet process, the need to automate and miniaturize sample addition is paramount. In the development of droplet microfluidics, injector modules were developed early due to the necessity of these operations in most HTS schemes. Successful addition devices have high consistency (e.g. each droplet is dosed with reagent), low droplet-to-droplet carryover, and reliable volume addition. In addition to these basic requirements, flexibility in addition ratios (typically presented as fold-increase in droplet volume) and high throughput of addition are beneficial.

The first example of addition in the droplet format was achieved by directly injecting reagent into pre-formed droplets using a T-channel.[1] In this design, aqueous plugs flow past a perpendicular channel containing a second aqueous stream, which pushes reagent into the plug (Figure 4-1A). This strategy is extremely reliable, with early examples reporting 100% success[1] since plugs necessarily interact with the reagent stream due to a single flow path. This style of direct injection was used for protein crystal formation,[1] organic reaction screening,[2] and

nanoparticle synthesis,[3] with maximum throughputs up to 600 droplets/s and injection ratios of 1.5-fold.[2,3] However, authors reported high sample carryover, unquantified, between adjacent droplets.[1,2] Carryover occurred due to mixing between the plug and the reagent stream during injection, contaminating the reagent stream for subsequent droplet additions. The carryover was reduced to < 1% by integrating alternating blank plugs which effectively washed the reagent stream at the expense of reagent and time economy.[2]

Multiple strategies have been presented to reduce carryover in a direct-injection format. A multi-injector unit was developed to reduce carryover without wash plugs by fabricating small, sequential hydrophilic channels, which reduce the convection occurring when the plug interacts with the reagent stream.[4] This strategy quantified carryover between adjacent plugs as 0.1%, and achieved a maximum injection ratio of 1.5-fold initial droplet volume with 3% RSD.[4] A microfluidic "K-channel" was also developed to address carryover concerns.[5] After the droplet is dosed with reagent in the K-channel, the stream is flushed to an outlet which eliminated carry-over. Addition in this format was achieved at 300 droplets/s with injection ratios < 2-fold increase in volume.

Despite the development of low-carryover injection systems, a "pico-injector" design has been used most widely for droplet HTS. The pico-injector only slightly differs from a traditional T-geometry by a decrease in the injection interface and the inclusion of an electric field which facilitates addition to surfactant stabilized droplets.[6] The pico-injection strategy has been widely applied to droplets over the last ten years for the droplet PCR,[7,8] enzyme kinetics,[9] particle synthesis,[10] among many other applications[11] at rates exceeding 1000 droplets/s.[8] As the design functions in the same way as T-injectors, 100% success rate for addition has been demonstrated,[6]

but it resulted in the same cross-contamination as the T-geometry discussed previously. By using multiple injectors the cross-contamination was reduced to 1%.[8]

While strategies have been discussed for reducing carryover in direct injection designs, a major limitation remains the limited volume addition ratio. Pico-injectors consistently achieve 0.5-fold increase in droplet volume,[6] but no increases of > 2-fold increases have been reported. Low volume addition is acceptable for some applications, such as adding a reaction substrate or buffer, but higher degrees of addition are sometimes needed. For example, significant volume addition is needed to effectively dilute the sample matrix, quench a reaction, or increase droplet size. For ESI-MS in particular, each of these factors affects analytical sensitivity significantly.[12]

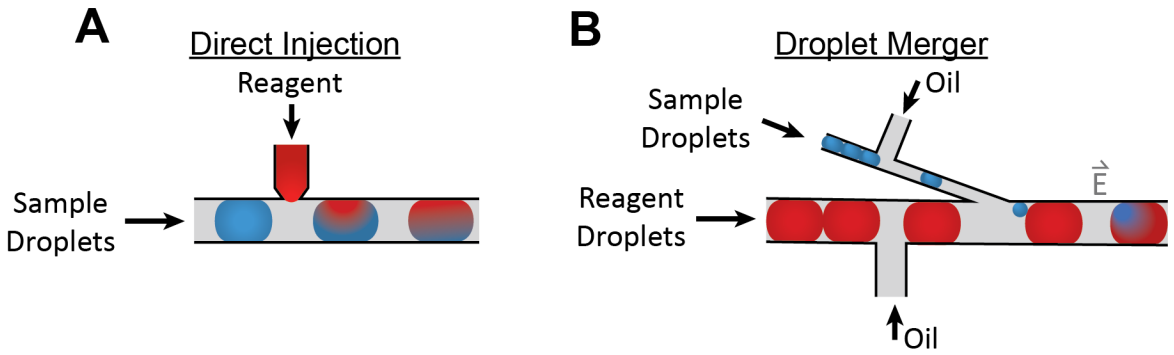

Figure 4-1: Generalized designs for direct injection and droplet merger for droplet addition. (A) Direct injection is achieved by flowing sample droplets by a continuous reagent stream, which doses each droplet. Shown here is the injection design typically used with pico-injection. (B) Droplet merger is achieved by synchronizing the injection of sample and reagent droplets, then merging them typically using an electric field.

An alternative to the direct-injection strategies above is addition via droplet merger. In this format, addition is achieved by merging two droplets. Two populations of droplets ("sample" and "reagent" droplets) are generated and stored. The droplets are pumped into a merger device where the droplets are "re-spaced" by oil, which introduces oil between droplets that have been close packed in storage. The droplets are pumped together to pair them one-to-one then they are merged (Figure 4-1B).[13,14] This merger strategy addresses two concerns with the direct-injection model. Primarily, by removing any interaction with a continuous reagent stream, sample carryover is

eliminated. Additionally, higher degrees of dilution can be achieved, as the volume added is a function of the size of reagent droplet rather than the volume injected into a sample droplet as in direct injection. For example, DNA containing sample droplets have been paired and merged with droplets containing *in vitro* transcription/translation (ivTT) reagents to express an enzyme at 250 droplets/s with a range of 4-10-fold increase in droplet volume.[15] The same design was used to perform 25-fold dilution for the same application of ivTT expression at 20 droplets/s.[16]

However, droplet merger strategies have not been widely used because the fluidics are more complicated than direct-injection strategies. The primary challenge is the need to synchronize the two streams of droplets. For this reason, the highest success rate reported was only 86%.[15] The merger design resulted in 5% of final droplets that received no sample droplet (e.g. a blank reagent droplet was generated), 3% of droplets were made from two diluent droplet and one sample droplet, 4% of droplets made from two sample droplets and one diluent droplet, and 2% of droplets were unmerged sample droplets.[15] This poor performance also resulted in high variation in final droplet volume (droplet diameter ranging from 3 – 110 μm).[15] The difficulty in synchronizing the droplets one-to-one was attributed to the difficulty to balance the four fluidic inlets corresponding to sample droplet reinjection, diluent droplet reinjection, oil spacer for sample droplets, and oil spacer for diluent droplets. While the merger strategy of addition allows for high dilution with no carryover, the low success rate and high-volume variability has resulted in few uses of this design.

Large volume changes are necessary for workflows such as mass activated droplet sorting (MADS), where small droplets (~1 nL in volume) are generated using a BioRad droplet generation system, but the droplet size required for MADS is 25 – 45 nL for compatibility with ESI-MS after splitting. Similarly, for droplet ESI-MS analysis of samples in complex matrices (e.g. high salt reaction buffers,[17] human samples[18] or cell media[19]), a dilution step via droplet addition can

improve sensitivity. For these applications, neither the direct injection nor droplet merger designs have achieved low carryover, high success rate, and large addition ratios. Therefore, development of addition strategies is needed to improve the analytical performance of these screening applications.

In this chapter, we describe two reagent addition modules that address the concerns and challenges outlined above. The first module functions like direct injection models with a key difference of a rapid channel expansion. The channel expansion is necessary to generate large, diluent droplets, which are merged during generation with smaller sample droplets (Figure 4-2A). The design has the benefits of direct injection designs, such as a high success rate, but also provides large volume additions which has not been described before. The second device presented improves upon existing droplet merger strategies by simplifying two key aspects. Reagent droplets are generated on the device, and a single oil inlet is used for both sample droplet respacing and diluent droplet generation (Figure 4-2B). By simplifying the flows into the device, a significant improvement in success rate for merger devices is achieved.

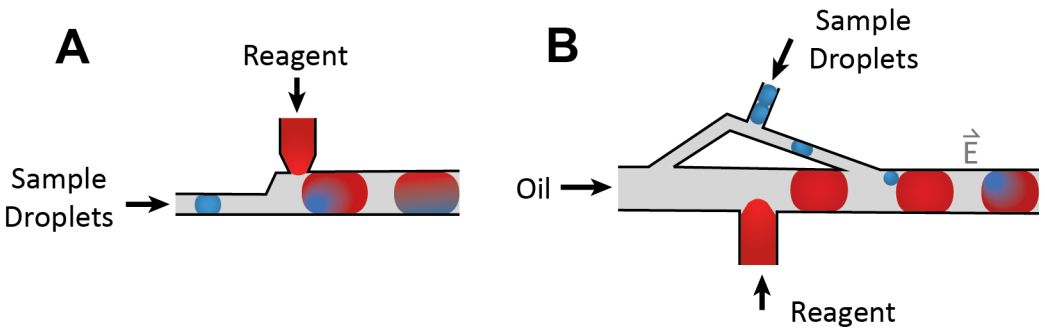

Figure 4-2: Generalized depictions of the two modules developed. (A) A step-injection design for high-dilution addition. (B) An improved droplet merger design using on-chip reagent droplet generation and a single oil inlet.

4.2 Materials and Methods

Reagents and materials. All chemicals were purchased from SigmaAldrich unless otherwise specified. HFE-7500 (3M) was used as fluorinated carrier fluid with 2 wt. % 008-

fluorosurfactant (RAN Biotechnologies). *In vitro* transcription/translation mix was purchased from New England Biolabs. Plasmid encoding green fluorescent protein was provided by Merck & Co. Reactants for Smiles-Truce rearrangement were provided by the Stephenson Lab at University of Michigan.

Device fabrication. Device design was performed using AutoCAD (Autodesk, Inc.) and a corresponding transparent mask was produced (Fineline Imaging). Standard photolithography procedures were followed.[20] Briefly, SU8 2075 negative epoxy photoresist (MicroChem Corp.) was spun to the desired thickness (200 μm) on silicon wafers (University Wafer). Wafers were patterned with the desired geometry with ultraviolet irradiation through the mask. Undeveloped photoresist was removed to produce a negative mold of the device. Polydimethylsiloxane (PDMS, Curbell Plastics) was mixed in a 1:10 activator to monomer ratio and poured over the patterned wafer. Cured devices were punched with a 30-gauge needle to add flow ports then bonded to glass slides with oxygen plasma activation (PDC-32G, Harrick Plasma, Inc.). Bound devices were flushed with perfluorodecalin (Oakwood Products Inc.) with 2% tridecafluoro-1,1,2,2-tetrahydrooctyl tricholorosilane for surface treatment.

Device operation. Device flow control was performed using an Elveflow OB1 MK3+ pressure controller supplied with nitrogen gas. Pressure was applied to the headspace of reagent vials with 30 ga PTFE tubing (Cole-Parmer) inserted into the device ports. Pressures were modulated using Elveflow Smart Interface software. Electric fields were generated using a home built high voltage system. Electrode channels were connected to syringes filled with 3 M NaCl. The voltage generator was attached to these NaCl filled syringes with alligator clips. A true ground moat was generated by connecting a salt-water electrode with a wire connected to house ground.

Device operation was performed and monitored using a Nikon TS100 inverted microscope equipped with a Phantom Miro C110 high speed camera used for visualization and data collection. Data analysis was performed using ImageJ (NIH). For tests using droplets generated in bulk, surfactant stabilized droplets were generated using flow focusing devices and stored in a modified vial as reported elsewhere.[16,21] For droplet generation from a multi well plate, samples were drawn into 150 μm inner diameter x 360 μm outer diameter PFA tubing from IDEX using a PHD 2000 Programmable syringe pump (Harvard Apparatus). 10 μL samples were deposited into 384 PCR multi well plates (Corning) with perfluorodecalin placed on top. While solution was being withdrawn through the tubing, an XYZ-position manipulator moved the tubing between sample wells and fluorous phase to form alternating droplet/carrier phase trains.

ESI-MS experiments. Two mass spectrometers were used in this work: an Agilent 6135b single quadrupole and an Agilent 6419 triple quadrupole fitted with a capillary electrophoresis sheath flow electrospray source (G1607B). Electrospray was achieved with 2.5 kV, with 350 °C drying gas set at 30 L/min, a source pressure of 10 psi, and 135 eV of fragmentor energy. The sheath liquid was water pumped at 30 μL/min. The mass spectrometers were operated in selected ion mode, monitoring for the nominal protonated mass for each of the test analytes and the nominal molecular weight of the marker compounds which each carry a permanent positive charge.

4.3 Results and Discussion

Characterization of step-injection module. To perform high-dilution addition, a step-injection device was designed as in Figure 4-3A. Droplets were first generated using standard flow focusing devices and stored in a tube as described previously.[16] As the droplets close pack during storage, the first region of the addition device is for re-injecting the pre-formed droplets and respacing them with fresh oil. The respacing oil (inlet 1 in Figure 4-3A) functions both to space

close packed droplets (inlet 2), but also to segment an additional stream of aqueous reagent (inlet 3). As the droplets are surfactant stabilized in this format, the merger of the re-injected droplet and the reagent diluent droplet is facilitated by an electric field generated via independent electrode channels (inlets 5 and 6). To reduce undesirable droplet merger of re-injected droplets, a grounded moat was designed to reduce the electric field (inlet 7), improving re-injected droplet stability. Once droplets are merged, they are exported to a single outlet (inlet 4). In the merger region, the channel is increased ("stepped") to accommodate the formation of a large diluent droplet. The step also serves to reduce flow velocity, which slows the initial sample droplet prior to merger. The electrodes are positioned such that in addition to destabilizing the droplets for merger, a DEP force is also applied to droplets in the channel. This design feature was included for extremely high dilution applications, where small droplets are pulled into the diluent stream rather than following the oil flow under the forming droplet (thereby missing reagent addition).

In an initial test of the device, a population of 800 pL droplets was produced with a droplet generation device, and the resulting emulsion was pumped into the step-injection device (Figure 4-3B). The re-injection of 800 pL droplets was synced to the formation of the ~20 nL droplets after establishing a reagent droplet generation rate. During operation, high-speed videos were acquired to evaluate the system. Figure 4-3C shows an image of the merger region, with one 800 pL droplet entering from left, and a 22 nL droplet (post-merger) flowing to the right, a 27-fold increase in droplet volume. In a video collected over 30 s, 309 additions were performed, successfully generating 22.3 nL droplets (3.8% RSD, 10 droplets/s, n = 309). No double or missed additions were observed. The droplet sizes presented here are directly applicable for the MADS experiment, where the BioRad droplet generator uses 0.8-1 nL droplets, and the MADS device requires 20-40

nL droplets.[16] This experiment demonstrates the largest fold-increase in droplet size using a direct injection device design.

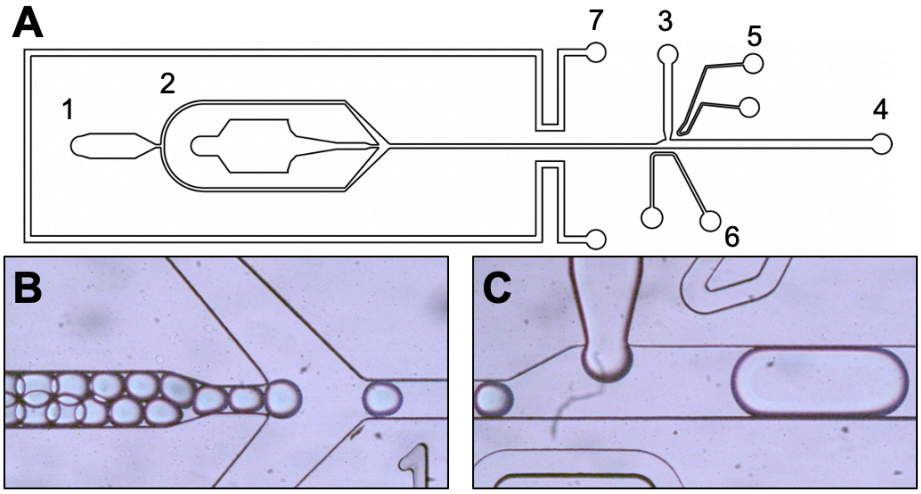

Figure 4-3: Design and example of the step-injection device. (A) Fluidic inlets are labelled; 1 – fluorinated oil, 2 – droplet re-injection, 3 – diluent stream, 4 – fluidic outlet, 5 – high-field electrode, 6 – grounding electrode, 7 – grounded moat electrode. (B) Photomicrograph of 800 pL droplet reinjection into the device. (C) Photomicrograph of the merger region, where a 28 nL droplet has been merged with an 800 pL droplet.

Evaluation of dilution factor. A primary limitation of direct-injection designs (e.g. pico-injectors) is the ability to significantly change the dilution factor. Using the step-injection device, the pressure applied to the diluent stream can be altered to change the dilution factor. To test this, 800 pL droplets were pumped into the device as before, and the pressure applied to the diluent stream was ranged from 0.6 PSI to 0.9 PSI. Droplet sizes (measured post-merger) were 14.8 nL (6.3 % RSD, n = 8 droplets), 24.1 nL (3.2% RSD, n = 13 droplets), and 29.3 nL (1.5% RSD, n = 9 droplets) when applying 0.6, 0.8, and 0.9 PSI, respectively (Figure 4-4), resulting in a 2-fold range of final droplet volumes achieved, with dilution factors up to 36-fold. In this test, pressures exceeding 0.9 PSI resulted in multiple merger events due to the forming diluent stream occupying a high volume of the merger region, so an upper limit was observed. The pressures shown here are relative to the applied pressures to the oil and reinjection inlets (0.6 PSI and 1 PSI respectively)

and attempts to increase throughput of reagent addition will require higher pressures applied to each of the ports.

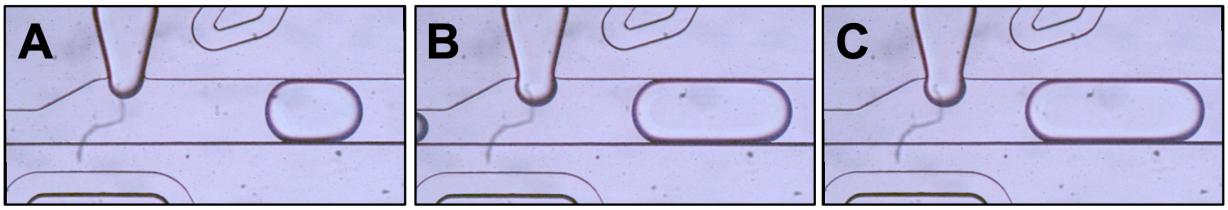

Figure 4-4: Dilution range using step-injector. Photomicrographs of diluted 800 pL droplets resulting in 14.2 nL (0.6 PSI applied, A), 23.9 nL (0.8 PSI, B), and 29.8 nL droplets (0.9 PSI, C).

While the above test showed the ability to change the final droplet volume after dilution with a fixed initial droplet volume and one device, the design also allows for different initial droplet sizes. Three droplet populations were generated (~200 – 3500 pL) and pumped into the device in Figure 4-3A. While maintaining the reagent stream pressure, a range of 8.5-fold to 146.5-fold addition was achieved with low variability on final droplet volume (Table 4-1). During these tests, missed additions were observed particularly when infusing smaller droplets. This is the result of variable re-injection frequency for smaller droplets. In the re-injection region (Figure 5-3B), the re-injected droplets are focused into single-file as the channel reduces to 150 x 100 µm cross-section. However, when the diameter of re-injected droplets approaches 100 µm (520 pL), they begin to stack, causing less consistent re-injection and therefore addition. This effect can be remediated by reducing the injection channel width or height such that the droplets do not stack. In the case of reducing the height of the channel, a multi-layer fabrication protocol must be followed to maintain the height of the channel in the merger region, which can complicate fabrication by aligning exposure masks for the two channel heights.

Table 4-1: Ranges of initial and final droplet volumes for effective dilution factor and rate of addition.

Initial Volume	Final Volume	Dilution Factor	% RSD on Final Volume	n (droplets)	Rate of 1:1 addition
3.4 nL	28.9 nL	8.5	1.5 %	41	100%
705 pL	29.6 nL	42.0	2.0 %	35	94.2%
200 pL	29.3 nL	146.5	0.9 %	44	93.2%

Evaluation of carryover. A primary concern with direct-injection modes for reagent addition is carryover between droplets via the reagent stream.[4] Carryover has been quantified when using wash droplets and multiple injectors as 0.1-1%.[3,8] To visualize the interaction between the initial droplet and the dilution stream in this format, 1.6 nL (0.5% RSD, n = 18) droplets containing 5% dye were injected into the step-injection device in Figure 4-3A. High-speed videos were obtained, and time-course images are presented in Figure 4-5. Over 31 droplets imaged, there were no instances of missed or double additions, and the final droplet volume was 16.3 nL (3.4% RSD, n = 31) representing a 10-fold dilution. The initial orange droplet interacts with the stream as a droplet is formed (Figure 4-5A) and is merged by the electric field (Figure 4-5B). The relatively high flow rate of the dilution stream pushes the dye into the forming droplet, reducing the interaction with the initial stream.

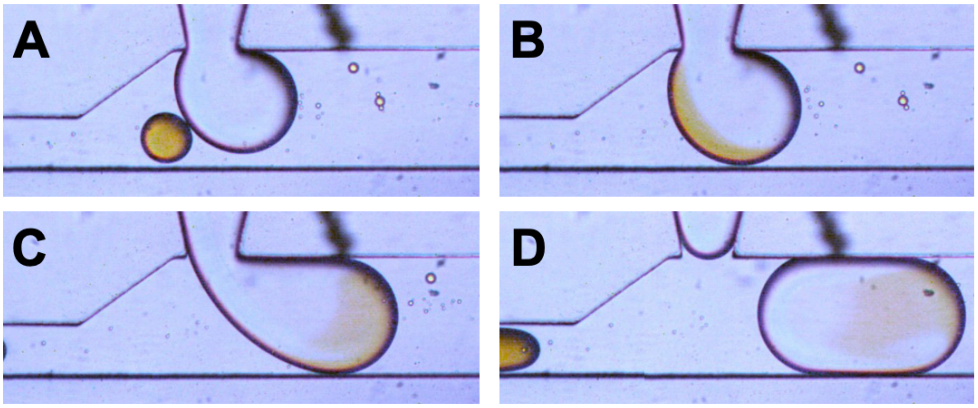

Figure 4-5: Time-course photomicrographs of a droplet merging with the dilution stream. (A) Initial droplet approaches the larger droplet forming from the reagent stream. (B) The droplets are merged due to the electric field on chip. (C) The final droplet is formed, pushing the initial droplet contents into the front of the droplet. (D) The final droplet is formed and separated from the reagent stream.

To quantify the carryover, ImageJ was used to determine the color with maximum intensity for the dye in the initial droplet, and images were processed in grayscale for the color intensity (Figure 4-6A). The gray values of the incoming droplet channel (region 1 in 4-6A) and of the reagent stream (region 2 in 4-6A) were normalized to background gray value intensity (region 3 in 4-6A) to account for differences in lighting throughout the video. The signals were then plotted as a percentage of the darkest incoming droplet in Figure 4-6B, representing a percentage (e.g. gray value of 100 represents 100% orange intensity). There are 14 initial droplets observed over 1.5 s monitored in region 1. While noise is detected monitoring the reagent stream, the signal never exceeds a value of 1, which indicates the contamination of the reagent stream remains less than 1% throughout experimentation. This level of contamination of the reagent stream is equal to that of the multiple pico-injectors used to reduce carryover in a single injector design.[8]

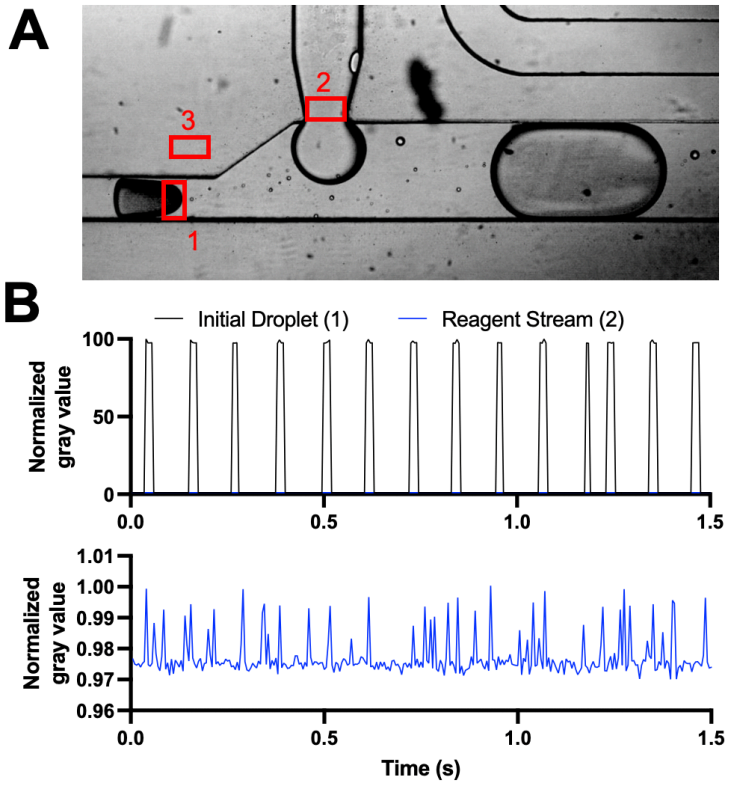

Figure 4-6: Carryover analysis of the step-injection addition device. (A) Representative grayscale image of the experiment, where darkness is a function of yellow intensity. Boxes are labelled where average grayscale values were monitored: 1 is the incoming droplet, 2 is the reagent stream, and 3 is the background signal. (B) trace of gray scale values monitored over 1.5 seconds. The top trace shows the normalized gray values for the initial droplet and reagent stream. The trace of the reagent stream is shown on a scaled axis below for interpretation.

Well-plate droplet compatibility. The presented devices have been shown for droplets generated, stored in glass vials, then re-injected into the addition device; however, some droplet based high-throughput screening is achieved by generating droplets from a modified multi-well plate.[22,23] These formats readily translate samples arrayed in wells into droplets, which can be analyzed using the same methods such as ESI-MS. The droplet dilution device was augmented to be compatible with droplets in this format by removing the droplet reinjection module and replacing it with a single channel (Figure 4-7A). The core of the device geometry was kept consistent as previously. As droplets generated from a wellplate are typically segmented with oil without surfactant, the design was made to be compatible with in-plane droplet injection and export. Additionally, droplets from a wellplate stay separated with the carrier oil during storage,

so no additional oil is needed for segmenting. While this does slighly change the fluidic dynamics within the merger region, the basic principles are the same.

The device was tested for use in a screen of organic reactions. To test the reagent addition in this format, 4 nL acetonitrile droplets were generated from a multiwell plate. The droplets were pumped into the device at 800 nL/min, and a trifluoromethylation reagent (yellow) was added to the droplets (Figure 4-7B) at 200 nL/min. The droplets post addition were 7.98 nL (4% RSD, n = 20 droplets), representing a 2-fold increase in droplet volume. This test demonstrates the utility of the device for droplets generated from a multi-well plate. To test carryover, droplets were generated with a 10x10 alternating pattern of acetonitrile with and without the reagent. Addition was performed with the same specifications as above, and acetonitrile droplets following droplets with the reagent were observed not to contain observable yellow coloration (Figure 4-7C). Based on color intensity analysis by ImageJ as in Figure 4-6, < 1% yellow signal was measured in the droplets not containing the trifluoromethylation reagent.

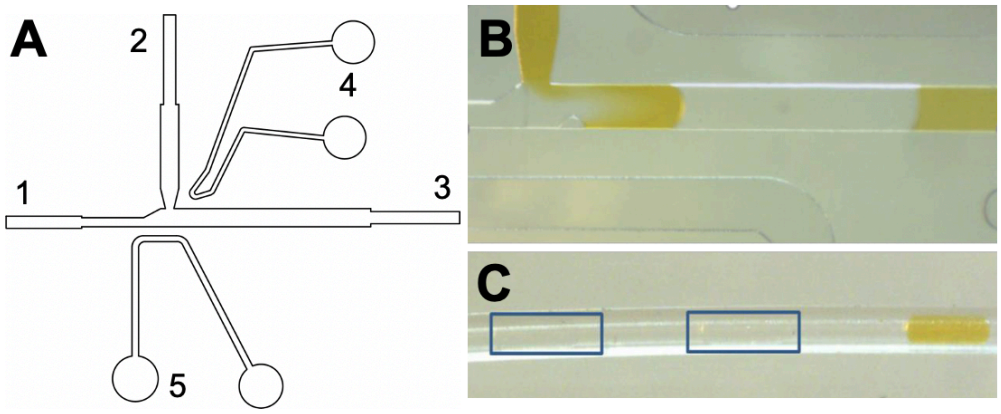

Figure 4-7: Droplet reagent addition using droplets generated from a well plate. (A) Design of the chip used for compatibility of non-surfactant stabilized droplets. Inlets are labelled; 1 – droplet injection capillary, 2 – reagent capillary, 3 – outlet capillary, 4 – high-voltage electrode and 5 – grounded electrode. (B) Image of droplet reagent addition with acetonitrile and a trifluoromethylation reagent (yellow). (C) Droplets in export capillary testing for carryover. Droplets in blue boxes do not show the yellow reagent, indicating low carryover.

The device was then applied to a proof of concept workflow for an in-flow screening platform for photocatalysis reactions. 4 nL Acetonitrile droplets containing the reaction substrate

(N-((4-cyanophenyl)sulfonyl)acetamide) were pumped into the device at 800 nL/min and dosed with photocatalyst at 200 nL/min. The outlet tubing was irradiated in a custom photoreactor for 7 minutes, and the droplets were immediately analyzed with ESI-MS at 0.3 droplets/s. The Smiles-Truce reaction product was monitored showing signal corresponding with the reaction product (Figure 4-8A) for each of the 60 droplets analyzed, suggesting every droplet was successfully dosed with photocatalyst. When the irradiation was not used, 20-fold lower MS signal was observed (Figure 4-8B), suggesting the reaction product was not successfully formed. This test demonstrates the applicability of the step-injection platform is a useful component to larger high-throughput screening efforts. By dosing reactant droplets with photocatalyst rather than adding photocatalyst to each reaction well in the MWP, this workflow consumes < 1% of the photocatalyst, increasing reagent economy.

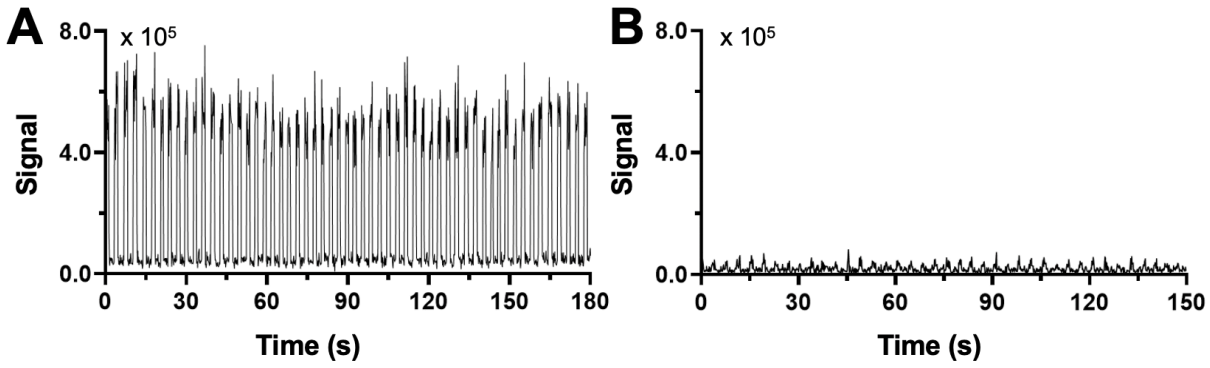

Figure 4-8: ESI-MS traces following addition of photocatalyst. ESI-MS traces for a product (EIC 309 m/z) of a Smiles-Truce rearrangement performed in-droplet. Substrate droplets were dosed with photocatalyst using reagent addition design. (A) Trace when droplets are irradiated in flow and (B) trace without irradiation.

Split droplet merger module. While the results above suggest the step-injection design is a versatile method for high-dilution droplet addition with low carryover, the design necessitates an interaction between the initial droplet and the dilution stream. While the carryover was observed to be < 1%, the possibility exists for contamination. To address this concern, we designed a variation on the step-injection module that decouples the dilution droplet generation and the merger of the initial sample droplet, which eliminates the possibility of carryover (Figure 4-9A).

The design differs from traditional pairwise-merger strategies by using a single oil stream split for both segmenting and re-spacing droplet samples. In existing pairwise merger devices (Figure 4-9B), two oil streams are used and adjusted to synchronize the two droplet streams merging, which complicates flow and set-up procedures, and has been reported as only 86% successful at achieving one-to-one addition.[15] Others have attempted to reinject droplets without oil spacing, but this method is only < 92% successful.[16] The approach presented in Figure 4-9A is a hybrid of both approaches which is beneficial for the ease of use and reliability of merger. Once the droplets are paired, they are merged by downstream electrodes which can be used in multiple orientations.

The droplet merger device operates differently from the step-injection model discussed previously. Thee critical dimension in the device is the channel size during droplet pairing and merging. The device operates on the principal that larger droplets make contact with the channel walls, where small droplets can freely flow and merge with the larger droplet. Therefore, the limits on final droplet volume are dictated by the channel dimensions, which are 450x150 μm (width x height) as designed in Figure 4-9A. To maintain contact with the channel walls the minimum final droplet size is 15.9 nL, and to maintain spatial separation between droplet pairs the maximum is 63.6 nL. Since the droplet re-injection geometry is the same as the step-injection device, the range of dilutions achievable is 3.9 – 318-fold dilution.

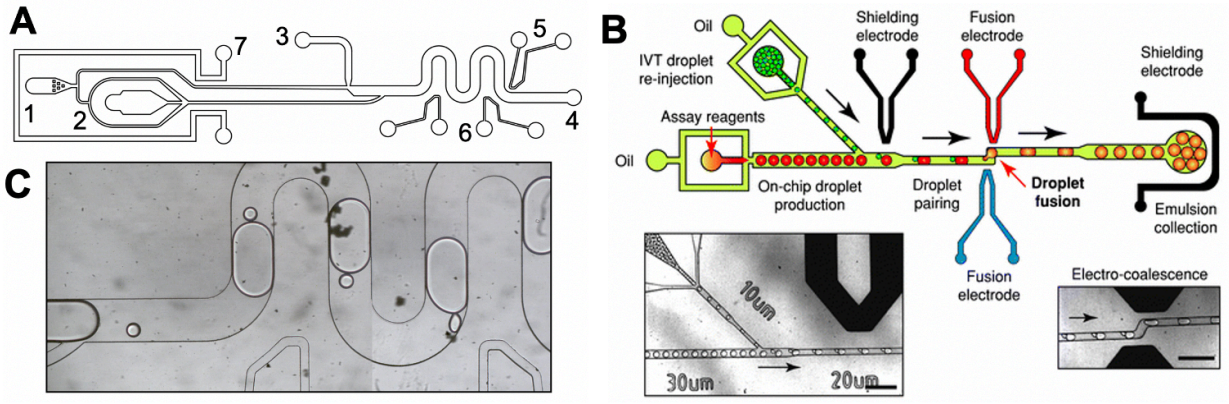

Figure 4-9: Design of the split droplet merger design for high-dilution reagent addition. (A) Fluidic inlets are labelled 1 – fluorinated oil, 2 – droplet re-injection, 3 – diluent stream, 4 – fluidic outlet, 5 – high-field electrode, 6 – grounding electrode, 7 – grounded moat electrode. (B) Design and images of a pairwise reagent addition device used by Mazutis et al. adapted with permission from the Royal Society of Chemistry (C) Image of device operation, showing the pairing of 1 nL droplets with 25 nL diluent droplets. Droplets pair and merge in the presence of an electric field.

The device was tested by pumping a population of surfactant stabilized, 1 nL droplets into the re-injection region at 25 droplets/s. Droplets from the reagent stream were generated to be 25 nL. The droplet streams were synchronized by first establishing droplet generation size and frequency from the reagent stream, then increasing the 1 nL droplet re-injection pressure until the rate of droplet generation matched the rate of reinjection (Figure 4-9C). Droplets were observed to pair and merge observed in the rightmost two droplets in Figure 4-9, resulting in 26.3 nL droplets (0.9% RSD, n = 29 droplets), which is a 27-fold addition. In this format, no contact between the reagent stream and the initial sample droplets is made, so the potential of carryover is eliminated.

Since the droplet merger method shown in Figure 4-9A relies on the pairing of droplets for effective dilution, the concern is the frequency of double or missed merging events, which has been high using other droplet merger designs.[15,24] To test this, 1 nL droplets were generated containing 50 µM choline. The choline droplets were merged with 30.3 nL droplets (0.5 % RSD, n = 13 droplets) containing 20 µM neostigmine using the droplet dilution device at 42 droplets/s. The resulting droplets were collected in bulk, re-spaced using a microfluidic device, and analyzed using ESI-MS monitoring for the two analytes (see methods). The unformatted droplet traces for

neostigmine and choline are shown in Figure 4-10A and B respectively. A correlation plot between the peak signal intensity for neostigmine and choline is shown in Figure 4-10C. Based on the clustering observed, three general signal levels appear for choline. Assuming the signals are a reflection of reagent addition instead of detector noise, of the 107 droplets analyzed, two are characterized with double addition (based on signal intensity of a choline droplet), and one appears to have been a missed addition. Using this population as representative of performance, the split droplet merger device successfully pairs and merges droplets 97.2% of the time, with a 1.8% double addition rate and a 0.9% missed addition rate. These rates surpass previously published success rates (86 – 92% success).[15,16,24]

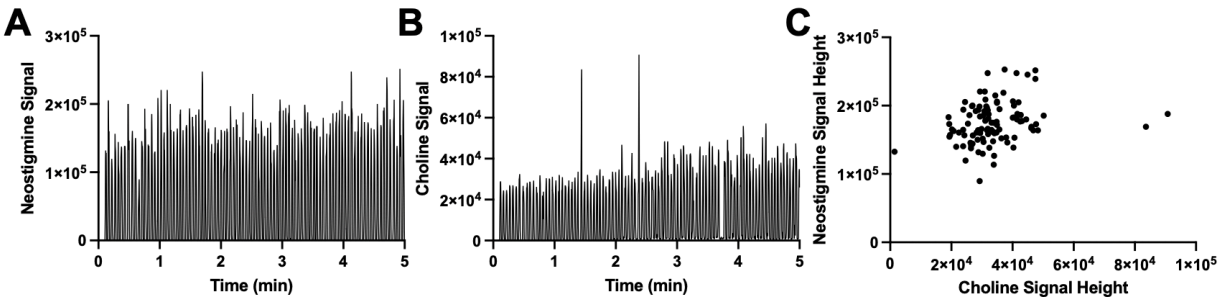

Figure 4-10: Test for consistency of droplet pairing and merging. Large droplets were marked with neostigmine, and small droplets were marked with choline. (A) ESI-MS trace of neostigmine and (B) choline. (C) Plot comparing the droplet signal heights for the two analytes. Two droplets are observed with significantly high signal for choline, indicating a double addition. One droplet is observed with low signal for choline, suggesting a missed addition.

The summarized results from the development presented are in Table 4-2. The table shows the compiled data from published results, showing the best-reported systems as representative of the design. Module 1 (step-injection model) and module 2 (split droplet merger) are presented with the compiled results of the testing presented. By comparing each entry, improvements are observed on the success rate and final RSD, as well as the fold-dilution achieved. The primarily limitation of the work presented here is the improvement on throughput. The modest frequency of additions presented in this work mat be attributed for the success of the devices, but even at the lower throughputs 10^5 samples can be processes per hour.

Table 4-2: Benchmarks for addition for established and developed device designs.

Design	Success rate (%)	RSD on final volume (%)	Frequency (droplets/s)	Carryover	Dilution (fold-increase)
Pico-injector	100	0.2 – 3	600	0.1 – 1%	0.1 – 2
Module 1	93-100	0.9 – 4	25	< 1%	2 – 150
Droplet Merger	86	22	250	n/a	4 – 10
Module 2	97	0.5 – 0.9	47	n/a	4 – 320

4.4 Conclusions

Two reagent addition strategies have been presented to accomplish high dilution of droplet samples. The first uses a step-injection model, where small droplets are merged with a high-flow stream of dilution solution. The device was characterized for flexibility in output droplet volume as well as range of dilution factors. It was shown to be compatible with both droplets generated in bulk, as well as from a multi-well plate for applications in reaction screening. The second device shows the feasibility of decoupling droplet reinjection from merger for carryover-free addition with ease of synchronization and use. The device was characterized with a high degree of consistency, with a ~97% success rate.

The suite of devices presented are applicable to many applications and are envisioned to be used where a large droplet is needed for analysis, or where matrix effects are significant. The dilution range afforded by these devices can be used in a variety of contexts for high-throughput screening.

4.5 References

(1) Zheng, B.; Ismagilov, R. F. A Microfluidic Approach for Screening Submicroliter Volumes against Multiple Reagents by Using Preformed Arrays of Nanoliter Plugs in a Three-Phase Liquid/Liquid/Gas Flow. *Angewandte Chemie International Edition* **2005**, *44* (17), 2520–2523. https://doi.org/10.1002/anie.200462857.

(2) Hatakeyama, T.; Chen, D. L.; Ismagilov, R. F. Microgram-Scale Testing of Reaction Conditions in Solution Using Nanoliter Plugs in Microfluidics with Detection by MALDI-MS. *J. Am. Chem. Soc.* **2006**, *128* (8), 2518–2519. https://doi.org/10.1021/ja057720w.

(3) Shestopalov, I.; D. Tice, J.; F. Ismagilov, R. Multi-Step Synthesis of Nanoparticles Performed on Millisecond Time Scale in a Microfluidic Droplet-Based System. *Lab on a Chip* **2004**, *4* (4), 316–321. https://doi.org/10.1039/B403378G.

(4) Li, L.; Boedicker, J. Q.; Ismagilov, R. F. Using a Multijunction Microfluidic Device To Inject Substrate into an Array of Preformed Plugs without Cross-Contamination: Comparing Theory and Experiments. *Anal. Chem.* **2007**, *79* (7), 2756–2761. https://doi.org/10.1021/ac062179n.

(5) Doonan, S. R.; Bailey, R. C. K-Channel: A Multifunctional Architecture for Dynamically Reconfigurable Sample Processing in Droplet Microfluidics. *Anal. Chem.* **2017**, *89* (7), 4091–4099. https://doi.org/10.1021/acs.analchem.6b05041.

(6) Abate, A. R.; Hung, T.; Mary, P.; Agresti, J. J.; Weitz, D. A. High-Throughput Injection with Microfluidics Using Picoinjectors. *PNAS* **2010**, *107* (45), 19163–19166. https://doi.org/10.1073/pnas.1006888107.

(7) Cui, J. Q.; Liu, F. X.; Park, H.; Chan, K. W.; Leung, T.; Tang, B. Z.; Yao, S. Droplet Digital Recombinase Polymerase Amplification (DdRPA) Reaction Unlocking via Picoinjection. *Biosensors and Bioelectronics* **2022**, *202*, 114019. https://doi.org/10.1016/j.bios.2022.114019.

(8) Eastburn, D. J.; Sciambi, A.; Abate, A. R. Picoinjection Enables Digital Detection of RNA with Droplet RT-PCR. *PLOS ONE* **2013**, *8* (4), e62961. https://doi.org/10.1371/journal.pone.0062961.

(9) L. Sjostrom, S.; N. Joensson, H.; Andersson Svahn, H. Multiplex Analysis of Enzyme Kinetics and Inhibition by Droplet Microfluidics Using Picoinjectors. *Lab on a Chip* **2013**, *13* (9), 1754–1761. https://doi.org/10.1039/C3LC41398E.

(10) Du, L.; Li, Y.; Gao, R.; Yin, J.; Shen, C.; Wang, Y.; Luo, G. Controllability and Flexibility in Particle Manufacturing of a Segmented Microfluidic Device with Passive Picoinjection. *AIChE Journal* **2018**, *64* (11), 3817–3825. https://doi.org/10.1002/aic.16356.

(11) Li, S.; Zeng, M.; Gaule, T.; McPherson, M. J.; Meldrum, F. C. Passive Picoinjection Enables Controlled Crystallization in a Droplet Microfluidic Device. *Small* **2017**, *13* (41), 1702154. https://doi.org/10.1002/smll.201702154.

(12) Sun, A. C.; Steyer, D. J.; Allen, A. R.; Payne, E. M.; Kennedy, R. T.; Stephenson, C. R. J. A Droplet Microfluidic Platform for High-Throughput Photochemical Reaction Discovery. *Nature Communications* **2020**, *11* (1), 6202. https://doi.org/10.1038/s41467-020-19926-z.

(13) Ahn, K.; Agresti, J.; Chong, H.; Marquez, M.; Weitz, D. A. Electrocoalescence of Drops Synchronized by Size-Dependent Flow in Microfluidic Channels. *Appl. Phys. Lett.* **2006**, *88* (26), 264105. https://doi.org/10.1063/1.2218058.

(14) Lee, M.; W. Collins, J.; M. Aubrecht, D.; A. Sperling, R.; Solomon, L.; Ha, J.-W.; Yi, G.-R.; A. Weitz, D.; N. Manoharan, V. Synchronized Reinjection and Coalescence of Droplets in Microfluidics. *Lab on a Chip* **2014**, *14* (3), 509–513. https://doi.org/10.1039/C3LC51214B.
(15) Mazutis, L.; Baret, J.-C.; Treacy, P.; Skhiri, Y.; Fallah Araghi, A.; Ryckelynck, M.; Taly, V.; D. Griffiths, A. Multi-Step Microfluidic Droplet Processing: Kinetic Analysis of an in Vitro Translated Enzyme. *Lab on a Chip* **2009**, *9* (20), 2902–2908. https://doi.org/10.1039/B907753G.
(16) Holland-Moritz, D. A.; Wismer, M. K.; Mann, B. F.; Farasat, I.; Devine, P.; Guetschow, E. D.; Mangion, I.; Welch, C. J.; Moore, J. C.; Sun, S.; Kennedy, R. T. Mass Activated Droplet Sorting (MADS) Enables High-Throughput Screening of Enzymatic Reactions at Nanoliter Scale. *Angewandte Chemie International Edition* **2020**, *59* (11), 4470–4477. https://doi.org/10.1002/anie.201913203.
(17) Sun, S.; C. Buer, B.; G. Marsh, E. N.; T. Kennedy, R. A Label-Free Sirtuin 1 Assay Based on Droplet-Electrospray Ionization Mass Spectrometry. *Analytical Methods* **2016**, *8* (17), 3458–3465. https://doi.org/10.1039/C6AY00698A.
(18) Wells, S. S.; Kennedy, R. T. High-Throughput Liquid–Liquid Extractions with Nanoliter Volumes. *Anal. Chem.* **2020**, acs.analchem.9b04915. https://doi.org/10.1021/acs.analchem.9b04915.
(19) Schirmer, M.; Wink, K.; Ohla, S.; Belder, D.; Schmid, A.; Dusny, C. Conversion Efficiencies of a Few Living Microbial Cells Detected at a High Throughput by Droplet-Based ESI-MS. *Anal. Chem.* **2020**, *92* (15), 10700–10708. https://doi.org/10.1021/acs.analchem.0c01839.
(20) Xia, Y.; Rogers, J. A.; Paul, K. E.; Whitesides, G. M. Unconventional Methods for Fabricating and Patterning Nanostructures. *Chem. Rev.* **1999**, *99* (7), 1823–1848. https://doi.org/10.1021/cr980002q.
(21) Mahler, L.; Tovar, M.; Weber, T.; Brandes, S.; Rudolph, M. M.; Ehgartner, J.; Mayr, T.; Figge, M. T.; Roth, M.; Zang, E. Enhanced and Homogeneous Oxygen Availability during Incubation of Microfluidic Droplets. *RSC Adv.* **2015**, *5* (123), 101871–101878. https://doi.org/10.1039/C5RA20118G.
(22) Pei, J.; Li, Q.; Lee, M. S.; Valaskovic, G. A.; Kennedy, R. T. Analysis of Samples Stored as Individual Plugs in a Capillary by Electrospray Ionization Mass Spectrometry. *Anal. Chem.* **2009**, *81* (15), 6558–6561. https://doi.org/10.1021/ac901172a.
(23) Sun, S.; Slaney, T. R.; Kennedy, R. T. Label Free Screening of Enzyme Inhibitors at Femtomole Scale Using Segmented Flow Electrospray Ionization Mass Spectrometry. *Anal. Chem.* **2012**, *84* (13), 5794–5800. https://doi.org/10.1021/ac3011389.
(24) Ahn, K.; Kerbage, C.; Hunt, T. P.; Westervelt, R. M.; Link, D. R.; Weitz, D. A. Dielectrophoretic Manipulation of Drops for High-Speed Microfluidic Sorting Devices. *Appl. Phys. Lett.* **2006**, *88* (2), 024104. https://doi.org/10.1063/1.2164911.

Chapter 5 Continuous and Automated Slug Flow Nanoextraction for Rapid Partition Coefficient Measurements

Reproduced from Payne, E.M. *et al, Analyst* **2021** *146,* 5722-5731 with permission from the Royal Society of Chemistry

5.1 Introduction

Liquid-liquid extractions (LLEs) are a fundamental tool useful for sample clean-up in complex matrices, determination of partition coefficients, and isolation of target compounds. A common use of LLE is for determining octanol-water partition coefficients (log K_{ow}). Log K_{ow} (often given as K_{ow}, log K, or log P) is routinely used in both drug development, to estimate bioavailability of pharmaceuticals,[1–3] and environmental studies to better understand aqueous remediation techniques.[4] The standard method for determination of log K_{ow} is the shake-flask method.[5] In this method, the two phases are shook to form an emulsion which facilitates transfer between phases. The phases are then re-separated for determination of the concentration of analyte in each phase. Ultimately, the shake-flask method has large volume requirements (mL), long procedures (hours), and remains difficult to automate.[6,7] A miniaturized, automated method for rapid determination of log K_{ow} values could be useful in a pharmaceutical environment when determinations are needed on large compound libraries or at early stages of drug development where material is limited. Chromatographic methods have been used to automate log K_{ow} screening; however, these methods approximate log K_{ow} based on calibration curves using compounds with known log K_{ow}.[8,9] Additionally, chromatographic methods for log K_{ow} determination are limited to analytes that retain well on columns. In this work, we describe a

microfluidic chip interfaced with an autosampler and UV-absorbance detector for rapid and automated LLE and apply it to log K_{ow} determinations using one microliter of sample.

Microfluidics has previously been applied to LLE. Parallel flow is a continuous microfluidic LLE technique in which two immiscible streams are co-flowed forming an extraction interface.[10] Several variations have been reported, demonstrating extractions from biological,[11,12] environmental,[13] and other complex matrices.[14,15] However, parallel flow and similar continuous flow approaches generally require long equilibration times (minutes) and long co-flow distances, which in turn limits parallel flow methods to low-throughput applications and extraction of analytes with rapid partitioning dynamics.[11,16] Additionally, longitudinal sample diffusion in these methods limit sequential analysis of different samples, and must be accounted for when determining extraction coefficients.[12]

Droplet microfluidics, which uses encapsulation of individual femtoliter to nanoliter droplets within an immiscible carrier fluid, has also been used for LLE.[17] Segmented flow, in which aqueous plugs are segmented by an extraction phase, has been shown for a variety of applications including the study of mass transfer,[18–20] preconcentration,[21] sample preparation,[22,23] and continuous synthesis.[24] One study reported using segmented flow of water and octanol to measure partition coefficients of a fluorophore.[25] Although this approach to segmented flow LLE has many applications, it is not applicable to high-throughput log K_{ow} measurements because analytes can transfer from plug-to-plug. This effect results from using the segmenting phase as the extraction solvent and prevents discrete extractions within a train of plugs.[23] Recently, a hybrid liquid-liquid-liquid microfluidic system has been reported to minimize inter-sample interactions;[26] but, as yet no three-liquid phase segmented flow has been described. Automation and rapid sample introduction that would allow high-throughput log K_{ow} have also not been developed.

Recently, our group demonstrated slug flow nanoextraction (SFNE) in which 5 nL plugs of extraction phase and aqueous sample are juxtaposed within a tube and separated from adjacent pairs by a third, fluorous phase to form a linear array of discrete "phase pairs" for extraction.[27] The extractions are rapid due to enhanced mass transfer by internal recirculation within each droplet as the phase pairs flow towards a detector (e.g., UV, fluorescence, mass spectrometry). The use of a fluorinated oil carrier phase allows for sample containment with minimal interaction between phase pairs.[28,29] Phase pairs were generated by "sipping" from 384-well plates with individual wells containing aqueous sample, organic extraction phase, and fluorous carrier fluid. SFNE was shown for in-line sample cleanup of biofluids for analysis by mass spectrometry (MS) and for log K_{ow} determination.[27]

The SFNE method previously described achieved miniaturized log K_{ow} determination with good throughput; however, the approach has limitations that may prevent easy adoption. A disadvantage is that the technique requires moving tubing containing an array of samples from the sipper to a flow-through detector, a manual step requiring fluidic disconnection and reconnection that is not easily automated.[27] As a result, the system cannot be operated unattended. Although advances in microfluidic sampling may ultimately enable such a system to be fully automated, we sought to develop a log K_{ow} measurement system that took advantage of the speed of extraction in droplets but relied more on conventional and readily available automated fluid handling, e.g. autosamplers, to create an easier to use system with mostly off-the-shelf components.

We demonstrate a system that uses an autosampler to inject compounds for log K_{ow} measurement into a microfluidic device that segments the sample into droplets to form aqueous-octanol phase pairs bound by an immiscible carrier phase. The resulting pairs flow through a UV

absorbance detector to measure concentration in the phases. The pairing of the autosampler with microfluidic phase-pair generation allows the system to operate continuously without operator intervention. Sample loading is comparable to HPLC and other systems and is easily achieved without making new fluidic connections. As the system is fluidically closed, no air bubbles are incorporated in the droplet train, unlike what we observed with the sipper method.[27] The removal of air has the advantage of preventing spikes in the detector output signal associated with the bubbles. The only custom component is a microfluidic chip which is the first to allow generation of three-liquid phase slug flow.[26] The automated SFNE method reduces preparation and analysis time by 10-fold and sample/extraction phase volume requirements by 40-fold compared to a microshake-flask method.[30]

5.2 Materials and Methods

Reagents and Materials. All chemicals and solvents were purchased from Sigma-Aldrich (St. Louis, MO) unless stated otherwise. PFD was purchased from Oakwood Chemical (Colombia Hwy, Estill, SC). Drug compounds were prepared in HPLC-grade water and 1-octanol at 1-10 mM (for compounds requiring calibrations), aliquoted, and stored at -80 °C. Standards were thawed daily for use and diluted to the desired concentration. For droplet visualization, dyes were diluted to an arbitrary concentration with strong visibility and used for experimentation. The red dye mixture used in some experiments consisted of equal parts rhodamine B, methyl orange, erythrosine B, phenol red, and neutral red.

Device Design and Fabrication. Microfluidic devices were designed using Autodesk Inc. AutoCAD software (San Rafael, CA) and printed onto a Fineline Imaging transparency (Colorado Springs, CO). Microfluidic master molds were generated with 150 μm feature height using standard photolithography procedures; SU8 2075 negative epoxy photoresist was spun onto silicon

wafers from University Wafer (South Boston, MA), patterned with ultraviolet irradiation through the transparent mask, and developed to leave polymerized features. Curbell Plastics Polydimethylsiloxane (PDMS) (Livonia, MI) was prepared 1:10 activator to monomer ratio, degassed, and poured over the SU8 master. Fluidic ports were produced in the PDMS stamps. PDMS stamps fabricated with fluidic channels were bound to either glass slides (PDMS/glass devices) or to PDMS slabs (PDMS/PDMS devices) using oxygen plasma activation generated by a Harrick Plasma Inc. PDC-32G (Ithaca, NY). Microfluidic devices were flushed with 2% tridecafluoro-1,1,2,2-tetrahydrooctyl tricholorosilane in PFD for surface treatment.

Device Operation and Phase Pair Generation. All flow was applied using Hamilton (Reno, NV) gastight syringes (250 µL, 500 µL, 1 mL) with Chemyx Inc. Fusion 400 syringe pumps. Syringes filled with octanol, PFD, and water (or aqueous sample) were connected to their respective fluidic ports of the phase pair generator via 150 inner diameter (i.d.) 360 outer diameter (o.d.) fused silica capillary coated with polyimide from Polymicro Technologies (Phoenix, AZ). Connections were made using low dead volume unions from Valco Instruments Co., Inc. (Houston, TX). For two-phase slug generation, 2.0 and 1.5 µL/min flow rates were applied for aqueous and PFD, respectively, unless stated otherwise. For three-phase slug generation (phase pairs), 2.0, 2.0, and 1.5 µL/min flow rates were applied for aqueous, octanol, and PFD, respectively, unless stated otherwise. Phase pairs (or droplets for two-phase) are segmented from one another as they reach the continuous PFD flow in the device, discretizing individual samples or extractions. These are exported from the device using 51 cm of 100 µm i.d. 360 o.d. PFA tubing from IDEX (Lake Forest, IL), which is also positioned within an online UV detector. UV detection used a Linear (Auburn, CA) UVIS 200 variable wavelength absorbance detector or a Linear UVIS 205 variable wavelength absorbance detector slotted for capillary flow cells. The wavelength was adjusted to

the various analytes being screened or assessed. National Instruments (Austin, TX) LabView UV data acquisition software was used for UV absorbance data acquisition and analysis.

For automation, the device is interfaced to a Thermo Fisher Scientific (Waltham, MA) UltiMate 3000 Autosampler using a Thermo Fisher Scientific 1 µL nanoViper sample loop. A syringe pump was interfaced to the six-port valve for aqueous flow. This flow acted as the water/aqueous flow during device operation. The complete set up is shown in Figure S1. Injection and wash parameters optimized to provide frequent injections for HTS. Briefly, wash speed and waste dispense was maximized to 8.33 µL/s and no delay in syringe draw or dispense was implemented. Full loop sample mode was found to be slightly faster than partial loop mode, and the loop overfill factor was kept low (2) and a small flush volume was used (5 loop volumes) to achieve 78 second injection rate. In initial experiments, standards were injected from 100 µL of solution in polypropylene autosampler vials. For HTS, standards were injected from 100 µL of solution in a 384-microwell plate. For the automated screen, the octanol syringe pump was programmed to automatically switch between calibration and log K_{ow} determination modes.

For validation of the HTS via microshake-flask method, offline extractions were performed, and each phase was injected using the LC autosampler through the UV detector. The microshake-flask method was performed by placing 500 µL of aqueous extraction standard and 500 µL of octanol in vial, shaking for 60 min, and centrifuging for 10 min.[30] Both phases were pipetted into an autosampler vial and injected for UV analysis with calibration curves in the aqueous phase.

A camera and microscope were often used to capture video of slug formation and export during experiments. For this an AmScope (Irvine, CA) MU500 camera was positioned onto an AmScope microscope to capture video of slugs forming or being exported before going to the

online UV detector. Video was captured using AmScope 3.7 digital camera software and edited using NIH (Bethesda, MD) ImageJ software. High resolution images and videos were taken using a Phantom Miro C110 (Wayne, NJ) on a Nikon (Tokyo, Japan) TS100 inverted microscope and Phantom Camera Control (PCC) software.

HPLC-MS of Eserine Samples. To determine if eserine was degrading due to ambient conditions, HPLC-MS was performed to analyze changes in analyte and degradation product signals. An eserine (Sigma Aldrich) stock was dissolved to 50 uM in 10 mM Tris buffer at pH 7.4. Samples were analyzed before and after a two-hour shake time at 22 ºC under ambient light conditions. The samples were analyzed with an Agilent 1290 Infinity II outfitted with a Phenomenex Kinetex C18 column (2.1 x 100 mm, 1.7 μm) and an Agilent 6410 mass spectrometer. The mobile phase was ramped from 5% to 50% acetonitrile in water with 0.1% formic acid over 7 minutes. The column was re-equilibrated at 5% acetonitrile for 1.5 minutes. Full mass spectra were collected, and the extracted ion chromatograms were integrated.

5.3 Results and Discussion

Device Characteristic and Features. The design of the system used for rapid log K_{ow} measurement is shown in Figure 5-1. Analytes dissolved in water are aliquoted into a well-plate that is placed into an autosampler. The autosampler injects samples into a continuous aqueous stream connected to the PDMS microfluidic device for segmentation into phase-pairs. Multiple microfluidic geometries were tested for three liquid phase plug generation. In-series T-junctions and sample "choppers" have been shown to generate alternating aqueous droplet types.[31] However, these designs were unable to generate the three liquid phase plugs due to differences in surface wettability, viscosity, and surface tension which caused inconsistent phase pair generation.[26] Additionally, devices in which both aqueous and octanol plugs were independently generated then

paired were unsuccessful due to surface interactions between octanol and PDMS. It was discovered that consistent three-phase slug generation was possible using a standard flow focusing device with two aqueous inlets.[32] Traditionally, the multiple input streams combine prior to segmentation then form plugs with both reagents; however, consistent three-phase flow could be achieved here due to immiscibility between water, octanol, and PFD. Evaluating extraction solvents such as ethyl acetate also resulted in phase-pair generation, but with prolonged experimentation (>2 minutes) PDMS swelling was observed, inhibiting further phase-pair generation. It is recommended that microfluidic devices made from glass or other inert materials are used if applying this microfluidic method for SFNE generation with organic solvents that swell PDMS.[33]

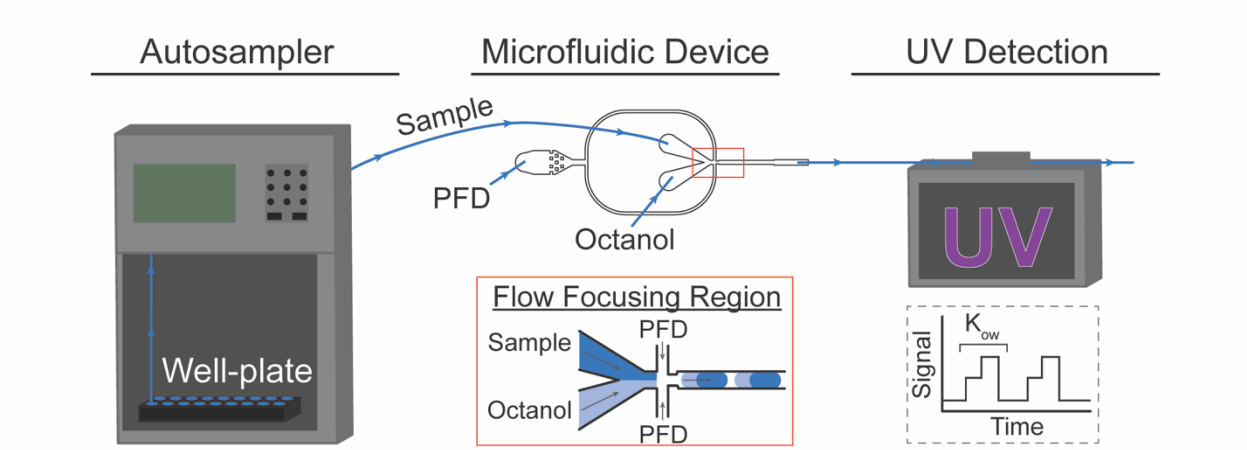

Figure 5-1: Automated log K_{ow} determination using slug flow nanoextraction. Compounds are aliquoted into a well-plate and injected by an autosampler. A microfluidic device generates phase-pairs by segmenting sample and octanol with PFD. Inset shows schematic of the flow focusing region where phase pairs are generated. Aqueous and octanol phases are briefly co-flowed before segmentation by PFD. Phase pairs are exported parallel with the channel into tubing or capillary. An in-line UV detector is used for the analysis of analytes in both aqueous and octanol phases

After phase pair generation, extractions occur at the interface between the octanol and aqueous phases as they flow through capillary to the online detector, where the signal in each phase can be measured and processed for the log K_{ow} of the injected analyte. As reported previously, extractions using SFNE are extremely rapid due to constant recirculation of the extraction interface.[27] Studies investigating mass transfer in similar sized emulsions also find sub-second

equilibration.[34,35] Between generation and analysis, the phase-pairs are in contact for >40 s, which is ample equilibration time for the extraction to occur.

The throughput is limited by injection frequency of the autosampler.[36] To maximize injection frequency, autosampler settings were adjusted for sample loading (draw speed, dispense speed, inter-step delays, injection volume), wash (wash speed, wash volume, inter-step delays), and injection loop control (overfill factor, flush volume, loop volume). By maximizing most draw rates and dispense rates during sample loading and washing, an injection cycle of 78 s was achieved. Some autosamplers have reported faster injections and may enable higher throughput log K_{ow} determination.[37–39] Flow rates were an important parameter for successful operation. Injections began to overlap with an aqueous flow rate under 1 µL/min. Co-flowing of the phases rather than segmentation (during phase pair generation) intermittently occurred with an aqueous flow rate under 2 µL/min. High flow rates result in fewer data points collected by the detector per slug phase-pair. To maximize data points per slug, while maintaining stability of generation, 2 µL/min was used.

Generalization of this technique for purposes beyond K_{ow} determination should consider the parameter selection process described. Phase pair generation is governed by the Capillary number, a measure inversely proportional to the interfacial tension between phases.[40,41] Octanol has a high viscosity (7.66 cP) and low surface tension (27.3 mN/m) relative to water (1 cP and 72.8 mN/m, respectively),[42,43] which limited phase pair generation to higher flow rates at these microchannel dimensions. Replacing octanol with other common extraction solvents such as ethyl acetate, chloroform, and hexane may allow for a wider range of flow rates available at these channel dimensions as the viscosities are more comparable to water (0.40, 0.52, and 0.31 cP

respectively).[44] However, surface tensions of these solvents remain comparable to octanol, so tuning of flow rates to achieve consistent phase-pair volume will be necessary.

Figure 5-2A illustrates online SFNE wherein a sample of red dye is injected and forms phase pairs with octanol segmented by PFD that then flow to a UV detector. Figure 5-2B illustrates that the UV detector trace from the droplets is a sequence of peaks for absorbance of each phase. Distinct signals of each phase were observed corresponding to PFD (minima) and different concentrations of dye in each phase at equilibrium. In a 6 min window of continuous phase pair generation interfaced with online UV analysis, 194 replicate extractions were performed (0.5 phase pairs/s) with relative standard deviation of signal intensity from the aqueous layer (RSD_{AQ}) of 6.8%. Equal volume ratio of aqueous and octanol was used for log K_{ow} determination; however, the relative ratios of water and organic phase can be regulated by the relative flow rates entering the microfluidic system.

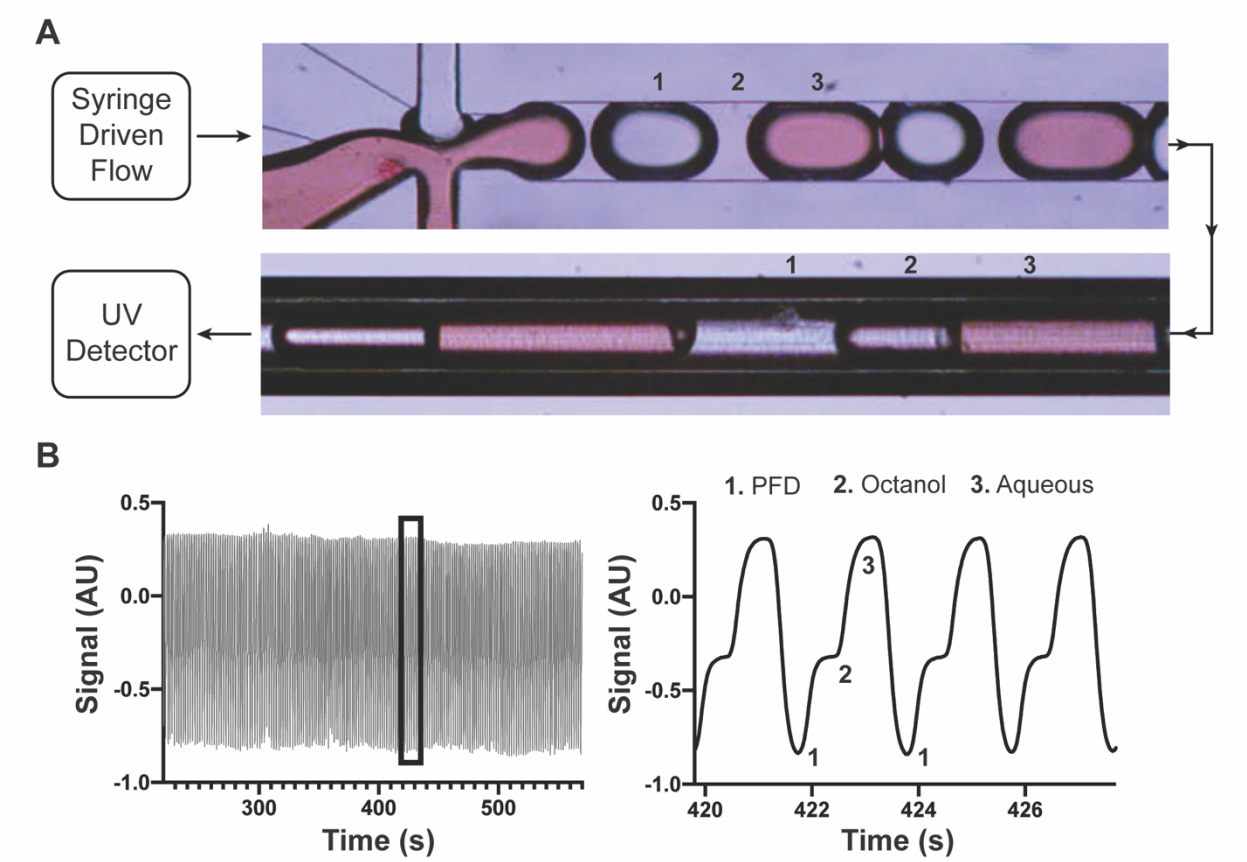

Figure 5-2: Online SFNE generation and detection. (A) A mixture of red dyes (aqueous, 3) and extraction phase (octanol, 2) are segmented into 8 nL phase pairs by PFD (fluourous, 1). (B) Continuous online UV Vis detection of the phase pairs in Teflon tubing for an extended period. Expansion of the trace is shown of distinct signals for each phase. Phase pairs are generated and analyzed at 0.5 phase pairs/s.

Phase pair generation is dependent on the flow of three different phases, where the relative flow rates into the generation device control the aqueous to organic volume ratio in the device. Manipulation of the volume ratio (V_R), expressed as,

Equation 5-1 $$V_R = V_{org}/V_{aq}$$

which, in phase pairs or general LLE, allows for preconcentration or dilution during extraction. V_R modulation was also demonstrated using the online generation device (Figure 5-3). For example, when using flow rates of 1.5, 1.0, and 0.8 µL/min for PFD, octanol, and aqueous, respectively, a V_R of ~0.75 was observed (Figure 5-3A). By adjusting the PFD, octanol, and aqueous flow rates to 0.6, 0.5, and 1.0 µL/min, respectively, the V_R was reduced by a factor of 2.2

to ~0.34 (Figure 5-3B); however, V_R is not directly proportional to flow ratio ($Flow_{org}/Flow_{aq}$, $F_{R)}$, as demonstrated above (i.e. V_R = 0.75 when F_R = 1.25, V_R = 0.34 when F_R = 0.5).

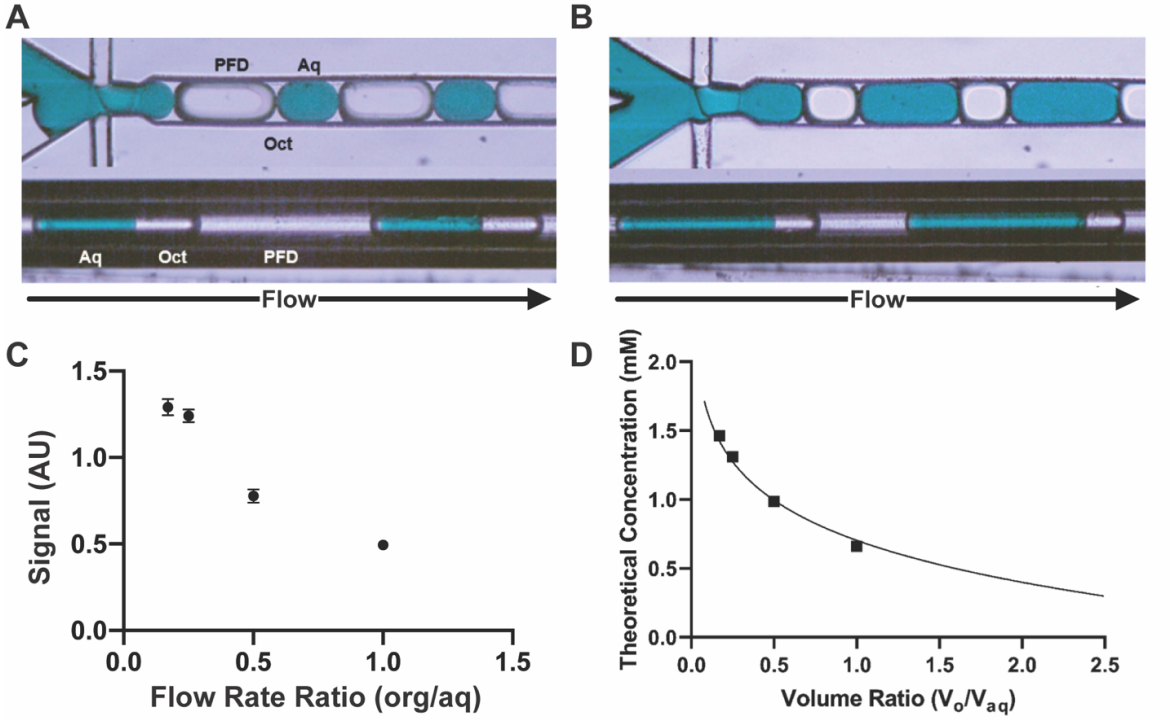

Figure 5-3: Volume manipulation via flow rate changes. (A) Images using flow rates of 1.5, 1.0, and 0.8 µL/min for PFD, octanol, and aqueous, respectively. A V_R of ~0.75 was observed. (B) By adjusting the PFD, octanol, and aqueous flow rates to 0.6, 0.5, and 1.0 µL/min, respectively, the V_R was reduced by a factor of 2.2 to ~0.34 (C) Using 1 mM ACP in water, flow rate ratio was varied from 1.0 to 0.17 and signal intensity in octanol are reported. Signal increases as the flow ratio decreases, showing the effective preconcentration. At least 400 replicates (equilibrium octanol plugs) were measured for each flow ratio. (D) Theoretical concentrations for acetaminophen (initial concentration in aqueous of 1 mM) as volume ratio is adjusted to achieve preconcentration.

Preconcentration effects can be achieved through modulation of the F_R. As a demonstration, the online SFNE device was used to perform an extraction of 1 mM ACP with several different flow ratios (Figure 5-3C). Reduction of the F_R resulted in the increase of the final signal intensity in octanol, showing a 2.6-fold increase in signal intensity when the ratio was reduced from 1.0 to 0.17 (Figure 5-3C). Based on a theoretical concentration curve as volume ratio is adjusted (Figure 5-3D), ACP equilibrium concentration in octanol should increase by 220% as V_R is decreased from 1.0 to 0.17. Experimentally, the signal intensity increased by 260% ± 20%

as F_R was decreased from 1.0 to 0.17. Though the signal intensity change does not perfectly reflect concentration change, this comparison demonstrates F_R modulation can achieve similar preconcentration effects as expected by V_R modulation.

This demonstration of preconcentration may provide a valuable tool for droplet microfluidics. Online LLE using SFNE with preconcentration could increase signal response when screening systems beyond partition coefficients. For example, in many directed evolution methods using droplet microfluidics, the ability to screen enzyme activity is limited by the detector. There have been recent advances in the throughput of droplet analysis with UV and absorbance detection,[45,46] but each demonstration has mentioned poor sensitivity at higher throughputs. Preconcentration could circumvent this significantly. Similarly, for MS based approaches,[47,48] preconcentration and salt removal would be beneficial for electrospray-based approaches.

Phase Toggle and Calibration. Quantitative log K_{ow} determination requires measuring concentration in each phase. UV absorbance is a generalizable detector for measuring concentrations, but calibration is required for quantitative results. To simplify calibration, the phase pair generation device was designed to allow the organic flow to be toggled on and off. When organic flow is off, a segmented flow of aqueous solution and PFD is formed so that the UV absorbance of known injected concentrations in aqueous phase can be measured allowing calibration. When organic flow is on, phase pair generation occurs where extractions can occur during transit. This feature allows for single phase calibrations in water and multi-phase extractions to occur, enabling quantitative determination of unknown equilibrium concentrations without disassembly of the system components or an additional microfluidic device. The system stabilizes from aqueous droplet generation to phase pair generation in under 5 s after toggling the organic phase, providing rapid switching between calibration and unknown determination modes.

Automated Log K_{ow} Measurements. For K_{ow} measurement, aqueous calibrations were performed by sequential injection of five to six concentrations of analyte while in two phase (aqueous/fluorinated) generation mode. Analyte dissolved in water was then injected at a known concentration (typically both 1 mM and 10 mM) while in three phase generation mode and measuring the resulting equilibrium concentration in water on-line by UV absorbance. Figure 5-4A illustrates a UV detector trace for K_{ow} determination of acetaminophen (ACP). Six aqueous calibration standards ranging from 0.1 – 1.0 mM in water as well as a blank were injected, followed by triplicate injection of the extraction sample (1 mM ACP in water). At the beginning of every screen, the absorbance value was set to zero for PFD for convenience. Differences in refractive index between the three phases resulted in negative absorbance readings of ACP in water and octanol at some concentrations. Quantification was based on measuring absorbance from the top of each peak for the aqueous plugs (Figure 5-4B).

Log K_{ow} was determined using:

Equation 5-2 $$\log K_{ow} = \log (C_{oct,eq}/C_{aq,eq})$$

Because the extraction uses equal volumes of octanol and aqueous sample for each phase pair, $C_{oct,eq}$ can be calculated once $C_{aq,eq}$ is known by:

Equation 5-3 $$C_{oct,eq} = C_{inital} - C_{aq,eq}$$

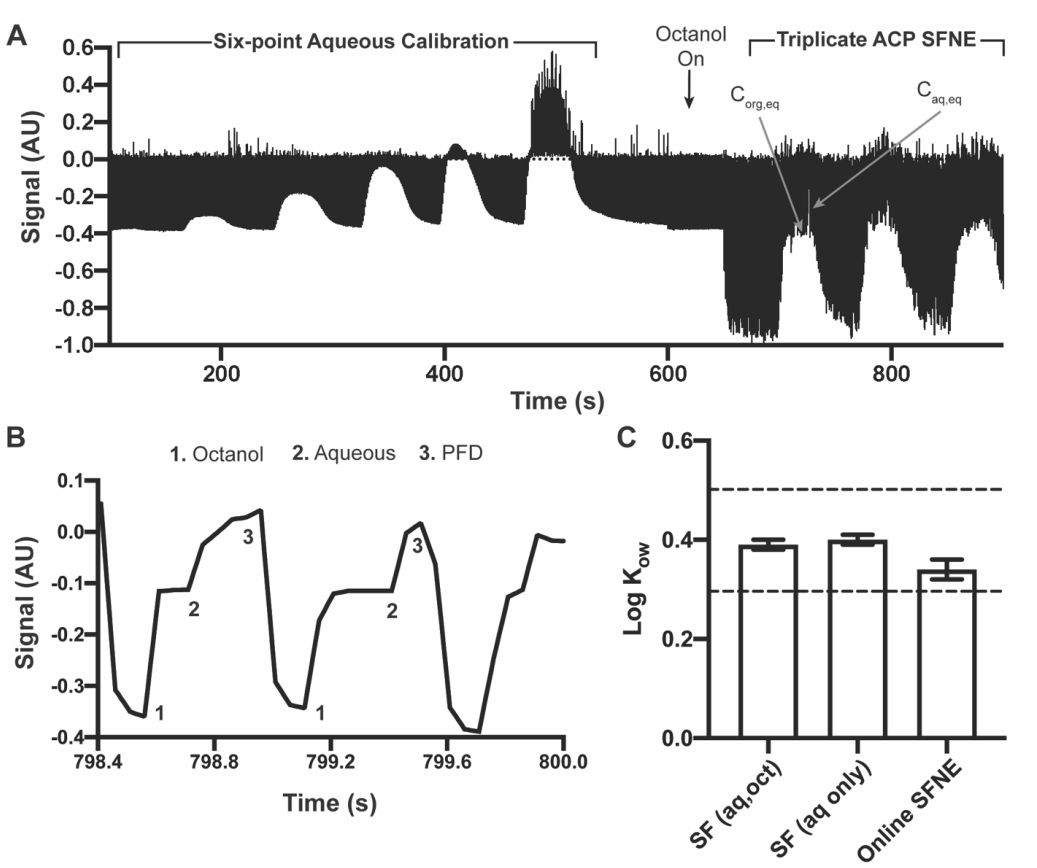

Figure 5-4: Full LC-SFNE-UV workflow for acetaminophen. (A) In a single automated run, a calibration in water was performed followed by triplicate injections with SFNE to determine log K_{ow} for acetaminophen. (B) Expansion of a portion of the trace, showing examples of the phase pairs that were used to determine equilibrium concentrations of acetaminophen in water post-extraction. (C) Value comparisons and validations in this study for online SFNE by comparison to microshake-flask (aq,oct), and microshake-flask (aq only) log K_{ow} values for ACP. Microshake-flask is denoted as SF. Range of previously published ACP log K_{ow} values are denoted with dashed lines.

The log K_{ow} determined by SFNE (0.28 ± 0.01) is comparable to previously reported values[1,49–51] and values determined by the microshake-flask method (Figure 5-4C). To determine the effect of only measuring concentration in aqueous phase, Log K_{ow} was determined by the microshake-flask method twice, once using calibrations in both octanol and water with direct measurements of each extraction layer to determine $C_{oct,eq}$ and $C_{aq,eq}$ (log K_{ow} = 0.28 ± 0.01), and once using only an aqueous calibration and measurement of the aqueous extraction layer, using Equation 5-3 to calculate $C_{oct,eq}$ (log K_{ow} 0.31 ± 0.005). The difference between these two modes of determining log K_{ow} using the microshake-flask method is low (6%), indicating that log K_{ow}

can be accurately measured using aqueous-only measurements. In principle, calibration in both solvents is possible on the automated SFNE method but using just the aqueous phase allows better throughput. The log K_{ow} determined by online SFNE demonstrates suitable accuracy, as it fits within the range of previously reported log K_{ow} values for ACP and reasonably matches the microshake-flask determined log K_{ow}.

The good linearity of the calibration suggested that fewer points could be used to increase throughput. Therefore, further log K_{ow} determination applications of this method only use five concentration levels (one of which is a blank) and single extraction standard injections, as each extraction standard injection generates several quantifiable phase pairs since multiple phase pairs are compartmentalized during injecting (Figure 5-4B).

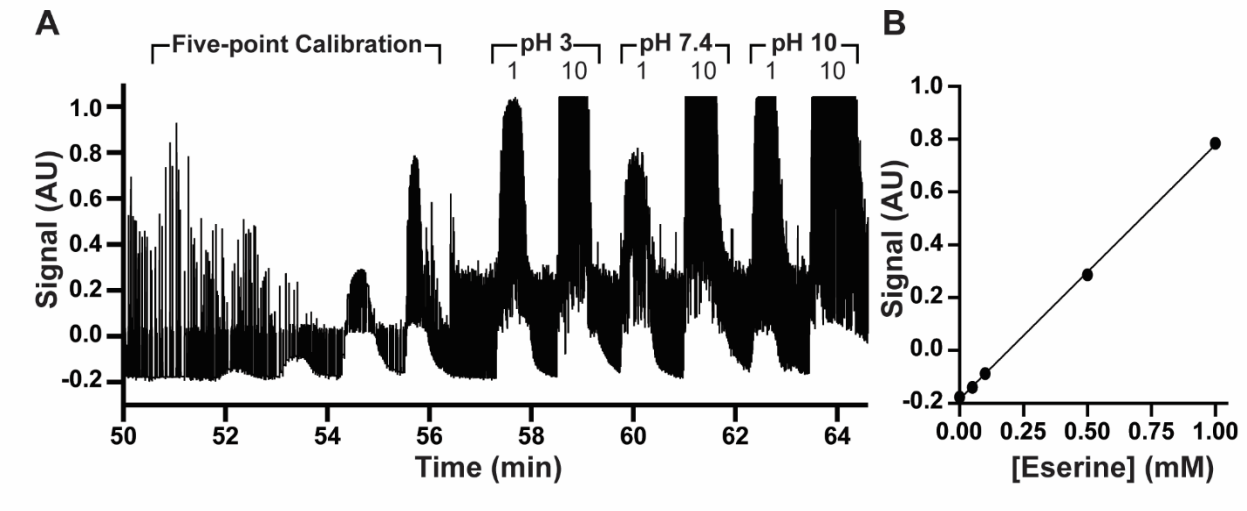

Figure 5-5: Log K_{ow} determination of eserine. (A) Example trace of eserine from full log K_{ow} screen. A five-point aqueous calibration curve in water was injected and generated into aq slugs. Organic (octanol) flow was started at 57 minutes. Unknown determination traces of eserine at pHs 3, 7.4, and 10, at both 1 and 10 mM concentrations. Organic flow was stopped at 65 min in preparation for the next compound screen. (B) Calibration curve generated from the trace ($R^2 > 0.99$).

The microshake-flask method used for validation required substantially higher volumes (500 µL of sample and octanol per extraction) and much longer equilibration times (1 h of shaking, 10 min of centrifugation).[5] Additionally, triplicate analysis of each microshake-flask extraction was required. In contrast, for SFNE the segmentation of each injection into compartmentalized

phase-pairs allows for triplicate (or more) analysis per injection since each phase pair is a separate extraction. When applying the microshake-flask method to large compound or condition panels, it is possible to simultaneously shake and centrifuge samples to decrease total extraction time, but at a theoretical maximum efficiency will still require an additional 1.2 h compared to the online SFNE system.

Rapid Log K_{ow} Determination. The system was applied to determining log K_{ow} for an array of compounds and conditions. Injections were performed from 20 μL of each sample in 384-microwell plate that contained a total of seven pharmaceutical compounds at three different pHs (pH 3, 7.4, and 10) and their corresponding five calibration standards. The compounds were injected at both 1 mM and 10 mM for each pH condition to increase the range of measurable log K_{ow}, as 1 mM standards are more likely to be below the LOD at partition equilibrium if log K_{ow} > 1.5. A trace for extraction of eserine, is shown in Figure 5-5. Octanol flow was automatically turned on at approximately 57 min, following the final calibration standard. The standard curve demonstrates linearity (Figure 5-5B) with $R^2 > 0.99$. After injection of the compounds at each of the pH levels, octanol flow was stopped (approximately 65 min) to allow for the standards of the next compound to be analyzed. Blank buffer injections were performed separately for baseline subtractions.

Table 5-1: Log K_{ow} values determined from screen and microshake-flask validation.

Compound	pKa Values	log K_{ow} (pH 3)	log K_{ow} (pH 7.4)	log K_{ow} (pH 10)	log K_{ow} (SF, pH 7.4)
Acetaminophen	-4.40, 9.46	0.29 ± 0.11	0.29 ± 0.07	0.28 ± 0.07	0.29 ± 0.02
Fexofenadine	4.04, 9.01	2.03 ± 0.24	0.42 ± 0.01	0.48 ± 0.03	0.30 ± 0.03
Caffeine	-0.92	0.03 ± 0.05	-0.02 ± 0.08	0.05 ± 0.06	-0.30 ± 0.01
Nicotinamide	3.63	0.11 ± 0.04	-0.58 ± 0.04	-0.31 ± 0.08	-0.44 ± 0.02

Eserine	6.59	0.07 ± 0.08	-0.29 ± 0.05	0.52 ± 0.04	0.16 ± 0.02
Neostigmine	n/a	-0.59 ± 0.04	< -1	< -1	< -1
Yohimbine	7.65, 14.68	< -1	0.16 ± 0.06	0.4 ± 0.02	0.40 ± 0.02

Twenty-one log K_{ow} measurements were attempted, with 5 calibration and 6 extraction sample injections per compound (84 total injections), using the automated system. This screen was performed in under 2 h, consuming 5 µL of extraction standard and 2.9 µL of octanol per compound analyzed. From the seven compounds screened at the three pH conditions, 18 log K_{ow} values were successfully determined (Table 5-1). The three log K_{ow} values that are unable to be measured in the screen (yohimbine pH 3, neostigmine pH 7.4 and 10) were due to insufficient sensitivity to measure the minimal amount of analyte that partitioned out of aqueous indicating that the log K_{ow} was less than -1.

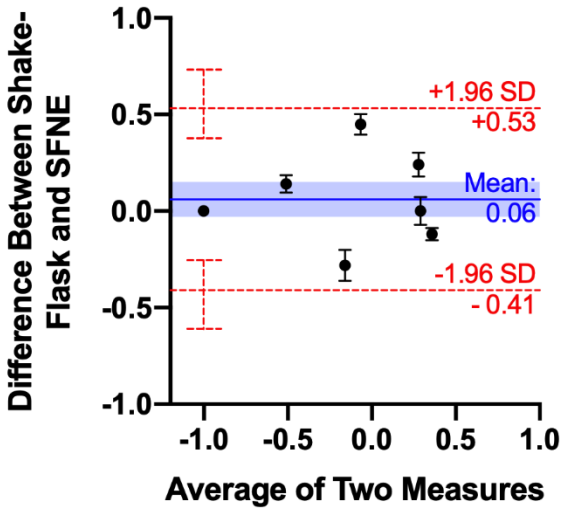

*Figure 5-6: Bland-Altman plot comparing the log K_{ow} determined at pH 7.4 for each compound by SFNE and microshake-flask extraction. Bias with standard error (0.06 ± 0.09) is shown. The limits of agreement (or 95% confidence interval) is shown as calculated by bias ± 1.96*standard deviation of the differences between the two methods*

To assess the accuracy of the measurements, each log K_{ow} at pH 7.4 was determined using the microshake-flask method (Table 5-1). Bland-Altman analysis was performed to quantitatively compare the two methods (Figure 5-6).[52,53] The Bland-Altman graph plots the average of the log

K_{ow} determinations for each method versus the difference between the determinations for each method. A 95% confidence interval is calculated to estimate the range of differences for the methods.[54] The average of the differences can indicate the presence of bias between the two methods. The low bias (0.06 ± 0.09) indicates no systematic error in the online SFNE method compared to the microshake-flask method.

Whether or not the calculated confidence interval is sufficient depends on the goals of the experiment. The mean absolute error of log K_{ow} of our measurements (assuming that the shake-flask method is the standard) was 0.17 log units. This error is comparable to mean absolute errors reported for HPLC,[43–45] NMR,[51] micellar electrokinetic chromatography,[58] and calculation methods,[59] which ranged from 0.11 to 0.50 (Table 5-2); however, such comparisons should be viewed with caution since different sets of compounds were used in each study. Previous studies have claimed that errors less than 0.30 are suitable for most applications.[58,59] Based on these comparisons, it seems that this method, at least for this limited dataset, provides comparable agreement to the shake flask method as other newer methods.

Table 5-2: Mean absolute errors and SD of errors from other methods.

Reference	Mean absolute error (log units)	SD of error (log units)
This work	**0.17**	**0.22**
[55]	0.11	0.08
[59]	0.50	N/A
[56]	0.10	0.19
[58]	0.26	0.32
[51]	0.12	0.21
[57]	0.42	0.52

	0.34	0.23

Most alternatives to the shake-flask method require calibration of a method against standards with known log K_{ow}. Errors in those methods can be attributed in part to lack of perfect correlation of the methods, e.g. of an HPLC column to the octanol/water system. In the droplet method, since partitioning is nominally the same environment, errors are likely different. We considered the possibility that analyte degradation during extraction, a potential problem with the shake-flask method, was a source of error. The compound with the highest variability between the two methods, eserine, was investigated for this possible source of error since it has been reported to degrade.[60] Electrospray MS was performed to identify parent masses for the common degradants (rubeserine, eseroline), where each analyte was observed with the M+H ion in positive mode (Figure 5-7A). Using LC-MS, an eserine solution was analyzed before and after 2 h shaking at ambient conditions mimicking the shake-flask method. No significant differences in eserine concentration or the common degradants were observed (Figure 5-7B), suggesting that degradation is not contributing to method variability. This finding is encouraging as the methods are comparable for labile compounds. However, when studying even more labile analytes, it is expected that the SFNE method will outperform bulk measurement due to the lower exposure time. Possible sources of error include impurity of compounds and analyte losses in the droplet system (e.g., adsorption to walls or the interface of carrier fluid).

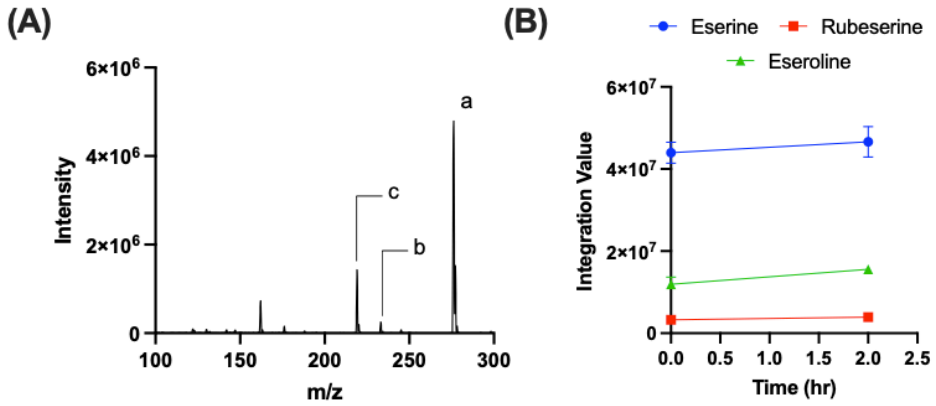

Figure 5-7: Investigation into possible degradation of eserine. (A) Mass spectrum of a eserine, eseroline, and rubeserine solution. Three peaks labelled correspond to a: eserine (M+H, 276 m/z), b: rubeserine (M+H, 233 m/z), and c: eseroline (M+H, 219 m/z). The signal of eseroline (c) may be artificially high due to an in-source fragment of eserine (57 m/z corresponding to losses of both C_2H_3NO and C_3H_7N). (B) Signal integration values from LC-MS of the selected ions in [A] before and after two-hours shaking at ambient conditions. Error bars represent standard error with n = 3. No significant changes were measured, suggesting no substantial degradation of eserine over the two-hour shake times.

One notable test compound was yohimbine, which demonstrates significantly different partitioning across the pH ranges tested (Table 5-1). Yohimbine has multiple ionizable groups including both basic and acidic moieties. The pKas are 7.6 and 14.7, indicating that at the lowest pH the compound is cationic, limiting its extraction into octanol. Upon raising the pH, the compound is neutral, allowing for octanol extraction. Additionally, fexofenadine appears to be more lipophilic in acidic environments, possibly due to its cationic charge shielded by large steric effects, but more hydrophilic when the surface acid group is charged (pH 7.4 and 10). These variations in the log K_{ow} (more properly, log D where D is distribution coefficient) are of interest for understanding the bioavailability in both basic and acidic regions of the body such as absorption through the acidic stomach versus the more alkaline colon or small intestine.[61,62]

5.4 Conclusions

A system has been developed for rapid determination of log K_{ow} using an autosampler coupled to a microfluidic chip and UV detector. The method provides convenient and automated

operation without operator intervention once samples are mounted in the autosampler. A key feature is rapid extraction. In a conventional shake-flask method, an emulsion is formed which improves contact between phases to decrease partitioning time; however, the phases must be re-segregated for analysis. The microfluidic chip used here essentially forms a controlled emulsion as fixed volume phase pairs that allow fast partitioning and then direct analysis of the phases for determination of log K_{ow}. Unlike a previous segmented flow method that used a robot to "sip" different phases into a tube that was then connected to a detector, the current system can operate continuously without the need for fluidic disconnect and reconnect; however, this convenience does require larger volumes of sample since the autosampler requires microliter volumes to inject.

This approach allowed for seven compounds to be screened for log K_{ow} values in under one hour including calibration curves for each compound, allowing for direct and accurate measurement of partition coefficients. This system has several limitations, primarily associated with the UV detection. Though suitable for in-line use and small volume analysis, capillary UV detection has poor sensitivity, ultimately limiting the method to use with chromophores. Possible solutions include use of larger droplets and thicker channels to enhance absorbance. Also, alternative detectors such as mass spectrometry might prove useful for these measurements. Throughput could be increased with newer/faster autosamplers, with injection cycles down to 22 s,[37] and using fewer calibration points. This method is also potentially adaptable for other extractions, such as sample clean-up of complex matrices. However, extraction solvent compatibility must be considered since chloroform, ethyl acetate, and dichloromethane can swell PDMS channels. Therefore, translation of the microfluidic geometry into glass-glass devices may be necessary.

5.5 References

(1) Liu, X.; Tu, M.; Kelly, R. S.; Chen, C.; Smith, B. J. Development of a Computational Approach to Predict Blood-Brain Barrier Permeability. *Drug Metab Dispos* **2004**, *32* (1), 132–139. https://doi.org/10.1124/dmd.32.1.132.

(2) Colmenarejo, G. In Silico Prediction of Drug-Binding Strengths to Human Serum Albumin. *Medicinal Research Reviews* **2003**, *23* (3), 275–301. https://doi.org/10.1002/med.10039.

(3) Hsieh, C.-M.; Wang, S.; Lin, S.-T.; Sandler, S. I. A Predictive Model for the Solubility and Octanol−Water Partition Coefficient of Pharmaceuticals. *J. Chem. Eng. Data* **2011**, *56* (4), 936–945. https://doi.org/10.1021/je1008872.

(4) Valsaraj, K. T.; Thibodeaux, L. J. Relationships between Micelle-Water and Octanol-Water Partition Constants for Hydrophobic Organics of Environmental Interest. *Water Research* **1989**, *23* (2), 183–189. https://doi.org/10.1016/0043-1354(89)90042-0.

(5) OECD. *Test No. 107: Partition Coefficient (n-Octanol/Water): Shake Flask Method*; OECD Guidelines for the Testing of Chemicals, Section 1; OECD, 1995. https://doi.org/10.1787/9789264069626-en.

(6) Chiou, C. T.; Schmedding, D. W.; Manes, Milton. Partitioning of Organic Compounds in Octanol-Water Systems. *Environ. Sci. Technol.* **1982**, *16* (1), 4–10. https://doi.org/10.1021/es00095a005.

(7) Danielsson, L.-G.; Zhang, Y.-H. Methods for Determiningn-Octanol-Water Partition Constants. *TrAC Trends in Analytical Chemistry* **1996**, *15* (4), 188–196. https://doi.org/10.1016/0165-9936(96)00003-9.

(8) Ogden, P. B.; Dorsey, J. G. Reversed Phase HPLC with High Temperature Ethanol/Water Mobile Phases as a Green Alternative Method for the Estimation of Octanol/Water Partition Coefficients. *Journal of Chromatography A* **2019**, *1601*, 243–254. https://doi.org/10.1016/j.chroma.2019.05.002.

(9) Poole, S. K.; Poole, C. F. Separation Methods for Estimating Octanol–Water Partition Coefficients. *Journal of Chromatography B* **2003**, *797* (1), 3–19. https://doi.org/10.1016/j.jchromb.2003.08.032.

(10) Tokeshi, M.; Minagawa, T.; Kitamori, T. Integration of a Microextraction System on a Glass Chip: Ion-Pair Solvent Extraction of Fe(II) with 4,7-Diphenyl-1,10-Phenanthrolinedisulfonic Acid and Tri-n-Octylmethylammonium Chloride. *Anal. Chem.* **2000**, *72* (7), 1711–1714. https://doi.org/10.1021/ac991147f.

(11) Reddy, V.; Zahn, J. D. Interfacial Stabilization of Organic–Aqueous Two-Phase Microflows for a Miniaturized DNA Extraction Module. *Journal of Colloid and Interface Science* **2005**, *286* (1), 158–165. https://doi.org/10.1016/j.jcis.2004.12.052.

(12) Žnidaršič-Plazl, P.; Plazl, I. Steroid Extraction in a Microchannel System—Mathematical Modelling and Experiments. *Lab Chip* **2007**, *7* (7), 883–889. https://doi.org/10.1039/B704432A.

(13) Kolar, E.; Catthoor, R. P. R.; Kriel, F. H.; Sedev, R.; Middlemas, S.; Klier, E.; Hatch, G.; Priest, C. Microfluidic Solvent Extraction of Rare Earth Elements from a Mixed Oxide Concentrate Leach Solution Using Cyanex® 572. *Chemical Engineering Science* **2016**, *148*, 212–218. https://doi.org/10.1016/j.ces.2016.04.009.

(14) Aota, A.; Nonaka, M.; Hibara, A.; Kitamori, T. Countercurrent Laminar Microflow for Highly Efficient Solvent Extraction. *Angewandte Chemie International Edition* **2007**, *46* (6), 878–880. https://doi.org/10.1002/anie.200600122.
(15) Minagawa, T.; Tokeshi, M.; Kitamori, T. Integration of a Wet Analysis System on a Glass Chip: Determination of Co(Ii) as 2-Nitroso-1-Naphthol Chelates by Solvent Extraction and Thermal Lens Microscopy. *Lab on a Chip* **2001**, *1* (1), 72–75. https://doi.org/10.1039/B102790P.
(16) Assmann, N.; Ładosz, A.; Rohr, P. R. von. Continuous Micro Liquid-Liquid Extraction. *Chemical Engineering & Technology* **2013**, *36* (6), 921–936. https://doi.org/10.1002/ceat.201200557.
(17) Chiu, D. T.; Lorenz, R. M.; Jeffries, G. D. M. Droplets for Ultrasmall-Volume Analysis. *Anal. Chem.* **2009**, *81* (13), 5111–5118. https://doi.org/10.1021/ac900306q.
(18) Kashid, M. N.; Harshe, Y. M.; Agar, D. W. Liquid−Liquid Slug Flow in a Capillary: An Alternative to Suspended Drop or Film Contactors. *Ind. Eng. Chem. Res.* **2007**, *46* (25), 8420–8430. https://doi.org/10.1021/ie070077x.
(19) Mary, P.; Chen, A.; Chen, I.; R. Abate, A.; A. Weitz, D. On-Chip Background Noise Reduction for Cell-Based Assays in Droplets. *Lab on a Chip* **2011**, *11* (12), 2066–2070. https://doi.org/10.1039/C1LC20159J.
(20) Lubej, M.; Novak, U.; Liu, M.; Martelanc, M.; Franko, M.; Plazl, I. Microfluidic Droplet-Based Liquid–Liquid Extraction: Online Model Validation. *Lab on a Chip* **2015**, *15* (10), 2233–2239. https://doi.org/10.1039/C4LC01460J.
(21) Chen, H.; Fang, Q.; Yin, X.-F.; Fang, Z.-L. Microfluidic Chip-Based Liquid–Liquid Extraction and Preconcentration Using a Subnanoliter-Droplet Trapping Technique. *Lab Chip* **2005**, *5* (7), 719–725. https://doi.org/10.1039/B416964F.
(22) Peroni, D.; van Egmond, W.; Kok, W. Th.; Janssen, H.-G. Advancing Liquid/Liquid Extraction through a Novel Microfluidic Device: Theory, Instrumentation and Applications in Gas Chromatography. *Journal of Chromatography A* **2012**, *1226*, 77–86. https://doi.org/10.1016/j.chroma.2011.08.001.
(23) He, Y.; Pei, J.; Srinivasakannan, C.; Li, S.; Peng, J.; Guo, S.; Zhang, L.; Yin, S. Extraction of Samarium Using a Serpentine Y-Junction Microreactor with 2-Ethylhexyl Phosphonic Acid Mono-2-Ethylhexyl. *Hydrometallurgy* **2018**, *179*, 175–180. https://doi.org/10.1016/j.hydromet.2018.06.006.
(24) Sahoo, H. R.; Kralj, J. G.; Jensen, K. F. Multistep Continuous-Flow Microchemical Synthesis Involving Multiple Reactions and Separations. *Angewandte Chemie International Edition* **2007**, *46* (30), 5704–5708. https://doi.org/10.1002/anie.200701434.
(25) Marine, N. A.; Klein, S. A.; Posner, J. D. Partition Coefficient Measurements in Picoliter Drops Using a Segmented Flow Microfluidic Device. *Anal. Chem.* **2009**, *81* (4), 1471–1476. https://doi.org/10.1021/ac801673w.
(26) Wang, T.; Xu, C. Liquid–Liquid–Liquid Three-Phase Microsystem: Hybrid Slug Flow–Laminar Flow. *Lab on a Chip* **2020**, *20* (11), 1891–1897. https://doi.org/10.1039/D0LC00292E.
(27) Wells, S. S.; Kennedy, R. T. High-Throughput Liquid–Liquid Extractions with Nanoliter Volumes. *Anal. Chem.* **2020**, *92* (4), 3189–3197. https://doi.org/10.1021/acs.analchem.9b04915.
(28) Roach, L. S.; Song, H.; Ismagilov, R. F. Controlling Nonspecific Protein Adsorption in a Plug-Based Microfluidic System by Controlling Interfacial Chemistry Using Fluorous-

Phase Surfactants. *Anal. Chem.* **2005**, *77* (3), 785–796. https://doi.org/10.1021/ac049061w.
(29) Payne, E. M.; Holland-Moritz, D. A.; Sun, S.; Kennedy, R. T. High-Throughput Screening by Droplet Microfluidics: Perspective into Key Challenges and Future Prospects. *Lab Chip* **2020**, *20* (13), 2247–2262. https://doi.org/10.1039/D0LC00347F.
(30) Andrés, A.; Rosés, M.; Ràfols, C.; Bosch, E.; Espinosa, S.; Segarra, V.; Huerta, J. M. Setup and Validation of Shake-Flask Procedures for the Determination of Partition Coefficients (LogD) from Low Drug Amounts. *European Journal of Pharmaceutical Sciences* **2015**, *76*, 181–191. https://doi.org/10.1016/j.ejps.2015.05.008.
(31) Deal, K. S.; Easley, C. J. Self-Regulated, Droplet-Based Sample Chopper for Microfluidic Absorbance Detection. *Anal. Chem.* **2012**, *84* (3), 1510–1516. https://doi.org/10.1021/ac202791d.
(32) Nisisako, T.; Torii, T.; Takahashi, T.; Takizawa, Y. Synthesis of Monodisperse Bicolored Janus Particles with Electrical Anisotropy Using a Microfluidic Co-Flow System. *Advanced Materials* **2006**, *18* (9), 1152–1156. https://doi.org/10.1002/adma.200502431.
(33) Lee, J. N.; Park, C.; Whitesides, G. M. Solvent Compatibility of Poly(Dimethylsiloxane)-Based Microfluidic Devices. *Anal. Chem.* **2003**, *75* (23), 6544–6554. https://doi.org/10.1021/ac0346712.
(34) Kumemura, M.; Korenaga, T. Quantitative Extraction Using Flowing Nano-Liter Droplet in Microfluidic System. *Analytica Chimica Acta* **2006**, *558* (1), 75–79. https://doi.org/10.1016/j.aca.2005.10.086.
(35) Zhao, C.-X.; Middelberg, A. P. J. Microfluidic Mass-Transfer Control for the Simple Formation of Complex Multiple Emulsions. *Angewandte Chemie International Edition* **2009**, *48* (39), 7208–7211. https://doi.org/10.1002/anie.200902485.
(36) Equitz, T. R.; Rodriguez-Cruz, S. E. High-Throughput Analysis of Controlled Substances: Combining Multiple Injections in a Single Experimental Run (MISER) and Liquid Chromatography–Mass Spectrometry (LC-MS). *Forensic Chemistry* **2017**, *5*, 8–15. https://doi.org/10.1016/j.forc.2017.05.001.
(37) Welch, C. J.; Gong, X.; Schafer, W.; Pratt, E. C.; Brkovic, T.; Pirzada, Z.; Cuff, J. F.; Kosjek, B. MISER Chromatography (Multiple Injections in a Single Experimental Run): The Chromatogram Is the Graph. *Tetrahedron: Asymmetry* **2010**, *21* (13), 1674–1681. https://doi.org/10.1016/j.tetasy.2010.05.029.
(38) Zawatzky, K.; Barhate, C. L.; Regalado, E. L.; Mann, B. F.; Marshall, N.; Moore, J. C.; Welch, C. J. Overcoming "Speed Limits" in High Throughput Chromatographic Analysis. *Journal of Chromatography A* **2017**, *1499*, 211–216. https://doi.org/10.1016/j.chroma.2017.04.002.
(39) Leveridge, M.; Collier, L.; Edge, C.; Hardwicke, P.; Leavens, B.; Ratcliffe, S.; Rees, M.; Stasi, L. P.; Nadin, A.; Reith, A. D. A High-Throughput Screen to Identify LRRK2 Kinase Inhibitors for the Treatment of Parkinson's Disease Using RapidFire Mass Spectrometry. *J Biomol Screen* **2016**, *21* (2), 145–155. https://doi.org/10.1177/1087057115606707.
(40) Thorsen, T.; Roberts, R. W.; Arnold, F. H.; Quake, S. R. Dynamic Pattern Formation in a Vesicle-Generating Microfluidic Device. *Phys. Rev. Lett.* **2001**, *86* (18), 4163–4166. https://doi.org/10.1103/PhysRevLett.86.4163.
(41) Dendukuri, D.; Tsoi, K.; Hatton, T. A.; Doyle, P. S. Controlled Synthesis of Nonspherical Microparticles Using Microfluidics. *Langmuir* **2005**, *21* (6), 2113–2116. https://doi.org/10.1021/la047368k.

(42) Shan, Z.; Asfour, A.-F. A. Viscosities and Densities of Nine Binary 1-Alkanol Systems at 293.15 K and 298.15 K. *J. Chem. Eng. Data* **1999**, *44* (1), 118–123. https://doi.org/10.1021/je980177x.
(43) Ye, C. W.; Li, J. Density, Viscosity, and Surface Tension of n-Octanol-Phosphoric Acid Solutions in a Temperature Range 293.15–333.15 K. *Russ. J. Phys. Chem.* **2012**, *86* (10), 1515–1521. https://doi.org/10.1134/S0036024412100263.
(44) Oswal, S.; Rathnam, M. V. Viscosity Data of Binary Mixtures: Ethyl Acetate + Cyclohexane, + Benzene, + Toluene, + Ethylbenzene + Carbon Tetrachloride, and + Chloroform at 303.15 K. *Can. J. Chem.* **1984**, *62* (12), 2851–2853. https://doi.org/10.1139/v84-482.
(45) Gielen, F.; Hours, R.; Emond, S.; Fischlechner, M.; Schell, U.; Hollfelder, F. Ultrahigh-Throughput–Directed Enzyme Evolution by Absorbance-Activated Droplet Sorting (AADS). *PNAS* **2016**, *113* (47), E7383–E7389. https://doi.org/10.1073/pnas.1606927113.
(46) Duncombe, T. A.; Ponti, A.; Seebeck, F. P.; Dittrich, P. S. UV–Vis Spectra-Activated Droplet Sorting for Label-Free Chemical Identification and Collection of Droplets. *Anal. Chem.* **2021**, *93* (38), 13008–13013. https://doi.org/10.1021/acs.analchem.1c02822.
(47) Steyer, D. J.; Kennedy, R. T. High-Throughput Nanoelectrospray Ionization-Mass Spectrometry Analysis of Microfluidic Droplet Samples. *Anal. Chem.* **2019**, *91* (10), 6645–6651. https://doi.org/10.1021/acs.analchem.9b00571.
(48) Holland-Moritz, D. A.; Wismer, M. K.; Mann, B. F.; Farasat, I.; Devine, P.; Guetschow, E. D.; Mangion, I.; Welch, C. J.; Moore, J. C.; Sun, S.; Kennedy, R. T. Mass Activated Droplet Sorting (MADS) Enables High-Throughput Screening of Enzymatic Reactions at Nanoliter Scale. *Angewandte Chemie International Edition* **2020**, *59* (11), 4470–4477. https://doi.org/10.1002/anie.201913203.
(49) Carlsson, K.; Karlberg, B. Determination of Octanol–Water Partition Coefficients Using a Micro-Volume Liquid-Liquid Flow Extraction System. *Analytica Chimica Acta* **2000**, *423* (1), 137–144. https://doi.org/10.1016/S0003-2670(00)01078-3.
(50) Baena, Y.; Pinzón, J. A.; Barbosa, H. J.; Martínez, F. Temperature-Dependence of the Solubility of Some Acetanilide Derivatives in Several Organic and Aqueous Solvents. *Physics and Chemistry of Liquids* **2004**, *42* (6), 603–613. https://doi.org/10.1080/00319100412331284413.
(51) Mo, H.; Balko, K. M.; Colby, D. A. A Practical Deuterium-Free NMR Method for the Rapid Determination of 1-Octanol/Water Partition Coefficients of Pharmaceutical Agents. *Bioorganic & Medicinal Chemistry Letters* **2010**, *20* (22), 6712–6715. https://doi.org/10.1016/j.bmcl.2010.08.145.
(52) Bland, J. M.; Altman, D. G. Measuring Agreement in Method Comparison Studies. *Stat Methods Med Res* **1999**, *8* (2), 135–160. https://doi.org/10.1177/096228029900800204.
(53) Martin Bland, J.; Altman, DouglasG. STATISTICAL METHODS FOR ASSESSING AGREEMENT BETWEEN TWO METHODS OF CLINICAL MEASUREMENT. *The Lancet* **1986**, *327* (8476), 307–310. https://doi.org/10.1016/S0140-6736(86)90837-8.
(54) Giavarina, D. Understanding Bland Altman Analysis. *Biochem Med (Zagreb)* **2015**, *25* (2), 141–151. https://doi.org/10.11613/BM.2015.015.
(55) Han, S.; Qiao, J.; Zhang, Y.; Yang, L.; Lian, H.; Ge, X.; Chen, H. Determination of N-Octanol/Water Partition Coefficient for DDT-Related Compounds by RP-HPLC with a Novel Dual-Point Retention Time Correction. *Chemosphere* **2011**, *83* (2), 131–136. https://doi.org/10.1016/j.chemosphere.2011.01.013.

(56) Tetko, I. V.; Bruneau, P. Application of ALOGPS to Predict 1-Octanol/Water Distribution Coefficients, LogP, and LogD, of AstraZeneca in-House Database. *J Pharm Sci* **2004**, *93* (12), 3103–3110. https://doi.org/10.1002/jps.20217.
(57) Ayouni, L.; Cazorla, G.; Chaillou, D.; Herbreteau, B.; Rudaz, S.; Lantéri, P.; Carrupt, P.-A. Fast Determination of Lipophilicity by HPLC. *Chroma* **2005**, *62* (5), 251–255. https://doi.org/10.1365/s10337-005-0608-6.
(58) Smith, J. T.; Vinjamoori, D. V. Rapid Determination of Logarithmic Partition Coefficients between N-Octanol and Water Using Micellar Electrokinetic Capillary Chromatography. *Journal of Chromatography B: Biomedical Sciences and Applications* **1995**, *669* (1), 59–66. https://doi.org/10.1016/0378-4347(95)00082-T.
(59) Paschke, A.; Neitzel, P. L.; Walther, W.; Schüürmann, G. Octanol/Water Partition Coefficient of Selected Herbicides: Determination Using Shake-Flask Method and Reversed-Phase High-Performance Liquid Chromatography. *J. Chem. Eng. Data* **2004**, *49* (6), 1639–1642. https://doi.org/10.1021/je049947x.
(60) Hemsworth, B. A.; West, G. B. Anticholinesterase Activity of Some Degradation Products of Physostigmine. *Journal of Pharmaceutical Sciences* **1970**, *59* (1), 118–120. https://doi.org/10.1002/jps.2600590128.
(61) Ashford, M.; Fell, J. Targeting Drugs to the Colon: Delivery Systems for Oral Administration. *Journal of Drug Targeting* **1994**, *2* (3), 241–257. https://doi.org/10.3109/10611869408996806.
(62) Bajpai, S. K.; Bajpai, M.; Dengre, R. Chemically Treated Hard Gelatin Capsules for Colon-Targeted Drug Delivery: A Novel Approach. *Journal of Applied Polymer Science* **2003**, *89* (8), 2277–2282. https://doi.org/10.1002/app.12478.

Chapter 6 Mass-Activated Droplet Sorting for Selection of Lysine-Producing *Escherichia coli*

This was performed in collaboration with Bridget E. Murray (BEM), Laura I. Penabad-Peña (LIP), and Dr. Eric Abbate (EA). BEM developed the methods for cell culture and LC-MS/MS analysis of lysine and glutamine. LIP performed LC-MS/MS validation and data analysis resulting in Figures 6-8D and 6-10C. EA performed the phenotyping analysis presented in Figure 6-12.

6.1 Introduction

Directed evolution (DE) has been demonstrated as a powerful method for designing biological means to chemical production. DE is achieved by iterative rounds of genetic mutation, screening activity of interest, and selection of desired phenotypes.[1] This process is meant to mimic natural evolution of cell or enzyme catalysts for the production of a valuable pharmaceutical or agricultural chemical. Recent evolution experiments have uncovered enzyme variants with high yields and enantiomeric selectivity for the anti-HIV drug islatravir,[2] the diabetes drug sitagliptin,[3] and a small cell lung cancer drug in clinical trials.[4] While extremely promising as a technique, DE methods are limited by the ability to screen the increasing size of variant libraries to uncover rare variants with high efficiency. Typically, samples are analyzed using liquid-chromatography, but these methods are often hindered by long analysis times and significant waste generation. Higher throughput analytical tools are needed to fully realize the power of DE. In this report, we describe a method for high-throughput analysis using droplet microfluidics coupled to mass spectrometry to reliably screen and sort cell mutants.

Droplet microfluidics enables high-throughput screening with reduced waste. Encapsulating chemical or biological material in water-in-oil droplets allows for discrete processing and analysis, which has been applied to many applications including directed evolution. Significant development in droplet microfluidics has translated many bulk processes into automated and miniaturized devices, such as sample generation,[5,6] dilution or reagent addition,[7,8] sampling or splitting,[6,8] and incubation.[9,10] Using these modules, droplet systems can be engineered to mimic traditional bulk screening. Desirable droplets can be selected in flow using dielectrophoresis (DEP),[11] which can be activated using logic-driven analysis.

While droplet processing and sorting has advanced significantly, droplet analysis remains a bottleneck to the field.[12] The most common method for analyzing droplets and actuating DEP is using fluorescence. Fluorescence activated droplet sorting (FADS) has been performed at rates up to 30 kHz and has been applied to screening many enzyme systems.[13] FADS has been used to screen *E. coli* variants for the synthesis of unnatural amino acids,[14] yeast variants producing α-amylase at high concentrations,[15] and β-galactosidase variants expressed *in vitro*.[16] While these applications have demonstrated impressive droplet manipulations at very high-throughputs, the methods are limited to screening systems with fluorescent products, or the ability to use a fluorescent reporter system. For most industrially relevant systems, evolution campaigns are not compatible with fluorescent detection.

The development of label-free droplet analysis methods has been explored to address these concerns. Alternatives to FADS have emerged such as absorbance activated droplet sorting,[17] UV-activated droplet sorting,[18] and Raman activated droplet sorting.[19] These strategies expand the available analytes that can be screened in droplet but have drawbacks due to the high background noise associated with the analytical methods. While optical approaches have rapid detection and

processing, the aforementioned droplet techniques have lagged behind the success achieved using FADS.

Direct mass spectrometry (MS) of droplets has become a reliable method for droplet analysis. Droplet samples have been analyzed with matrix-assisted laser desorption ionization (MALDI)-MS and electrospray ionization (ESI)-MS which provides label-free analysis of analytes with ionizable groups. Droplet MALDI-MS was recently applied to the DE of type-3 polyketide synthase.[20] While this method provides rich metabolite profiles for each variant, the analysis is offline which reduces automation and throughput, and MALDI leads to high variability for quantitative analysis.[21,22] In contrast, ESI can be integrated into the flow path of droplet microfluidic systems and has higher reproducibility than MALDI. Droplet ESI-MS approaches have been used to analyze biological catalysis for a variety of systems.[23–26] However, ESI-MS is a destructive technique, so performing droplet sorting with this method is challenging.

Our group recently described mass-activated droplet sorting (MADS) which is a strategy for circumventing the destructive nature of ESI-MS.[27] In brief, droplets are introduced to a microfluidic device that splits the droplet; one of the subsequent droplets is analyzed by ESI-MS, and the other is sorted based on the ion intensity of interest using DEP. The original demonstration of MADS used ESI-MS to analyze the conversion of a non-native, non-fluorescent amine substrate into a ketone product by a transaminase enzyme. While this report remains the only demonstration of droplet sorting actuated by ESI-MS analysis, it used an *in vitro* transcription/translation (ivTT) to express enzyme variants. This approach is limited because many enzymes are not easily *in vitro* expressed, genetic material had to be amplified using PCR, and the downstream analysis of selected variants requires amplification, transformation into cells, culture, and sequencing.[28] Each step of this process increases variability in the genetic material confined to the droplets, so

screening and validation becomes more complicated. Additionally, the method was restricted to enzyme evolution, where related applications in bioengineering such as synthetic biology and metabolic engineering show promise for chemical production. Each of these concerns are readily addressed by investigating the use of living cells for MADS.

Many DE workflows use microbes such as *E. coli* or *S. cerevisiae* for synthetic biology.[28] These cells have the advantage of rapid growth under mild conditions and can be easily scaled up for production. In addition to use for expression of an enzyme for enzyme engineering, entire pathways can be optimized for chemical production.[28] Validation of a screen using living cells requires fewer steps; in principle, the selected cells could be viable for bulk verification though culture and downstream analysis such as sequencing.

A small number of reports have used ESI-MS to analyze whole cells encapsulated in droplets. Two examples have focused on the encapsulation, growth, and analysis of different actinobacteria strains in the genus *Streptomyces* for the production of antibiotics.[24,29] Recently, the conversion rate of D-glucose to L-lysine by *C. glutamicum* was measured using droplet ESI-MS.[23] Notably, these reports used MS only to analyze the droplet samples and no sorting was performed. The glucose turnover report aimed to understand the catalysis of individual cells rather than for developing production-ready biocatylsts;[23] however, for the discovery of cell variants that can be used in production, high biomass in the droplets is essential.

Here, we demonstrate MADS for the selection of whole-cell variants producing L-lysine with high biomass. Lysine is a vital small molecule used in many industries such as agriculture, pharmaceuticals, and cosmetics,[30] but is not produced by humans or animals. Living foundries such as microbes show promise to continuously generate lysine to match multibillion-dollar demand.[31] To this end, some studies have focused on understanding pathways to develop *E. coli*

variants that overproduce lysine.[31,32] We present a method for analyzing lysine directly from droplet cell cultures using ESI-MS and discuss in-droplet growth conditions for biocatalyst discovery. An integrated workflow for cell sorting using MADS is demonstrated (Figure 6-1). The utility of the system is shown with the selection a known high-producer of lysine.[31] In the final workflow, cells are encapsulated in droplets, grown to form isogenic colonies, sorted using MADS, then collected for validation. The selected cells are shown to be readily grown in liquid cultures, enabling standard validation techniques.

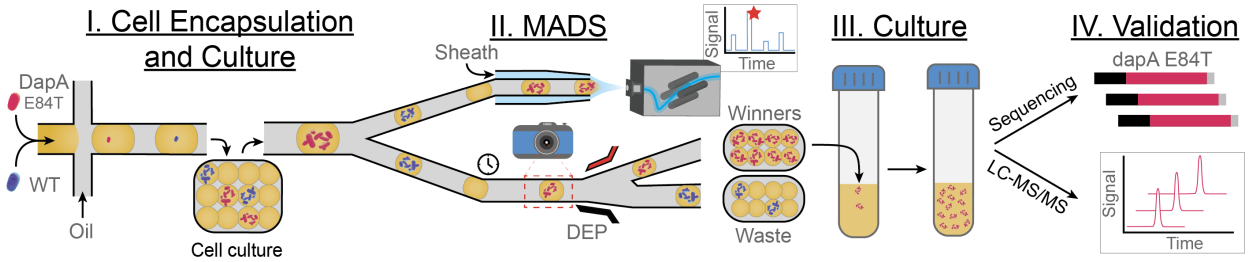

Figure 6-1: Workflow for E. coli cell sorting with MADS. Droplets are generated with single E. coli cells then cultured to create isogenic colonies. Droplets are split where one is analyzed by ESI-MS, and the other is sorted using DEP based on the MS signal intensity. Selected droplets are added to fresh cell media for bulk culture, enabling validation by LC-MS/MS and sequencing.

6.2 Materials and Methods

Reagents and Materials. All chemicals and solvents were purchased from Sigma Aldrich (St. Louis, MO) unless otherwise stated. Novec 7500 oil was purchased from Oakwood Chemical (Colombia Hwy, Estill, SC), and was mixed with 008-Fluorosurfactant from RAN Biotechnologies (Beverly, MA) to a concentration of 2 wt.%. Lysine deficient Neidhardt ("EZ Media - Lys") was purchased from Teknova (Hollister, CA) and was prepared according to manufacturer suggestions. Carbenicillin (Teknova) and Chloramphenicol (Teknova) were added to the media at 100 µg/mL and 25 µg/mL respectively as antibiotics. Blue dye was purchased from Kroma Kolors (Torrance, CA).

Device Design and Fabrication. All microfluidic devices were produced using standard protocols. Devices were designed using AudoCAD from Autodesk Inc (San Rafael, CA). Exposure masks were generated for photolithography. SU8 master molds were prepared at 150 μm feature height by spin-coating and exposing SU8 2075 negative epoxy photoresist from Kayaku Advanced Materials (Westborough, MA) onto silicon wafers from University Wafer (South Boston, MA) through the photomasks. Device master molds were developed after UV irradiation, and degassed polydimethylsiloxane (PDMS) was poured and cured. Fluidic ports were produced in the PDMS stamps. PDMS stamps fabricated with fluidic channels were bound glass slides using oxygen plasma activation generated by a Harrick Plasma Inc. PDC-32G (Ithaca, NY). Microfluidic devices were flushed with 2% tridecafluoro-1,1,2,2-tetrahydrooctyl tricholorosilane in perfluorodecane for surface treatment.

Cell Culture. Glycerol stocks of wild-type (WT) and DapA E84T *E. coli* were provided by Inscripta, Inc. To initiate cell growth, 2 μL of the glycerol stock was added to 2 mL freshly prepared cell media under flame. Cell density measurements at optical density 600 nm (OD_{600}) were taken using a WPA CO8000. For bulk experiments, tubes were incubated at 30 °C shaking at 250 rpm using a Thermo MaxQ 4450 until absorbance readings were > 2, approximately 18 h. For in-droplet cell culture experiments, the initial culture generated from the glycerol stock with absorbance < 0.05 was used for droplet generation. Droplet cell culture was achieved at 30 °C with periodic mixing of the droplets.

Device Operation and MADS. Flow was achieved through both pressure-driven and syringe-driven flow. For pressure-driven flow, an Elveflow (Paris, France) OB1 MK4 was supplied with dry nitrogen. Syringe-driven flow was achieved using Hamilton (Reno, NV) gastight syringes with Chemyx Inc. Fusion 400 syringe pumps. Pressurized vials or syringes were

connected to microbore polytetrafluoroethylene tubing from Cole Parmer (Vernon Hills, IL) which was inserted into the microfluidic device ports. When applicable, devices were coupled to the electrospray ionization source with 150 μm x 300 μm perfluoroalkoxy alkane tubing from IDEX (Lake Forest, IL).

To generate droplets, flow focusing devices were used to segment aqueous flow with fluorinated oil. Droplets were stored in glass vials which were capped with stoppers as described previously.[27] After storage, droplets were pumped into subsequent devices by displacing droplets in the sealed containers with fresh oil.

For MADS experiments, droplet and respacing oil was driven by syringes at 1.5 and 15 μL/min respectively. To maintain constant flow to the MS arm and the sorting arm, back pressure was applied to the oil accelerator region and the outlet using the OB1 with a 0.1 PSI offset respectively.

The mass spectrometer was an Agilent 6135b single quadrupole outfitted with a capillary electrophoresis sheath flow electrospray source. Electrospray was achieved with 2.5 kV, with 350 °C drying gas set at 30 L/min, a source pressure of 10 psi, and 135 eV of fragmentor energy. The sheath liquid was water pumped at 30 μL/min unless otherwise stated. The mass spectrometer was operated in selected ion mode, monitoring for the nominal protonated mass for each of the test analytes and the nominal molecular weight of the marker compounds which each carry a permanent positive charge (lysine; 147 m/z, arginine 174 m/z, neostigmine 223 m/z). Dwell time on the instrument was set at 2 ms per mass.

MADS was achieved by scanning and processing voltages for each selection ion as described in depth previously.[27] Briefly, a modified fraction collection board exported voltages from the instrument to amplifiers which were read by a microcontroller. The microcontroller was

also connected to a Cognex (Natick, MA) In-Sight 7600 tracking camera, which processed droplets on chip discriminating between marker (containing 1% blue dye) and non-marker droplets. Arginine present in the cell media was used for droplet detection, neostigmine (50 μM) was used to track marker droplets, and lysine was monitored to determine hits. A custom LabView software package was used to align the MS trace with the camera tracking, and to threshold for sorting the droplets of interest. DEP was achieved by applying 1 kV to 3 M NaCl electrodes on chip. Droplets were collected into a pressurized vial with glass inserts to contain the selected and waste droplets.

LC-MS/MS Validation. For the bulk-grown cell screen, droplets from the hit and pre-sorted pool were collected. The droplet samples were merged with 0.5 μL of perfluorooctanol with vortexing. 15 μL of the subsequent aqueous sample was quenched with three volume equivalents of cold methanol. Prior to encapsulation for MADS, control samples of the WT and DapA variant cultures were collected and quenched with three volume equivalents. For the droplet grown screen, droplets were collected, merged, and 2 μL of the aqueous pool was immediately added to 2 mL of fresh cell media, and 2 μL of the control WT and DapA cultures was added to 2 mL of fresh media. Samples for LC-MS/MS were obtained after 24 h culture.

Samples for quantitation and validation were prepared using benzoyl chloride derivatization described previously.[33] Calibration samples were prepared in fresh cell media then were diluted three-fold in cold methanol. Sample and calibration samples were centrifuged for 15 min. Supernatant was mixed 2:1:1:1 with 100 mM sodium carbonate and 2% benzoyl chloride, vortexed for 10s, then sulfuric acid in acetonitrile/water for quenching. Solutions were filtered, diluted 1:1000 in HPLC-grade water and added to autosampler vials.

LC-MS/MS was performed using an Agilent 1290 Infinity II outfitted with a Phenomenex Kinetex C18 column (2.1 mm x 100 mm, 1.7 μm) interfaced to an Agilent 6410 triple quadrupole

mass spectrometer. Mobile phase A (MPA) was 10 mM ammonium formate in HPLC-grade water and MPB was HPLC-MS grade acetonitrile, held at a total flow rate of 0.5 mL/min. MPB was initially held at 20% for 3.5 min then ramped to 70% over 1 min. Benzylated lysine and glutamine were monitored with multiple reaction monitoring; the lysine mass transition was 355.2 to 188.1 *m/z* and the glutamine was 251.7 to 105.2 *m/z*. Peaks were integrated using the Agilent software.

Phenotyping analysis. Glycerol stocks generated from overnight cultures were diluted and plated onto an LB agar plates (Teknova) containing 100 µg/mL carbenicillin and 25 µg/mL chloramphenicol. The plate was incubated at 30 °C for 16 h, then an QPix 420 automated colony picker (Molecular Devices) was used for depositing colonies into sterile 1.2 mL square 96-well plates (Thomas Scientific). Colonies were grown in 300 µL of fresh cell media for 19 h in a shaker incubator (Climo-Shaker ISF-X (Kuhner), 30°C, 85% humidity, 250 rpm). Cultures were diluted 20-fold into new 96-well plates containing fresh media, followed by 24 h in the shaker incubator.

Plates were centrifuged at 3,000 g for 10 min, and the supernatant was diluted 100-fold in water, then 10-fold in 50:50 acetonitrile and water. Lysine concentration was measured using a RapidFire high-throughput mass spectrometry system (Agilent) coupled to a 6460 triple quadruple mass spectrometer (Agilent). The RapidFire conditions were as follows: Pump 1: 80% acetonitrile (LC/MS grade, Fisher), 20% water (LC/MS grade, Fisher), 1.5 mL/min, Pump 2: 100% water, 1.25 mL/min, Pump 3: 5% acetonitrile, 95% water, 1.25 mL/min. RapidFire method: Aspirate: 600 ms, Load/wash: 2000 ms, Extra wash: 0 ms, Elute: 3000 ms, Re-equilibrate: 500 ms. 10 µL injection loop. Lysine quantification was achieved for ion abundance of lysine (147.1 – 84 m/z).

6.3 Results and Discussion

Direct MS detection of lysine. A challenge with direct MS without a separation method is ionization suppression during ESI. In particular, the suppression is severe for complex matrices such as cell media, which contains essential nutrients and salts.[34] Previously, matrix effects for detection of lysine were reduced by using alternatives to standard cell media.[23] However, it is preferable to use established growth media as to maintain consistency between screening and validation conditions. Droplet ESI has been achieved previously using a coaxial sheath flow source which facilitates the ionization without droplet transfer to stainless steel emitters.[26,35] In principle, the use of a sheath flow can also reduce matrix effects by performing on-line dilution during ESI, which has been studied in depth in application with capillary electrophoresis.[36]

We investigated the ability to detect lysine from lysine-deficient growth media using a sheath flow source by generating droplets using a microfluidic "chopper" described previously.[37] For a first test, droplets were generated from two streams; one comprised of lysine deficient Neidhardt media and the other was Neidhardt media containing 250 μM lysine. The droplets were analyzed using the sheath flow source with water as the sheath, and the flow rate was varied from 0 – 50 μL/min. The 0 μL/min condition mimics standard electrospray without sheath flow, and the 50 μL/min is the upper range of acceptable flow rates using the sprayer. ~70 droplets were analyzed for each flow rate, and all droplet signal intensities were retrieved using the maximum signal height for each droplet. Histograms of all droplet signals are shown in Figure 6-2A. At low sheath flow rates, no differentiation between the two populations was observed, owing to the lack of dilution and make-up flow that facilitates ESI. Above 10 μL/min sheath flow, a bimodal distribution is observed corresponding to droplets with and without 250 μM lysine added. The conditions with two signal populations (10 – 50 μL/min sheath) were compared quantitatively by

calculating Z-factors (Figure 6-2B). For the 10, 20, 40, and 50 µL/min conditions, the Z-factor was calculated as negative, indicating the variation between the population signals overlaps and the method is not suitable for screening.[38] The 30 µL/min sheath flow rate performed the best for differentiation of the two signal populations as it was the only condition to demonstrate a positive Z-factor. However, as the Z-factor was calculated as 0.2, the method for screening these two concentrations is marginal.[38]

The sheath flow both facilitates the spray of the droplets and provides dilution to the droplets as they are ionized. The 30 µL/min performs best likely due to adequate dilution of the salts in the cell media and facilitation of droplet electrospray without having detrimentally high flow rates which contributes to signal variability during electrospray. The total flow rate from the microfluidic device (oil and aqueous flow) in this experiment was 2.3 µL/min, so effective dilution was 13-fold. For all future experiments, 30 µL/min of water was used for sheath flow.

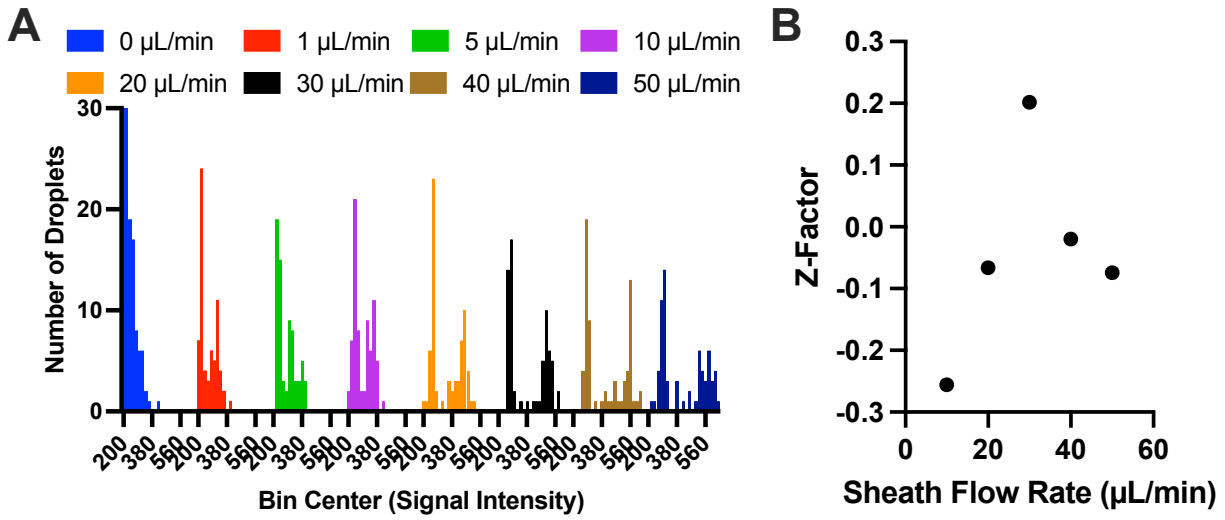

Figure 6-2: Testing droplet ESI-MS of lysine by varying sheath flow rate. (A) Histograms of 0 µM lysine and 250 µM lysine signal intensities with various sheath flow rates. Low sheath flow rates do not produce bimodal distributions of signals until 10 µL/min. Higher sheath-flow rates provide better separation between populations, but the highest flow rates have higher variability. (B) Z-factors calculated from the different sheath flow rates. Z-factor peaks at 30 µL/min.

A second challenge for screening using droplet microfluidics is the diffusion of target analytes between droplets.[12,39] If the target analyte of the screen can transfer between droplets, the reliability of sorting hits from the larger pool becomes challenging. We have previously demonstrated a method for testing droplet crosstalk in surfactant stabilized systems using the chopper device but did not investigate crosstalk in complex matrices such as cell media. We tested the transfer using the chopper device by comparing droplets which do not have lysine with and without exposure to droplets that do contain lysine (Figure 6-3). No statistically significant increase in the signal intensity was observed when the empty droplets are exposed to lysine-containing droplets, suggesting lysine is contained to the original droplet, and is a viable target for screening using a droplet-based high-throughput screen.

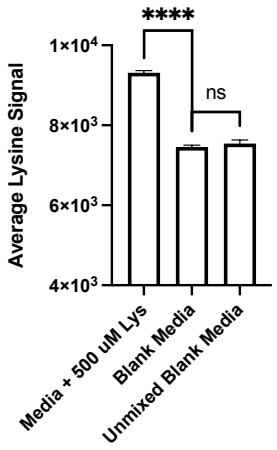

Figure 6-3: Crosstalk test of lysine in cell media. Results from chopper experiment comparing lysine-doped media to blank media mixed and unmixed for testing crosstalk. A significant difference ($P < 0.0001$) difference is observed between the lysine added and blank media populations. No significant difference is calculated between blank droplets when mixed and unmixed with lysine-containing droplets.

We next tested various lysine concentrations in cell media to determine if variable lysine production would be detectable from cells. Droplets were analyzed with ESI-MS with concentrations up to 1 mM. The average signal increased with concentration (Figure 6-4A) which suggests that cells producing variable amounts of lysine will be detectable using droplet ESI. From this calibration curve, the LoD was calculated as 80 μM. The MS signal during oil introduction

(e.g. background for the sheath flow) is shown with the dashed line. The variability in signals was calculated for each of these populations and Z-factors were calculated between each of the population combinations (Figure 6-4B). Z-factors between 0.5-1 are considered to provide excellent separation of signal populations.[38] These Z-factors show the differences that droplet ESI-MS is able to screen in this format, roughly >2-fold increase in lysine concentration. Under ideal conditions (e.g. maximum cell density at peak lysine production), WT *E. coli* produce 25 mg/L lysine corresponding with 171 µM, and *E. coli* variants such as the DapA E84T variant can produce almost 1000-fold more than the WT.[31] In the context of these benchmarks, the droplet ESI method is sensitive enough to detect the lysine produced by the *E. coli* strains of interest over the complex media background, and reliable enough to screen populations of WT and DapA variant lysine production, which is representative of an unknown variant in a potential screen.

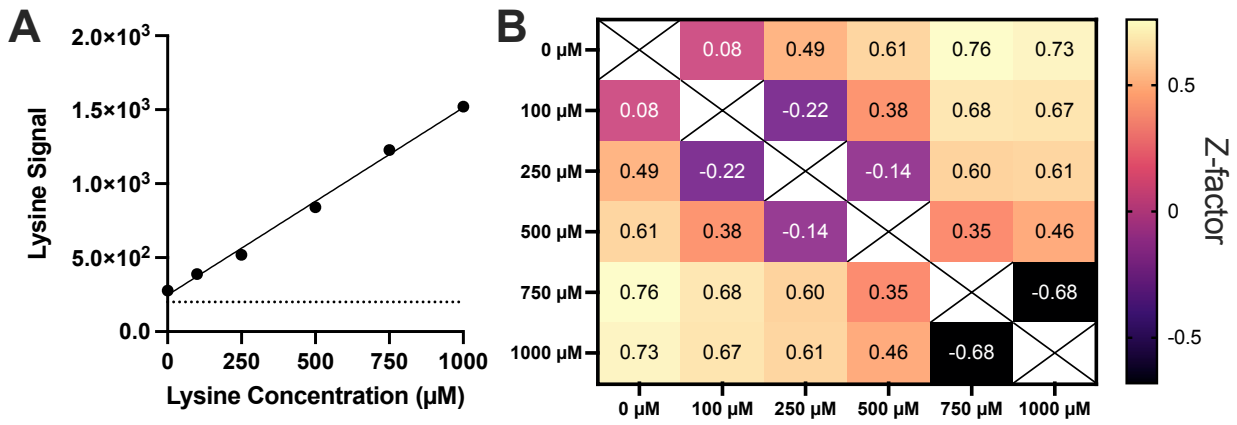

Figure 6-4: Lysine calibration curve and Z-factors from droplet ESI-MS. (A) Droplets were generated with increasing lysine in cell media. Each point represents 30 droplets with SEM. A line of best fit (R^2 >0.99) is included. The dashed line represents the background signal when no droplet is introduced. (B) Heatmap of the Z-factors comparing each droplet population from the calibration curve. Values <0 represent differences that are not adequate enough to screen, Z-factors 0 – 0.5 represent a marginal assay, and >0.5 represent an excellent assay.

It is notable that while the blank cell media does not contain lysine, it does contain glutamine which has the same nominal mass. Therefore, this method measures a cumulative signal intensity for both lysine and glutamine present in the media. The media contains 0.6 mM

glutamine,[34] which will be consumed by the cell during cell growth. For the experiments presented above, the background signal for glutamine was consistent; however, after cell growth the background signal can be affected by the consumption of glutamine. This presents a small issue since the signal intensity in the unspent cell media is very low compared to the background signal (Figure 6-4, dashed line).

Cell growth and lysine production. While the previous results suggested droplet-ESI is appropriate for detecting lysine from cell media, cell biology is another required step for droplet screening. Our previous work with MADS required 20 – 40 nL droplets as input, so cells must be cultured in this range of droplet sizes. There has been some work reported on *E. coli* culture in 8 – 500 nL droplets.[40–43] However, both cell culture and lysine production must be feasible. We tested growth first by diluting cells to < 0.05 OD_{600} in fresh Neidhardt media, which is the lower limit of the OD meter. We then generated 20 nL droplets using the suspension. The droplets were incubated with periodic mixing, then imaged. While cells were not observed at early time points due to the small size of *E. coli* (Figure 6-5A), significant growth was observed after 48 h (Figure 6-5B), indicated by the turbidity best observed at 20x magnification. As expected by the low cell density, 64% droplets remained empty because no cell was encapsulated by the droplet. By calculating the Poisson distribution based on the degree of occupancy, ~29% of droplets contained a signal cell while ~8% of droplets contained two or more cells initially.[44]

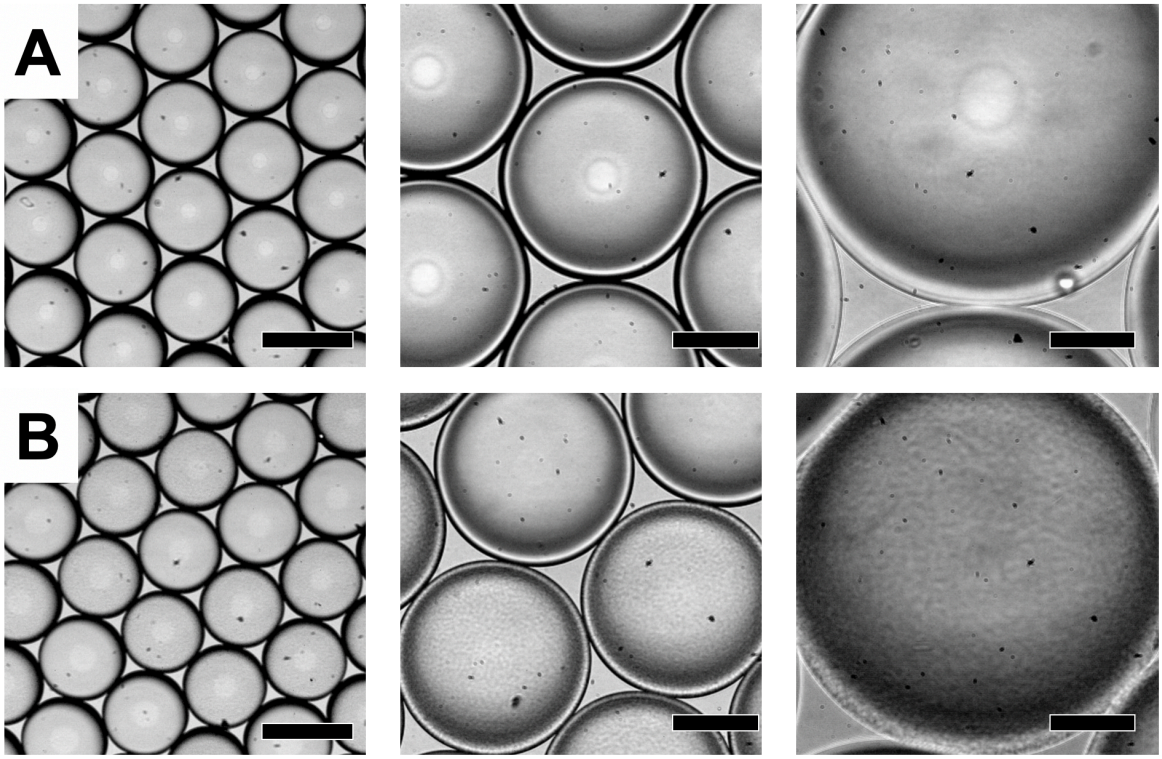

Figure 6-5: Images of E. coli cell growth in droplets. (A) Initial and (B) 48-hour time point images. Panels show images using a 4x, 10x, and 20x objective. Scale bars represent 500 um, 200 um, and 100 µm for 4x, 10x and 20x objectives, respectively.

We next attempted to detect lysine from the cells that were grown in droplets. For this test, we encapsulated WT *E. coli* and the DapA variant E84T.[31] A population of droplets was generated intentionally empty, marked by 50 µM neostigmine which is a small molecule that is easily detected by ESI-MS. The droplets were generated, incubated for 48 h, then infused through a microfluidic device which re-spaces droplets with oil for analysis. An example of the droplet ESI-MS trace is shown in Figure 6-6. The trace shows mixed droplets from the incubation, where the order of droplet introduction is random. None of the droplets with high lysine correspond to droplets containing neostigmine, which marks known empty droplets. This reduces the likelihood that the high lysine signals observed are random detector noise. Only two levels of lysine signal are observed, suggesting that droplets that contain WT cell cultures are not immediately recognizable over the unspent cell media background (marked with neostigmine). We hypothesize

that since the WT *E. coli* produces relatively low lysine, the degree of glutamine consumption during growth offsets the lysine production in these droplets. A primary concern when designing microfluidic systems using dense cell suspensions is the clogging of microfabricated channels and emitters during ESI-MS. This test demonstrated the feasibility of using high-density cell suspensions in this system, as no clogging or detrimental effects were observed throughout the duration of this experiment (75 min, >2000 droplets).

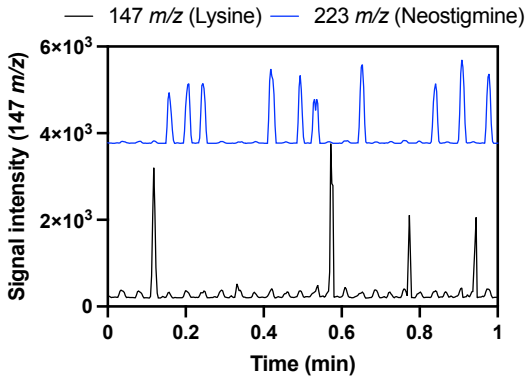

Figure 6-6: ESI-MS following E. coli growth in droplets. Lysine trace (black, 147 m/z) and neostigmine (blue, 223 m/z, offset) are shown. High lysine signal is observed in four of the droplets. Neostigmine marks droplets intentionally left empty.

MADS of lysine. The previous results suggest that droplet microfluidics and ESI-MS are suitable methods for growing and analyzing cell variants. However, MADS must be implemented to preserve sample for sorting. MADS has been shown using *in vitro* transcription/translation buffers,[27] but thus far cells in droplets have not been investigated. Beyond this example, no other report has achieved droplet sorting based on MS.

The success of MADS relies on the intermittent and random introduction of marker droplets used for alignment between ESI-MS and sorting. Alignment is achieved by monitoring a unique mass (223 *m/z*, neostigmine) by ESI-MS and correlating that signal with a blue dye in the droplet that can be observed with camera tracking on chip. The initial demonstration of MADS used differential flow rates and delay lines to offset the analysis by MS from the tracking camera,

typically 50 – 70 droplets in "queue" for sorting. The alignment is performed by matching the pattern of non-marker droplets to marker droplets, then initiates the sorting based on thresholds set in the program. However, it was observed during testing that having a substantial delay between the MS and the on-chip camera resulted in misalignment due to the many droplets in the queue. Modifications were made to the MADS system for this demonstration by shortening the delay between the MS and camera (Figure 6-7A). In the updated design, the delay between the MS analysis and the replicate droplet arriving to the sorting region was designed to be 5 – 10 droplets, which provides less opportunity for misalignment.

During preliminary testing it was also observed that *E. coli* growth in-droplet changes the color of the droplet from colorless to gray/brown. As the camera uses the detection of a blue dye to recognize marker droplets from non-marker droplets, we verified the ability for the camera to distinguish between blue and cell containing droplets. After training the camera processing program, droplet classification was achieved between the blue marker droplets and droplets containing cells (Figure 6-7B). With the updated camera settings and device design, a test experiment was performed to sort any cell containing, non-marker droplets from marker droplets as determined by the MS; the MS settings were set to select any droplet not containing the marker molecule, neostigmine, and to send marker droplets to waste. DEP sorting of non-marker droplets was observed (Figure 6-7C) suggesting the updated system could be used in replacement of the original MADS design.[27]

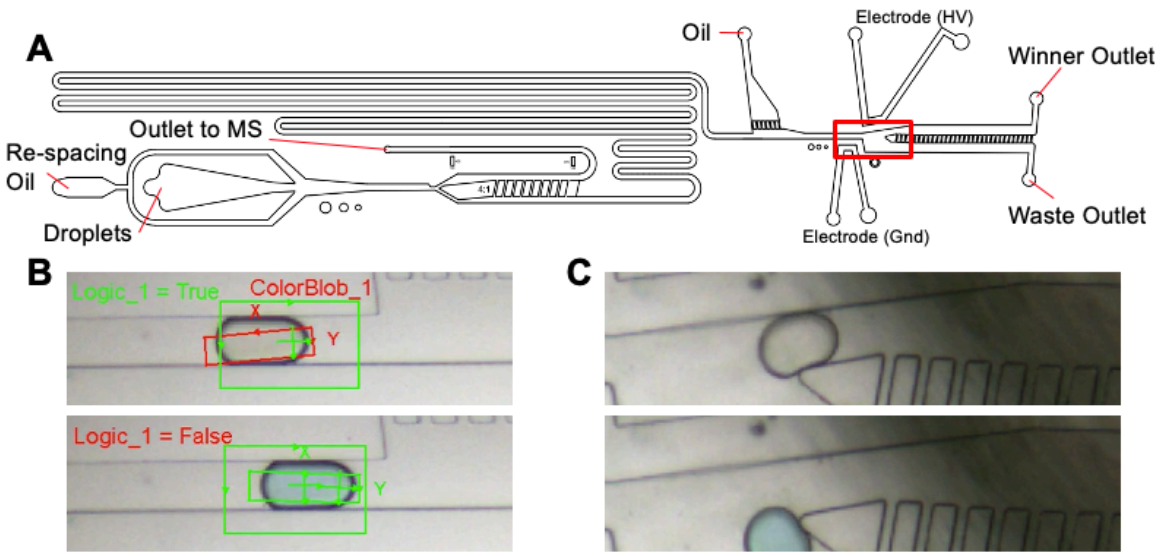

Figure 6-7: Design and example of MADS experiment. (A) Design of MADS device with labelled fluidic ports. The delay channel to the sorting region was shortened to reduce delay between MS and sorting outlets. (B) Images from camera tracking of a turbid cell sample versus a blue marker droplet. (C) Images of sorting non marker droplets from marker droplets.

We applied MADS to the sorting of cell samples that were grown in bulk liquid cultures. WT and DapA E84T variants ("DapA") were grown in standard liquid cultures for 48 h. The cell suspensions were infused through the chopper device to determine the signal differences between the two cultures. Two distinct populations were observed, correlating with the WT and DapA variant cultures. Using the droplet signals from this experiment, a Z-factor of 0.623 was calculated (Figure 6-8A),[45] suggesting the populations means are significantly different from each other accounting for signal variability. A lysine signal threshold for sorting was selected based on the marker droplet mean signal plus three standard deviations of the population. This threshold accounts for the variance in WT signal, providing a 99.7% confidence interval of not sorting from the WT population.

Using the liquid culture cell outgrowth and a solution of cell media containing blue dye and neostigmine (marker), droplet populations were generated with 60% WT, 20% DapA, 20% marker. Droplets were infused into the MADS system and screened for ~3 h. Approximately 5000 droplets were analyzed, and the system remained in-sync for ~85% of the time, resulting in 4230

droplets processed by the system. An example trace from this experiment is shown in Figure 6-8B. The system was out of sync for ~750 droplets, so all droplets were sent to the waste collection during these periods. The non-synced intervals are primarily due to the introduction of merged droplets into the system. When merged droplets enter the MADS chip, the stream is segmented by the re-spacing oil (Figure 6-7A); however, the merged droplets often contain neostigmine which the MS recognizes as a marker droplet, but the blue dye is too dilute to be recognized by the camera. In these instances of droplet merger, the MS classifies merged droplets as marker droplets, and the camera classifies the identical droplets as non-markers, which causes the interval alignment to fail.

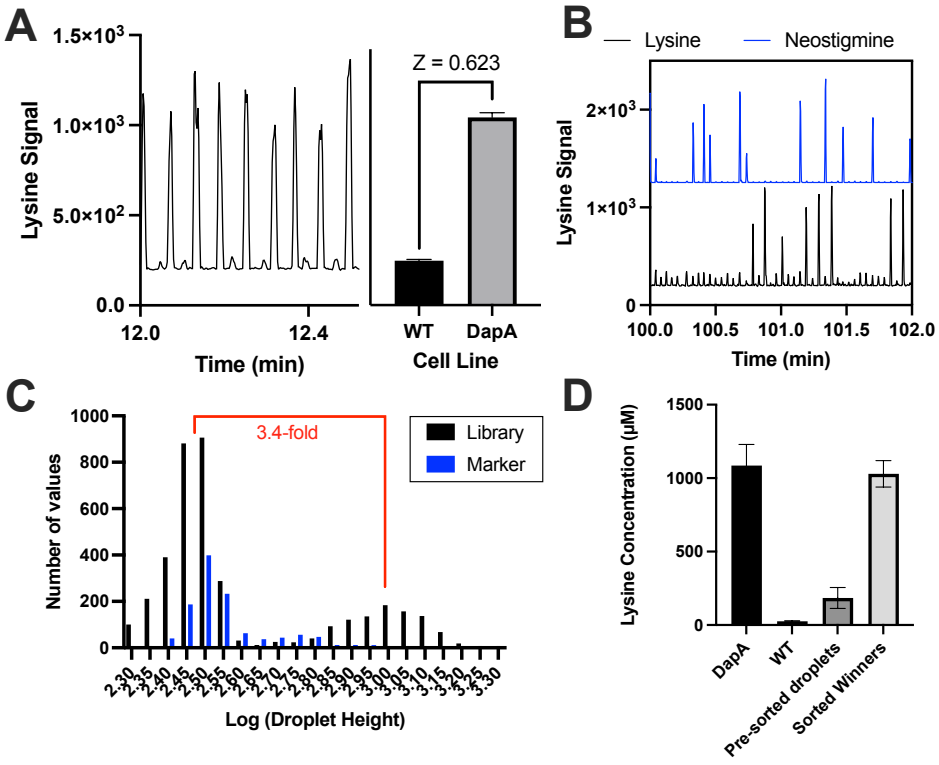

Figure 6-8: Results from MADS of droplets generated from E. coli liquid cultures. (A) Chopper experiment to compare WT and DapA signals when grown in bulk cultures. The average signals are differentiable with a Z-factor of 0.623. (B) Example trace from MADS experiment of bulk grown cells. Neostigmine trace (blue, offset) signifies marker droplets. (C) Histogram from all droplets analyzed in the experiment. The black bars represent a library (WT or DapA) droplet, whereas blue bars represent marker droplets. (D) Concentrations of lysine determined by LC-MS/MS. DapA and WT control samples were obtained at the time of droplet generation for the MADS screen.

A histogram of all droplets analyzed is shown in Figure 6-8C. Non-marker droplets are labelled as "library" droplets, which represent droplets generated from either the WT or DapA solutions. Two distributions of library signals are observed from the histogram, correlating with high and low lysine signal. By applying a signal threshold to the library droplets, WT and DapA classifications are assigned after data collection. Statistics from this experiment are shown in Table 6-1. The threshold resulted in droplet populations roughly equal to those generated and pumped into the MADS device. The percentage of marker droplets is artificially high due to the previous discussion of merged droplets.

Table 6-1: Results from MADS screen of cells grown in liquid cultures.

Population	Number of Droplets	Percentage of Total	Average Signal ± SD	% RSD
WT	2827	57%	291 ± 41	14%
DapA	1001	20%	998 ± 247	25%
Marker	1148	23%	373 ± 127	34%

The sorting experiment was validated using LC-MS/MS (see methods). The samples were derivatized using benzoyl chloride described previously,[33] which enhances separation of glutamine from lysine. Lysine concentrations from the initial cell cultures, pre-sorted droplets, and sorted winners are shown in Figure 6-8D. The control DapA culture used to droplet generate hit droplets for the experiment produced ~1 mM lysine and the WT culture had 10-fold lower lysine production. The pre-sorted droplet population had higher lysine than the pure WT control owing to the 20% of the population which was generated from the DapA culture suspension. The sorted droplets had significant lysine, equal to the DapA initial culture within error. Based on these concentrations, the sorted winners had 5.6-fold higher lysine than the pre-sorted pool, and 40.9-fold higher lysine than the WT control culture, demonstrating enrichment of the desired droplets.

The glutamine signal for all samples was less than half of that in the blank unspent cell media, suggesting that the droplet sorting was unaffected by glutamine signal in the droplets, and that glutamine was consumed during cell growth.

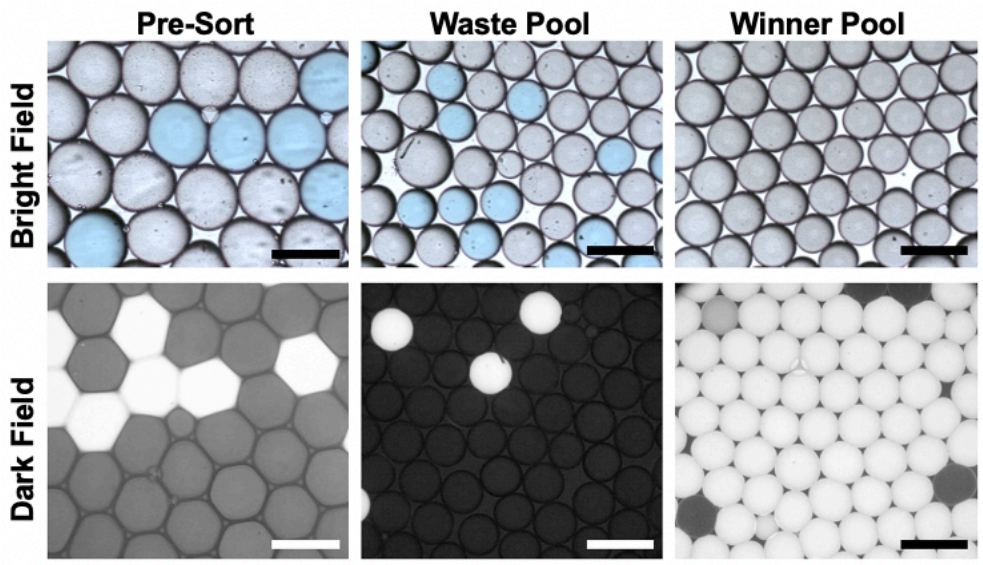

Figure 6-9: Fluorescent validation of MADS experiment. Representative images of droplet populations in bright and dark field. Blue droplets represent marker droplets used for alignment, and fluorescent droplets were generated from the desired DapA cell suspension. Scale bars are 500 µm.

To further validate the false positive and false negative sorting rate, a similar sorting experiment was undergone, but the DapA liquid culture was marked with 10 µM fluorescein prior to droplet generation. The droplets were imaged pre- and post-MADS to quantify ratios of DapA droplets. Representative bright and dark field images are presented in Figure 6-9. In bright field, the abundance of markers can be determined by the presence of the blue dye. In dark field, abundance of DapA droplets can be observed. The results from this sorting experiment are summarized in Table 6-2. The pre-sorted pool was measured with 14.3% DapA, 68.4% WT, and 17.3% marker droplets. After sorting, 97.1% of droplets collected were from the DapA culture, suggesting a 2.9% false positive rate (e.g. WT droplets in the sorted pool). No marker droplets were observed in the winner pool. In the waste pool, 4.3% of the droplets were DapA, which is a sufficiently low false negative rate. In comparison to our prior work with *in vitro* expression for

MADS, this report has similarly high success rate (previously reported as 91.6 – 98.7%) with a slightly higher false negative rate (previously reported as 1.5 – 4.1%).[27]

Table 6-2: Percentages of droplet populations pre- and post-MADS determined with bright and dark field imaging.

Droplet Pool	DapA	WT	Marker
Pre-sort	14.3%	68.4%	17.3%
Waste	4.3%	73.7%	22.0%
Winner	97.1%	2.9%	0.0%

MADS of cell variants. The bulk screen demonstrated potential to select active from less active variants; but it does not represent a workflow compatible for selecting active variants from a population. Therefore, we sought to select cell samples grown in droplets. For this test, dilute cell solutions of WT and DapA were prepared (OD_{600} < 0.05), then droplets were generated. Marker droplets were generated at a 20% ratio to the total amount of droplets generated. The droplet storage vial was incubated as previously shown, then droplets were screened using MADS.

Droplets were infused for 160 min, and droplets with high lysine signal were sorted as above. Figure 6-10A shows a trace where each point represents the height of a library or marker droplet. A histogram showing the total droplets analyzed in this system is shown in Figure 6-10B. As previously, a bimodal distribution of library droplets is observed; the lower signal population are droplets that were generated with a single WT cell or were empty due to the low cell density. The higher signal population which was sorted with MADS represents droplets that were generated with a single DapA variant cell encapsulated. Isogenic cell colonies were grown in the droplets from the initially encapsulated single cells, which then produced lysine contained to the droplet analyzed and sorted with MADS. Interestingly, the lower signal population had lower lysine signal than the marker droplets, which were made with fresh media without lysine. This signal shift

indicates the consumption of the glutamine during growth by the WT cells, without sufficient lysine production to offset the glutamine depletion.

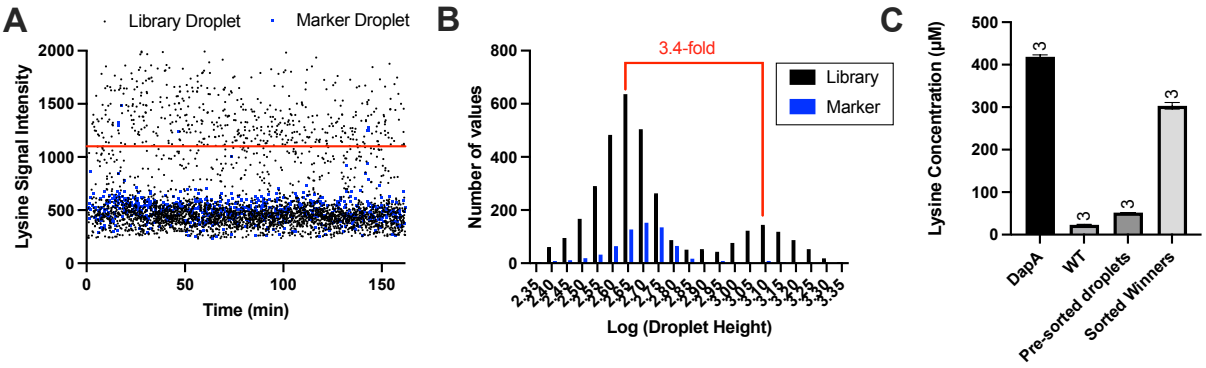

Figure 6-10: Results from MADS following in droplet E. coli growth. (A) Reformatted trace of droplet heights for 160 minutes of screening. (B) Histogram of all analyzed droplet heights. (C) LC-MS/MS quantitation results from cultures generated from droplet seeded into media.

To validate the selected droplets, liquid cultures were generated by seeding sorted and pre-sorted droplets into fresh media (see methods). Initially, the cell density for each culture was low (OD_{600} < 0.05) but after 24 h of growth each culture showed significant growth (OD_{600} measurements > 2, Figure 6-11). This finding demonstrates that cells that have been cultured in-droplet and screened using MADS are viable and can be used for validation. Cell contamination resulting in the growth observed in Figure 6-11 is unlikely as the cell media contained antibiotics and the cells used for the experiment had antibiotic resistance. The ability to culture selected droplets after sorting is a considerable benefit to using whole cells for DE, as no genetic recovery, amplification, or transfection is required for validation.

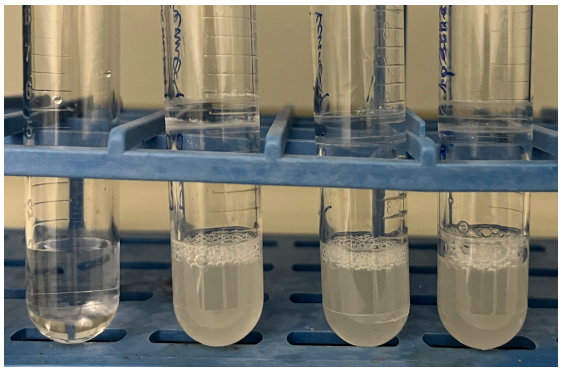

Figure 6-11: Image of bulk cultures generated after the in-droplet grown MADS experiment. From left to right, cultures are blank media, positive control DapA, sorted droplets, and pre-sorted droplets.

The bulk cultures were each sampled for analysis by LC-MS/MS. The resulting concentrations are shown in Figure 6-10C. The trends are similar to the previous screen: pre-sorted droplets have higher lysine production than the pure WT culture, and the sorted winners have higher lysine than the pre-sorted droplets. The sorted droplets resulted in a culture with 5.8-fold higher lysine than the pre-sorted pool, showing enrichment of a mixed population of WT and DapA. Similarly, the winner cultures had 13.1-fold higher lysine than the WT control cultures. These results suggest that MADS was successful at selecting DapA droplets from WT grown in droplets. The winner culture had less lysine compared to the DapA control, which could be a result of unequal growth following droplet seeding compared to the control culture, or from WT droplets sorted into the winner pool. Based on the enrichment from pre-sorted droplets to the winners, the false positive rate appears low, but more advanced validation can be performed to quantify the false positive rate. After the initial cultures were produced from the droplet and control groups, glycerol stocks were prepared.

To measure the accuracy of the sorting, the liquid cultures were analyzed using phenotyping of colonies generated from individual cells. Briefly, glycerol stocks were spread onto an agar plate, resulting in colonies grown from single cells adhered to the agar. A subsection of 96 colonies per glycerol stock were sampled into a multiwell plate and the production of lysine was

quantified compared to control DapA and WT samples. Based on the phenotype of individual colonies (e.g. the lysine concentration compared to control samples), the frequency of WT and DapA was determined. Glycerol stocks generated from the control WT and DapA cultures resulted in 100% frequency of the respective target cell line (Figure 6-12). Samples from the pre-sort droplet populations resulted in mixed populations of the two cell lines; on average, 78% of the cells were WT, 20% were DapA and 2% were intermediate, meaning both WT and DapA cells grew together in one agar colony sampled for analysis. Four sorted winner pools were collected throughout the experiment with sample collection occurring every 40 minutes. The four pools are shown in Figure 6-12, where "Win 1" represents the first 40 minutes, "Win 2" is the second 40-minute interval, and so forth. The winning pools resulted in 68-100% DapA, demonstrating 3.3 – 4.9-fold enrichment of DapA from the pre-sorted droplets. Based on the increase from 68% DapA to 100% DapA, the sorting success rate improved throughout the experiment. This is likely due to misaligned sorting events early in the experiment, which is less frequent when the MADS system has more time to properly align. Based on these results, MADS was effective at selecting for the high producing cell variant for lysine.

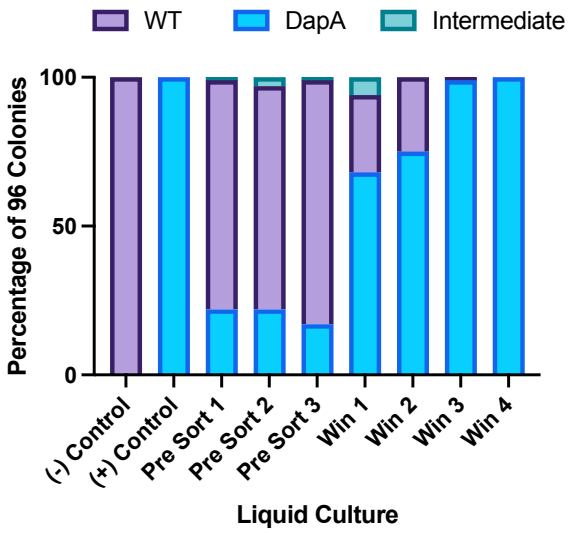

Figure 6-12: Phenotyping analysis of cultures generated from MADS experiment. Percentage of colonies formed from liquid cultures. Positive and negative control cultures were pure WT and DapA cultures respectively. Pre-sort pools represent liquid cultures generated by adding merged droplets to fresh media. Winner pools represent droplets collected from sorting at four time points.

Variability with droplet ESI. The experiments above have showed the analysis of lysine in droplets in a variety of formats. By compiling this data, it is possible to examine variability in different formats to understand where sources of error will arise when applying this to an unknown high-throughput screen. The results from LC-MS/MS validation in Figure 6-8D showed that the DapA variant produced roughly 1 mM lysine, corresponding to ~1000 counts using droplet ESI-MS. Using this concentration, MADS was tested using 1 mM lysine standard in cell media to quantify the variability in droplet signal. Figure 6-13 shows compiled data for lysine analyzed by droplet ESI. The %RSD is shown for five formats of lysine analysis. The chopper device with 1 mM standards resulted in the lowest variation with an RSD of 5%. When the experiment was repeated with the bulk-cultures of DapA, the variation increased to 9% RSD. The variability increased further when using the MADS device with 1 mM lysine standards to 18% RSD. When performing MADS on the cell suspensions grown in bulk (data from experiment in Figure 6-8C), the % RSD was 25%. Finally, the most complex workflow where cells were grown in droplets and

the droplets were analyzed during MADS, the RSD increased once again to 31% (data from experiment in Figure 6-10B).

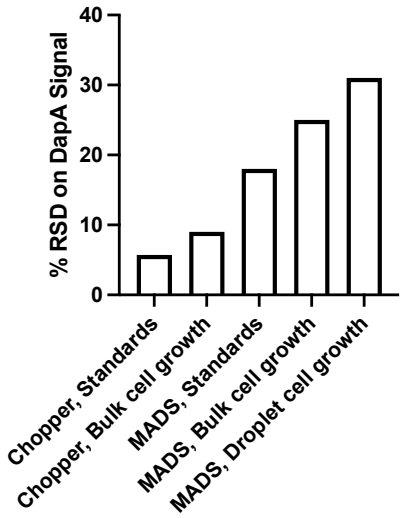

Figure 6-13: Variability of droplet-ESI MS experiments. Comparison of % relative standard deviation between droplet-ESI MS experiments for 1 mM lysine. The condition lists first the microfluidic device used for droplet introduction to MS then the method for lysine production. Standards signifies 1 mM lysine in unspent cell media, bulk cell growth indicates cells grown before droplet generation, and droplet cell growth means single cells were encapsulated then grown for lysine production.

These results indicate multiple sources of variability. The first source of variability is droplet ESI during MADS, resulting in increases when using both standards and cell-produced lysine. The complexity of the MADS device results in flow changes to the ESI source, which is the most likely cause for increased variability. Another source of variability appears to result from the inclusion of cells in the droplet, resulting in increases in the chopper and MADS experiment. This may be due to lysine sequestration or variable electrospray when whole-cells are present. A final source of variability is the biological variability occurring in the droplet. When cells were grown in the droplet, variability was higher than when a cell suspension was encapsulated after growth and lysine production. While this degree of variability is undesirable, the differential lysine levels between the DapA variants and WT was sufficient to account for the increased variability.

6.4 Conclusions

A system has been developed for the high-throughput sorting of cell variants using droplet microfluidics and ESI-MS. Lysine detection from an industry standard cell media is shown using droplet ESI-MS, facilitated by the use of a sheath flow ESI source. *E. coli* growth and metabolism is shown in large droplets, which is immediately usable for MADS. MADS was improved from a previous report for ease of sorting alignment and to be applicable for cell samples. Droplets generated using bulk grown cultures were screened, showing strong enrichment from the pre-sorted pool. Finally, a full workflow was demonstrated for *E. coli* encapsulation, growth, and screening, which yields viable cells for downstream analytical and biological validation with 68-100% success.

The workflow presented here has potential to enable high-throughput screening for a variety of evolution workflows. The system is generalizable for many synthetic biology approaches where the development whole-cell catalysts is limited by the sample processing and analytical screening.

6.5 References

(1) Arnold, F. H.; Volkov, A. A. Directed Evolution of Biocatalysts. *Current Opinion in Chemical Biology* **1999**, *3* (1), 54–59. https://doi.org/10.1016/S1367-5931(99)80010-6.

(2) Huffman, M. A.; Fryszkowska, A.; Alvizo, O.; Borra-Garske, M.; Campos, K. R.; Canada, K. A.; Devine, P. N.; Duan, D.; Forstater, J. H.; Grosser, S. T.; Halsey, H. M.; Hughes, G. J.; Jo, J.; Joyce, L. A.; Kolev, J. N.; Liang, J.; Maloney, K. M.; Mann, B. F.; Marshall, N. M.; McLaughlin, M.; Moore, J. C.; Murphy, G. S.; Nawrat, C. C.; Nazor, J.; Novick, S.; Patel, N. R.; Rodriguez-Granillo, A.; Robaire, S. A.; Sherer, E. C.; Truppo, M. D.; Whittaker, A. M.; Verma, D.; Xiao, L.; Xu, Y.; Yang, H. Design of an in Vitro Biocatalytic Cascade for the Manufacture of Islatravir. *Science* **2019**, *366* (6470), 1255–1259. https://doi.org/10.1126/science.aay8484.

(3) Savile, C. K.; Janey, J. M.; Mundorff, E. C.; Moore, J. C.; Tam, S.; Jarvis, W. R.; Colbeck, J. C.; Krebber, A.; Fleitz, F. J.; Brands, J.; Devine, P. N.; Huisman, G. W.; Hughes, G. J. Biocatalytic Asymmetric Synthesis of Chiral Amines from Ketones Applied to Sitagliptin Manufacture. *Science* **2010**. https://doi.org/10.1126/science.1188934.

(4) Schober, M.; MacDermaid, C.; Ollis, A. A.; Chang, S.; Khan, D.; Hosford, J.; Latham, J.; Ihnken, L. A. F.; Brown, M. J. B.; Fuerst, D.; Sanganee, M. J.; Roiban, G.-D. Chiral Synthesis of LSD1

Inhibitor GSK2879552 Enabled by Directed Evolution of an Imine Reductase. *Nat Catal* **2019**, *2* (10), 909–915. https://doi.org/10.1038/s41929-019-0341-4.
(5) Thorsen, T.; Roberts, R. W.; Arnold, F. H.; Quake, S. R. Dynamic Pattern Formation in a Vesicle-Generating Microfluidic Device. *Phys. Rev. Lett.* **2001**, *86* (18), 4163–4166. https://doi.org/10.1103/PhysRevLett.86.4163.
(6) Link, D. R.; Anna, S. L.; Weitz, D. A.; Stone, H. A. Geometrically Mediated Breakup of Drops in Microfluidic Devices. *Phys. Rev. Lett.* **2004**, *92* (5), 054503. https://doi.org/10.1103/PhysRevLett.92.054503.
(7) Abate, A. R.; Hung, T.; Mary, P.; Agresti, J. J.; Weitz, D. A. High-Throughput Injection with Microfluidics Using Picoinjectors. *PNAS* **2010**, *107* (45), 19163–19166. https://doi.org/10.1073/pnas.1006888107.
(8) Doonan, S. R.; Bailey, R. C. K-Channel: A Multifunctional Architecture for Dynamically Reconfigurable Sample Processing in Droplet Microfluidics. *Anal. Chem.* **2017**, *89* (7), 4091–4099. https://doi.org/10.1021/acs.analchem.6b05041.
(9) Cochrane, W. G.; Hackler, A. L.; Cavett, V. J.; Price, A. K.; Paegel, B. M. Integrated, Continuous Emulsion Creamer. *Anal. Chem.* **2017**, *89* (24), 13227–13234. https://doi.org/10.1021/acs.analchem.7b03070.
(10) Frenz, L.; Blank, K.; Brouzes, E.; D. Griffiths, A. Reliable Microfluidic On-Chip Incubation of Droplets in Delay-Lines. *Lab on a Chip* **2009**, *9* (10), 1344–1348. https://doi.org/10.1039/B816049J.
(11) Ahn, K.; Kerbage, C.; Hunt, T. P.; Westervelt, R. M.; Link, D. R.; Weitz, D. A. Dielectrophoretic Manipulation of Drops for High-Speed Microfluidic Sorting Devices. *Appl. Phys. Lett.* **2006**, *88* (2), 024104. https://doi.org/10.1063/1.2164911.
(12) Payne, E. M.; Holland-Moritz, D. A.; Sun, S.; Kennedy, R. T. High-Throughput Screening by Droplet Microfluidics: Perspective into Key Challenges and Future Prospects. *Lab Chip* **2020**, *20* (13), 2247–2262. https://doi.org/10.1039/D0LC00347F.
(13) Sciambi, A.; Abate, A. R. Accurate Microfluidic Sorting of Droplets at 30 KHz. *Lab on a Chip* **2015**, *15* (1), 47–51. https://doi.org/10.1039/C4LC01194E.
(14) Vallejo, D.; Nikoomanzar, A.; Paegel, B. M.; Chaput, J. C. Fluorescence-Activated Droplet Sorting for Single-Cell Directed Evolution. *ACS Synth. Biol.* **2019**, acssynbio.9b00103. https://doi.org/10.1021/acssynbio.9b00103.
(15) Sjostrom, S. L.; Bai, Y.; Huang, M.; Liu, Z.; Nielsen, J.; Joensson, H. N.; Andersson Svahn, H. High-Throughput Screening for Industrial Enzyme Production Hosts by Droplet Microfluidics. *Lab Chip* **2014**, *14* (4), 806–813. https://doi.org/10.1039/C3LC51202A.
(16) Fallah-Araghi, A.; Baret, J.-C.; Ryckelynck, M.; D. Griffiths, A. A Completely in Vitro Ultrahigh-Throughput Droplet-Based Microfluidic Screening System for Protein Engineering and Directed Evolution. *Lab on a Chip* **2012**, *12* (5), 882–891. https://doi.org/10.1039/C2LC21035E.
(17) Gielen, F.; Hours, R.; Emond, S.; Fischlechner, M.; Schell, U.; Hollfelder, F. Ultrahigh-Throughput–Directed Enzyme Evolution by Absorbance-Activated Droplet Sorting (AADS). *PNAS* **2016**, *113* (47), E7383–E7389. https://doi.org/10.1073/pnas.1606927113.
(18) Duncombe, T. A.; Ponti, A.; Seebeck, F. P.; Dittrich, P. S. UV–Vis Spectra-Activated Droplet Sorting for Label-Free Chemical Identification and Collection of Droplets. *Anal. Chem.* **2021**, *93* (38), 13008–13013. https://doi.org/10.1021/acs.analchem.1c02822.
(19) Wang, X.; Ren, L.; Su, Y.; Ji, Y.; Liu, Y.; Li, C.; Li, X.; Zhang, Y.; Wang, W.; Hu, Q.; Han, D.; Xu, J.; Ma, B. Raman-Activated Droplet Sorting (RADS) for Label-Free High-Throughput Screening of Microalgal Single-Cells. *Anal. Chem.* **2017**, *89* (22), 12569–12577. https://doi.org/10.1021/acs.analchem.7b03884.
(20) Xu, L.; Chang, K.-C.; Payne, E. M.; Modavi, C.; Liu, L.; Palmer, C. M.; Tao, N.; Alper, H. S.; Kennedy, R. T.; Cornett, D. S.; Abate, A. R. Mapping Enzyme Catalysis with Metabolic Biosensing. *Nat Commun* **2021**, *12* (1), 6803. https://doi.org/10.1038/s41467-021-27185-9.

(21) Ucal, Y.; Durer, Z. A.; Atak, H.; Kadioglu, E.; Sahin, B.; Coskun, A.; Baykal, A. T.; Ozpinar, A. Clinical Applications of MALDI Imaging Technologies in Cancer and Neurodegenerative Diseases. *Biochimica et Biophysica Acta (BBA) - Proteins and Proteomics* **2017**, *1865* (7), 795–816. https://doi.org/10.1016/j.bbapap.2017.01.005.
(22) Diehl, H. C.; Beine, B.; Elm, J.; Trede, D.; Ahrens, M.; Eisenacher, M.; Marcus, K.; Meyer, H. E.; Henkel, C. The Challenge of On-Tissue Digestion for MALDI MSI— a Comparison of Different Protocols to Improve Imaging Experiments. *Anal Bioanal Chem* **2015**, *407* (8), 2223–2243. https://doi.org/10.1007/s00216-014-8345-z.
(23) Schirmer, M.; Wink, K.; Ohla, S.; Belder, D.; Schmid, A.; Dusny, C. Conversion Efficiencies of a Few Living Microbial Cells Detected at a High Throughput by Droplet-Based ESI-MS. *Anal. Chem.* **2020**, *92* (15), 10700–10708. https://doi.org/10.1021/acs.analchem.0c01839.
(24) Mahler, L.; Wink, K.; Beulig, R. J.; Scherlach, K.; Tovar, M.; Zang, E.; Martin, K.; Hertweck, C.; Belder, D.; Roth, M. Detection of Antibiotics Synthetized in Microfluidic Picolitre-Droplets by Various Actinobacteria. *Scientific Reports* **2018**, *8* (1), 13087. https://doi.org/10.1038/s41598-018-31263-2.
(25) E. Kempa, E.; A. Hollywood, K.; A. Smith, C.; E. Barran, P. High Throughput Screening of Complex Biological Samples with Mass Spectrometry – from Bulk Measurements to Single Cell Analysis. *Analyst* **2019**, *144* (3), 872–891. https://doi.org/10.1039/C8AN01448E.
(26) Diefenbach, X. W.; Farasat, I.; Guetschow, E. D.; Welch, C. J.; Kennedy, R. T.; Sun, S.; Moore, J. C. Enabling Biocatalysis by High-Throughput Protein Engineering Using Droplet Microfluidics Coupled to Mass Spectrometry. *ACS Omega* **2018**, *3* (2), 1498–1508. https://doi.org/10.1021/acsomega.7b01973.
(27) Holland-Moritz, D. A.; Wismer, M. K.; Mann, B. F.; Farasat, I.; Devine, P.; Guetschow, E. D.; Mangion, I.; Welch, C. J.; Moore, J. C.; Sun, S.; Kennedy, R. T. Mass Activated Droplet Sorting (MADS) Enables High-Throughput Screening of Enzymatic Reactions at Nanoliter Scale. *Angewandte Chemie International Edition* **2020**, *59* (11), 4470–4477. https://doi.org/10.1002/anie.201913203.
(28) Wang, Y.; Xue, P.; Cao, M.; Yu, T.; Lane, S. T.; Zhao, H. Directed Evolution: Methodologies and Applications. *Chem. Rev.* **2021**, *121* (20), 12384–12444. https://doi.org/10.1021/acs.chemrev.1c00260.
(29) Wink, K.; Mahler, L.; Beulig, J. R.; Piendl, S. K.; Roth, M.; Belder, D. An Integrated Chip-Mass Spectrometry and Epifluorescence Approach for Online Monitoring of Bioactive Metabolites from Incubated Actinobacteria in Picoliter Droplets. *Anal Bioanal Chem* **2018**, *410* (29), 7679–7687. https://doi.org/10.1007/s00216-018-1383-1.
(30) Tonouchi, N.; Ito, H. Present Global Situation of Amino Acids in Industry. In *Amino Acid Fermentation*; Yokota, A., Ikeda, M., Eds.; Advances in Biochemical Engineering/Biotechnology; Springer Japan: Tokyo, 2016; Vol. 159, pp 3–14. https://doi.org/10.1007/10_2016_23.
(31) Becker, J.; Wittmann, C. Systems and Synthetic Metabolic Engineering for Amino Acid Production – the Heartbeat of Industrial Strain Development. *Current Opinion in Biotechnology* **2012**, *23* (5), 718–726. https://doi.org/10.1016/j.copbio.2011.12.025.
(32) Bassalo, M. C.; Garst, A. D.; Choudhury, A.; Grau, W. C.; Oh, E. J.; Spindler, E.; Lipscomb, T.; Gill, R. T. Deep Scanning Lysine Metabolism in Escherichia Coli. *Molecular Systems Biology* **2018**, *14* (11), e8371. https://doi.org/10.15252/msb.20188371.
(33) Song, P.; Mabrouk, O. S.; Hershey, N. D.; Kennedy, R. T. In Vivo Neurochemical Monitoring Using Benzoyl Chloride Derivatization and Liquid Chromatography–Mass Spectrometry. *Anal. Chem.* **2012**, *84* (1), 412–419. https://doi.org/10.1021/ac202794q.
(34) Neidhardt, F. C.; Bloch, P. L.; Smith, D. F. Culture Medium for Enterobacteria. *Journal of Bacteriology* **1974**, *119* (3), 736–747. https://doi.org/10.1128/jb.119.3.736-747.1974.
(35) Sun, A. C.; Steyer, D. J.; Allen, A. R.; Payne, E. M.; Kennedy, R. T.; Stephenson, C. R. J. A Droplet Microfluidic Platform for High-Throughput Photochemical Reaction Discovery. *Nature Communications* **2020**, *11* (1), 6202. https://doi.org/10.1038/s41467-020-19926-z.

(36) Monton, M. R. N.; Soga, T. Metabolome Analysis by Capillary Electrophoresis–Mass Spectrometry. *Journal of Chromatography A* **2007**, *1168* (1), 237–246. https://doi.org/10.1016/j.chroma.2007.02.065.
(37) Deal, K. S.; Easley, C. J. Self-Regulated, Droplet-Based Sample Chopper for Microfluidic Absorbance Detection. *Anal. Chem.* **2012**, *84* (3), 1510–1516. https://doi.org/10.1021/ac202791d.
(38) Zhang, J. H.; Chung, T. D.; Oldenburg, K. R. A Simple Statistical Parameter for Use in Evaluation and Validation of High Throughput Screening Assays. *J Biomol Screen* **1999**, *4* (2), 67–73. https://doi.org/10.1177/108705719900400206.
(39) Chen, Y.; Wijaya Gani, A.; Tang, S. K. Y. Characterization of Sensitivity and Specificity in Leaky Droplet-Based Assays. *Lab on a Chip* **2012**, *12* (23), 5093. https://doi.org/10.1039/c2lc40624a.
(40) Baraban, L.; Bertholle, F.; M. Salverda, M. L.; Bremond, N.; Panizza, P.; Baudry, J.; Visser, J. A. G. M. de; Bibette, J. Millifluidic Droplet Analyser for Microbiology. *Lab on a Chip* **2011**, *11* (23), 4057–4062. https://doi.org/10.1039/C1LC20545E.
(41) Duarte, L. C.; Figueredo, F.; Ribeiro, L. E. B.; Cortón, E.; Coltro, W. K. T. Label-Free Counting of Escherichia Coli Cells in Nanoliter Droplets Using 3D Printed Microfluidic Devices with Integrated Contactless Conductivity Detection. *Analytica Chimica Acta* **2019**, *1071*, 36–43. https://doi.org/10.1016/j.aca.2019.04.045.
(42) Shemesh, J.; Ben Arye, T.; Avesar, J.; Kang, J. H.; Fine, A.; Super, M.; Meller, A.; Ingber, D. E.; Levenberg, S. Stationary Nanoliter Droplet Array with a Substrate of Choice for Single Adherent/Nonadherent Cell Incubation and Analysis. *Proceedings of the National Academy of Sciences* **2014**, *111* (31), 11293–11298. https://doi.org/10.1073/pnas.1404472111.
(43) Leung, K.; Zahn, H.; Leaver, T.; Konwar, K. M.; Hanson, N. W.; Pagé, A. P.; Lo, C.-C.; Chain, P. S.; Hallam, S. J.; Hansen, C. L. A Programmable Droplet-Based Microfluidic Device Applied to Multiparameter Analysis of Single Microbes and Microbial Communities. *PNAS* **2012**, *109* (20), 7665–7670. https://doi.org/10.1073/pnas.1106752109.
(44) Matuła, K.; Rivello, F.; Huck, W. T. S. Single-Cell Analysis Using Droplet Microfluidics. *Advanced Biosystems* **2020**, *4* (1), 1900188. https://doi.org/10.1002/adbi.201900188.
(45) Iversen, P. W.; Eastwood, B. J.; Sittampalam, G. S.; Cox, K. L. A Comparison of Assay Performance Measures in Screening Assays: Signal Window, Z' Factor, and Assay Variability Ratio. *J Biomol Screen* **2006**, *11* (3), 247–252. https://doi.org/10.1177/1087057105285610.

Chapter 7 Conclusions and Future Directions

7.1 Conclusions

This thesis describes investigation and development of droplet microfluidics for high-throughput experimentation. The challenges facing droplet microfluidics detailed in Chapter 1, including the understanding of molecular transport between droplets, development of flexible unit operations, and the need for information-rich analysis have each been explored. Various applications have been presented, such as screening enzyme variants, reaction conditions, physiochemical properties, and cell variants. Progress towards advancing droplet microfluidics as a screening technology will increase the reliability beyond what has been presented here. ESI-MS has the potential to increase the application of droplets, including for the discovery of new biocatalysts, development of synthetic catalysts, measurement of chemical descriptors, and sampling for high temporal *in vivo* sensing. Taken holistically, this work serves to enable and improve the ability to screen with low reagent consumption, high efficiency, and improved automation.

In Chapter 2, the transfer of small molecules between droplets was investigated. This challenge is a significant hurdle in the application of droplet microfluidics for screening, and a limited body of work has investigated the phenomenon with non-fluorescent analytes. Using ESI-MS, the transfer was investigated for a structurally diverse panel of analytes for the first time, unraveling both the extent of the transfer and variables driving it. We uncovered new mechanisms for small molecule transport, which is a launching point for the development of surfactants with improved analyte retention. To this end, we demonstrated for the first time the selective retention

of small molecules by using designed surfactants. The work was limited to studying rapid transfer occurring during flow. While measuring crosstalk during flow uncovered important properties (surfactant structure, oil composition, flow duration), it is not fully representative of all droplet-based screening workflows. To build on this work, crosstalk in applied formats (e.g. droplets in storage for prolonged time) must also be investigated. Additionally, while driving variables for crosstalk were uncovered, no clear solution to droplet crosstalk was identified.

Chapters 3 and 4 detailed effort into developing fundamental droplet operations: splitting and reagent addition. In the first chapter, splitting using an electric field was discovered. Microfluidic droplets were split using an AC field employing a floated ground, which serves to induce opposing DEP on droplets in flow. Based on the mechanism, droplets with a range of sizes can be split which is an improvement upon existing splitting designs. An added feature is the ability to easily actuate the split, which geometrical splitters are unable to achieve without valving which requires complex fabrication and pressure control. While controlled splitting occurring due to the electric field has not been described previously, no application of the operation was demonstrated in Chapter 3. Other on-demand droplet splitters (e.g. using pressure driven valving or surface acoustic waves) have been used for combinatorial droplet merging, where droplet arrays are selectively split and combined with each other to form complex reaction vessels. Additionally, application in selectively splitting merged droplets to regain size homogeneity may be of use but was not demonstrated.

In the Chapter 4, two reagent addition tools were developed that are flexible for droplet size (200 pL – 4 nL), generation format (droplets from microfluidic devices and with MWPs), and dilution factor (2 – 150-fold dilution). The reagent addition geometry was used in a proof of concept high-throughput experiment for discovery of photocatalysts, which consumed only 1% of

the photocatalyst compared with MWP methods. A module was developed to decouple the incoming droplet with the diluent droplet, which eliminates the possibility for carryover. The devices achieved the highest dilution to date but did not significantly investigate the throughput limits of the system. The devices were tested up to 50 additions/s, which is sufficient to process 1.8 x 10^5 samples per hour, but the throughputs of existing designs can be as high as 1000 additions/s. Further development using the reagent addition modules should focus on this limitation.

In Chapter 5, the development of an automated workflow was designed for droplet based LLE. This work built on previous development of SFNE,[1] which has utility in droplet extraction and partition coefficient measurement. A new microfluidic device was developed which showed the ability for three-liquid phase droplet generation (aqueous, organic, and fluorinated) for the first time. The device was coupled to an autosampler, which addresses the limitations of droplet microfluidics as an expert-only method. Using the autosampler, sample formats that are used in existing workflows can be processed using droplet operations. The system was used to screen octanol-water partitioning coefficients, representing the highest-throughput approach for K_{ow} measurement developed at time of publication. K_{ow} values were screened for an example small molecule library, which showed value agreement suitable for industrial screening. The workflow relied on an autosampler for sample introduction, which provided automation and ease of use, but does not maximize the throughput available by droplet microfluidics. Investigation into integrating LLE as a cleanup step in larger workflows (e.g. for the cell screening in Chapter 6) could prove useful for HTS.

Finally, Chapter 6 demonstrated the first reported selection of cell variants in droplets using ESI-MS. This work builds upon previous work developing MADS for *in vitro* expressed enzyme.[2]

In the presented workflow, lysine production from *E. coli* in droplets is shown without additional preparation of workup by ESI-MS. The screen shows the feasibility of using cells for droplet based ESI-MS screening, even with high biomass in a commercial growth medium. The enrichment of a known *E. coli* variant from a wild-type strain was shown by using industry standard validation methods. The workflow is compatible with industrially available methods for cell variant generation as input, and industry acceptable methods for downstream validation and sequencing. The workflow is limited to screening applications such as synthetic biology, where a cell generates the desired product through metabolic pathways. Additionally, the small molecule target, lysine, is a favorable analyte due to the high ionization efficiency and the high production by the cell variants. Efforts into expanding the workflow need to assess sensitivity for targets which are not as favorable for ESI-MS or are not as highly expressed by the cell variant.

In addition to the limitations described above, development based on the progress presented in this dissertation focuses on expanding the investigation of molecular transport in other formats, applying the extraction method to activity assays, and further engineering of the MADS system. For the carryover work, the principles developed in Chapter 2 can be applied to other workflows where droplets are used, and the transfer is still relevant. For the extraction work in Chapter 5, the developed protocol can be applied with minor modifications for the rapid clean-up and label-free measurement of enzyme activities using ESI-MS. For MADS presented in Chapter 6, the platform can be improved by increasing throughput, deceasing droplet consumption, improving reliability, and engineering droplet collection for sequence-activity relationships.

7.2 Crosstalk in storage

Chapter 2 developed a method to understand small molecule carryover between droplets segmented with a fluorinated oil. The method primarily relied on a chopper-based design,[3] where

droplet generation is alternated between two aqueous streams containing an analyte and one kept blank (Figure 7-1). The method was developed for easy comparisons, ensuring a controlled ratio of analyte and blank droplets. Variables (e.g. analytes, oils, or other conditions) were tested in under 15 minutes with a few exceptions. While the method showed good reproducibility and uncovered many driving aspects for droplet crosstalk, it was primarily focused on droplets in flow, where no direct contact was made between adjacent droplets. An important aspect that was not investigated in depth is droplets in storage (i.e. stored in a vial with a close-packed structure). For many of the significant effects uncovered in Chapter 2, the crosstalk in storage was examined, but no thorough testing was performed to examine the dynamics occurring between droplets in storage.

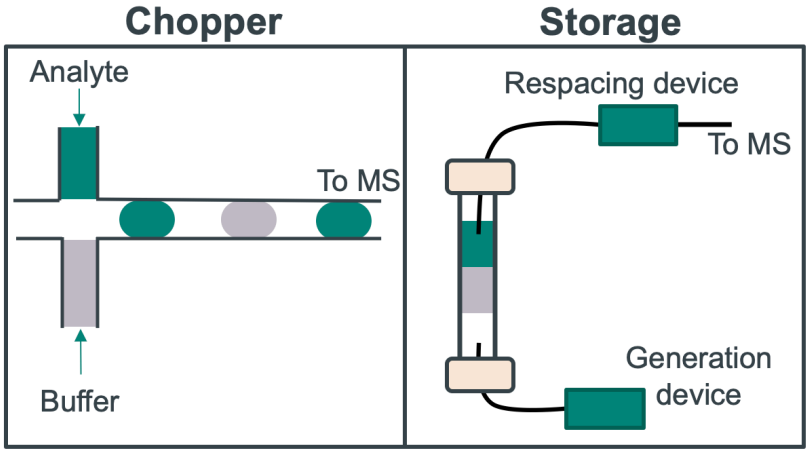

Figure 7-1: Schematics of the main two methods for testing crosstalk presented in Chapter 2. The chopper design alternates generation between analyte containing (green) and buffer (gray) droplets. The droplets remain separated and are directly analyzed by the MS. In storage experiments, populations of analyte and buffer droplets were generated and stored in glass vials, mixed (not shown), and infused through a respacing device which pushes droplets to the MS.

For the storage experiments in Chapter 2, droplets were generated using a generation device into glass storage vials, with an approximate ratio of 50% analyte containing droplets and 50% blank droplets (~30 min). The two layers of droplets were mixed (~10 min) then pumped to a secondary microfluidic device, which re-spaces the tightly packed droplets (15 min). However, this method (Figure 7-1) was too slow to observe the dynamics of the transfer, since most analytes

examined demonstrated 100% carryover at the time of analysis. From a measurement approach, this method also presented two variables which are difficult to control for, namely the ratio and perfect mixing of the two populations, and the exposure time that the droplets had to each other. Similarly, this workflow introduces variables such as the tubing that carries formed droplets into the storage vial, the tubing that carries droplets to the re-spacing device, and the fresh oil which is used to respace droplets. Lastly, the workflow does not lend itself to screening many variables quickly (e.g. different analytes, oil compositions, or droplet sizes), as each experiment takes ~ 1 hr and two microfluidic set ups (one for droplet generation, one for re-spacing and analysis) per condition.

To address these concerns, a hybrid device was developed. The device uses the principles of the original chopper device but includes an incubation step to bridge the gap to the bulk storage format (Figure 7-2A). The "incubated chopper" (abbreviated as InCh) device allows for the controllable flow rates, analyte/blank droplet ratio, and flow duration, while also providing an incubation channel for controlled exposure with droplet interaction. The latter feature is possible by using an oil drain, which pulls oil from the main fluidic channel after droplet generation (Figure 7-2B). After the incubation chamber, tightly packed droplets are re-spaced with oil, and the droplets are exported from the device for ESI-MS.

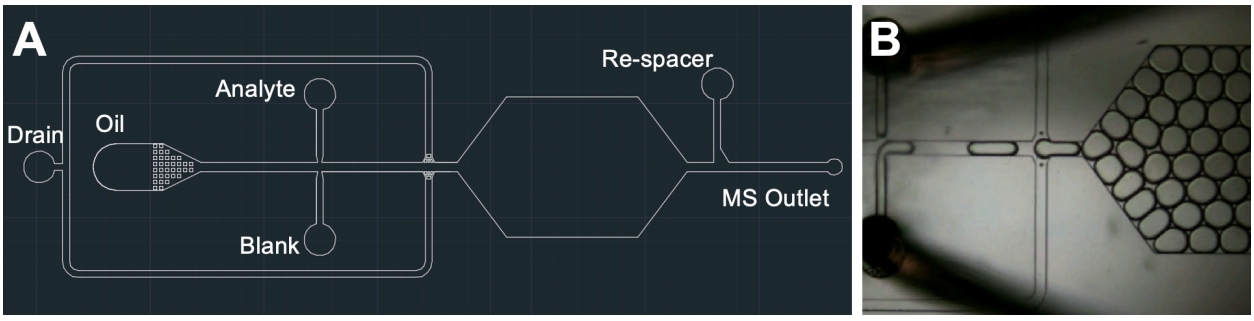

Figure 7-2: Design and example of incubated chopper (InCh) device. (A) Fluidic inlets are labelled according to the function. (B) Photomicrograh of the InCh device, focusing on the oil draining region. Droplet are generated from the two aqueous flows, then oil is drained perpendicular to the main channel, facilitated by microfabricated posts. The droplets are introduced into the incubation chamber with tight packing.

The InCh device was first tested by generating 25 nL droplets using caffeine as a test analyte. Caffeine had low crosstalk in the initial testing with the chopper device, but preliminary storage tests showed full carryover. Using the same flow rates, tubing lengths, and surfactant stabilized oil (variables known to affect crosstalk) as the chopper experiment, caffeine crosstalk increased with inclusion of an incubation step (Figure 7-3). When the droplets were tightly packed due to the oil drain (calculated as 37 droplets/mm^3, or 92.5% occupancy of droplets per unit volume), the crosstalk value increased from 0.05 to almost 0.5, representative of full carryover of caffeine. The flow rates used (1 μL/min oil, 0.6 μL/min combined aqueous) present a 37.5% composition of aqueous flow. Therefore, the oil drain was effective at removing 88% of the oil. When the oil drain was not used, droplet density was reduced to 15 droplets/mm^3 (consistent with the oil/aqueous flow ratios, 37.5% density) and an intermediate crosstalk value was measured for caffeine (Figure 7-3). These results taken together suggest another factor driving droplet crosstalk, relating to the density of droplets together. In the InCh test, droplets were still exported from the device and flowed through capillary to the MS, so the crosstalk resulting from the shear forces between the droplet and the tubing wall was still present. By subtracting the crosstalk value based on the chopper experiment (e.g. the crosstalk from shear stress during flow to the MS without incubation) the incubation of the droplets represented 26% caffeine carryover at 37.5% droplet density and 79% caffeine carryover at 92.5% droplet density.

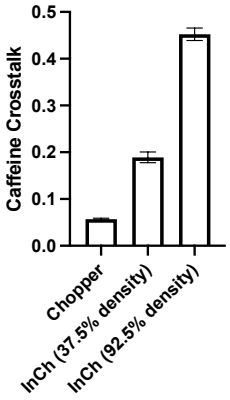

Figure 7-3: Comparison of crosstalk by different experiments. Crosstalk values for caffeine measured using the original chopper design, the InCh device without close packing, and the InCh device with close packing by utilizing an oil drain

The InCh device enables the crosstalk measurement with additional variables that can be controlled. One such variable is the length of time the droplets remain in contact with each other, easily designed with increasing incubation channel size. Three devices were designed to this end, which were tested with three analytes, all with intermediate degrees of crosstalk. As the incubation time increased, no significant effect on crosstalk was observed (Figure 7-4). This finding suggests that the effect of crosstalk when droplets are in contact with each other is very rapid, consistent with our early experiments using the traditional incubation experiment. Interestingly, the crosstalk of tryptamine was measurable using the InCh device. This analyte was included in the original library screen of crosstalk using the chopper device in Chapter 2 and included in the PCA model. However, this analyte was one that had undetectable crosstalk with the chopper device, but the PCA predicted the carryover was still possible. The two methods (InCh and storage experiments) may not be directly equivalent as there are a number of variables that differ, but the InCh device appears to uncover more dynamics than the chopper device (shown with the solid lines, color coded to the analyte), which might provide insight into crosstalk in storage.

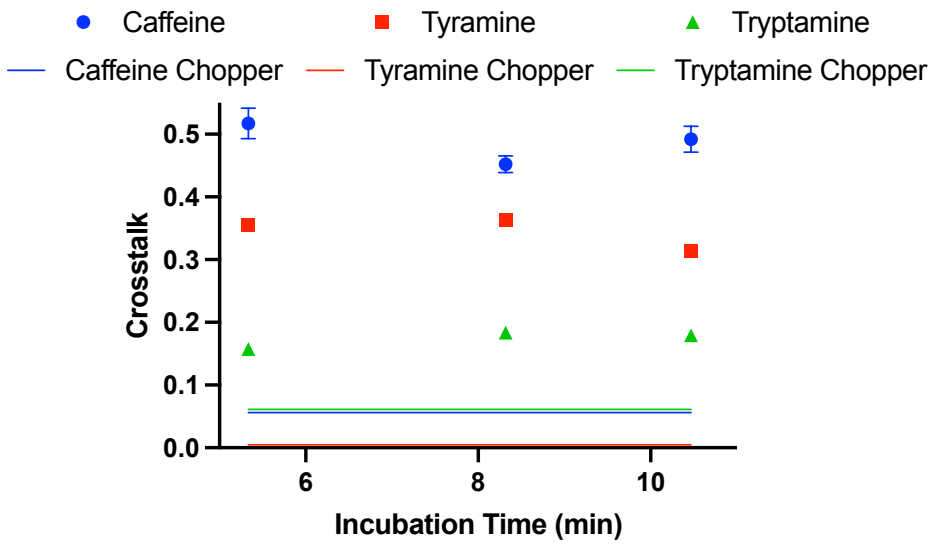

Figure 7-4: Effect of incubation channel length on crosstalk. Incubation time was controlled using three devices, and the incubation time was calculated by calculating volume of the incubation channel designed. The solid colored lines represent the value calculated with the chopper device for caffeine, tryramine, and tryptamine

The previous finding of crosstalk reduction by decreasing the droplets density was further investigated by increasing the flow rate of the segmenting oil without oil draining. The oil flow rate was increased into the incubation chamber, decreasing droplet density from 37.5% at 1 µL/min to 16.6% at 3 µL/min oil. Caffeine crosstalk was reduced with increasing oil but it leveled at ~0.1 (Figure 7-5A). As in previous experiments, the droplets were still flowed through capillary to the MS, which results in ~0.06 crosstalk of caffeine. The difference of 0.04 caffeine crosstalk may be due to experimental variability (8% difference could be due to error in measurement) or it could be due to a physical effect such as shear between the droplets and the incubation channel walls.

We also tested the feasibility of performing an oil-replacement prior to transport by generating droplets with 37.5% droplet density, followed by the addition of FC-40 oil containing no surfactant. Results presented in Chapter 2 suggested that FC-40 with 2 wt.% 008-FS is a favorable oil composition for small molecule retention, resulting in caffeine crosstalk of 0.01 in the chopper experiment. In principle, adding FC-40 to the surfactant stabilized oil can reduce surfactant micelle concentration, which can reduce the transport by shear-driven micelle

formation. Compared to an identical experiment in which surfactant stabilized Novec oil was used, caffeine crosstalk was reduced by almost half (Figure 7-5B). The reduction, 0.1, is the equivalent value as the caffeine crosstalk from the chopper using 2 wt% 008-FS in Novec oil (Figure 7-3), so this finding suggests it is possible to mitigate the flow-based effects by stripping surfactant. However, the measured crosstalk value of 0.1 is still relatively high. This degree of crosstalk with FC 40 may be due to interaction between droplets in the storage chamber (37.5% density) prior to the oil dilution, or it may be a combination of flow-based factors and the interaction in the storage chamber. This finding suggests there is feasibility for mixed oil replacements, which can mitigate flow-driven crosstalk even after incubation experiments.

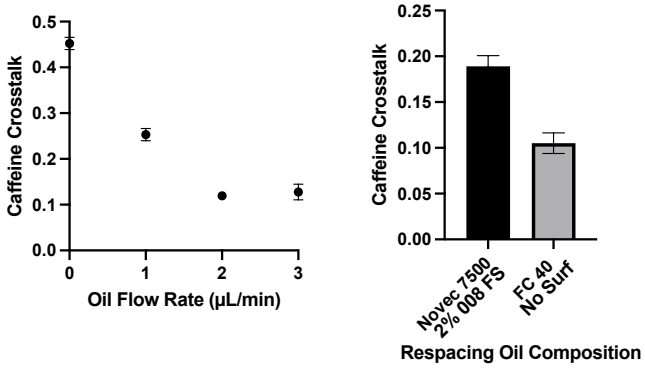

Figure 7-5: Effect of droplet density on crosstalk. (A) Effect of oil flow rate into the incubation chamber. Oil was increased without draining and the droplets were analyzed. Higher oil flow rates leads to lower droplet density in the chamber. With lower droplet density, caffeine crosstalk is reduced. (B) Changing the composition of the respacing oil after droplet incubation. When the respacing oil was changed to FC40 without surfactant, a reduction is observed.

7.3 SFNE for activity assays

Chapter 4 detailed the use of a microfluidic device for the generation of droplet phase-pairs of octanol and water segmented by PFD. The full platform demonstrated a user-friendly interface for analyzing samples in a multi-well plate. While it was applied to the study of octanol-water partitioning coefficients, the demonstration can be applied for a more generalizable platform.

Liquid-liquid extractions can be used for rapid analyte extraction relating to many applications. For example, standard workflows for protein engineering experiments, e.g. those in Chapter 6, typically rely on cells as biocatalytic hosts. For analysis of cell variants, a sample cleanup is typically used to isolate the targets of the screen from the complex cell media and cell debris background. Typically, this is done by quenching the reaction with an organic solution, centrifuging the mixture, and performing dilution on the supernatant. However, using the online SFNE method presented in Chapter 5, most of these steps could be replaced using droplet based LLE.

A challenge associated with translating the presented online SFNE system to generalizable biological workup is the compatibility of the system with organic solvents. A PDMS device was used for phase-pair generation with octanol, however; PDMS is largely incompatible with organic solvents.[4] Alternative materials have been used for microfabrication of microfluidic device, such as glass, silicon, and a variety of thermostable plastics.[5] Glass has the benefits of transparency, allowing for monitoring of on-chip operations, but suffers from lengthy fabrication protocols. However, for proof of principle, the SFNE devices used in Chapter 5 were replicated using glass fabrication by hydrofluoric acid etching. A representative image of the fabricated glass SFNE device is shown in Figure 7-6.

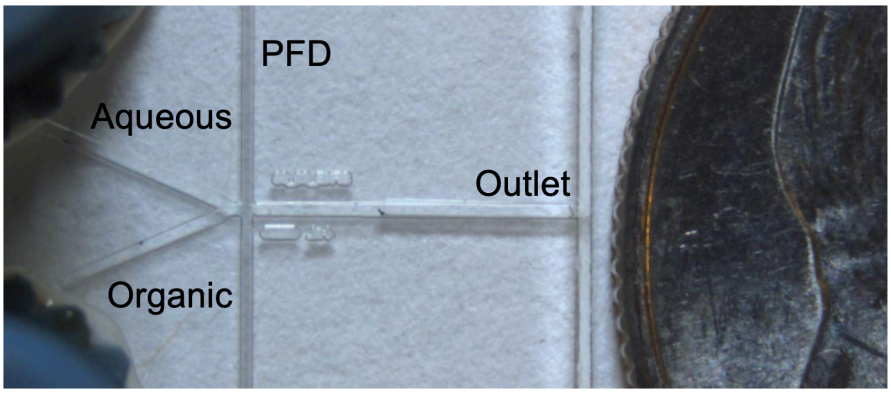

Figure 7-6: Image of glass SFNE generation device. The channels are labelled according to their function. The device is positioned next to a dime for scale.

The primary difference between the glass device developed and the PDMS device used previously is the challenges associated with using a rigid material compared to the elastomeric PDMS. As the phase-pairs are not surfactant stabilized to facilitate the transfer of chemical material between the aqueous phase and the organic phase, the resulting flow is not facilitated by the stability provided by the surfactant. Therefore, the phase pairs must exit the device in the plane of flow rather than perpendicularly through flow outlets. To accommodate this in the glass device, both the top and the bottom of the device were etched to create an outlet in the plane of the fluidic channels. A fused silica capillary was inserted into the outlet, and wax was used to seal the capillary to the chip.

To demonstrate the utility of the new device material, the device was coupled with ESI-MS. A solution of 1 μM fexofenadine in artificial cerebrospinal fluid (aCSF) was infused into the device without organic flow but was segmented by PFD (Aqueous droplets). The outlet capillary was inserted into a CE-ESI-MS source as in Chapters 2, 4 and 6. The signal was very low for fexofenadine in aCSF due to the significant ionization suppression which has been discussed previously.[1,6] The flow of the organic (ethyl acetate) into the microfluidic device was started which initiated SFNE phase pairs. Upon the introduction of an extraction phase for fexofenadine, the MS

signal was increased 100-fold (Figure 7-7). This shows the improvements possible for using SFNE using the microfluidic device for complex matrices.

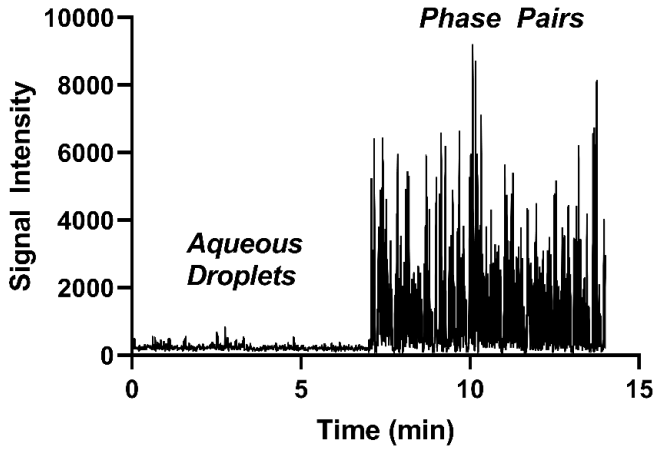

Figure 7-7: Example trace using SFNE with ESI-MS for complex matrices. For 7 minutes, 1 uM fexofenadine was infused without extraction, then ethylacetate was infused to generate phase-pairs. Significant signal improvement was observed with SFNE.

The glass device presented can be used in tandem with the existing system for online SFNE as in Figure 7-8. The new material allows for extraction using a range of organic solvents. Samples can be plated into a well-plate, such as for enzyme or cell variants, or plasma or urine samples. The samples can be injected into the glass device, which will segment into SFNE phase-pairs. The resulting pairs can be analyzed using ESI-MS, which can be used to scan for a range of small molecules such as reaction products or biomarkers from human samples.

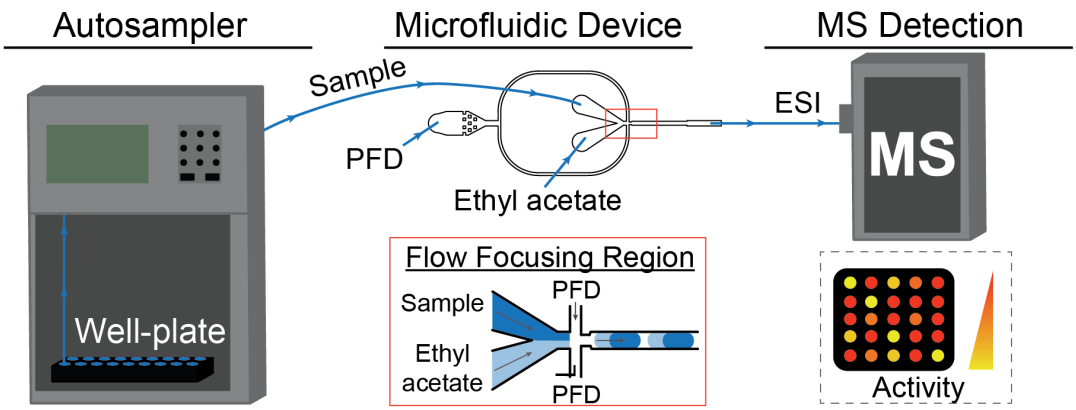

Figure 7-8: Proposed schematic for using the online SFNE platform for activity or biomarker analysis. Samples in a well plate are pumped into the microfluidic device for phase pair generation. Resulting phase pairs are analyzed with ESI-MS

7.4 Advanced screening and collection for MADS

Chapter 6 outlined the application of MADS for the selection of cell samples. The utilization of whole cells as biocatalysts simplified the workflow of the original MADS demonstration. Cells are capable of growing without DNA amplification and expression needed using *in vitro* expression, which eliminated the PCR steps originally required. Additionally, the cells were engineered to synthetize lysine via glucose metabolism, so no substrate or induction addition step was needed. The final workflow presented was aided by the necessary biology (cell growth and metabolism) occurring in a single reaction vessel.

While the workflow presented is a significant step toward a generalizable method for cell variant screening, it is currently applicable for cell systems that do not require induction or substrate addition. While some reports have shown the utility of autoinduction media and adding the substrate to the initial growth cultures,[7] the added flexibility of reagent addition could provide temporal control for quenching or cell lysis. In these cases, an additional reagent step is required. In particular the high-dilution reagent addition presented in Chapter 4 are appropriate to achieve

this goal. As standard reagent addition methods have been shown to result in chemical and biological carryover, the touch-free, high-dilution reagent addition system is suggested.

While *E. coil* were shown to grow effectively in 30 nL droplets in Chapter 6, the droplet size is associated with instability due to low surface tension. We hypothesize that adjusting to a smaller droplet size is beneficial for the reliability of the screen, due to both improved droplet stability and reduction in reaction chamber for the cells to grow. With smaller droplets, nutrients and space deplete faster, which initiates the maximum lysine production available by the cells at an earlier time point. To test the feasibility of using smaller droplets, DapA expressing *E. coli* were grown from single cells in both 3 and 30 nL droplets for 24 h (cell stocks were diluted to < 0.05 OD_{600} prior to droplet generation). Images taken of the droplets after 24 h showed the frequency of cell growth was 8% for 3 nL droplets and 14% for 30 nL droplets, which is consistent with Poisson loading of single cells in droplets. The droplets were analyzed by ESI-MS by respacing the droplets after bulk growth (Figure 7-9). Droplets with high lysine signal were observed in both droplet sizes. Therefore, the cells are capable of growing and producing lysine in both formats.

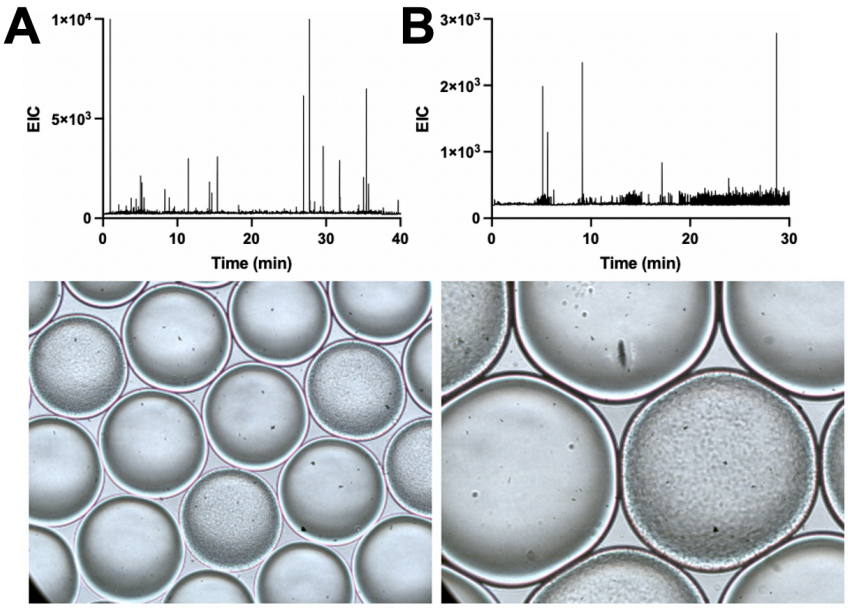

Figure 7-9: Images of E. coli growth in different droplet sizes. (A) ESI-MS trace and photomicrograph of 3 nL droplets that were used for E. coli cell culture. Maximum lysine signal was observed at 10000 counts. (B) Trace and photomicrograph of 30 nL droplet cultures, where maximum signal is observed at 2500 counts.

The use of smaller droplets allows for manipulations such as dynamic droplet mixing. This strategy is reported to increase the homogeneity of in-droplet cell growth by constantly refreshing the oil in the droplet storage vial.[8] This serves to both circulate droplets, mimicking the shaking that is commonly performed with bulk cell cultures, as well as provide oxygen which is dissolved in the fresh oil. The re-circulator was built based on previous reports and tested, showing significant droplet mixing over time (Figure 7-10). While the dynamic mixer can be used for a variety of droplet sizes, the constant flow of oil can break or merge more unstable droplets. It is proposed that the dynamic mixer be used for future in-droplet growth experiments to increase cell growth homogeneity.

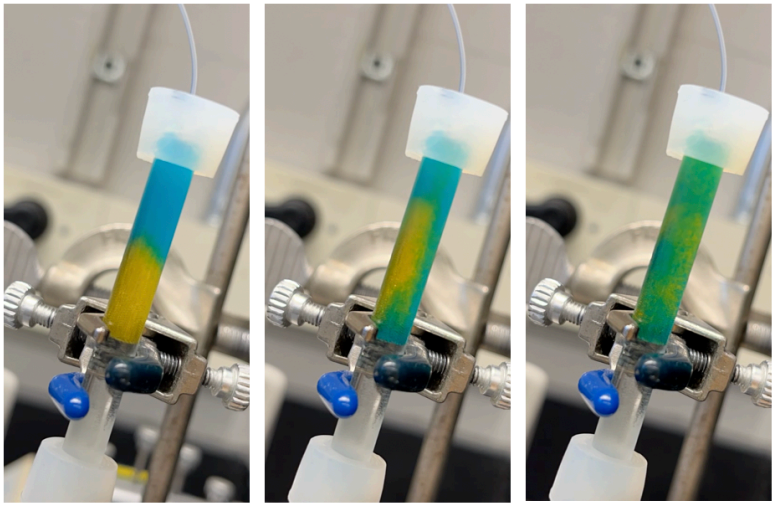

Figure 7-10: Dynamic droplet mixer. Photos from a time-course experiment testing the dynamic droplet mixer with 3 nL droplets. Two populations of droplets were generated (maize and blue), and oil was recirculated passively using a peristaltic pump. After 15 min, substantial mixing had occurred.

The use of small droplets also has disadvantages compared to 30 nL droplets, primarily the incompatibility with the current MADS set-up. Therefore, two options exist to couple the two: use of reagent addition as discussed above, or the re-design of MADS for smaller droplets. The use of reagent addition is promising, as it enables more abilities for cell screening (i.e. lysis, reaction quenching), but it requires the inclusion of another microfluidic operation which increases potential droplet size variability and the complexity of the method. Based on the benchmarks presented in Chapter 4, the touch-free addition module showed 97% success rate, so the variability introduced to MADS is minimal.

If the need for reagent addition is not required and the increase in workflow difficulty (i.e. another microfluidic operation) is undesirable, MADS channel dimensions can be scaled down and smaller inner diameter capillary can be used to MS analysis. While droplets must make contact with tubing/channel walls for consistency of flow in the current design, reduction from 150 µm to 50 µm inner diameter capillary changes the minimum droplet size compatible with ESI from ~5 nL to ~200 pL (as determined by 3x the volume of a sphere in the capillary). Based on the splitting

ratio occurring during MADS, the minimum input droplet size changes from ~15 nL to ~600 pL. Achieving this goal enables MS based screening with significantly smaller droplets, which can facilitate both upstream operations (cell growth, droplet stability) and downstream operations (DEP sorting).

A final limitation of MADS is the inability to match MS signal with verified sequence information. In the system presented in Chapter 6, all selected droplets are pooled and verified together. In an unknown screen, a second-tier screen would be needed to identify the degree of improvements made for individual variants captured. An efficient collection system will deposit selected droplets into independent reservoirs, where the MS signal can be analyzed compared to a verified sequence. Droplet deposition methods have been presented before using DEP trapping electrodes.[9] While this strategy shows good spatial separation of droplets, the trapping is most effective with picoliter size droplets, the fabrication of such trapping substrates is complicated, and the success is contingent on sophisticated detection and actuation.

For cell-based screening such as Chapter 6, an ideal substrate for droplet deposition will promote cell growth, such as agar or cell media. We tested the ability for droplet deposition of cell-containing droplets in both formats. An agar substrate was first patterned using an SU8 stamp to generate microwells in the surface, and cell containing droplets were manually deposited into the wells. After 24 h, the cells adhered and grew significantly on the agar (Figure 7-11A). We also tested the feasibility of cell growth in microwell plates seeded with cell media (Figure 7-11B). In both formats, cell growth is feasible. In future work, deposition from the splitting device must be engineered to actuate the movement of a depositing capillary.

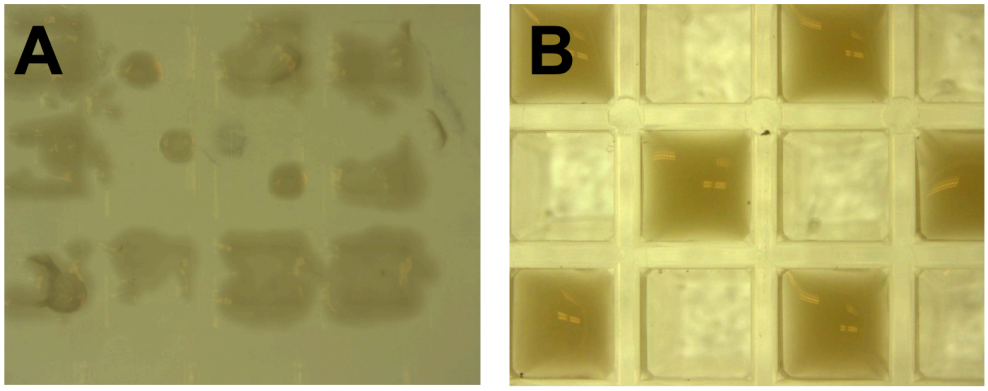

Figure 7-11: E. coli droplet deposition and growth. (A) Cell-containing droplets spotted onto a micropatterned agar plate after 24 h of incubation. (B) Cells contained within microwells in a checkerboard pattern, where brown wells contain cells and clear wells contain blank cell media.

This final demonstration of the feasibility of droplet deposition and subsequent cell growth also shows the feasibility of a full structure-activity relationship study for DE. While the primary goal of DE workflows is to identify variants with superior chemical production, computational efforts can use analyze both beneficial and detrimental mutations with respect to activity to generate enzyme or metabolic profiles that predict combinatorial variants.[10] By screening and sequencing all variants, rich databases of residue contributions can be generated. In this format, no droplet sorting is needed, since each droplet can be split for ESI-MS and deposition. Without the sorting needed with MADS, both droplet operations and MS operations are simplified; the microfluidic device is a simple droplet splitter, and the MS can be a fast-scanning, high-resolution, or more selective instrument such as a qTOF, orbitrap, or triple-quadrupole mass spectrometer.

7.5 References

(1) Wells, S. S.; Kennedy, R. T. High-Throughput Liquid–Liquid Extractions with Nanoliter Volumes. *Anal. Chem.* **2020**, *92* (4), 3189–3197. https://doi.org/10.1021/acs.analchem.9b04915.

(2) Holland-Moritz, D. A.; Wismer, M. K.; Mann, B. F.; Farasat, I.; Devine, P.; Guetschow, E. D.; Mangion, I.; Welch, C. J.; Moore, J. C.; Sun, S.; Kennedy, R. T. Mass Activated Droplet Sorting (MADS) Enables High-Throughput Screening of Enzymatic Reactions at Nanoliter Scale. *Angewandte Chemie International Edition* **2020**, *59* (11), 4470–4477. https://doi.org/10.1002/anie.201913203.

(3) Deal, K. S.; Easley, C. J. Self-Regulated, Droplet-Based Sample Chopper for Microfluidic Absorbance Detection. *Anal. Chem.* **2012**, *84* (3), 1510–1516. https://doi.org/10.1021/ac202791d.
(4) Lee, J. N.; Park, C.; Whitesides, G. M. Solvent Compatibility of Poly(Dimethylsiloxane)-Based Microfluidic Devices. *Anal. Chem.* **2003**, *75* (23), 6544–6554. https://doi.org/10.1021/ac0346712.
(5) Scott, S. M.; Ali, Z. Fabrication Methods for Microfluidic Devices: An Overview. *Micromachines* **2021**, *12* (3), 319. https://doi.org/10.3390/mi12030319.
(6) Ngernsutivorakul, T.; Steyer, D. J.; Valenta, A. C.; Kennedy, R. T. In Vivo Chemical Monitoring at High Spatiotemporal Resolution Using Microfabricated Sampling Probes and Droplet-Based Microfluidics Coupled to Mass Spectrometry. *Anal. Chem.* **2018**, *90* (18), 10943–10950. https://doi.org/10.1021/acs.analchem.8b02468.
(7) Eenink, B. D. G.; Kaminski, T. S.; Bornberg-Bauer, E.; Jose, J.; Hollfelder, F.; van Loo, B. Vector Redesign and In-Droplet Cell-Growth Improves Enrichment and Recovery in Live Escherichia Coli. *Microbial Biotechnology* **2022**, *15* (11), 2845–2853. https://doi.org/10.1111/1751-7915.14144.
(8) Mahler, L.; Tovar, M.; Weber, T.; Brandes, S.; Rudolph, M. M.; Ehgartner, J.; Mayr, T.; Figge, M. T.; Roth, M.; Zang, E. Enhanced and Homogeneous Oxygen Availability during Incubation of Microfluidic Droplets. *RSC Adv.* **2015**, *5* (123), 101871–101878. https://doi.org/10.1039/C5RA20118G.
(9) Cole, R. H.; Tang, S.-Y.; Siltanen, C. A.; Shahi, P.; Zhang, J. Q.; Poust, S.; Gartner, Z. J.; Abate, A. R. Printed Droplet Microfluidics for on Demand Dispensing of Picoliter Droplets and Cells. *PNAS* **2017**, *114* (33), 8728–8733. https://doi.org/10.1073/pnas.1704020114.
(10) Benítez, A. R.; Tweedy, S.; Baker Dockrey, S. A.; Lukowski, A. L.; Wymore, T.; Khare, D.; Brooks, C. L.; Palfey, B. A.; Smith, J. L.; Narayan, A. R. H. Structural Basis for Selectivity in Flavin-Dependent Monooxygenase-Catalyzed Oxidative Dearomatization. *ACS Catal* **2019**, *9* (4), 3633–3640. https://doi.org/10.1021/acscatal.8b04575.

Appendix

Supporting information for Chapter 2

For crosstalk dataset analysis, 36 analytes were tested in triplicate for crosstalk using 2 wt.% 008 FS in HFE 7500. The values are presented in Table A-1, alongside the normalized chemical descriptors as determined by ChemAxon.

The analytes were compared using a Tanimoto similarity matrix shown in Figure A-1. Principle component analysis presented in Chapter 2 was generated using the variable contributions outlined in Figure A-2, with the following principle components:

PC-1 = 0.27 LogS - 0.44 LogD -0.42 LogP + 0.31 HBA + 0.35 HBD - 0.19 MPb + 0.40 PSAc + 0.37 HLBd

PC-2 = 0.52 LogS - 0.24 LogD - 0.24 LogP - 0.46 HBA - 0.33 HBD - 0.42 MPb - 0.35 PSAc + 0.03 HLBd

Table A-1: Dataset of measured crosstalk values and normalized physicochemical descriptors

Entry	Compound	Crosstalk Value ± SEM	LogS (pH8.46)	LogD (pH8.46)	LogP	H-Bond Acceptor	H-Bond Donor	MPb	PSAc (pH8.46)	HLBd
1	Triethylamine	0.222 ± 0.013	1.62	-0.11	0.40	-0.87	-1.01	-0.60	-1.21	0.13
2	Acetylpyridine	0.376 ± 0.011	-0.41	0.50	0.14	-0.09	-1.01	-0.63	-0.37	-1.32
3	Caffeine	0.056 ± 0.002	-0.12	-0.14	-0.43	0.69	-1.01	0.03	0.56	0.14
4	Oxymetazoline	0.086 ± 0.002	-0.87	1.05	1.21	0.69	0.72	1.77	0.16	-0.66
5	Aminoantipyrine	0.053 ± 0.003	-0.90	0.31	-0.02	0.69	-0.14	0.62	0.27	1.39
6	Imidazole	0.039 ± 0.002	0.19	0.06	-0.24	-0.87	-0.14	-1.47	-0.41	-0.17
7	3,4-Diaminopyridine	0.184 ± 0.003	1.18	-0.64	-0.59	0.69	0.72	-0.83	0.82	-0.47
8	Nicotinamide	0.025 ± 0.001	-0.07	-0.06	-0.36	-0.09	-0.14	-0.75	0.48	-0.68

9	Acetaminophen	0.016 ± 0.001	-0.69	0.58	0.24	-0.09	0.72	-0.26	0.26	-1.26
10	Aniline	0.480 ± 0.011	-0.72	0.78	0.40	-0.87	-0.14	-0.86	-0.50	-1.88
11	p-anisidine	0.414 ± 0.012	-0.79	0.64	0.27	-0.09	-0.14	-0.51	-0.20	-1.08
12	N-Methylmorpholine	0.206 ± 0.011	0.95	0.10	-0.19	-0.09	-1.01	-0.87	-0.95	1.39
13	Eserine	0.220 ± 0.012	-1.01	1.27	0.84	0.69	-0.14	1.73	0.12	0.33
14	Pyridine	0.442 ± 0.024	0.18	0.52	0.17	-0.87	-1.01	-1.15	-0.93	-1.34
15	N-Methylpiperidine	0.189 ± 0.009	1.67	-0.02	0.30	-0.87	-1.01	-0.71	-1.21	0.17
16	1-pyridin-3-yl-ethylamine	0.073 ± 0.001	0.82	-0.11	-0.04	-0.09	-0.14	-0.42	-0.03	0.08
17	2-methylimidazole	0.086 ± 0.002	0.53	0.11	-0.19	-0.87	-0.14	-1.23	-0.41	-0.60
18	Benzylamine	0.492 ± 0.009	0.21	0.24	0.32	-0.87	-0.14	-0.55	-0.45	-0.62
19	Tripropylamine	0.473 ± 0.010	0.74	0.39	1.11	-0.87	-1.01	0.18	-1.21	-0.40
20	Tryptamine	0.061 ± 0.003	-0.26	0.24	0.50	-0.87	0.72	0.44	0.07	-0.38
21	Diaminoheptane	<0.005	-1.11	0.57	0.43	-0.09	0.72	-0.13	0.41	0.89
22	Tyramine	<0.005	0.78	0.00	0.13	-0.09	0.72	-0.22	0.21	-0.22
23	Serotonin	<0.005	-0.26	0.10	0.04	-0.09	1.58	0.52	0.73	0.08
24	Uracil	<0.005	-0.36	-0.37	-0.57	-0.09	0.72	-1.12	0.55	-0.16
25	n-Acetylputrescine	<0.005	1.82	-1.12	-0.65	-0.09	0.72	-0.44	0.51	0.66
26	Uridine	<0.005	-0.15	-1.10	-1.28	3.03	2.45	0.46	2.56	0.67
27	Kynurenic acid	<0.005	0.26	-0.72	0.54	1.47	0.72	0.12	1.05	0.30
28	Arginine	<0.005	1.06	-1.86	-1.66	3.03	2.45	-0.10	3.03	2.43
29	Acetylcholine	<0.005	N/A	-2.00	-2.10	-0.87	-1.01	-0.25	-0.49	1.32
30	Choline	<0.005	N/A	-2.23	-2.31	-0.87	-0.14	-0.79	-0.69	1.32
31	Lysine	<0.005	1.27	-1.89	-1.64	1.47	1.58	-0.32	1.77	2.12
32	Neostigmine	<0.005	N/A	-1.00	-1.20	-0.87	-1.01	0.99	-0.39	0.90
33	Dextromethorphan	>0.500	-1.07	1.20	1.42	-0.09	-1.01	2.06	-0.91	-0.75
34	Diphenhydramine	>0.500	-1.75	1.71	1.49	-0.09	-1.01	1.94	-0.91	-0.62
35	Imipramine	>0.500	-2.40	1.90	1.78	-0.09	-1.01	2.40	-1.10	-0.88
36	Tributylamine	>0.500	-0.33	1.07	1.72	-0.87	-1.01	0.96	-1.21	-0.78

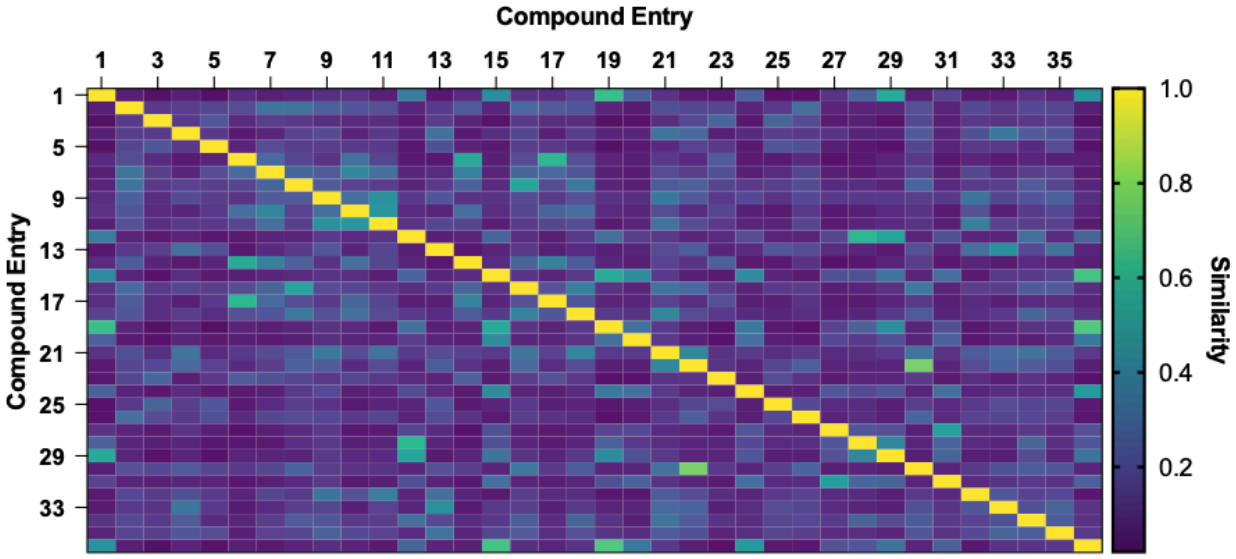

Figure A-1: Tanimoto similarity matrix for compounds in the database. Row and column numbers correspond with the compound entry listed in Table S2. A similarity score of 1 represents identical chemical structures. Compounds are largely dissimilar. Highest similarity score is 0.78 for compounds 22 and 30 (serotonin and tryptamine). The average score is 0.15.

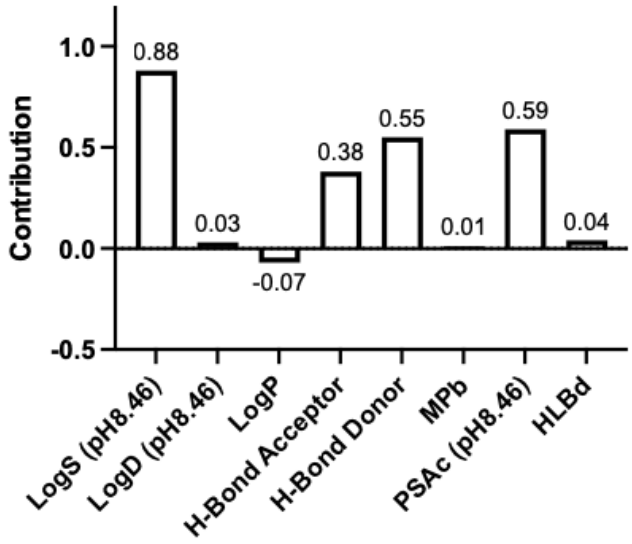

Figure A-2: Variable contributions of physicochemical descriptors to PCA.